

Conflict Analysis for Cooperative Maneuvering using Vehicle-to-everything (V2X) Communication

by

Hao Wang

A dissertation submitted in partial fulfillment
of the requirements for the degree of
Doctor of Philosophy
(Mechanical Engineering)
in the University of Michigan
2024

Doctoral Committee:

Professor Gábor Orosz, Chair
Dr. Onur Altintas, Toyota InfoTech Labs
Professor Necmiye Ozay
Professor Jing Sun

Hao Wang

haowangm@umich.edu

ORCID iD: 0000-0002-0707-7129

© Hao Wang 2024

ACKNOWLEDGEMENTS

I would like to express my deepest gratitude to my advisor, Professor Gábor Orosz, whose support, guidance, and mentorship have been invaluable throughout the entirety of my Ph.D. journey. I would like to extend my sincere appreciation to my committee members, Dr. Onur Altintas, Professor Necmiye Ozay, and Professor Jing Sun, for their constructive feedback and insightful suggestions. I am also grateful to all my collaborators, both in academia and in industry, especially, Dr. Sergei Avedisov at Toyota InfoTech Labs, for their helpful comments and discussions.

TABLE OF CONTENTS

ACKNOWLEDGEMENTS	ii
LIST OF FIGURES	v
LIST OF TABLES	xi
LIST OF APPENDICES	xii
ABSTRACT	xiii
CHAPTER	
1 Introduction	1
1.1 Motivation: Conflict Resolution in Mixed Traffic	1
1.2 Cooperation using V2X Communication	3
1.3 Contributions and Outline	6
2 Establishing the Conflict Analysis Framework	8
2.1 Modeling Vehicle Dynamics	9
2.2 Conflict Analysis	11
2.2.1 Conflict charts	14
2.2.2 Communication range and decision making rule	15
2.3 Conflict Analysis with Intent Information	19
2.4 Controller Design	21
2.5 Experiments and Simulations	26
2.5.1 Experiments on test track with real vehicles	26
2.5.2 Simulations using real highway data	29
2.6 Summary	31
3 Opportunistic Strategy in Conflict Analysis	32
3.1 Opportunistic Strategy	32
3.1.1 Conservative strategy and potential opportunity	32
3.1.2 Decision checking mechanism	34
3.1.3 Opportunistic controller	35
3.2 Simulation with Real Highway Data	37
3.3 Summary	40

4 Multi-Vehicle Conflict Analysis under Time Delays	41
4.1 Modeling Vehicle Dynamics and Communication	43
4.2 Multi-Vehicle Conflict Analysis with Status-sharing	46
4.2.1 Conflict analysis with time delay in dynamics	47
4.2.2 Conflict analysis with time delays in communication	52
4.3 Multi-Vehicle Conflict Analysis with Intent Information	57
4.4 Controller Design and Simulation	61
4.4.1 Goal-oriented control	62
4.4.2 Simulations with real highway data	63
4.5 Summary	66
5 Scalability of Conflict Analysis	68
5.1 Extending Multi-Vehicle Conflict Analysis	68
5.1.1 Conflict analysis under additional maneuver constraints	68
5.1.2 Conflict analysis with more remote vehicles	78
5.2 Controller Design and Simulation	81
5.3 Summary	83
6 Intent-based Conflict Analysis and Experimental Evaluation	84
6.1 Generalizing Motion Intent of Vehicles	85
6.2 Generalizing Conflict Analysis	87
6.2.1 Intent-based conflict analysis	87
6.2.2 Communication setup	91
6.2.3 Conflict analysis for a merge scenario	92
6.3 Experiments at Mcity Test Track	96
6.3.1 Creating intent messages	97
6.3.2 Experiments in Mcity	98
6.3.3 Evaluating benefits of intent sharing	101
6.3.4 Validating intent-based conflict analysis	102
6.4 Evaluating Intent Sharing using Real Highway Data	104
6.4.1 Packet delivery ratios on public highways	104
6.4.2 Effects of communication conditions	106
6.5 Summary	110
7 Conclusions and Future Work	111
7.1 Conclusions	111
7.2 Future Work	112
 APPENDICES	 114
 BIBLIOGRAPHY	 134

LIST OF FIGURES

FIGURE

1.1	Different levels of cooperation enabled by V2X communication, defined in SAE J3216 standard.	3
1.2	Levels of automation and cooperation targeted in this dissertation (green shading). . .	4
1.3	Conflict prevention performed by an ego vehicle under status sharing and intent sharing.	5
2.1	Cooperative maneuvers at (a) highway on-ramp, (b) expressway entrance, (c) highway off-ramp. (d) Model used for conflict analysis. A conflict happens if both vehicles are present (even partially) in the conflict zone, and thus, the key parameter $s = L + l$ is the sum of conflict zone length and the vehicle length.	9
2.2	Conceptual illustrations of proposition P in panel (a) and proposition Q in panel (b). .	12
2.3	(a)-(c) Conflict charts in the (v_2, r_2) -plane for given v_1, r_1 values as indicated. (a) Conflict charts for merge ahead. (b) Conflict charts for merge behind. (c) Unified conflict charts combining (a) and (b). (d)-(f) Conflict charts in the (r_1, r_2) -plane for given v_1, v_2 values as indicated.	16
2.4	(a)-(d) Conflict charts in the (v_2, r_2) -plane when the remote vehicle is approaching with a constant speed. (e)-(h) Conflict charts in the (r_1, r_2) -plane when the remote vehicle travels at constant speed while the ego vehicle is accelerating. According to the decision making rule (2.24), the decision in the green region below the blue boundary is merge ahead while the decision in the green region above the blue boundary is merge behind.	17
2.5	Communication range as a function of (a) $a_{\max,2}$, (b) $a_{\min,2}$ and (c) $v_{\max,2}$, where the parameters of the remote vehicle are given in Table 2.1.	19
2.6	(a)-(c) Conflict charts in the (v_2, r_2) -plane given the intent of the remote vehicle: $v_1 \in [25, 30]$ [m/s] and $u_1 \in [-2, 1]$ [m/s ²]. (a) Conflict charts for merge ahead. (b) Conflict charts for merge behind. (c) Unified conflict charts combining (a) and (b). (d)-(f) Conflict charts in the (r_1, r_2) -plane given the same intent of the remote vehicle.	22
2.7	Change of decision charts under the same intent as in Fig. 2.6 when the communication range requirement in Theorem 1 is satisfied (a) and when it is not satisfied (b). Conflict cannot be prevented without intent for the points marked A, B, and C. With intent the decisions become: A - merge behind; C - merge ahead; B - conflict is not preventable.	23
2.8	Block diagram of the decision making and control logic of the CAV under the communication requirement in Theorem 1.	24
2.9	Velocity profiles when applying controller $u_2^{\mathcal{P}_g}$ when the speed limit $v_{\max,2}$ is not reached (a) and when it is reached (b).	24

2.10	Velocity profiles for the controller $u_2^{Q_g}$. The different panels correspond to the cases in Fig. 2.8. Here, t_{q1} is the time when the remote vehicle clears the conflict zone under $u_1(t) \equiv a_{\min,1}$ (or $u_1(t) \equiv \underline{a}_1$ when intent is available).	25
2.11	Experimental setup. (a) Layout of the test track with merge zone (yellow rectangle), conflict zone (red rectangle), and start positions of the ego vehicle (magenta dots). (b-f) Snapshots from an experiment with panels (d) and (e) highlighting the conflict.	27
2.12	(a) Experimental data (initial conditions of both vehicles) superimposed on the conflict chart. Green circles mark non-conflicting merges ahead, blue circles denote non-conflicting merges behind and magenta crosses correspond to conflicts. (b)-(d) Position, speed and acceleration profiles of both vehicles corresponding to the initial conditions of points A and B. The red shaded region in panel (b) highlights the time interval where both vehicles are inside the conflict zone in case B.	28
2.13	Simulation results with the initial condition of point B in Fig. 2.12(a). Position, speed, and acceleration profiles of the vehicles are plotted in panels (a), (b), and (c), respectively for the experimental run and when the CAV uses the controller (2.36,2.38,2.39,2.40) with different status update rates as indicated. The red shaded region in panel (a) highlights the time interval where both vehicles are inside the conflict zone in case B.	29
2.14	Simulation results when a CAV utilizes traffic data received from the remote vehicle and applies the controller (2.36,2.37,2.38,2.39,2.40) with different status update rates and intent as indicated. Position, speed, and acceleration profiles of the vehicles are plotted in panels (a), (b), and (c), respectively. Observe that with intent information the CAV's decision changes from merge behind to merge ahead.	30
2.15	(a) Change of decision chart corresponding to the initial condition of the remote vehicle in Fig. 2.14. (b) Time needed for the CAV to execute the maneuver when choosing the initial condition along the dashed vertical line.	31
3.1	Conflict charts in the (r_1, r_2) -plane for $v_1 = 28$ [m/s] and $v_2 = 25$ [m/s]. (a)-(c) Conflict charts for merge ahead, merge behind, and the unified conflict chart. The opportunity region in panel (c) is highlighted by stripes. Here, we used $a_{\max,2} = 2$ [m/s] and $a_{\min,2} = -4$ [m/s ²], while other parameters are the same as in Table 2.1.	33
3.2	Block diagram of the opportunistic strategy.	35
3.3	Optimal solution $u_2^*(t)$ for the time interval $t \in [t_k, t_{k+1})$ (between receiving two adjacent status sharing packets) when $t_k^* \geq t_{k+1}$ (a) and when $t_k^* < t_{k+1}$ (b). Here t_k^* predicts the time when the state will reach the black boundary of set Q_g	36
3.4	Simulation results of conservative and opportunistic strategies with initial state $r_1(0) = 201.57$ [m], $v_1(0) = 22.63$ [m/s], $r_2(0) = 210$ [m], and $v_2(0) = 25$ [m/s] when status sharing packets are received every 0.1 [s]. (a) initial state in conflict chart (magenta cross). (b)-(c) trajectories under conservative and opportunistic strategies (magenta crosses); (d)-(f): position, speed and acceleration profiles.	38

3.5	Sequences of trajectories with and without regular status update. (a)-(e) ego vehicle changes decision to merge ahead based on status update at 1.4 [s] and keeps using $u_2(t) \equiv a_{\max,2}$ to merge ahead. (a)-(b), (f)-(i) opportunity to merge ahead is missed without status update. Here, the state evolves out of \mathcal{P}_g at 4.3 [s] since the input $u_2(t) \equiv a_{\min,2}$ is used after 3.1 [s] to keep the state inside \mathcal{Q}_g and the ego vehicle eventually merges behind.	39
4.1	Potential conflict scenario in a cooperative maneuver between three vehicles. (a)-(b) Ego vehicle 0's view from its front and rear cameras when performing a lane change between the remote vehicles 1 and 2. (c) Model showing the general scenario. Here, the front and rear conflict zones are highlighted by rectangles with red shadings. . . .	42
4.2	Time delays in the ego vehicle's dynamics and in the V2X communication between ego and remote vehicles.	43
4.3	Conflict charts in (h_{10}, h_{02}) -plane under delay σ in the ego vehicle's dynamics and communication delay $\tau_1 = \tau_2 = \tau$. (a) For initial velocities $(v_0(0), v_1(0), v_2(0)) = (27, 29, 28)$ [m/s] without delays. (b) For the same velocities as (a) with delay σ and control input history $u_0(t) = 0$ [m/s ²], $t \in [-\sigma, 0]$. (c) For velocities $(v_0(0), v_1^{\text{est}}(0), v_2^{\text{est}}(0)) = (27, 26.7, 28.85)$ [m/s] with communication delay τ , where $v_1^{\text{est}}(0), v_2^{\text{est}}(0)$ are estimated based on Theorem 4. (d) For the same velocities as (c) with both delays σ and τ	48
4.4	Opportunity set Γ for the indicated values of time delays with: (a)-(d) initial states corresponding to point A $(h_{10}(0), h_{02}(0)) = (63, 4)$ [m] and point B $(h_{10}(0), h_{02}(0)) = (3, 52)$ [m] in Fig. 4.3(a)-(b); (e)-(h) estimated initial states under communication delays corresponding to point \tilde{A} $(h_{10}^{\text{est}}(0), h_{02}^{\text{est}}(0)) = (62.43, 3.79)$ [m] and point \tilde{B} $(h_{10}^{\text{est}}(0), h_{02}^{\text{est}}(0)) = (2.43, 51.79)$ [m] in Fig. 4.3(c)-(d). Here, the input history $u_0(t) = 0$ [m/s ²], $t \in [-\sigma, 0]$ is used for delay $\sigma > 0$	49
4.5	(a) Heat map showing the decrease of opportunity window $\Delta T_\Gamma = \hat{T}_\Gamma - T_\Gamma $ when delay in the ego vehicle's dynamics increases from $\sigma = 0$ [s] to $\sigma = 0.5$ [s]. (b) Opportunity window length evaluated as a function of delay σ for initial state cases represented by points A-D in Fig. 4.3(a)-(b), where $(v_0(0), v_1(0), v_2(0)) = (27, 29, 28)$ [m/s], and A $(h_{10}(0), h_{02}(0)) = (63, 4)$ [m], B $(h_{10}(0), h_{02}(0)) = (3, 52)$ [m], C $(h_{10}(0), h_{02}(0)) = (52, 2)$ [m], and D $(h_{10}(0), h_{02}(0)) = (-0.5, 43)$ [m].	53
4.6	Conceptual illustration of estimating current system state at the initial time $t = 0$ under communication delays τ_1 and τ_2 . The dashed curves represent the remote vehicles' true behaviors during the time intervals $[-\tau_1, 0]$ and $[-\tau_2, 0]$, while the solid curves represent the worst case estimation according to Theorem 4.	54
4.7	The length of the opportunity window evaluated as a function of communication delay τ for initial state cases A-D and different delays σ in the dynamics of ego vehicle. . . .	57
4.8	(a) Length of the opportunity window while varying the delay σ in the dynamics and communication delay τ with and without the intent information from remote vehicles for initial state case A. (b) Contours of opportunity window of the lower 3D surface (no-intent case).	57

4.9	Conflict analysis with intent $v_1(t), v_2(t) \in [27, 30]$ [m/s], $u_1(t), u_2(t) \in [-1, 1]$ [m/s ²], and $\Delta t_1 = \Delta t_2 = 5$ [s]. (a)-(c) Conflict chart and opportunity set without time delays for the same initial velocities as in Fig. 4.3(a). (d)-(f) Conflict chart and opportunity set with delay in dynamics $\sigma = 0.5$ [s] and communication delay $\tau = 0.5$ [s]. The gray regions indicate the corresponding opportunity sets in Fig. 4.4(a)-(b) and (g)-(h) without intent.	59
4.10	(a) Chart showing the decision change under the same intent information, time delays, and estimated initial velocities as in Fig. 4.9(d)-(f). (b) Heat map of opportunity window expansion $\Delta T_\Gamma = \bar{T}_\Gamma - T_\Gamma $	61
4.11	(a) Length of the opportunity window as a function of intent horizon for initial state cases A-D and time delays indicated. (b) Mechanism behind the saturation of the opportunity window.	62
4.12	Evolution of opportunity set $\bar{\Gamma}$, goal point, and trajectory $h_{02}^{\text{est}}(t)$ under delay $\sigma = 0.5$ [s] in the ego vehicle's dynamics, and communication delay $\tau = 0.1$ [s], with intent information $v_1 \in [34.9, 36.7]$ [m/s], $v_2 \in [36.5, 37.2]$ [m/s], $u_1 \in [-0.6, 0.4]$ [m/s ²], $u_2 \in [-1.5, 0.5]$ [m/s ²], $\Delta t_1 = \Delta t_2 = 10$ [s]. The goal-oriented controller $u_0(t) = u_0^G$ is used with status and intent updates every 0.1 [s]. (a)-(d) Case (i) where the ego vehicle is initially traveling behind the remote vehicles. (e)-(h) Case (ii) where the ego vehicle is initially traveling in front of the remote vehicles.	64
4.13	Simulation results under the same time delays, initial states, and intent as in Fig. 4.12. (a)-(c) Results for case (i). (d)-(f) Results for case (ii). The dashed magenta curves in (b) and (e) correspond to status and intent updates every 1 [s].	65
5.1	(a) A merge scenario involving an ego vehicle 0, and two remote vehicles 1 and 2. The ego vehicle must form necessary front and rear gaps inside the merge zone to enable a conflict-free merge. (b) Generalized model of the merge scenario.	69
5.2	Extending multi-vehicle conflict analysis to the merge scenario. (a)-(b) Checking $x(0) \in \mathcal{M}_g$ according to Theorem 5 with initial condition $(h_{10}(0), h_{02}(0), r_0(0)) = (-17.3, 52.3, 46)$ [m] and $(v_0(0), v_1(0), v_2(0)) = (25, 24.22, 24.09)$ [m/s], where (a) constructs the lane change opportunity set Γ , and (b) constructs the corresponding merge opportunity set Θ ; (c)-(d) Checking $x(0) \in \mathcal{M}_r$ according to Theorem 6 with initial condition $(h_{10}(0), h_{02}(0), r_0(0)) = (76.7, -35.7, 30)$ [m] and $(v_0(0), v_1(0), v_2(0)) = (25, 24.25, 23.99)$ [m/s], where (c) and (d) visualize the constructions of the sets Γ and Θ , respectively. Here, the merge zone is located at [100, 200] [m] and time delay $\sigma = 0.5$ [s] is used in the ego vehicle's dynamics. Intent of remote vehicles are assumed to be $v_1(t) \in [24.22, 25.04]$ [m/s], $u_1(t) \in [-0.2, 0.3]$ [m/s ²], $v_2(t) \in [23.70, 25.36]$ [m/s], and $u_2(t) \in [-0.3, 0.7]$ [m/s ²], with intent horizons $\Delta t_1 = \Delta t_2 = 10$ [s].	74

5.3	Conflict charts in the plane of front and rear gaps corresponding to different remote vehicle pairs in Fig. 5.4, under delay $\sigma = 0.5$ [s] in the ego vehicle's dynamics and delay $\tau = 0.1$ [s] in the remote vehicles' V2X information, for velocities (a) $(v_0(0), v_1(-0.1), v_2(-0.1)) = (25, 24.58, 24.22)$ [m/s]; (b) $(v_0(0), v_2(-0.1), v_3(-0.1)) = (25, 24.22, 24.02)$ [m/s]; (c) $(v_0(0), v_3(-0.1), v_4(-0.1)) = (25, 24.02, 25.50)$ [m/s]; and (d) $(v_0(0), v_4(-0.1), v_5(-0.1)) = (25, 25.50, 26.28)$ [m/s]. Here, the ego vehicle's initial position is given as $r_0(0) = 0$ [m] and the merge zone is located at [100,200] [m]. The estimated initial state encoded in $x_{\text{est}}(0)$ for each panel is summarized in Table 5.2.	77
5.4	An extended merge scenario where the ego vehicle 0 attempts to merge onto the main road as a chain of remote vehicles are approaching. (a) Pairwise conflict analysis when five remote vehicles are inside the ego vehicle's communication range. (b) Remote vehicles' behaviors represented by real highway driving data.	79
5.5	Evolution of merge opportunity set Θ , goal point $(t^G, r_0^G) \in \Theta$, and positions r_0, r_2 , and r_3 , corresponding to the merge scenario in Fig. 5.4. Here, the ego vehicle 0 pursues merge opportunity between remote vehicles 2 and 3 using goal-oriented controller $u_0(t) = u_0^G$ with status and intent updates every 0.1 [s].	82
5.6	Simulation results of the ego vehicle 0 pursuing merge opportunity between remote vehicles 2 and 3, corresponding to Fig. 5.5.	82
6.1	Modeling vehicle intent from dynamical systems viewpoint. (a) Diagram showing the input/output representation of a vehicle's motion. (b) Conceptual illustration of a vehicle's longitudinal motion intent.	85
6.2	Schematic diagram of on-board conflict analysis that provides real-time decision assistance to the ego vehicle based on the remote vehicles' status and intent messages.	88
6.3	Visualizing packet receiving timing of V2X messages. (a) When intent packet has sufficient horizon. (b) When intent packet has short horizon while being sent with a low rate or when packet drops occur.	91
6.4	Validating intent sharing cooperation in a merge scenario using real vehicles at Mcity test track. (a) Experiments where intent-based conflict analysis provides on-board decision assistance to an ego vehicle attempting to merge. The rear mirror views of the ego vehicle are shown in the left column. (b) A generalized model of the merge scenario.	93
6.5	Implementing intent messages using the V2X protocol WSMP. (a) Commercially available V2X Onboard Unit (OBU). (b)-(c) Examples of intent messages transmitted in the experiments.	97
6.6	Benefits evaluation of intent sharing in Mcity experiments where the ego vehicle performed on-board conflict analysis while maintaining standstill. (a)-(b) Ego vehicle's behavior preference. (c)-(d) Remote vehicle's maneuvers while using cruise control and when the human driver decreases the speed. Examples of intent bounds are highlighted as blue shadings. (e)-(f) Evolution of estimated times T_0^H and T_1 under the aforementioned two different behaviors of the remote vehicle. The warning issuance times T_w highlight the benefits of intent sharing in mitigating false positive decisions.	100

6.7	Two examples of Mcity experiments where the remote vehicle approaches with cruise control and the ego vehicle driver merges after the issuance of warning. (a)-(c) A scenario where the warning disappears automatically during the maneuver based on the ego vehicle's actual behavior and the updated V2X messages. No conflict happens after all as illustrated in panel (b). (d)-(f) A scenario where the warning persists after being issued. Here an actual conflict happens as shown in panel (e).	102
6.8	Experimental results validating the on-board decision assistance enabled by intent-based conflict analysis. Each data point marks an experiment, showing the merge starting time of the ego vehicle and the corresponding position of the remote vehicle. Colors indicate different merge results. (a) Remote vehicle uses cruise control. (b) Remote vehicle is human-driven.	104
6.9	Testing packet delivery ratio of intent messages (a) on a rural section of highway US-23, and (b) on an urban section of highway I-275. (c) The corresponding packet delivery ratios as a function of distance between intent sender and receiver.	105
6.10	Data-based simulation of a merge scenario at the on-ramp of highway M-14 near Barton Drive, Ann Arbor, Michigan. (a)-(b) Simulation setup where the ego vehicle merges from a stop sign. (c)-(d) The ego vehicle's behavior preference and remote vehicle's speed profile (extracted from a real human driver data). (e) Conflict analysis showing the estimated times T_0^H and T_1 . The warning issuance times are highlighted for different intent sending conditions.	108
6.11	Evaluating the effects of communication conditions (intent horizon, sending rate, and packet delivery ratio) on the benefits of intent sharing via simulations. The warning issuance time is plotted as a function of packet delivery ratio with the indicated intent horizons and sending rates. The dots mark mean values while the error bars show the standard deviations.	109

LIST OF TABLES

TABLE

2.1	Parameters values used in the Chapter 2.	11
2.2	Maneuver execution time of the CAV in Fig. 2.14.	30
3.1	Simulation results with ego vehicle's initial state $r_2(0) = 210$ [m] and $v_2(0) = 25$ [m/s].	40
4.1	Parameters values used in the Chapter 4.	45
4.2	Maneuver results under different V2X conditions.	63
5.1	Parameters values used in the Chapter 5.	69
5.2	Estimated initial state encoded in $x_{\text{est}}(0)$ for each panel of Fig. 5.3.	78
6.1	Parameters values used in the experiments at Mcity.	94

LIST OF APPENDICES

A Decoupling a conflict-free merge maneuver	114
B Conflict Chart Boundaries	116
C Proof of Theorem 1	118
D Proof of Theorem 2	119
E Prove the optimality of opportunistic control law	120
F Proof of Lemma 1	121
G Analytical forms of the boundaries that construct the opportunity set	122
H Proof of Theorem 3	124
I Proof of Theorem 4	125
J Analytical form of goal-oriented controller	126
K Proof of Lemma 2	127
L Proof of Lemma 3	128
M Proof of Theorem 5	129
N Proof of Theorem 6	130
O Proof of the relationship in equation 5.19	131
P Proof of Theorem 7	132
Q Proof of Theorem 8	133

ABSTRACT

Conflicts between traffic participants may arise when their spatio-temporal trajectories come sufficiently close. Without timely detection and appropriate management, these conflicts may lead to safety hazards and compromise the traffic efficiency. Emerging technologies in vehicular automation and vehicle-to-everything (V2X) communication opened up new opportunities to resolve conflicts between vehicles in a cooperative manner. On the other hand, a mixed-autonomy environment consisting of vehicles with different automation and cooperation capabilities is expected to bring additional challenges to conflict resolution over the next few decades.

In this dissertation we construct a framework of conflict analysis to detect, manage, and resolve conflicts arising in cooperative maneuvers between vehicles at different levels of automation and cooperation. In particular, two different classes of cooperation, enabled by V2X communication, are considered as means to prevent conflicts: status sharing and intent sharing. Status sharing allows vehicles to exchange their instantaneous states with each other (e.g., current velocity and position), whereas intent sharing enables further information exchange regarding the intended future motion of vehicles (e.g., velocity and acceleration bounds). In conflict analysis, we interpret the dynamical information encoded in the wireless status and intent messages by means of conflict charts, where the state space is partitioned into the so called no-conflict, uncertain, and conflict domains. This allows for efficient decision making and controller design.

We first establish the concept of conflict analysis to prevent conflicts between two vehicles. Conflict-free maneuvering strategies are developed and communication requirements for the existence of such strategies are determined. We then extend the established conflict analysis framework to study conflicts between multiple vehicles, while considering two types of time delays, one in vehicle dynamics and the other in V2X communication. Using reachability theory, conflict anal-

ysis allows us to examine the merits of communication in conflict prevention in the presence of delays. The effects of time delays on conflicts in a mixed-autonomy environment are systematically quantified. It is revealed that receiving status information can facilitate conflict-free maneuvers, but time delays can compromise such opportunities. It is also shown that receiving intent information compensates the effects of delays, removes unnecessary conservatism from decision making, and improves the efficiency of controllers of connected vehicles. We design a goal-oriented controller for connected automated vehicles to pursue conflict-free maneuvers, and demonstrate the framework using simulations with real highway data.

Our theoretical analysis is brought to practice by generalizing the representation of vehicles' motion intent from a dynamical systems viewpoint. This enables us to extend conflict analysis by incorporating intent information. Such an extension is used to assist the decision-making of intent-receiving vehicles, and can be tailored to both automated and human-driven cases. We create intent messages using commercially available V2X devices, and experimentally demonstrate the benefits of sharing intent in cooperative maneuvering. Experiments are performed at a test track where intent-based on-board decision assistance is provided to human drivers in merge scenarios. Furthermore, we test intent messages on public highways and evaluate the performance in terms of packet delivery ratio. The collected data are fed into numerical simulations to investigate the effects of intent transmission conditions (e.g., sending frequency, intent horizon, and packet drops) on conflict resolution.

In summary, this dissertation presents state-of-the-art results on V2X-based conflict management in cooperative maneuvering under mixed autonomy. The novel framework of conflict analysis provides a rigorous yet scalable means to enhance traffic safety and efficiency. This dissertation is among the very first efforts to systematically study the communication impact on conflicts in mixed traffic. In particular, our theoretical study and experimental evaluation on intent sharing cooperation are expected to benefit the on-going standardization and future real-world deployment.

CHAPTER 1

Introduction

1.1 Motivation: Conflict Resolution in Mixed Traffic

Conflicts between different traffic participants may arise when their spatio-temporal trajectories come adequately close [1]. Such conflicts often occur while multiple road users attempt to access the same road resource at the same time, for example, at intersections, roundabouts, lane changes, and highway merges. Without timely detection and appropriate management, these conflicts may lead to evasive maneuvers and safety hazards of individual vehicles, compromising the overall traffic flow efficiency [2, 3]. Human drivers use many cues from other road users to prevent conflicts, and yet, traffic accidents often happen due to human’s limited perception capability and incorrect evaluation of the situation, especially in uncertain driving environments [4, 5].

Over the past few decades, emerging technologies in vehicular automation [6, 7, 8], onboard sensing [9, 10], and wireless communication [11, 12, 13] have led to an increasing expectation for automated vehicles to possess better-than-human capabilities in conflict management. These technological advances opened up new opportunities for enhancing traffic safety and efficiency by allowing conflict resolution between vehicles in a cooperative manner [14, 15, 16, 17]. Vehicle-to-everything (V2X) communication is one of the most promising technologies, which allows vehicles to communicate beyond-line-of-sight information with other road participants [18, 19, 20]. Standardized protocols for V2X communication include dedicated short range communication (DSRC) [21, 22, 23, 24] and Cellular V2X (C-V2X) [25, 26, 27, 28].

Earlier results show that V2X communication may be utilized by automated vehicles to improve their performance according to multiple metrics while performing different maneuvers [29]. For example, vehicles with high levels of automation may cooperatively agree about what maneuvers to take using maneuver coordination messages [15, 30, 31, 32]. Focusing on higher-level decision-making, many different scheduling strategies are proposed to manage conflicts between multiple vehicles, using techniques such as graph-based modeling [33], formal verification [34], and assume-guarantee contracts [35]. A sizable literature of strategies also exist where even the control actions

of automated vehicles are carried out cooperatively. Such strategies include virtual platooning [36], optimal control [37, 38, 39, 40, 41], model predictive control [42, 43], and reachability analysis [44, 45, 46, 47]. Applications are not restricted to automated ground vehicles but may also be found on unmanned aerial and maritime vehicles [48, 49, 50]. The success of these strategies, however, relies on a strong assumption that all traffic participants possess high levels of automation.

Six different levels of automation have been defined by the Society of Automotive Engineers (SAE) [51]: level 0 – no driving automation; level 1 – driver assistance; level 2 – partial driving automation; level 3 – conditional driving automation; level 4 – high driving automation; and level 5 – full driving automation. In the near future, having a fully automated environment (with level 3-5 vehicles) is still very unlikely. It is becoming clear that the forthcoming decades will witness an autonomy evolution dominated by the so-called mixed traffic consisting of human-driven vehicles and vehicles of different automation levels [52, 53]. Managing conflicts in mixed-autonomy systems has generated growing interests in multiple research communities.

For example, in [54], a framework for robot-human collision avoidance was proposed, where the prediction of human behavior was achieved by a statistical model without considering the interaction, and robot trajectories were generated by sequential planning and tracked by robust reachability-based controllers. In [55], game theory was used to model human decision making, and reinforcement learning was used for intelligent agents to generate the optimal action sequence. To provide provable safety guarantees, in [56], safe maneuver of the ego vehicle was realized by computing a library of the so-called robust controlled invariant sets offline, while other vehicles' driving intentions were estimated online by solving a linear programming problem. Alternatively, safety-critical control may be realized by control barrier functions (CBFs) while incorporating environmental uncertainties and input delays [57]. From the perspective of formal methods, [58] reviewed recent works on correct-by-construction design for automated vehicles, where representative techniques include finite state abstraction [59], temporal logic-based verification [60], and control synthesis using automata [61] and/or optimization [62]. In [63], a reachable set-based trajectory prediction of road participants is proposed for provably safe motion planning, where the ego vehicle relies on on-board sensors without V2X communication, and the uncertainties of the future evolution of the environment are considered. Other methods include a variety of optimization techniques including optimal control [64, 65], dynamic programming [66], model predictive control [67, 68], and reinforcement learning [69, 70]. These approaches were used for decision making and action planning for automated vehicles when interacting with human-driven vehicles, in scenarios such as lane changes, roundabouts, and merges.

Despite the active research on conflict management in mixed traffic, several important questions still remain open. One of the challenging problems is the limited scalability due to the “curse of dimensionality”. This issue can arise in dynamic optimization [71], formal verification [72],

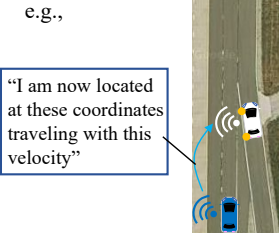
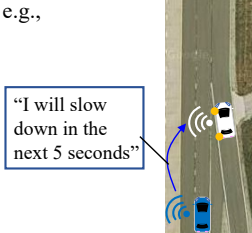
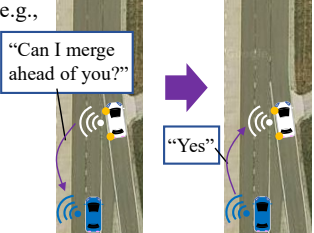
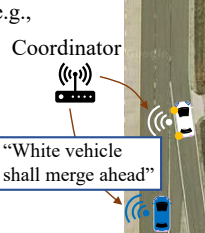
Status-Sharing: “Here I am/what I see”	Intent-Sharing: “Here is what I plan to do”	Negotiation (agreement-seeking): “Can we do this together?”	Prescriptive: “I will do as directed”
e.g., 	e.g., 	e.g., 	e.g., 
Standardized: Basic safety message Cooperative awareness message	New classes under standardization: e.g., SAE J3186 draft, ETSI TR 103 578		

Figure 1.1: Different levels of cooperation enabled by V2X communication, defined in SAE J3216 standard.

and reachability analysis [73], causing heavy computational load in existing conflict resolution algorithms and hindering their real-time implementations. Also, facing an uncertain environment, guaranteeing maneuver safety while maximizing efficiency in complex traffic scenarios is difficult. Moreover, the benefits of V2X communication on conflict resolution in mixed-autonomy environments are yet to be well investigated. A corresponding framework to systematically study conflicts under different levels of cooperation is missing. Meanwhile, effects of important V2X communication factors, such as information type, transmission rate, communication range, time delays, and packet drops, remain unclear in the context of conflict resolution.

In this dissertation, we develop new approaches and provide insights to these open research problems. A scalable and efficiently implementable framework of conflict analysis is developed for vehicles of various levels of automation to resolve conflicts under different cooperation classes. We utilize V2X communication as the enabling technology for conflict resolution in cooperative maneuvering. In the next section, we review the state-of-the-art of V2X-enabled cooperation and identify opportunities for cooperative conflict resolution in mixed traffic.

1.2 Cooperation using V2X Communication

The cooperation enabled by V2X communication is attracting considerable attentions from the automotive industry and standardization agencies [18, 74, 75]. The SAE standard J3216 categorizes four classes of cooperation between vehicles under V2X communication [18]: status sharing, intent sharing, negotiation, and prescriptive cooperation. Fig. 1.1 provides illustrative examples for different classes of cooperation. In status sharing, connected vehicles share instantaneous status information such as position and velocity, whereas in intent sharing, the information regarding

Automation level Cooperation level	Human-driven vehicles: SAE level 0 – No driving automation	Partially automated vehicles: SAE level 1 – Driver assistance SAE level 2 – Partial driving automation	Highly automated vehicles: SAE level 3 – Conditional driving automation SAE level 4 – High driving automation SAE level 5 – Full driving automation
Status sharing			
Intent sharing			
Negotiation			
Prescriptive			

Figure 1.2: Levels of automation and cooperation targeted in this dissertation (green shading).

future motion plans is exchanged (e.g., velocity and acceleration bounds over a time horizon). Negotiation further allows vehicles to seek agreements about their future maneuvers by actively requesting road space and responding to such requests. Finally, prescriptive cooperation relies on a traffic coordinator prescribing maneuvers for all road users in a centralized manner. In contrast, the cooperation under status sharing, intent sharing, and negotiation is decentralized, offering vehicles the advantage to decide on their own actions based on the shared information.

Fig. 1.2 summarizes V2X-enabled cooperation between road participants possessing different automation levels. As highlighted by the yellow shaded part, negotiation and prescriptive cooperation may only happen between highly automated vehicles. These classes of cooperation so far attracted most prior research efforts [15, 30, 31, 32, 76, 77, 78]. In a mixed-autonomy traffic environment, however, negotiating future trajectories may oftentimes be infeasible, while requiring all traffic participants to follow the prescribed actions may be impractical. Thus, the cooperation between vehicles shall stay within the two lower classes: status sharing and intent sharing. This dissertation focuses on these two classes of cooperation and studies the green shaded part in Fig. 1.2, where vehicles of different automation degrees cooperate to prevent conflicts.

Sharing status is well-standardized. Examples include basic safety messages (BSMs) [21] and cooperative awareness messages (CAMs) [79]. Status information allows a vehicle to gain instantaneous situational awareness, but it can also lead to inefficient decisions and abrupt maneuvers due to the absence of foresight into future uncertainties. The decision-making and control of an ego vehicle are illustrated in Fig. 1.3. Based on the available status information, the ego vehicle shall

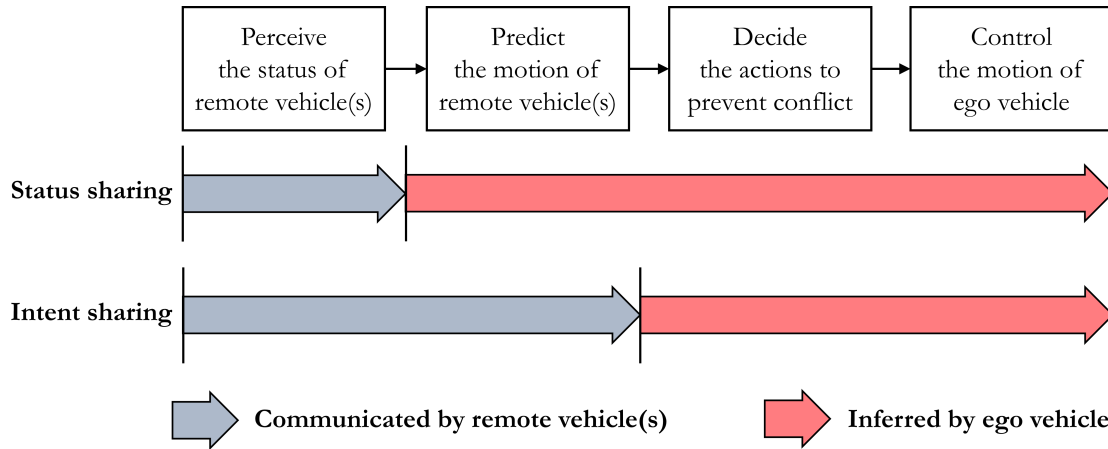


Figure 1.3: Conflict prevention performed by an ego vehicle under status sharing and intent sharing.

first predict the motion of remote vehicles and use these predictions when deciding what action to take so that no conflicts arise. Then the ego vehicle shall execute the chosen action through a control strategy. When the vehicle receives information only about the current status of other vehicles, the decisions that ensure conflict-free maneuvers are expected to be conservative, while the performance can be improved when intent information is also received from the surrounding vehicles. Consequently, intent sharing is an emerging form of cooperation, which is attracting increasing research attentions. Intent information can benefit a vehicle’s decision making and control design by providing a more accurate prediction for the evolution of future environments.

In the literature of intent-enhanced maneuver coordination, many works focus on scenarios where driving intent of other vehicles is estimated from the available status information, while the exact intent is not shared directly via communication. Estimation techniques include optimization [56], statistical inference [80], and learning based strategies [81]. However, such estimation can be inaccurate and may not always be completed in a timely manner due to large computational load. Instead of estimating intent, we focus on V2X communication-based intent sharing, which enables more detailed and precise interpretation of vehicle intent.

Standardization of intent sharing is currently in progress. For example, SAE is establishing maneuver sharing and coordination service [82], while the European Telecommunications Standards Institute (ETSI) is standardizing maneuver coordination service [74, 75]. These standards are still under development, and intent messages have not been created and field-tested so far. On the other hand, a noticeable amount of theoretical research has been triggered by the ongoing standardization. For instance, [30] and [83] studied maneuver coordination messages which contained the planned and desired trajectories (as polynomials of time) for automated vehicles. From a communication perspective, [84] studied generation rules of such messages, while [85] evaluated the impact of maneuver coordination in large-scale traffic via simulations. Also, a framework was proposed in

[86] where vehicles' intended trajectories are communicated using B-spline representation in a fully automated car-following scenario.

These prior studies on intent sharing were limited to theory, and a clear gap exists on evaluating the benefits of intent in the real world. To the best of our knowledge, no previous work has evaluated experimentally the benefits of intent sharing in conflict resolution, and the corresponding communication requirements for intent messages have been unclear. This dissertation provides a first effort to fill these gaps. Using status sharing as a baseline, the benefits of intent sharing are systematically studied through conflict analysis and experimentally evaluated using real vehicles.

1.3 Contributions and Outline

In this dissertation, we first establish the concept of conflict analysis for two vehicles of different levels of automation, and demonstrate its applicability to aid a fast and reliable decision making and control design. In particular, we assume that the participating vehicles are equipped with V2X communication, and study cooperative maneuvers under status sharing and intent sharing. In conflict analysis, we construct *conflict charts* to interpret the dynamical information encoded in the status and intent messages, where the state space is partitioned into the so-called no-conflict, uncertain, and conflict domains. Conflict-free maneuvering strategies are developed and communication requirements for such strategies are determined. To demonstrate the developed framework, we investigate a scenario with an ego connected automated vehicle (CAV) merging to a main road while a connected human-driven vehicle (CHV) is approaching on that road. The results are demonstrated both by experimental data using real vehicles on a test track and by simulations utilizing real highway data. The benefits of status and intent sharing in conflict resolution are systematically quantified. Moreover, based on conflict analysis, we propose a novel opportunistic strategy to improve the ego vehicle's decision and control, aiming to maximize its maneuver time efficiency.

We then scale up conflict analysis framework to multiple vehicles of different levels of automation, while utilizing reachability techniques. Two different types of time delays are considered, one in vehicle dynamics and the other in V2X communication. We systematically quantify the effects of time delays on conflicts in a mixed-autonomy environment. It is revealed that conflict-free maneuvers between multiple vehicles can be facilitated by receiving status information, but time delays can compromise such opportunities. It is also shown that receiving intent information compensates the effects of delays, removes the conservatism from decision making, and improves the efficiency of controllers for CAVs. We design a goal-oriented controller for a CAV to guarantee conflict-free maneuvers. This type of controller provides the designers with the freedom in choosing appropriate "goal state" to realize desired performances according to different design metrics (e.g., time and en-

ergy efficiencies, robustness). The benefits of different types of V2X information are demonstrated via simulations based on real highway data. We show that receiving the remote vehicles' status and intent information more frequently improves the passenger comfort and time efficiency of the CAV. The scalability and implementability of conflict analysis framework are demonstrated first in lane change scenarios and then in the more challenging multi-vehicle merge scenarios, where stricter maneuver constraints apply.

Furthermore, we propose a generalized representation of vehicles' motion intent from a dynamical systems viewpoint. Based on this, we extend the framework of conflict analysis and use the intent information to assist a personalized decision-making of an intent-receiving vehicle (which can be either automated or human-driven). We create intent messages using commercially available V2X radios using the communication protocol WSMP [87, 88], and demonstrate experimentally the benefits of sharing intent in cooperative maneuvering. This is validated via experiments at a test track where intent-based decision assistance is provided on-board to human drivers in merge scenarios. The experimental results reveal significant benefits of intent sharing in enhancing vehicle safety and time efficiency. We further test intent messages on public roads and evaluate the performance in terms of packet delivery ratio, i.e., the percentage of intent packets received out of those have been sent. Real highway data is collected and fed into numerical simulations to investigate the effects of intent transmission conditions (e.g., sending rate, intent horizon, and packet drops) on the benefits of intent sharing in conflict resolution.

This dissertation is developed based on our prior results reported in [89, 90, 91, 92, 93, 94, 95, 96, 97, 98, 99]. The remainder of this dissertation is organized as follows. In Chapter 2, we take an analytical approach to establish the framework of conflict analysis for two vehicles of different automation levels under status and intent sharing, and discuss the decision making and controller design. Benefits under different types of cooperation are quantified. Using such framework, we develop an optimization-based opportunistic strategy in Chapter 3 to further improve the efficiency in decision and control. In Chapter 4, we extend the conflict analysis framework to multiple vehicles by developing numerical tools, while incorporating time delays in vehicle dynamics and V2X communication. This extension is examined in lane change scenarios. Effects of time delays in conflict management are systematically studied. We further investigate the scalability of conflict analysis in Chapter 5 under additional maneuver safety constraints using multi-vehicle merge scenarios. In Chapter 6, we generalize the representation of vehicle motion intent and experimentally validate intent sharing in conflict resolution using real vehicles. Finally, we conclude the dissertation and lay out future research directions in Chapter 7.

CHAPTER 2

Establishing the Conflict Analysis Framework

In this chapter, we establish the framework of conflict analysis. We define conflict as an event when the trajectories of traffic participants come sufficiently close so that they may appear at the same location at the same time. Since vehicles have finite dimensions, we define a conflict zone of a finite size. For simplicity, in this chapter we focus on cooperative maneuvers where the conflict zone is fixed to the ground as depicted in Fig. 2.1(a)-(c). Note that this setup will be generalized in the subsequent chapters to accommodate moving conflict zones as well. To prevent conflicts, no more than one vehicle shall be present in the conflict zone at the same time. We develop conflict analysis using the representative example where the ego vehicle merges to a main road while a remote vehicle is approaching on that road [100]. However, the methods we develop can be applied to a larger set of maneuvers where multiple vehicles must enter a given spatial domain. Examples include intersections, roundabouts, and lane changes [101, 37, 102] with conflict zones of different shapes and sizes. We consider conflict prevention from the perspective of the ego vehicle which, according to the traffic rules, must yield to the other vehicle approaching the conflict zone on the main road. It is assumed that both vehicles are equipped with V2X communication devices and the ego vehicle is automated, thus, referred to as a connected automated vehicle (CAV); see Fig. 2.1(d). We demonstrate how conflict analysis can be utilized by the CAV for decision making under different levels of cooperation. Namely, we consider status sharing and intent sharing scenarios which can be supported by different types of wireless messages [18].

In conflict analysis, we consider the performance limits of both vehicles and calculate the so-called no-conflict, conflict, and uncertain domains in the state space for the cases when the ego vehicle merges ahead of the remote vehicle and when it merges behind. We demonstrate that the corresponding conflict charts can be used for decision making by the ego vehicle. Based on the conflict analysis, we also derive a V2X communication range requirement. If the ego vehicle receives status sharing messages before the remote vehicle enters this range, conflict-free maneuvers can be guaranteed independent of the remote vehicle's future motion. Then, we design a longitudinal controller for the ego CAV to execute the maneuver. We demonstrate that even a single status message from the remote vehicle can enable the vehicle to prevent conflicts and that

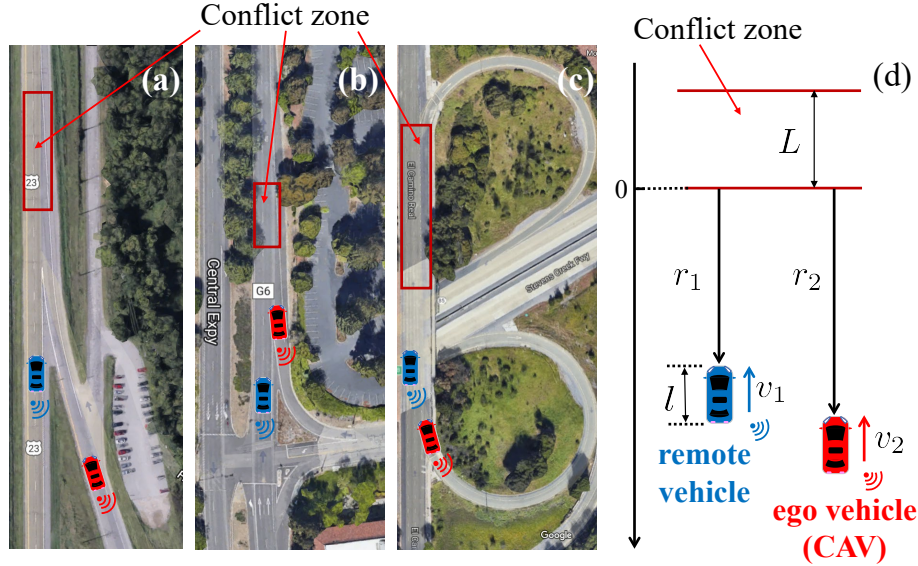


Figure 2.1: Cooperative maneuvers at (a) highway on-ramp, (b) expressway entrance, (c) highway off-ramp. (d) Model used for conflict analysis. A conflict happens if both vehicles are present (even partially) in the conflict zone, and thus, the key parameter $s = L + l$ is the sum of conflict zone length and the vehicle length.

the time efficiency can be significantly improved when receiving more status updates. We also show that by receiving intent information from the remote vehicle, a CAV can significantly enhance its capability of preventing conflicts and also improve its time efficiency. The developed conflict analysis framework is demonstrated by real vehicles via experiments performed at a test track and via simulations using highway traffic data collected at south-east Michigan.

The rest of this chapter is organized as follows. In Section 2.1 the mathematical model for vehicle dynamics is constructed. In Section 2.2 we establish the conflict analysis framework. We introduce the concept of conflict charts, derive the V2X communication range requirement, and use these results to construct a decision making rule for the ego vehicle. In Section 2.3 we investigate the scenario when the remote vehicle shares its intent with the ego vehicle via V2X communication. In Section 2.4 we design a controller that enables the ego CAV to execute non-conflicting maneuvers. In Section 2.5 experiments performed at a test track and simulations using real traffic data are presented. Finally, Section 2.6 concludes this chapter.

2.1 Modeling Vehicle Dynamics

Consider the scenarios in Fig. 2.1(a)-(c) where the conflict zones are indicated by red rectangles near the end of the ramps. The length of the conflict zone represents a safe distance between the vehicles which may vary according to the road configuration and traffic conditions. Here, to

simplify the matter, we ignore the lateral dynamics of the vehicles and consider the model shown in Fig. 2.1(d). The distances of the remote vehicle and ego vehicle from the conflict zone are denoted by r_1 and r_2 while their longitudinal velocities are v_1 and v_2 , respectively. Here, we use subscript 1 to refer to the remote vehicle and subscript 2 to refer to the ego vehicle. The length of the conflict zone is denoted by L , the length of both vehicles is l , and we define $s := L + l$ to account for the length of the vehicles in case of conflict. Note that the conflict analysis presented below can be adapted to many other conflict scenarios with conflict zones of various sizes and shapes by appropriately selecting the conflict zone parameters.

To highlight the main idea of conflict analysis, we adopt a simple model for the longitudinal dynamics of the vehicles. By neglecting the air drag and the rolling resistance we have

$$\begin{aligned} \dot{r}_1 &= -v_1, \\ \dot{v}_1 &= \text{sat}(u_1), \\ \dot{r}_2 &= -v_2, \\ \dot{v}_2 &= \text{sat}(u_2). \end{aligned} \tag{2.1}$$

Here the dot represents the derivatives with respect to time t and the negative signs appear since the vehicles are traveling towards the conflict zone. Moreover, u_1 and u_2 represent the control inputs, and the saturation function is included to take into account the acceleration limits of the ego and remote vehicles.

Assuming that the velocity is between the assigned limits $v \in (v_{\min}, v_{\max})$, we have

$$\text{sat}(u) = \begin{cases} a_{\min} & \text{if } u \in (-\infty, a_{\min}], \\ u & \text{if } u \in (a_{\min}, a_{\max}), \\ a_{\max} & \text{if } u \in [a_{\max}, \infty). \end{cases} \tag{2.2}$$

For $v = v_{\min}$, we substitute a_{\min} with 0, since the vehicle would not decelerate in this case. Similarly, when $v = v_{\max}$, we substitute a_{\max} with 0, since the vehicle would not exceed the speed limit. Indeed, the acceleration limits and the speed limits may be different for different vehicles; see Table 2.1. Notice that $v_{\min,2}$ is set to zero, that is, the ego vehicle is allowed to stop along the ramp. Since we are controlling the motion of the ego vehicle, we also assume that we are able to assign acceleration limits that correspond to emergency braking and full-throttle acceleration [52]. On the other hand, we do not have control over the remote vehicle (it may be a human-driven vehicle), and we assume that its acceleration and speed limits correspond to reasonable highway driving behavior. Note that this analysis could also be carried out for different parameter values.

Table 2.1: Parameters values used in the Chapter 2.

L	20 [m]	l	5 [m]
$a_{\min,1}$	-4 [m/s ²]	$a_{\min,2}$	-8 [m/s ²]
$a_{\max,1}$	2 [m/s ²]	$a_{\max,2}$	4 [m/s ²]
$v_{\min,1}$	20 [m/s]	$v_{\min,2}$	0 [m/s]
$v_{\max,1}$	35 [m/s]	$v_{\max,2}$	35 [m/s]

Now we define the state vector

$$x := \begin{bmatrix} r_1 & v_1 & r_2 & v_2 \end{bmatrix}^T \in \Omega, \quad (2.3)$$

where $\Omega := [-s, \infty) \times [v_{\min,1}, v_{\max,1}] \times [-s, \infty) \times [0, v_{\max,2}]$. These states can be made available for both vehicles via V2X connectivity (e.g., a status sharing message from the remote vehicle shall contain r_1 and v_1). However, when designing the decision making and control algorithms, we can only prescribe the input u_2 of the ego vehicle. The input u_1 of the remote vehicle cannot be prescribed, only its bounds (given by the saturation function) are assumed to be known. When the intent of the remote vehicle is shared via V2X communication, the ego vehicle may utilize this information to have a better prediction of the remote vehicle's motion, but one still has no control over u_1 . That is, the overall system (2.1) is not controllable, and our goal is to ensure that no conflict occurs under such assumptions.

2.2 Conflict Analysis

In this section, we provide a rigorous definition of conflict using mathematical logic and the model constructed above. Then, we calculate domains of different qualitative behaviors in the state space and display them on conflict charts.

As mentioned above, a conflict occurs if both vehicles appear in the conflict zone at the same time. This can be formalized as the proposition

$$C := \{\exists t, r_1(t) \in [-s, 0] \wedge r_2(t) \in [-s, 0]\}, \quad (2.4)$$

and a non-conflicting maneuver is given by

$$\neg C = \{\forall t, r_1(t) \notin [-s, 0] \vee r_2(t) \notin [-s, 0]\}, \quad (2.5)$$

where we use the symbols \wedge (and), \vee (or), and \neg (negation). This definition can be generalized for more than two vehicles and for different traffic scenarios such as intersections, roundabouts, and

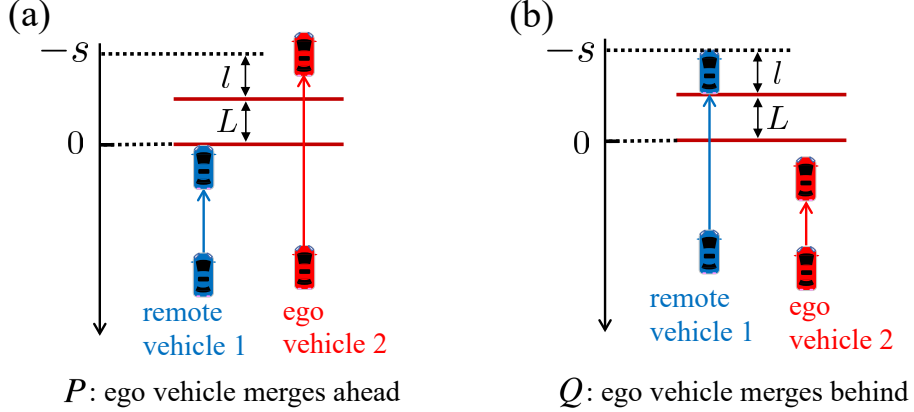


Figure 2.2: Conceptual illustrations of proposition P in panel (a) and proposition Q in panel (b).

lane changes.

We can decouple $\neg C$ into two cases where the ego vehicle merges ahead of the remote vehicle and where it merges behind:

$$\begin{aligned}
 P &:= \{\exists t, r_1(t) = 0 \wedge r_2(t) < -s\}, \\
 Q &:= \{\exists t, r_1(t) = -s \wedge r_2(t) > 0\}.
 \end{aligned}
 \tag{2.6}$$

As visualized in Fig. 2.2(a), proposition P describes that by the time the remote vehicle enters the conflict zone, the ego vehicle has already passed it. On the other hand, as shown in Fig. 2.2(b), proposition Q states that by the time the remote vehicle exits the conflict zone, the ego vehicle has yet to enter it. Furthermore, one can show that the relationship

$$P \vee Q \iff \neg C
 \tag{2.7}$$

holds (see Appendix A), leading to the definition of non-conflicting maneuver.

Definition 1. *Given the dynamics (2.1), a maneuver is non-conflicting if proposition P or proposition Q is true.* ■

Again, this definition may be extended to more than two vehicles by defining pairwise conflicts and can be generalized to a large variety of traffic scenarios. We remark that, from the perspective of the ego vehicle, deciding on whether to merge ahead or behind the approaching remote vehicle is analogous to the so-called “yellow light dilemma” [103], where a vehicle facing a yellow traffic light needs to decide on whether it can safely stop in front of or timely clear an intersection. Note that the yellow light dilemma is usually studied with only one vehicle considered and may be eliminated by properly designing the yellow light interval [104]. Our analysis in this chapter, however, involves

an additional vehicle which is out of our control, and the potential conflicts may only be resolved through proper decision-making and control design for the ego vehicle. This way, our study on conflicts may be seen as a generalization of the yellow light dilemma problems.

Proposition P can be decomposed into three cases:

- (1) No-conflict with respect to P : the ego vehicle is able to merge ahead without conflict independent of the subsequent motion of the remote vehicle.
- (2) Uncertain with respect to P : the ego vehicle may be able to merge ahead without conflict depending on the subsequent motion of the remote vehicle.
- (3) Conflict with respect to P : the ego vehicle is not able to merge ahead without conflict independent of the subsequent motion of the remote vehicle.

Mathematically these can be formulated as disjoint sets in state space:

$$\mathcal{P}_g := \{x(0) \in \Omega \mid \forall u_1(t), \exists u_2(t), P \text{ for } t > 0\}, \quad (2.8)$$

$$\mathcal{P}_y := \{x(0) \in \Omega \mid (\exists u_1(t), \forall u_2(t), \neg P \text{ for } t > 0) \wedge (\exists u_1(t), \exists u_2(t), P \text{ for } t > 0)\}, \quad (2.9)$$

$$\mathcal{P}_r := \{x(0) \in \Omega \mid \forall u_1(t), \forall u_2(t), \neg P \text{ for } t > 0\}, \quad (2.10)$$

and we refer to these as no-conflict set, uncertain set, and conflict set with respect to merge ahead, respectively. The subscripts g, y and r correspond to the colors green, yellow, and red that will be used to visualize the sets in state space. Similarly, based on proposition Q , the state space can be decomposed into no-conflict set, uncertain set, and conflict set with respect to the merge behind, that is,

$$\mathcal{Q}_g := \{x(0) \in \Omega \mid \forall u_1(t), \exists u_2(t), Q \text{ for } t > 0\}, \quad (2.11)$$

$$\mathcal{Q}_y := \{x(0) \in \Omega \mid (\exists u_1(t), \forall u_2(t), \neg Q \text{ for } t > 0) \wedge (\exists u_1(t), \exists u_2(t), Q \text{ for } t > 0)\}, \quad (2.12)$$

$$\mathcal{Q}_r := \{x(0) \in \Omega \mid \forall u_1(t), \forall u_2(t), \neg Q \text{ for } t > 0\}. \quad (2.13)$$

Note that the first and second predicates in (2.9) are the negation of the predicates in (2.8) and (2.10), that is,

$$\begin{aligned} (\exists u_1, \forall u_2, \neg P) &\iff \neg(\forall u_1, \exists u_2, P), \\ (\exists u_1, \exists u_2, P) &\iff \neg(\forall u_1, \forall u_2, \neg P), \end{aligned} \quad (2.14)$$

implying that \mathcal{P}_g , \mathcal{P}_y , and \mathcal{P}_r are pairwise disjoint and giving $\mathcal{P}_g \cup \mathcal{P}_y \cup \mathcal{P}_r = \Omega$. Similar relationships also exist in (2.11-2.13), yielding $\mathcal{Q}_g \cup \mathcal{Q}_y \cup \mathcal{Q}_r = \Omega$.

We remark that the formal logic-based set description can be naturally extended to more complex conflict scenarios (e.g., more vehicles or lanes), which guarantees mathematical strictness while keeping the definition concise and scalable. We also emphasize that the decoupling of the propositions P and Q breaks down the problem of preventing conflict into the merge ahead scenario and the merge behind scenario.

2.2.1 Conflict charts

Using model (2.1), the boundaries between the domains \mathcal{P}_g , \mathcal{P}_y , and \mathcal{P}_r in state space can be calculated analytically, and the same holds for \mathcal{Q}_g , \mathcal{Q}_y , and \mathcal{Q}_r . By superimposing these domains, we can create conflict charts that separate the state space into no-conflict, uncertain, and conflict domains.

First, we focus on the sets \mathcal{P}_g , \mathcal{P}_y , and \mathcal{P}_r . If $r_1(0) \in [-s, 0]$, the remote vehicle starts in the conflict zone and the ego vehicle has no chance to merge ahead without conflict. When $r_1(0) \in (0, \infty)$, we can describe two boundaries, $r_2 = p_1(r_1, v_1, v_2)$ and $r_2 = p_2(r_1, v_1, v_2)$, which separate \mathcal{P}_g , \mathcal{P}_y , and \mathcal{P}_r as visualized in the (v_2, r_2) -plane in Fig. 2.3(a). These boundaries are derived by considering that by the time the remote vehicle enters the conflict zone the ego vehicle just exits while applying the input bounds $(u_1(t), u_2(t)) \equiv (a_{\max,1}, a_{\max,2})$ and $(u_1(t), u_2(t)) \equiv (a_{\min,1}, a_{\max,2})$; see Fig. 2.2(a) and Appendix B.

It can be proven that $p_2(r_1, v_1, v_2) \geq p_1(r_1, v_1, v_2)$, $\forall r_1 \in (0, \infty)$, $v_1 \in [v_{\min,1}, v_{\max,1}]$, and $v_2 \in [0, v_{\max,2}]$. Thus, the regions \mathcal{P}_g , \mathcal{P}_y , and \mathcal{P}_r are given by

$$\mathcal{P}_g = \{x \in \Omega \mid r_2 < p_1(r_1, v_1, v_2)\}, \quad (2.15)$$

$$\mathcal{P}_y = \{x \in \Omega \mid p_1(r_1, v_1, v_2) \leq r_2 < p_2(r_1, v_1, v_2)\}, \quad (2.16)$$

$$\mathcal{P}_r = \Omega \setminus (\mathcal{P}_g \cup \mathcal{P}_y), \quad (2.17)$$

and these are shaded as green, yellow, and red in Fig. 2.3(a), respectively.

Similarly, consider the sets \mathcal{Q}_g , \mathcal{Q}_y , and \mathcal{Q}_r . There are two boundaries related to proposition Q : $r_2 = q_1(r_1, v_1, v_2)$ and $r_2 = q_2(r_1, v_1, v_2)$; see Fig. 2.3(b). These are calculated by considering that by the time the remote vehicle exits the conflict zone, the ego vehicle just enters while applying the input bounds $(u_1(t), u_2(t)) \equiv (a_{\min,1}, a_{\min,2})$ and $(u_1(t), u_2(t)) \equiv (a_{\max,1}, a_{\min,2})$; see Fig. 2.2(b). Note that boundaries q_1 and q_2 overlap for $v_2 \in [0, -t_{q2} a_{\min,2}]$, where t_{q2} represents the time needed for the remote vehicle to exit the conflict zone, with $u_1(t) \equiv a_{\max,1}$; see (B.10-B.12) in Appendix B. One can then prove that, $q_1(r_1, v_1, v_2) \geq q_2(r_1, v_1, v_2)$, $\forall r_1 \in [-s, \infty)$,

$v_1 \in [v_{\min,1}, v_{\max,1}]$, $v_2 \in (-t_{q2} a_{\min,2}, \infty)$. Thus, the regions \mathcal{Q}_g , \mathcal{Q}_y , and \mathcal{Q}_r are

$$\mathcal{Q}_g = \{x \in \Omega | r_2 > q_1(r_1, v_1, v_2)\} \quad (2.18)$$

$$\mathcal{Q}_y = \{x \in \Omega | q_2(r_1, v_1, v_2) < r_2 \leq q_1(r_1, v_1, v_2)\}, \quad (2.19)$$

$$\mathcal{Q}_r = \Omega \setminus (\mathcal{Q}_g \cup \mathcal{Q}_y). \quad (2.20)$$

These regions are shaded as green, yellow, and red in Fig. 2.3(b), respectively.

Figure 2.3(d)-(e) visualize the corresponding boundaries and regions in the (r_1, r_2) -plane, where the red square at the bottom left corner represents the conflict zone. Note that the sets partitioning the state space are obtained analytically using the simple model (2.1) without resistance terms. With more complicated models, analytical calculations may not be possible and numerical tools may be needed. Developing such tools will be discussed further below in Chapters 4 and 5.

Having introduced the boundaries and regions related to P and Q separately, we combine them together in Fig. 2.3(c) and (f). Each region in these graphs is given by the intersection of a set related to P and a set related to Q . We color the regions as follows: combining a green region with any other region gives green; combining a yellow region with a yellow or red region gives yellow; combining two red regions gives red. We refer to these as unified conflict charts. Such conflict charts can be used by the ego vehicle to locate the current system state, and thus reason about future conflicts, once a status of the remote vehicle is received (via V2X communication).

In the unified conflict chart in Fig. 2.3(f), the red-shaded region corresponds to the ‘‘capture set’’ computed in [46, 44]. However, here the decision making boundaries further divide the rest of the state space into different regions, enabling the ego vehicle to make decisions (and act on them) long before approaching the capture set. As will be explained below, the decision in the green region below the blue boundary shall be ‘‘merge ahead’’ and in the green region above the blue boundary shall be ‘‘merge behind’’ in order to prevent conflict independent of the future behavior of the remote vehicle.

Fig. 2.4(a)-(d) show a sequence of charts in the (v_2, r_2) -plane for fixed v_1 and different r_1 values as indicated. These charts illustrate the evolution of the boundaries while the remote vehicle approaches the conflict zone with constant speed. On the other hand, Fig. 2.4(e)-(h) show a sequence of conflict charts in the (r_1, r_2) -plane when the remote vehicle travels at constant speed while the ego vehicle is accelerating.

2.2.2 Communication range and decision making rule

The conflict charts introduced above provide a general tool for decision making. These, however, rely on having motion information available from the remote vehicle, which, in most cases,

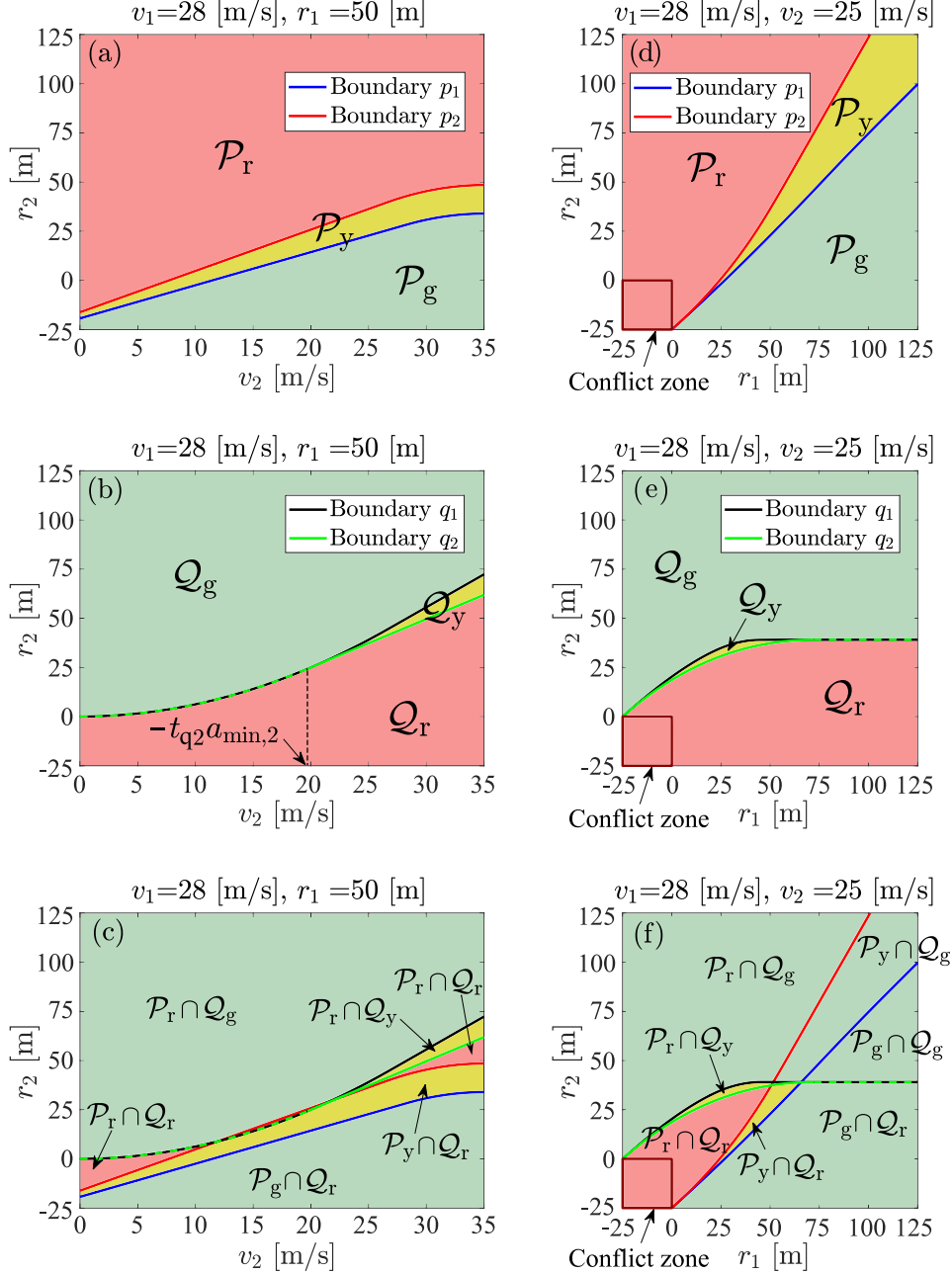


Figure 2.3: (a)-(c) Conflict charts in the (v_2, r_2) -plane for given v_1, r_1 values as indicated. (a) Conflict charts for merge ahead. (b) Conflict charts for merge behind. (c) Unified conflict charts combining (a) and (b). (d)-(f) Conflict charts in the (r_1, r_2) -plane for given v_1, v_2 values as indicated.

cannot be obtained using optical sensors, but require the use of V2X communication. Here we provide conditions for the required range of V2X communication in order to guarantee conflict free maneuvers.

For initial conditions $x(0) \in \mathcal{P}_g \cup \mathcal{Q}_g$ in the green region, there exists a controller $u_2(t)$ such

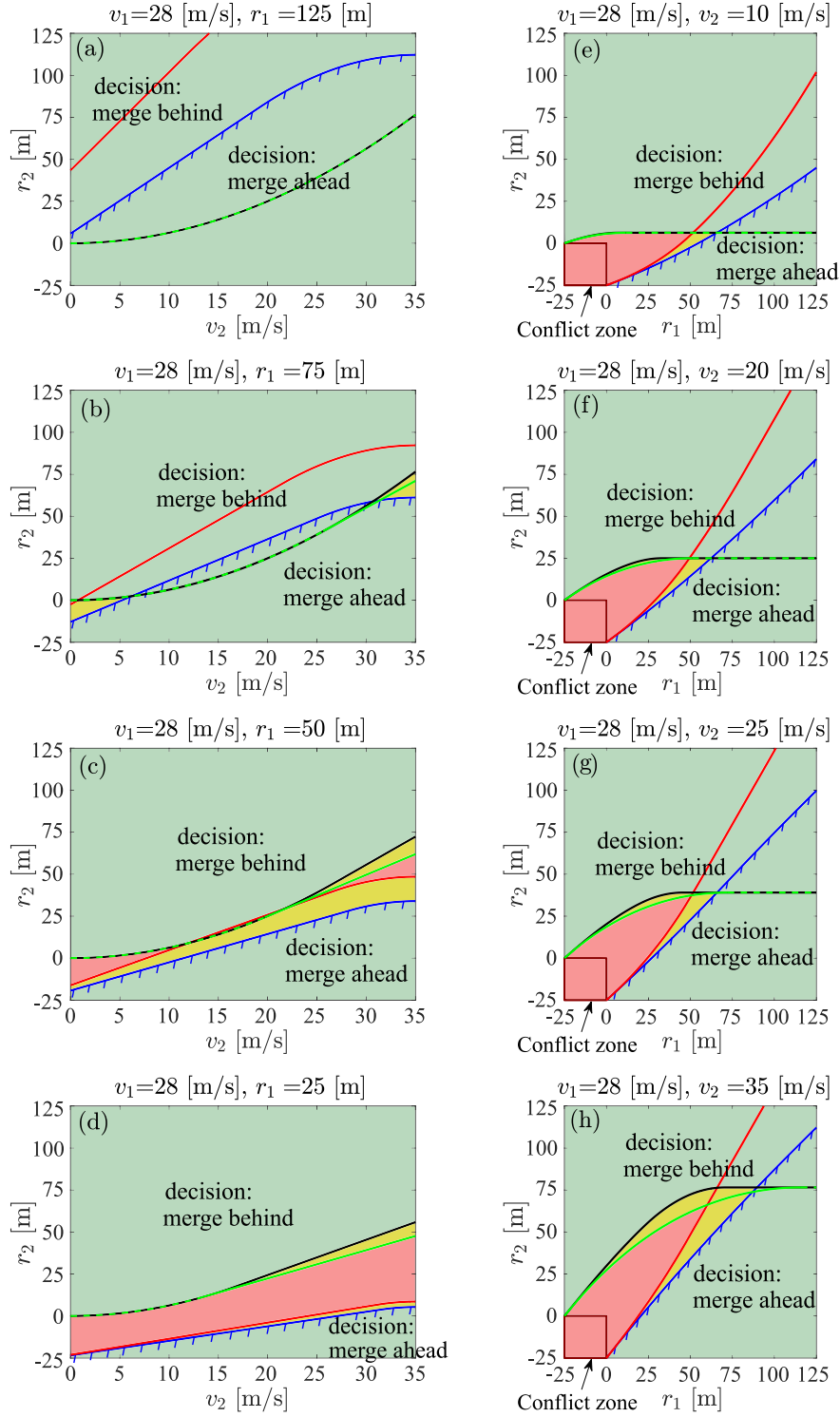


Figure 2.4: (a)-(d) Conflict charts in the (v_2, r_2) -plane when the remote vehicle is approaching with a constant speed. (e)-(h) Conflict charts in the (r_1, r_2) -plane when the remote vehicle travels at constant speed while the ego vehicle is accelerating. According to the decision making rule (2.24), the decision in the green region below the blue boundary is merge ahead while the decision in the green region above the blue boundary is merge behind.

that conflict can be prevented for $t > 0$, that is, $x(t) \in \mathcal{P}_g \cup \mathcal{Q}_g$. The following theorem relates this to a communication range requirement.

Theorem 1. *The statement $x(0) \in \mathcal{P}_g \cup \mathcal{Q}_g$ holds for $r_1(0) \geq r_1^*$ where*

$$r_1^* = \max\{\underline{r}_1, \bar{r}_1\}, \quad (2.21)$$

and

$$\underline{r}_1 = \begin{cases} \sqrt{\frac{2s}{a_{\max,2}}} v_{\max,1}, & \text{if } s a_{\max,2} \leq \frac{1}{2} v_{\max,2}^2, \\ \left(s + \frac{v_{\max,2}^2}{2a_{\max,2}}\right) \frac{v_{\max,1}}{v_{\max,2}}, & \text{otherwise,} \end{cases} \quad (2.22)$$

$$\bar{r}_1 = \left(s - \frac{v_{\max,2}^2}{2a_{\min,2}}\right) \frac{v_{\max,1}}{v_{\max,2}}. \quad (2.23)$$

Proof. See Appendix C. □

The proof is based on showing that, if $r_1(0) \geq r_1^*$, then $p_1(r_1, v_1, v_2) \geq q_1(r_1, v_1, v_2)$ independent of the values of v_1 and v_2 , meaning that the system state is guaranteed to stay in the green no-conflict domain $\mathcal{P}_g \cup \mathcal{Q}_g$; see Fig. 2.4(a). The theorem implies that if the ego vehicle receives a status packet from the remote vehicle (at $t = 0$) when the latter is at least r_1^* distance away from the conflict zone, then independent of the input $u_1(t)$, $t \geq 0$, there exists a controller $u_2(t)$, $t \geq 0$ which can prevent conflicts for $t > 0$. For the parameters in Table 2.1, we have $r_1^* = 124$ [m] which is possible to satisfy with current V2X technologies. Fig. 2.5(a)-(c) show how the communication range r_1^* is affected by the parameters of the ego vehicle. Notice that with lower capability of accelerating and decelerating, larger communication range is required to prevent conflict. This also implies that having a larger communication range may help one to improve passenger comfort.

Now we propose a decision making rule for the ego vehicle:

$$\text{decision} = \begin{cases} \text{merge ahead,} & \text{if } x(0) \in \mathcal{P}_g, \\ \text{merge behind,} & \text{if } x(0) \notin \mathcal{P}_g \wedge x(0) \in \mathcal{Q}_g. \end{cases} \quad (2.24)$$

That is, if the initial state $x(0) \in \mathcal{P}_g$, then independent of the motion of the remote vehicle, the ego vehicle is able to merge ahead without conflict, and the decision maximizes its time efficiency. On the other hand, if $x(0) \notin \mathcal{P}_g$ and $x(0) \in \mathcal{Q}_g$, then independent of the motion of the remote vehicle, the ego vehicle is able to merge behind without conflict.

If the communication range requirement in Theorem 1 is satisfied (see Fig. 2.4(a)), a non-conflicting decision is guaranteed by (2.24) for any initial state of the ego vehicle. Also, (2.24) suggests that for $x(0) \in \mathcal{P}_g \cap \mathcal{Q}_g$, the ego vehicle still chooses to merge ahead to increase its time

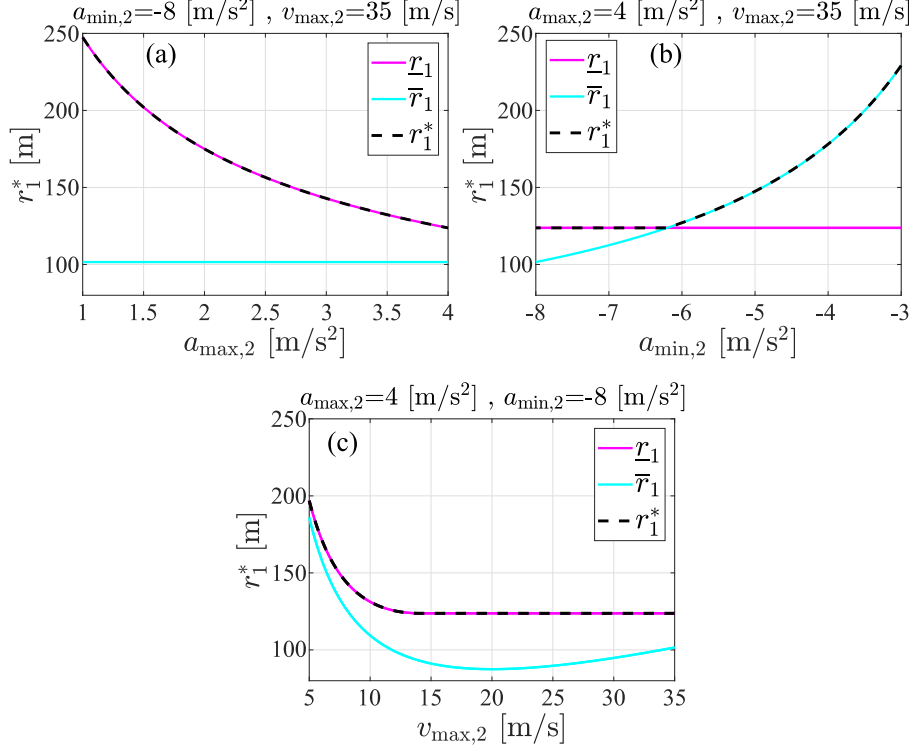


Figure 2.5: Communication range as a function of (a) $a_{\max,2}$, (b) $a_{\min,2}$ and (c) $v_{\max,2}$, where the parameters of the remote vehicle are given in Table 2.1.

efficiency. If the communication range requirement is not satisfied (see Fig. 2.4(b)-(d)), the decision making rule (2.24) can still be applied. However, if the initial state $x(0) \notin \mathcal{P}_g \cup \mathcal{Q}_g$ then a definite decision cannot be made due to the unknown future behaviors of the remote vehicle. In the next section, we provide a potential solution to this problem by making the intent of the remote vehicle available via V2X connectivity.

2.3 Conflict Analysis with Intent Information

In this section, we show that obtaining intent information from the remote vehicle can help the ego vehicle to make decisions since it decreases the uncertainty regarding the future behavior of the remote vehicle. We also demonstrate that making better decisions may significantly improve the time efficiency of the ego vehicle when merging. We note again that intent sharing is beneficial to cooperative driving as it can be used to improve the decision-making and control of an automated vehicle having at least partial automation; see Fig. 1.2.

First, we define the intent of the remote vehicle under the scenario described in Section 2.1.

Definition 2. *Given the dynamics (2.1,2.2), the intent of the remote vehicle is a restricted velocity*

domain $v_1(t) \in [\underline{v}_1, \bar{v}_1]$ and acceleration (input) domain $u_1(t) \in [\underline{a}_1, \bar{a}_1]$ over some time period $t \in [0, \Delta t]$, where $v_{\min,1} \leq \underline{v}_1 \leq \bar{v}_1 \leq v_{\max,1}$ and $a_{\min,1} \leq \underline{a}_1 \leq \bar{a}_1 \leq a_{\max,1}$. ■

For example, in a highway driving scenario with cruise control, an intent message may encode that for the next $\Delta t = 15$ seconds, the remote vehicle will travel with a speed between $\underline{v}_1 = 27$ [m/s] and $\bar{v}_1 = 29$ [m/s] while limiting its acceleration between $\underline{a}_1 = -1$ [m/s²] and $\bar{a}_1 = 1$ [m/s²].

For simplicity, we assume that the time interval Δt of the intent covers the time horizon until the remote vehicle clears the conflict zone. This assumption is realistic for merge, intersection crossing, and lane change maneuvers as those typically last for a few seconds. Thus, when the intent information is available, the boundaries in the conflict charts can be re-calculated using the formulas in Appendix B with the remote vehicle's velocity and acceleration limits given by its intent. Let us use $r_2 = \bar{p}_1(r_1, v_1, v_2)$, $r_2 = \bar{p}_2(r_1, v_1, v_2)$, $r_2 = \bar{q}_1(r_1, v_1, v_2)$, and $r_2 = \bar{q}_2(r_1, v_1, v_2)$ to denote the new boundaries. One can then define no-conflict, uncertain, and conflict sets with intent information. For proposition P we have

$$\bar{\mathcal{P}}_g = \{x \in \Omega | r_2 < \bar{p}_1(r_1, v_1, v_2)\}, \quad (2.25)$$

$$\bar{\mathcal{P}}_y = \{x \in \Omega | \bar{p}_1(r_1, v_1, v_2) \leq r_2 < \bar{p}_2(r_1, v_1, v_2)\}, \quad (2.26)$$

$$\bar{\mathcal{P}}_r = \Omega \setminus (\bar{\mathcal{P}}_g \cup \bar{\mathcal{P}}_y), \quad (2.27)$$

cf. (2.15-2.17), while for proposition Q we obtain

$$\bar{\mathcal{Q}}_g = \{x \in \Omega | r_2 > \bar{q}_1(r_1, v_1, v_2)\} \quad (2.28)$$

$$\bar{\mathcal{Q}}_y = \{x \in \Omega | \bar{q}_2(r_1, v_1, v_2) < r_2 \leq \bar{q}_1(r_1, v_1, v_2)\}, \quad (2.29)$$

$$\bar{\mathcal{Q}}_r = \Omega \setminus (\bar{\mathcal{Q}}_g \cup \bar{\mathcal{Q}}_y), \quad (2.30)$$

cf. (2.18)-(2.20).

The following Theorem gives the relationships between the sets with and without intent information.

Theorem 2. *Given the intent of the remote vehicle, we obtain*

$$\mathcal{P}_g \subseteq \bar{\mathcal{P}}_g, \quad \mathcal{P}_y \supseteq \bar{\mathcal{P}}_y, \quad \text{and} \quad \mathcal{P}_r \subseteq \bar{\mathcal{P}}_r, \quad (2.31)$$

$$\mathcal{Q}_g \subseteq \bar{\mathcal{Q}}_g, \quad \mathcal{Q}_y \supseteq \bar{\mathcal{Q}}_y, \quad \text{and} \quad \mathcal{Q}_r \subseteq \bar{\mathcal{Q}}_r. \quad (2.32)$$

Proof. See Appendix D. □

The relationships (2.31) and (2.32) reveal that with the intent both the no-conflict and conflict sets (with respect to P and Q) expand, while the uncertain sets (with respect to P and Q) shrink.

These are illustrated in the conflict charts in Fig. 2.6(a) and (d), and Fig. 2.6(b) and (e), respectively.

The following Corollary states that the uncertain sets $\bar{\mathcal{P}}_y$ and $\bar{\mathcal{Q}}_y$ disappear when considering a deterministic future motion (i.e., constant acceleration) for the remote vehicle.

Corollary 1. $\bar{\mathcal{P}}_y = \bar{\mathcal{Q}}_y = \emptyset$ if the intent of the remote vehicle satisfies

$$(\bar{a}_1 = \underline{a}_1) \vee (\bar{v}_1 = \underline{v}_1 = v_1(t)). \quad (2.33)$$

This corollary can be proved by noticing that (2.33) leads to the relationships $\bar{p}_1(r_1, v_1, v_2) = \underline{p}_1(r_1, v_1, v_2)$ and $\bar{q}_1(r_1, v_1, v_2) = \underline{q}_1(r_1, v_1, v_2)$ between the boundaries.

Combining the conflict charts associated with propositions P and Q , yields the following property for the unified conflict charts.

Corollary 2. *Given the intent of the remote vehicle, in the unified conflict charts we have*

$$\mathcal{P}_g \cup \mathcal{Q}_g \subseteq \bar{\mathcal{P}}_g \cup \bar{\mathcal{Q}}_g, \quad (2.34)$$

$$\mathcal{P}_r \cap \mathcal{Q}_r \subseteq \bar{\mathcal{P}}_r \cap \bar{\mathcal{Q}}_r. \quad (2.35)$$

This corollary can be proved from (2.31) and (2.32) with basic set operations. Practically, (2.34) and (2.35) mean that with intent the green and red regions expand, resulting in smaller yellow region in the state space Ω ; cf. Fig. 2.6(c,f) with Fig. 2.3(c,f). That is, having intent information reduces the uncertainty in the decision making of the ego vehicle and provides additional danger awareness. Also, the decision making rule (2.24) can be adapted by using $\bar{\mathcal{P}}_g$ and $\bar{\mathcal{Q}}_g$ instead of \mathcal{P}_g and \mathcal{Q}_g , respectively.

The charts in Fig. 2.7 quantify the benefits of using the intent information. These are obtained by superimposing the conflict charts with and without intent information; see Figs. 2.3, 2.4 and 2.6. In the gray-shaded regions, the decision remains unchanged. Fig. 2.7(a) shows that when the communication range requirement (2.21,2.22,2.23) is satisfied, there is a region where decision changes from merge behind to merge ahead. Fig. 2.7(b) depicts that when the communication range requirement is not satisfied, a previously yellow region changes to green and red. For example, points A, B, and C were in the yellow region in Fig. 2.3(c), while in Fig. 2.7(b) A and C are in the green region with decisions to merge behind and merge ahead, respectively. Point B is in the red region, giving the ego vehicle an awareness of danger that a conflict is not preventable.

2.4 Controller Design

Based on the conflict analysis presented above, we design a controller for the ego vehicle to execute a conflict-free merge. Recall that this vehicle is considered to be automated and we refer to this as

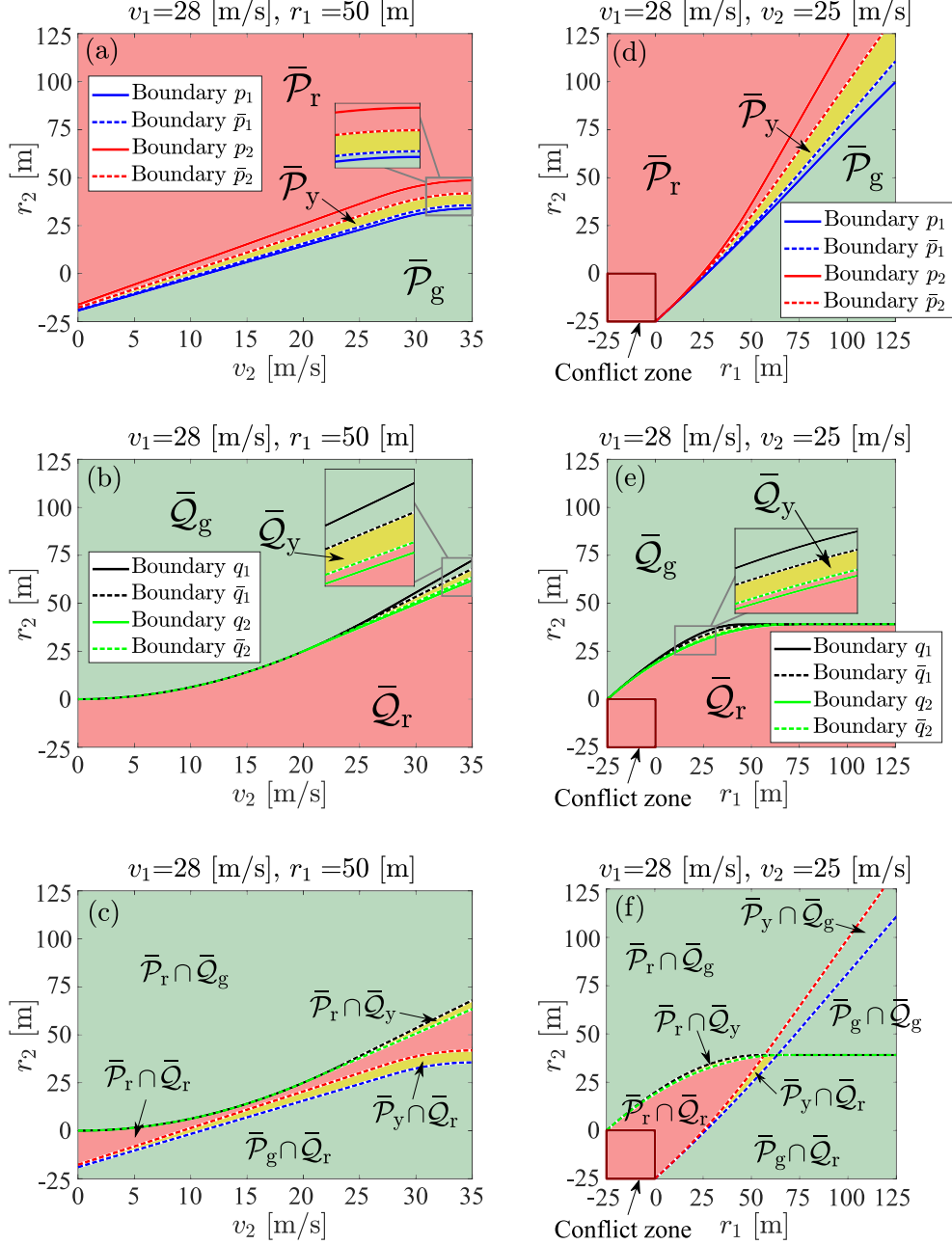


Figure 2.6: (a)-(c) Conflict charts in the (v_2, r_2) -plane given the intent of the remote vehicle: $v_1 \in [25, 30]$ [m/s] and $u_1 \in [-2, 1]$ [m/s²]. (a) Conflict charts for merge ahead. (b) Conflict charts for merge behind. (c) Unified conflict charts combining (a) and (b). (d)-(f) Conflict charts in the (r_1, r_2) -plane given the same intent of the remote vehicle.

a connected automated vehicle (CAV) in this section. On the other hand, no restriction is assumed for the remote vehicle, i.e., it can be human-driven or automated. Finally, we assume that the communication range requirement given in Theorem 1 holds, i.e., the CAV receives a status update from the remote vehicle before the latter one reaches the distance r_1^* from the conflict zone.

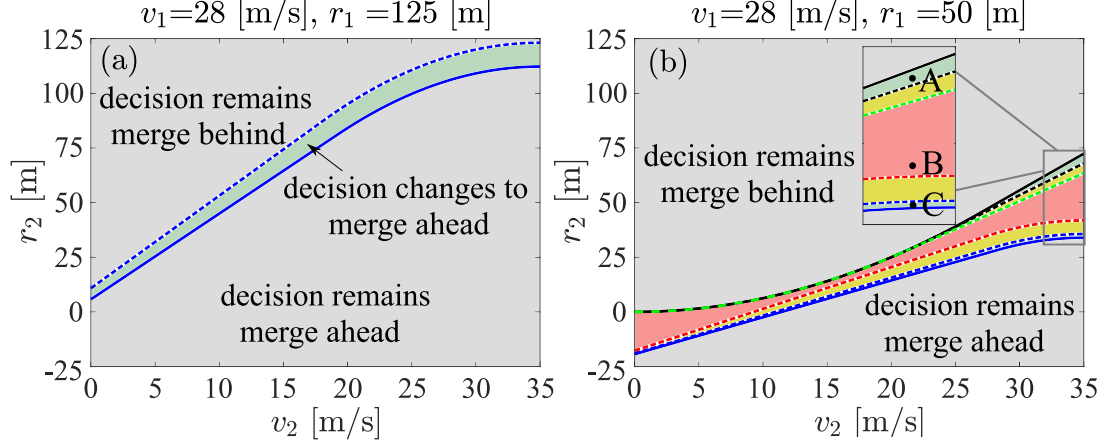


Figure 2.7: Change of decision charts under the same intent as in Fig. 2.6 when the communication range requirement in Theorem 1 is satisfied (a) and when it is not satisfied (b). Conflict cannot be prevented without intent for the points marked A, B, and C. With intent the decisions become: A - merge behind; C - merge ahead; B - conflict is not preventable.

To ensure a non-conflicting maneuver independent of the remote vehicle's future action $u_1(t)$, we propose the controller

$$u_2(t) = \begin{cases} u_2^{\mathcal{P}_g}, & \text{if decision = merge ahead,} \\ u_2^{\mathcal{Q}_g}, & \text{if decision = merge behind,} \end{cases} \quad (2.36)$$

for $t \geq 0$; see (2.24). Here, $u_2^{\mathcal{P}_g}$ ensures that the ego vehicle merges ahead of the remote vehicle without conflict, and $u_2^{\mathcal{Q}_g}$ ensures that it merges behind without conflict. A block diagram summarizing the decision making and control logic for the CAV is shown in Fig. 2.8, where the design of $u_2^{\mathcal{Q}_g}$ is divided into several cases as discussed below.

For merge ahead, the CAV chooses constant control input

$$u_2^{\mathcal{P}_g} = a_{\max,2}, \quad (2.37)$$

since it makes the maneuver the most time-efficient (from the CAV's perspective). Note that according to the saturation function (2.2) in (2.1), the CAV's acceleration becomes zero once its velocity reaches $v_{\max,2}$. Fig. 2.9 shows two different velocity profiles when $u_2^{\mathcal{P}_g}$ is applied to pass the conflict zone. Panels (a) and (b) correspond to cases when $v_{\max,2}$ is not reached and when it is reached, respectively.

For merge behind, the CAV uses the constant control input $u_2^{\mathcal{Q}_g}$ that is calculated by assuming the worst-case scenario $u_1(t) \equiv a_{\min,1}$ (or $u_1(t) \equiv \underline{a}_1$ when intent is available). To maximize the time efficiency (of the CAV), we set $u_2^{\mathcal{Q}_g}$ such that the CAV arrives at the front edge of conflict zone

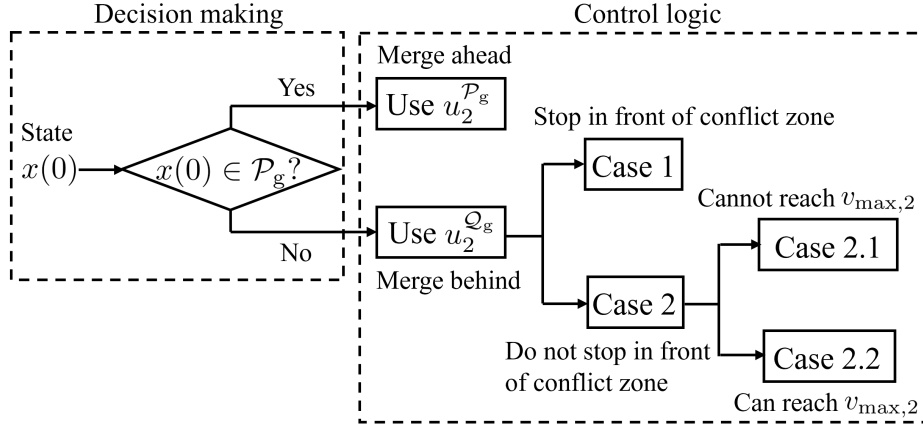


Figure 2.8: Block diagram of the decision making and control logic of the CAV under the communication requirement in Theorem 1.

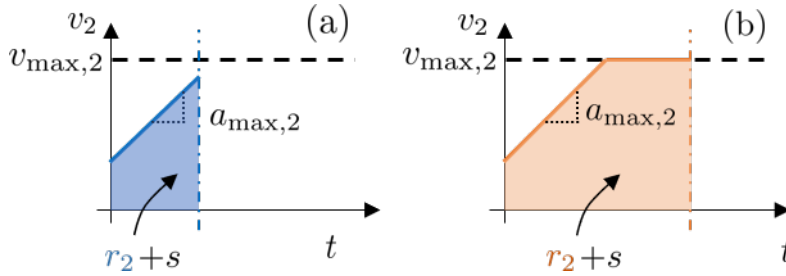


Figure 2.9: Velocity profiles when applying controller $u_2^{\mathcal{P}_g}$ when the speed limit $v_{\max,2}$ is not reached (a) and when it is reached (b).

at time t_{q1} , when the remote vehicle clears the conflict zone. In the formulas below, we drop the argument (0) when referring to the initial values of the state x , that is, we use r_1, v_1, r_2, v_2 instead of $r_1(0), v_1(0), r_2(0), v_2(0)$.

We distinguish two cases:

Case 1: $r_2 \leq \frac{1}{2}t_{q1}v_2 \implies$ the CAV must stop at the front edge of the conflict zone. Then the control input is given by

$$u_2^{\mathcal{Q}_g} = -\frac{v_2^2}{2r_2}, \quad (2.38)$$

which makes the CAV stop at the front edge of the conflict zone no later than the time t_{q1} ; see Fig. 2.10(a) where the area below the curve is the distance r_2 . Note that it can be shown from (2.38) that $u_2^{\mathcal{Q}_g} > a_{\min,2}$. Also, the control input $u_2^{\mathcal{Q}_g}$ saturates once the CAV's speed reaches $v_{\min,2} = 0$ [m/s].

Case 2: $r_2 > \frac{1}{2}t_{q1}v_2 \implies$ the CAV does not need to stop at the front edge of conflict zone. For this

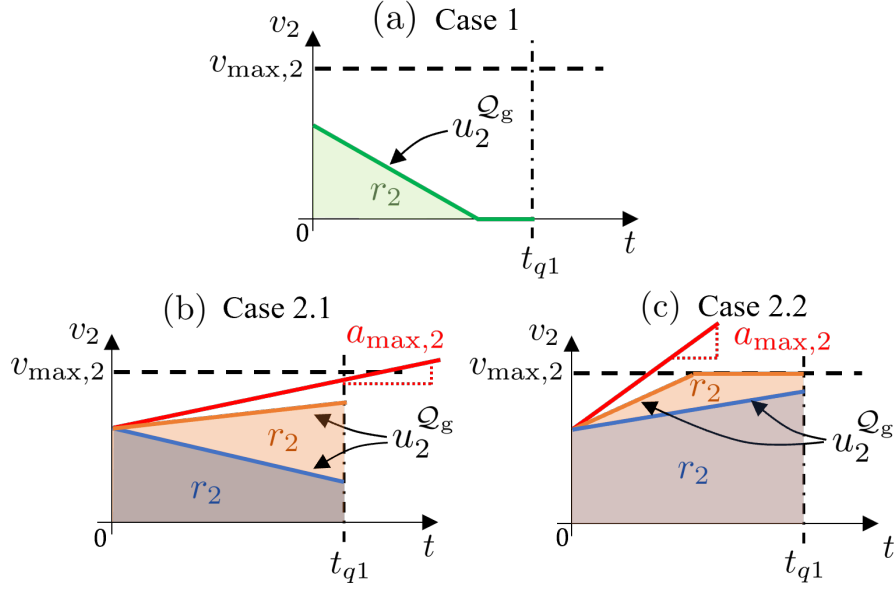


Figure 2.10: Velocity profiles for the controller $u_2^{Q_g}$. The different panels correspond to the cases in Fig. 2.8. Here, t_{q1} is the time when the remote vehicle clears the conflict zone under $u_1(t) \equiv a_{\min,1}$ (or $u_1(t) \equiv \underline{a}_1$ when intent is available).

case there are two subcases.

Case 2.1: $a_{\max,2} < (v_{\max,2} - v_2)/t_{q1} \implies$ the CAV's speed cannot reach $v_{\max,2}$ by time t_{q1} , not even by applying the maximum acceleration $a_{\max,2}$; see Fig. 2.10(b). In this case we use

$$u_2^{Q_g} = \begin{cases} \frac{2(r_2 - v_2 t_{q1})}{t_{q1}^2}, & \text{if } r_2 \in (\frac{1}{2}t_{q1}v_2, \frac{1}{2}t_{q1}^2 a_{\max,2} + v_2 t_{q1}], \\ a_{\max,2}, & \text{otherwise.} \end{cases} \quad (2.39)$$

Case 2.2: $a_{\max,2} \geq (v_{\max,2} - v_2)/t_{q1} \implies$ the CAV's speed can reach $v_{\max,2}$ by time t_{q1} ; see Fig. 2.10(c). In this case we use

$$u_2^{Q_g} = \begin{cases} \frac{2(r_2 - v_2 t_{q1})}{t_{q1}^2}, & \text{if } r_2 \in (\frac{1}{2}t_{q1}v_2, \frac{1}{2}t_{q1}(v_2 + v_{\max,2})], \\ \frac{(v_{\max,2} - v_2)^2}{2(t_{q1}v_{\max,2} - r_2)}, & \text{if } r_2 \in (\frac{1}{2}t_{q1}(v_2 + v_{\max,2}), -\frac{(v_{\max,2} - v_2)^2}{2a_{\max,2}} + t_{q1}v_{\max,2}], \\ a_{\max,2}, & \text{otherwise.} \end{cases} \quad (2.40)$$

Note that in Case 2.2 the control input $u_2^{Q_g}$ saturates once the CAV's speed reaches $v_{\max,2}$.

The proposed controller guarantees that region \mathcal{P}_g is invariant under $u_2^{\mathcal{P}_g}$, and \mathcal{Q}_g is invariant under $u_2^{Q_g}$. That is, $\mathcal{P}_g \cup \mathcal{Q}_g$ is control invariant under (2.36). Recall that $u_2^{Q_g}$ is derived by using a status packet received from the remote vehicle at $t = 0$ and it is assumed that the remote vehicle

is applying $u_1(t) \equiv a_{\min,1}$ (or \underline{a}_1) along $t > 0$. However, if the CAV receives status updates later, it can re-calculate (2.38), (2.39), and (2.40) using the most recent information, which results in larger value of $u_2^{Q_g}$, and consequently, better time-efficiency for the CAV. The benefits of receiving frequent status updates will be shown in the next section.

2.5 Experiments and Simulations

In this section, we show two applications of the conflict analysis framework developed above. First, we present experimental results obtained in a closed test track to demonstrate that (i) the theoretical conflict chart matches with data collected using real vehicles, and (ii) our conflict analysis can help a CAV to prevent conflicts that a human driver could not avoid. Second, we present numerical simulations by using real highway data for the remote vehicle to demonstrate that a CAV is able to prevent conflict when using the proposed decision making and control algorithms. We also demonstrate that the performance of CAV can be significantly enhanced when it utilizes intent information from the remote vehicle.

2.5.1 Experiments on test track with real vehicles

The experiments were performed at the test track of the University of Michigan called Mcity with two real vehicles; see the aerial view in Fig. 2.11(a). The remote vehicle (blue) traveled along the main road while the ego vehicle (white) merged onto the main road within the yellow rectangle of 50 meters length. The conflict zone is indicated by the red rectangle of 20 meters length. Fig. 2.11(b)-(f) show snapshots from one of the maneuvers where conflict arose. In the experiments both vehicles had human drivers, but the remote vehicle's speed was regulated by cruise control (set to 30 [mi/hr] = 13.4 [m/s]), which may be considered as a low level of automation. The ego vehicle started from standstill from the locations marked by magenta dots in panel (a) and it launched some time after the remote vehicle has passed a landmark (indicated by the red line). Thus, by varying the launching location and the launching time, a set of different initial conditions were explored. The ego vehicle's decision (and the corresponding act) on whether to merge ahead or behind the remote vehicle was made by the human driver. For each initial condition, multiple experiments were performed.

Both vehicles were equipped with GPS devices and V2X communication devices that allowed them to share their status (GPS-based position and speed) with a 10 Hz update rate using basic safety messages (BSMs) [21]. For intent sharing, the intended speed of the remote vehicle (13.4 [m/s]) was known by the driver of the ego vehicle. Correspondingly, when constructing the conflict chart in the (r_1, r_2) -plane in Fig. 2.12(a), we used velocity limits $\underline{v}_1 = 13$ [m/s] and $\bar{v}_1 = 14$ [m/s]

(corresponding to the speed error of the cruise control) and $v_{\min,2} = 0$ and $v_{\max,2} = 20$ [m/s] (the speed limits of the ego vehicle), while the other parameters are the same as in Table 2.1. In this figure only the conflict chart of merge ahead is shown (cf. Figs. 2.3(d) and 2.6(d)) as in the experiments the ego vehicle could always merge behind the remote vehicle without conflict, due to the standstill initial condition.

The initial condition for each experiment is displayed on the conflict chart in Fig. 2.12(a). Green and blue circles correspond to non-conflicting merge ahead and merge behind runs, respectively, while magenta crosses indicate runs with conflict. Observe that the theoretical boundaries match the data well. Most non-conflicting merge ahead cases are located in the $\bar{\mathcal{P}}_g$ region, while none of them appear in the $\bar{\mathcal{P}}_r$ region. On the other hand, most conflicting cases are located in the $\bar{\mathcal{P}}_y$ and $\bar{\mathcal{P}}_r$ regions. These correspond to the human driver attempting to merge ahead based on an incorrect assessment of the situation. We remark that if rolling and air resistances were included in the ego vehicle's model, one would expect a slightly smaller green region and a slightly larger red region. We leave the quantification of this difference for our future work as this requires additional

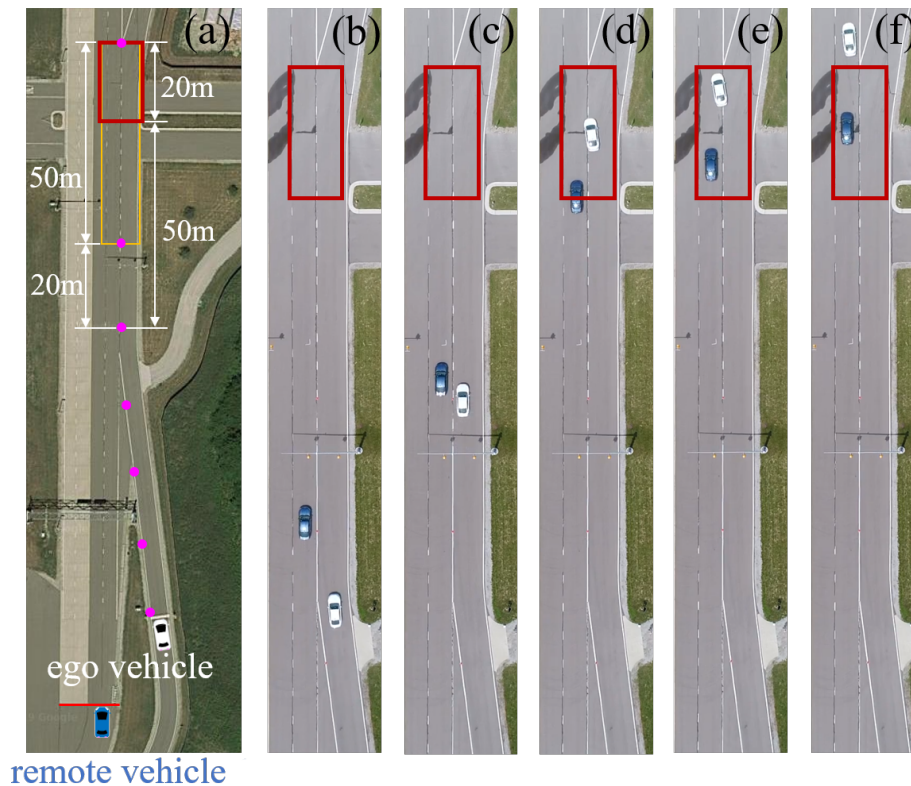


Figure 2.11: Experimental setup. (a) Layout of the test track with merge zone (yellow rectangle), conflict zone (red rectangle), and start positions of the ego vehicle (magenta dots). (b-f) Snapshots from an experiment with panels (d) and (e) highlighting the conflict.

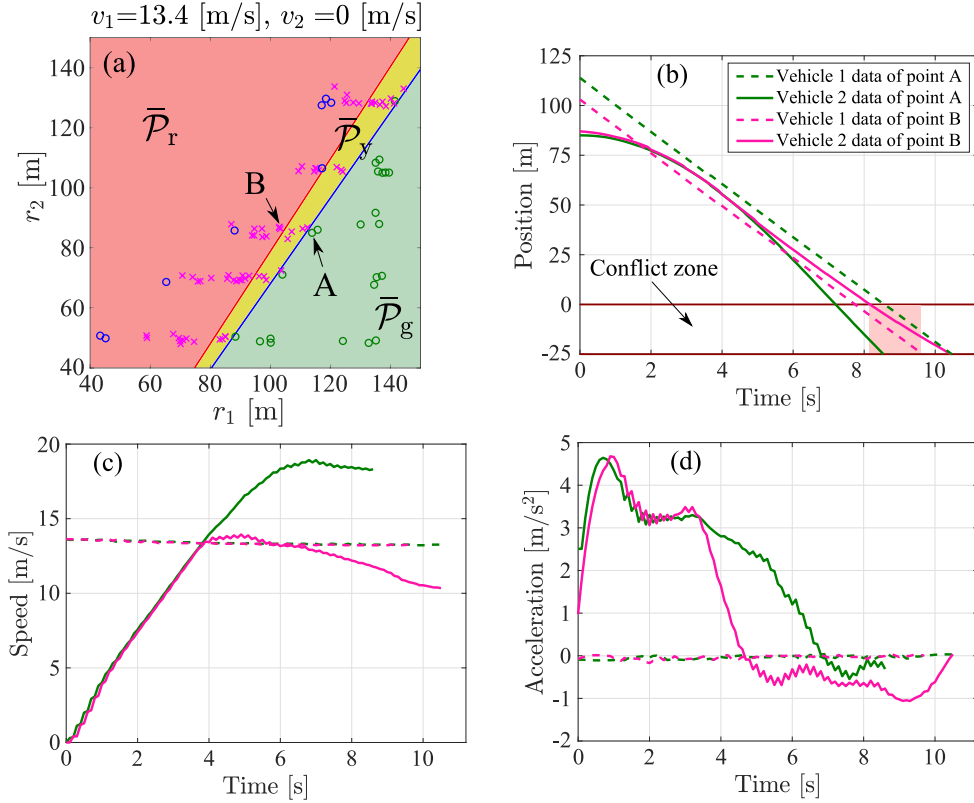


Figure 2.12: (a) Experimental data (initial conditions of both vehicles) superimposed on the conflict chart. Green circles mark non-conflicting merges ahead, blue circles denote non-conflicting merges behind and magenta crosses correspond to conflicts. (b)-(d) Position, speed and acceleration profiles of both vehicles corresponding to the initial conditions of points A and B. The red shaded region in panel (b) highlights the time interval where both vehicles are inside the conflict zone in case B.

numerical tools, which, however, can be developed based on the results of the subsequent chapters.

Fig. 2.12(b)-(c) show the vehicles' motion data corresponding to point A (no conflict) and point B (conflict) in Fig. 2.12(a). In both cases, the ego vehicle decides to merge ahead as shown by the similar speed and acceleration profiles within the first 3.5 seconds in Fig. 2.12(c) and (d). However, in the conflict chart point A is located in the $\bar{\mathcal{P}}_g$ region while point B is in the $\bar{\mathcal{P}}_r$ region where a non-conflicting merge ahead is not possible. Correspondingly, as revealed by the speed and acceleration profiles after 3.5 seconds, the ego vehicle successfully merges ahead in case A but runs into a conflict in case B. In the latter case, the ego vehicle reduces its speed and acceleration and eventually merges behind the remote vehicle. The conflict is illuminated in Fig. 2.12(b) by red shading, where the ego vehicle (solid magenta curve) appears in the conflict zone at the same time as the remote vehicle (dashed magenta curve).

The ego vehicle was able to prevent conflict in case A but failed to do so in case B due to the inability of the human driver to accurately assess the remote vehicle's state and intent and to make

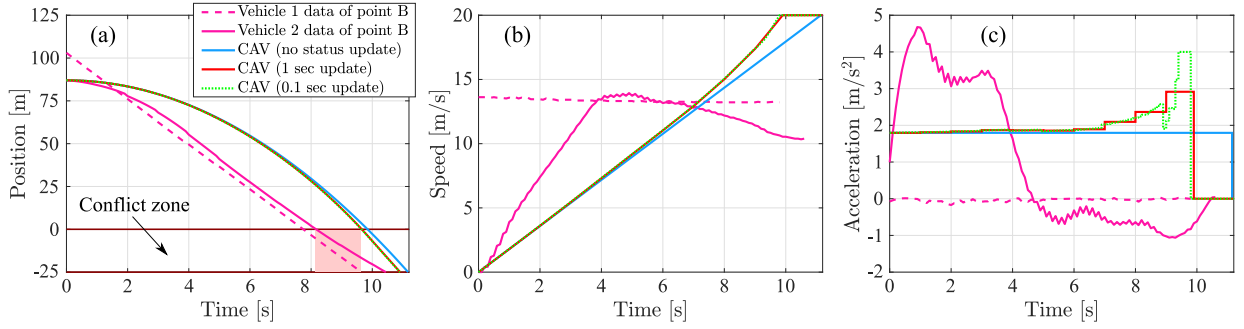


Figure 2.13: Simulation results with the initial condition of point B in Fig. 2.12(a). Position, speed, and acceleration profiles of the vehicles are plotted in panels (a), (b), and (c), respectively for the experimental run and when the CAV uses the controller (2.36,2.38,2.39,2.40) with different status update rates as indicated. The red shaded region in panel (a) highlights the time interval where both vehicles are inside the conflict zone in case B.

an informed decision. If the ego vehicle was a connected automated vehicle, it could utilize V2X connectivity to obtain accurate information about the motion of the remote vehicle. Then, with the help of conflict analysis, the CAV could make a decision to prevent the conflict and execute the corresponding maneuver using the controller designed above. To demonstrate this, we use the initial condition of the point B in Fig. 2.12(a) and show simulation results for a CAV equipped with the controller (2.36) in Fig. 2.13.

Since $x(0) \notin \bar{\mathcal{P}}_g$, according to (2.24), the CAV decides to merge behind the remote vehicle and applies (2.38)-(2.40). The position profiles in Fig. 2.13(a) show that the CAV enters the conflict zone just after the remote vehicle exits. The velocity and acceleration profiles in Fig. 2.13(b) and (c) highlight the differences caused by different V2X packet update rates. When no status updates are utilized (blue curves) the ego vehicle maintains a constant acceleration until it reaches the maximum speed. With status updates the control commands is updated every second (red curves) or every 0.1 seconds (green curves) yielding velocity and acceleration profiles which allow the CAV to execute the maneuver faster as can be observed in Fig. 2.13(a).

2.5.2 Simulations using real highway data

To further evaluate the efficiency of the decision making and control algorithms, we utilize data collected on US-23 near Ann Arbor, Michigan for the remote vehicle; see Fig. 2.1(a). The remote vehicle's position, velocity, and acceleration are shown by black curves in Fig. 2.14(a), (b), and (c), respectively. At the initial time the remote vehicle is 201.57 meters from the conflict zone traveling at a speed of 22.63 [m/s]. At the same time, the ego vehicle (CAV) is placed at the on-ramp 210 meters from the conflict zone traveling with speed of 25 [m/s]. This yields $x(0) \in \mathcal{P}_y \cap \mathcal{Q}_g$

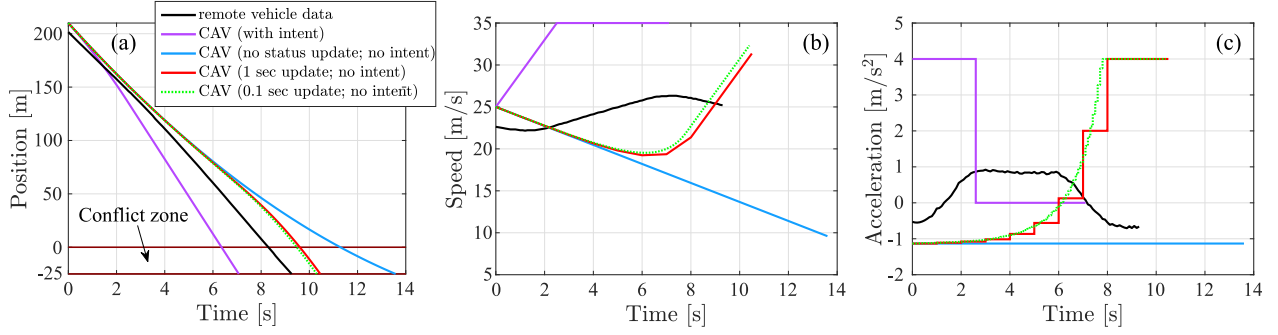


Figure 2.14: Simulation results when a CAV utilizes traffic data received from the remote vehicle and applies the controller (2.36,2.37,2.38,2.39,2.40) with different status update rates and intent as indicated. Position, speed, and acceleration profiles of the vehicles are plotted in panels (a), (b), and (c), respectively. Observe that with intent information the CAV’s decision changes from merge behind to merge ahead.

Table 2.2: Maneuver execution time of the CAV in Fig. 2.14.

	Execution time
No status update	13.58 [s]
Status update every 1 s	10.45 [s]
Status update every 0.1 s	10.31 [s]
Intent + Status	7.07 [s]

and, according to (2.24), the CAV decides to merge behind the remote vehicle while using the controller (2.36) with (2.38)-(2.40). In Fig. 2.14, the time profiles of the CAV are shown for different status update rates; see blue, red and green curves. Notice that the time needed for the CAV to execute the maneuver (i.e., execution time) decreases when status packets are received more frequently; as shown in Table 2.2. Less frequent status updates yield longer execution times due to the conservative prediction of remote vehicle’s future motion.

When intent information is available, the execution times can be further reduced. For example, extracting the bounds $\underline{v}_1 = 21$ [m/s], $\bar{v}_1 = 27$ [m/s], $\underline{a}_1 = -1$ [m/s²], $\bar{a}_1 = 1$ [m/s²] from the velocity and acceleration data of the remote vehicle, yields $x(0) \in \bar{\mathcal{P}}_g \cap \bar{\mathcal{Q}}_g$, that is, the CAV decides to merge ahead using the controller (2.36) with (2.37); see the purple curves in Fig. 2.14. This decision change leads to a significant improvement of the execution time as shown in Table 2.2.

Figure 2.15(a) depicts the domain in state space where the CAV changes its decision from merge behind to merge ahead if intent information becomes available. Considering the initial position $r_2(0) \in [-s, 300]$ [m] and initial speed $v_2(0) = 25$ [m/s] for the CAV (marked by the vertical dashed line in Fig. 2.15(a)), we simulated the CAV without and with intent while using the

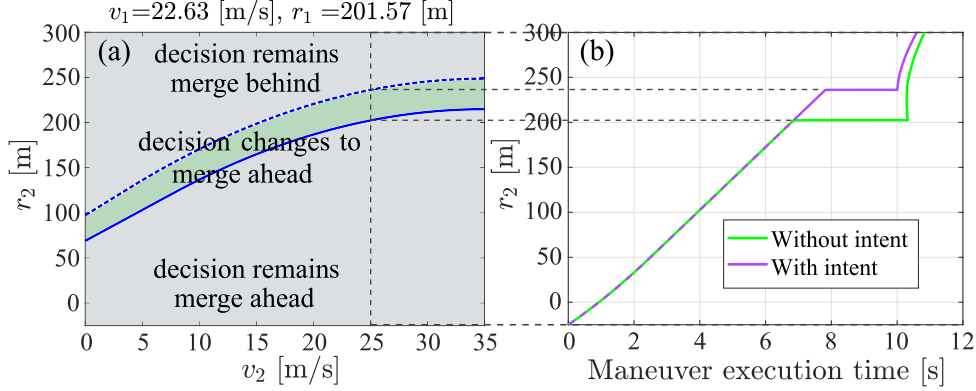


Figure 2.15: (a) Change of decision chart corresponding to the initial condition of the remote vehicle in Fig. 2.14. (b) Time needed for the CAV to execute the maneuver when choosing the initial condition along the dashed vertical line.

controller (2.36)-(2.40). The corresponding maneuver execution times are shown in Fig. 2.15(b) for status update rate 10 Hz. Observe that the execution time is significantly reduced in the domain where the decision changes due to intent. Even in the domain where the decision merge behind remains unchanged, having intent information still improves the time efficiency of the controller.

2.6 Summary

In this chapter, we established the concept of conflict analysis in order to help vehicles with different levels of automation and cooperation to prevent conflicts. We constructed conflict charts that allowed connected automated vehicles to make better decisions while utilizing status and intent messages received from remote vehicles via V2X communication. We also determined the communication range required to guarantee the existence of conflict-free maneuvers. We demonstrated that increasing the frequency of status updates can benefit the time efficiency of the ego vehicle. Moreover, we showed that sharing intent information that bounds the future speed and acceleration of remote vehicles leads to less conservatism in the decision making of the ego vehicle. Intent messages from remote vehicles also yield significant improvements in the time efficiency of the ego vehicle and such improvements cannot be replicated by merely sharing current status information more frequently. The results were demonstrated experimentally using real vehicles on a test track and by numerical simulations using real highway data.

In the next chapter, we will take a closer look at the conflict charts, and explore more efficient decision-making rules and control algorithms that can potentially maximize the time efficiency of the ego vehicle.

CHAPTER 3

Opportunistic Strategy in Conflict Analysis

In Chapter 2, we have established the concept of conflict analysis. This chapter extends conflict analysis framework by developing an optimization-based opportunistic strategy which can improve the ego vehicle's performance while guaranteeing a conflict-free maneuver at the same time.

We still use the merge scenario depicted in Fig. 2.1 in the previous chapter as an application example, which involves an ego vehicle and a remote vehicle. The vehicles' dynamical models are still given by (2.1). We assume that the ego vehicle receives status sharing messages via V2X, containing the current position and speed of the remote vehicle. For simplicity in stating the basic idea, in this chapter we restrict ourselves to status sharing without considering intent sharing. Note that, however, our analysis can be naturally extended to the intent sharing case.

Recall that in conflict analysis, we interpret messages transmitted by remote vehicles by means of conflict charts, which allow us to devise conflict-free controllers for the ego vehicle based on the message content and the state of the ego vehicle. By solving a constrained optimization problem, here we derive an opportunistic strategy that maximizes the possibility of the ego vehicle to merge ahead of the remote vehicle, while satisfying the conflict-free condition. This reduces the conservatism in the strategy proposed in Chapter 2 (referred to as conservative strategy in this chapter) in terms of the time efficiency of ego vehicle. These benefits are demonstrated by using traffic data taken on a highway in south-east Michigan.

3.1 Opportunistic Strategy

Let us first point out the conservatism of the decision making rule in Chapter 2 and highlight the potential benefits that may be obtained by the opportunistic strategy discussed further below.

3.1.1 Conservative strategy and potential opportunity

In Chapter 2, a conservative decision making rule 2.24 was proposed for the green region of the unified conflict chart. Within \mathcal{P}_g (green region below the blue boundary in Fig. 3.1(c)), there is

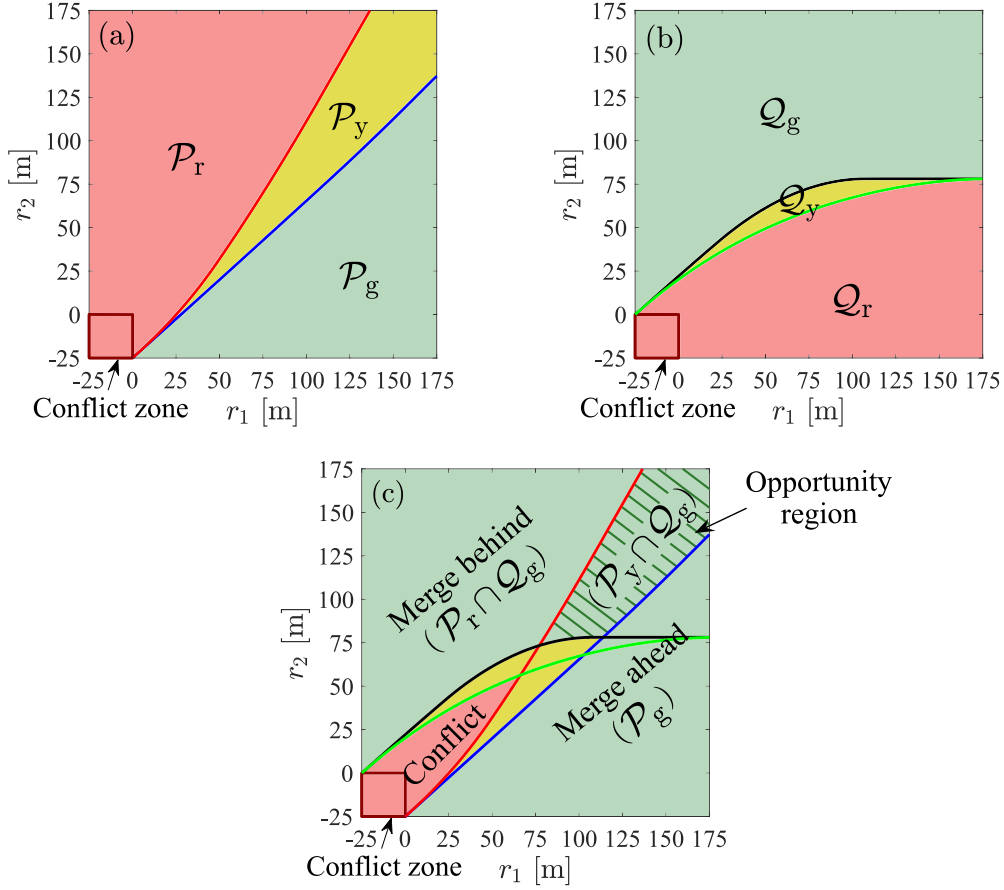


Figure 3.1: Conflict charts in the (r_1, r_2) -plane for $v_1 = 28$ [m/s] and $v_2 = 25$ [m/s]. (a)-(c) Conflict charts for merge ahead, merge behind, and the unified conflict chart. The opportunity region in panel (c) is highlighted by stripes. Here, we used $a_{\max,2} = 2$ [m/s] and $a_{\min,2} = -4$ [m/s²], while other parameters are the same as in Table 2.1.

no conflict with respect to proposition P and vehicle 2 is able to merge ahead without a conflict independent of the motion of vehicle 1. The decision for this region is indeed merge ahead. Note that merging ahead leads to higher time efficiency and thus has priority over merging behind. When merging ahead without conflict is not guaranteed but merging behind without conflict is guaranteed independent of the motion of vehicle 1 (green region above the blue boundary in Fig. 3.1(c)), then vehicle 2 decides to merge behind. Once the decision is made at the initial time, vehicle 2 sticks to it and executes it by choosing an appropriate control law. In Chapter 2, two separate controllers were designed for merging ahead and behind, which ensured conflict-free merge by keeping the evolution of the state inside the no-conflict sets \mathcal{P}_g and \mathcal{Q}_g , respectively. We refer to the above decision making rule and the corresponding control laws as the conservative strategy in the rest of this chapter.

To understand the conservatism one may notice that the merge behind decision is applied in two

different regions of the state space. In $\mathcal{P}_r \cap \mathcal{Q}_g$ (green region above the red boundary in Fig. 3.1(c)), merging ahead without conflict is not possible, and thus, merge behind is the only choice. On the other hand, in $\mathcal{P}_y \cap \mathcal{Q}_g$ (striped region between the red and blue boundaries in Fig. 3.1(c)), merging ahead without a conflict may be possible depending on the future behavior of vehicle 1. This may offer potential opportunities for vehicle 2 to merge ahead. The conservative strategy makes the decision of merge behind without pursuing the opportunity to merge ahead actively. We name this striped region in conflict chart the opportunity region, and we propose an opportunistic strategy, which tries to merge ahead in this region, while still ensuring a conflict-free merge.

In what following, we focus on the opportunity region $\mathcal{P}_y \cap \mathcal{Q}_g$ and discuss in detail an opportunistic strategy which consists of a decision checking mechanism and an optimization-based controller.

3.1.2 Decision checking mechanism

As conflict analysis shows, if the initial state is in the opportunity region (i.e., $x(0) \in \mathcal{P}_y \cap \mathcal{Q}_g$), then the ego vehicle may be able to merge ahead without a conflict depending on the motion of the remote vehicle. To prevent conflict, the ego vehicle decides to pursue the opportunity to merge ahead, while ensuring that a conflict-free merge behind is still guaranteed in the case that merge ahead is not possible. To execute this decision, one needs to solve a constrained optimization problem, which is discussed in detail in the next subsection. This initial decision will be revised later on as updates about the status of the remote vehicle become available. The decision can be changed to merge ahead if the system state evolves into the no-conflict set with respect to merge ahead (\mathcal{P}_g), i.e., the trajectory crosses the blue boundary in conflict charts (see Fig. 3.1(c)). On the other hand, the decision must be finalized as merge behind if the trajectory crosses the red boundary and enters $\mathcal{P}_r \cap \mathcal{Q}_g$ region.

This decision making rule is summarized as

$$\text{decision} = \begin{cases} \text{stick to merge ahead,} & \text{if } x(t_k) \in \mathcal{P}_g, \\ \text{pursue opportunity to merge ahead,} & \text{if } x(t_k) \in \mathcal{P}_y \cap \mathcal{Q}_g, \\ \text{stick to merge behind,} & \text{if } x(t_k) \in \mathcal{P}_r \cap \mathcal{Q}_g, \end{cases} \quad (3.1)$$

where $t_k, k = 0, 1, \dots$ represent the time when status sharing packets are received from the remote vehicle so that $t_0 = 0$ is the initial time. The left part of Fig. 3.2 visualizes this mechanism. At any t_k , if the state is in the opportunity region (i.e., $x(t_k) \in \mathcal{P}_y \cap \mathcal{Q}_g$), then the ego vehicle pursues the opportunity to merge ahead, but the decision will be reviewed at the next status update time t_{k+1} . If $x(t_k) \in \mathcal{P}_g$ (green region below the blue curve), the decision is set to merge ahead for $t \geq t_k$.

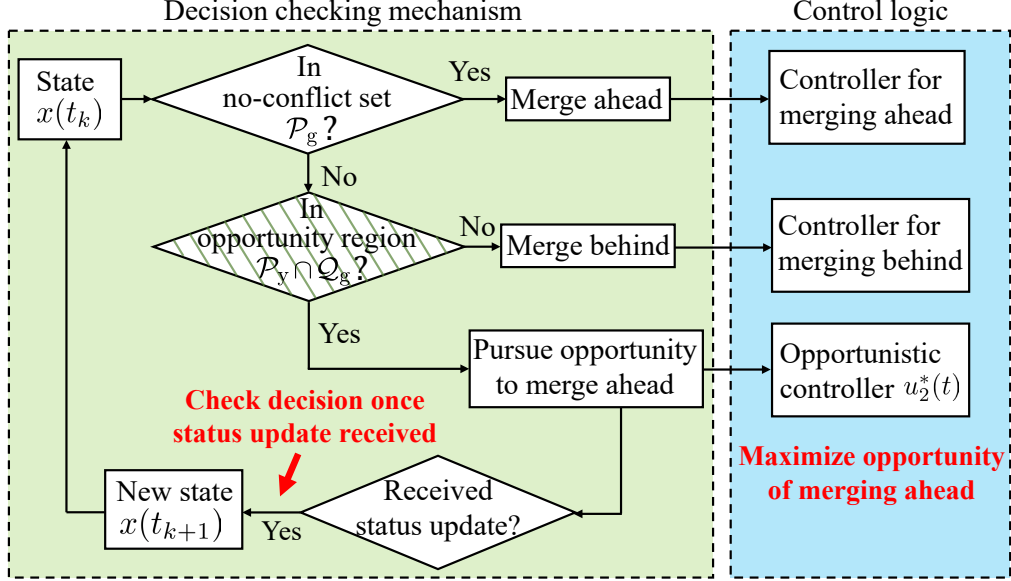


Figure 3.2: Block diagram of the opportunistic strategy.

Finally, if $x(t_k) \in \mathcal{P}_r \cap \mathcal{Q}_g$ (green region above the red boundary), then the decision is set to merge behind for $t \geq t_k$. We emphasize that in contrast to the conservative strategy (2.24) where the ego vehicle does not revise its decision, the decision checking (3.1) enables a potential decision change to merge ahead, which can improve the time efficiency of the ego vehicle.

3.1.3 Opportunistic controller

The decision checking mechanism allows the ego vehicle to take the opportunity of merging ahead, but whether it can merge ahead or not also depends on the future motion of the remote vehicle, which we do not have control over. Here we propose a control algorithm that maximizes the ego vehicle's chance to merge ahead while ensuring that it can still merge behind without conflict if its decision to merge ahead is not possible. The key idea is to “push” the system toward the blue boundary, i.e., toward set \mathcal{P}_g , while keeping it inside the no-conflict set \mathcal{Q}_g . This can be formulated as an optimization problem as discussed below.

Let $T_{\text{reach},1}(t)$ denote the time needed for the remote vehicle to reach the conflict zone and $T_{\text{exit},2}(t)$ the time needed for ego vehicle to exit the conflict zone, calculated at time t assuming $[u_1(t), u_2(t)]^\top \equiv [a_{\text{max},1}, a_{\text{max},2}]^\top$ as future inputs. Based on the definition of sets \mathcal{P}_g and \mathcal{P}_y , $x(t) \in \mathcal{P}_g$ if and only if $T_{\text{reach},1}(t) > T_{\text{exit},2}(t)$, while $T_{\text{reach},1}(t) \leq T_{\text{exit},2}(t)$ holds if $x(t) \in \mathcal{P}_y$. Define $\tilde{T}(t) := T_{\text{exit},2}(t) - T_{\text{reach},1}(t)$ and consider the state $x(t_k) \in \mathcal{P}_y \cap \mathcal{Q}_g$ such that $\tilde{T}(t_k) \geq 0$. In order for $x(t) \in \mathcal{P}_g$ at some $t > t_k$, $\tilde{T}(t) < 0$ must hold. Noting that $\tilde{T}(t)$ is a continuous function of t , pushing the state $x(t)$ from \mathcal{P}_y to \mathcal{P}_g is equivalent to decreasing $\tilde{T}(t)$ in t . Although we do not have

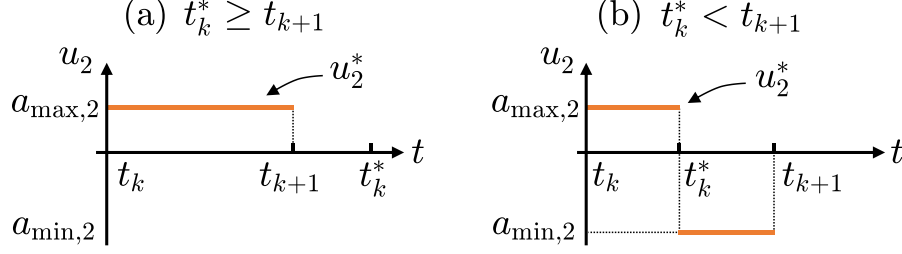


Figure 3.3: Optimal solution $u_2^*(t)$ for the time interval $t \in [t_k, t_{k+1})$ (between receiving two adjacent status sharing packets) when $t_k^* \geq t_{k+1}$ (a) and when $t_k^* < t_{k+1}$ (b). Here t_k^* predicts the time when the state will reach the black boundary of set \mathcal{Q}_g .

control over $T_{\text{reach},1}(t)$, we can ensure via $u_2(t)$ that $T_{\text{exit},2}(t)$ decreases the most.

Assuming $x(t_k) \in \mathcal{P}_y \cap \mathcal{Q}_g$, we formulate an optimization problem that minimizes the time derivative of $T_{\text{exit},2}(t)$ by shaping $u_2(t)$ within the time interval $[t_k, t_{k+1})$:

$$\begin{aligned}
 \min_{u_2(t) \in \mathbb{R}} \quad & J(t) = \frac{d}{dt} T_{\text{exit},2}(t), \quad \forall t \in [t_k, t_{k+1}), \\
 \text{subject to} \quad & \text{dynamics (2.1),} \\
 & x(t_k) \in \mathcal{P}_y \cap \mathcal{Q}_g, \\
 & x(t) \in \mathcal{Q}_g, \quad \forall t \in [t_k, t_{k+1}).
 \end{aligned} \tag{3.2}$$

Note that $\frac{d}{dt} T_{\text{exit},2}(t)$ depends on $u_2(t)$, and the optimal solution $u_2^*(t)$ ensures that $T_{\text{exit},2}(t)$ (and thus $\tilde{T}(t)$) decreases the most along $t \in [t_k, t_{k+1})$. This maximizes the opportunity of the state x evolving into the set \mathcal{P}_g . In the meantime, the last constraint ensures that a conflict-free merge behind is always possible.

Due to the simplicity of the dynamics (2.1), the optimal solution to (3.2) can be found analytically:

$$u_2^*(t) = \begin{cases} a_{\max,2}, & \text{if } t \in [t_k, t_k^*), \\ a_{\min,2}, & \text{if } t \in [t_k^*, t_{k+1}), \end{cases} \tag{3.3}$$

where t_k^* is the predicted time when the system state reaches the black boundary of set \mathcal{Q}_g assuming $[u_1(t), u_2(t)]^\top \equiv [a_{\min,1}, a_{\max,2}]^\top$ for $t \geq t_k$. Since the future motion of vehicle 1 is unknown, we must assume the “worst-case scenario” $u_1(t) \equiv a_{\min,1}$ to ensure $x(t) \in \mathcal{Q}_g$. Note that $a_{\max,2}$ minimizes the cost function, while $a_{\min,2}$ ensures that the constraints are satisfied under the “worst case scenario” (see Appendix E for the proof). Notice that $a_{\max,2}$ and $a_{\min,2}$ are not necessarily the physical limits of the ego vehicle, but can be parameters chosen by the users. In this chapter, we use $a_{\max,2} = 2$ [m/s] and $a_{\min,2} = -4$ [m/s²] (which are different from Table 2.1), while other parameters remain the same. We remark that if $t_k^* \geq t_{k+1}$, then we only need to assign $u_2^*(t) \equiv a_{\max,2}$

for $t \in [t_k, t_{k+1})$, otherwise we switch to $a_{\min,2}$ at time t_k^* ; see Fig. 3.3. Recursively, at t_{k+1} we check decision using $x(t_{k+1})$. If $x(t_{k+1}) \in \mathcal{P}_y \cap \mathcal{Q}_g$, then we calculate t_{k+1}^* and apply (3.3) again for $t \in [t_{k+1}, t_{k+2})$. One can prove that $t_{k+1}^* \geq t_k^*$, which means that status updates make the prediction less conservative.

Note that for $t_k^* < t_{k+1}$ (see Fig. 3.3(b)), if the remote vehicle's behavior does not follow the worst-case scenario, then $t_{k+1}^* > t_{k+1}$ holds. In this case, the optimal solution (3.3) switches from $a_{\max,2}$ to $a_{\min,2}$ at t_k^* and then back to $a_{\max,2}$ at t_{k+1} , which could result in passenger discomfort. Thus, for practical purposes, one may implement a sub-optimal solution, where after the earliest t_k^* such that $t_k^* < t_{k+1}$ holds, the decision is changed to merge behind and $u_2(t) = a_{\min,2}$ is applied without pursuing the opportunity again. The value of $u_2(t)$ may be updated to be less conservative as new status updates are received, similar to the controller for merging behind proposed in [89].

As a summary, the control law (3.3) pursues the opportunity of merging ahead but ensures that a conflict-free merge behind is always possible. The decision checking mechanism (3.1) together with the corresponding controller is referred to as the opportunistic strategy. We remark that V2X communication is essential to apply this strategy as this allows the ego vehicle to monitor whether and when it crosses the blue boundary of \mathcal{P}_g . This will be demonstrated in the next section by simulations.

3.2 Simulation with Real Highway Data

In this section, we demonstrate the benefits of opportunistic strategy using simulations with real highway data, and compare the results with the conservative strategy. We show that the opportunistic strategy can significantly improve the time efficiency of the ego vehicle by revising decisions as new information becomes available via V2X.

To represent the remote vehicle, we use data collected from a real human-driven vehicle approaching a junction on highway US-23 in south-east Michigan. The ego vehicle is assumed to be a connected automated vehicle merging from an on-ramp. At the initial time, the remote vehicle is 201.57 meters from the conflict zone traveling with speed 22.63 [m/s], while the ego vehicle is 210 meters from the conflict zone travelling with speed 25 [m/s]. The magenta cross in Fig. 3.4(a) marks the initial state in the conflict chart, which is located in the opportunity region. In this case, the conservative strategy decides to merge behind, while the opportunistic strategy applies the decision checking mechanism (3.1) and controller (3.3) allowing the ego vehicle to eventually change its decision and merge ahead. Fig. 3.4(b)-(c) depict the system state as time evolves until the ego vehicle exits the conflict zone. The magenta crosses are plotted every 100 ms corresponding to 10 Hz status updates rate. Although both strategies avoid conflict, the opportunistic strategy significantly improves time efficiency of the ego vehicle by merging ahead within 29% shorter

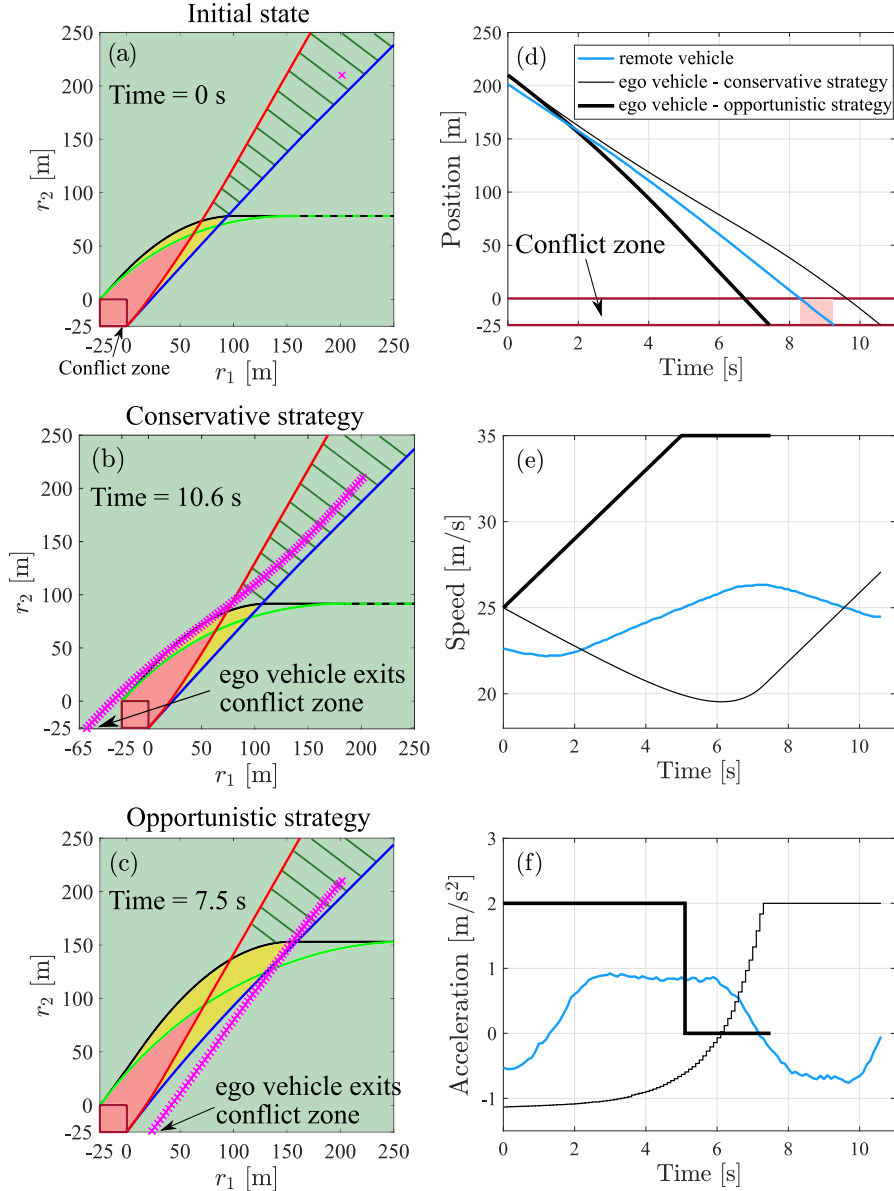


Figure 3.4: Simulation results of conservative and opportunistic strategies with initial state $r_1(0) = 201.57$ [m], $v_1(0) = 22.63$ [m/s], $r_2(0) = 210$ [m], and $v_2(0) = 25$ [m/s] when status sharing packets are received every 0.1 [s]. (a) initial state in conflict chart (magenta cross). (b)-(c) trajectories under conservative and opportunistic strategies (magenta crosses); (d)-(f): position, speed and acceleration profiles.

time. The corresponding time profiles are shown in Fig. 3.4(d)-(f) for the two different strategies. The conservative strategy updates the control input with status updates while keeping the decision the same. On the other hand, the opportunistic strategy is capable of updating the decision if such opportunity arises while still remaining conflict-free.

Figure 3.5(a)-(e) show the detailed evolution of trajectory under the opportunistic strategy. At

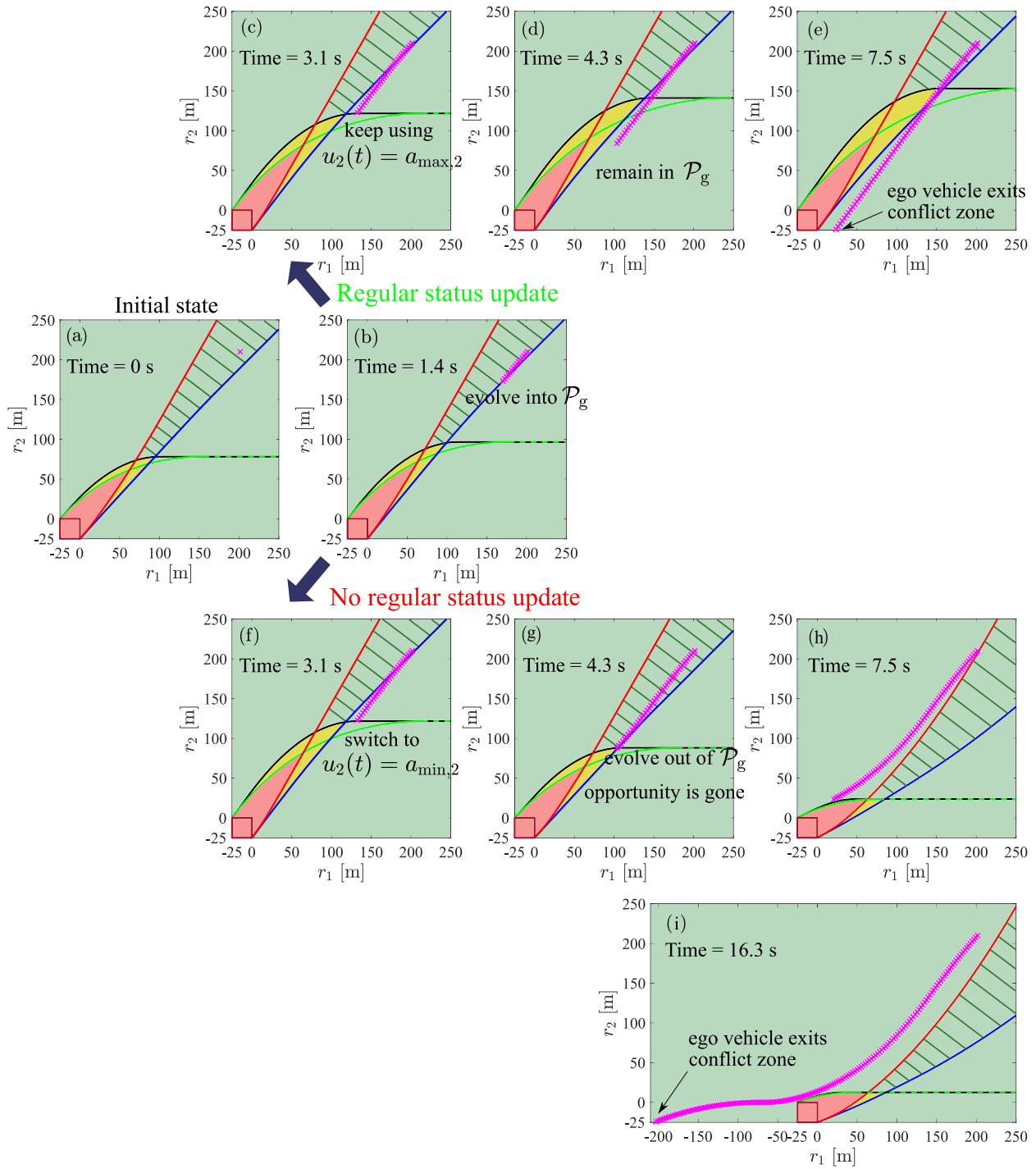


Figure 3.5: Sequences of trajectories with and without regular status update. (a)-(e) ego vehicle changes decision to merge ahead based on status update at 1.4 [s] and keeps using $u_2(t) \equiv a_{\max,2}$ to merge ahead. (a)-(b), (f)-(i) opportunity to merge ahead is missed without status update. Here, the state evolves out of \mathcal{P}_g at 4.3 [s] since the input $u_2(t) \equiv a_{\min,2}$ is used after 3.1 [s] to keep the state inside \mathcal{Q}_g and the ego vehicle eventually merges behind.

Table 3.1: Simulation results with ego vehicle’s initial state $r_2(0) = 210$ [m] and $v_2(0) = 25$ [m/s].

V2X condition	Regular status update		No regular status update	
Strategy	Conservative	Opportunistic	Conservative	Opportunistic
Maneuver result	merge behind	merge ahead	merge behind	merge behind

1.4 [s] (Fig. 3.5(b)), the trajectory crosses the blue boundary and enters set \mathcal{P}_g . Based on (3.1), the decision is changed to merge ahead, and the ego vehicle keeps using $a_{\max,2}$ to achieve this goal. However, if no status updates are available when the state enters set \mathcal{P}_g , then a decision change is not possible. Fig. 3.5(a)-(b), (f)-(i) show the evolution under opportunistic strategy without status update after the initial time. Although the trajectory crossed the blue boundary, the ego vehicle is not aware of it and, based on (3.3), the control input switches to $u_2(t) = a_{\min,2}$ at 3.1 [s] to keep the state inside Q_g (i.e., above the black boundary). At 4.3 [s], the state moves out of the \mathcal{P}_g region, and the opportunity to merge ahead is gone. Eventually, the ego vehicle merges behind the remote vehicle using 16.3 [s] compared to 7.5 [s] in the regular status update case. These results are summarized in Table 3.1. Consequently, maintaining regular V2X communication is essential to secure the benefits of opportunistic strategy.

3.3 Summary

In this chapter, we developed an opportunistic strategy for conflict prevention in cooperative maneuvering with the help of conflict analysis. We demonstrated that the proposed optimization-based strategy can significantly improve the time efficiency of the ego vehicle by revising its decision based on status updates received via V2X, while guaranteeing a conflict-free maneuver. The benefits are illustrated by simulations using real highway data. We showed that V2X connectivity is essential to apply this strategy as regular status updates are needed for successful decision revision.

So far conflict analysis has allowed us to study conflicts between two vehicles of different automation degrees. The corresponding decision-making and control strategies were investigated. In the following chapters, we will generalize conflict analysis to multi-vehicle cases, while considering more complex scenarios under more realistic models of vehicle dynamics and communication.

CHAPTER 4

Multi-Vehicle Conflict Analysis under Time Delays

In Chapters 2 and 3, we have developed the conflict analysis framework for two vehicles with different levels of automation. In this chapter, we scale up conflict analysis to accommodate more than two vehicles in mixed traffic. Moreover, in the previous chapters, perfect V2X communication (neglecting packet drops and information delays) was assumed, and a simplified vehicle dynamics model was used without considering computation and actuation delays. The ignored effects of time delays will be systematically studied in this chapter.

Prior studies have shown that time delay has significant influence on the performance of connected and automated vehicles, with most research efforts focusing on vehicle platooning scenarios [105, 106, 107, 108, 109, 110]. For example, time delay can contribute to the instability of vehicular chains, causing congestion and even accidents. A sizable amount of control strategies were also proposed to compensate the effects of time delay and to optimize vehicles' performances, including predictor feedback [111, 112] and data-based real-time optimization [113]. However, there exists a clear gap in the literature about how time delay affects conflict resolution, especially, in a mixed traffic environments in which vehicles possessing different cooperation capabilities and automation degrees interact with each other.

This chapter first develops necessary mathematical tools to generalize the framework of conflict analysis to multi-vehicle scenarios. Based on this, we systematically investigate the effects of delays in both vehicle dynamics and communications, considering both status-sharing and intent-sharing cooperation. Fig. 4.1(a)-(b) illustrate a cooperative maneuvering scenario where conflicts may arise. Here, a connected ego vehicle attempts to change to the right lane to move between two connected remote vehicles. To perform a lane change, the following two steps are needed for the ego vehicle: (i) keep its current lane and create adequate longitudinal distances from the two remote vehicles; (ii) change its lateral position to enter the target lane. In this study, we focus on the first step, while assuming the second step is conducted by lateral motion planning and control modules after the ego vehicle secures sufficient relative distances. We represent the safe distance buffers between the vehicles by two conflict zones attached to the remote vehicles (red rectangles in Fig. 4.1). To ensure a conflict-free maneuver, the ego vehicle must not overlap with either of these

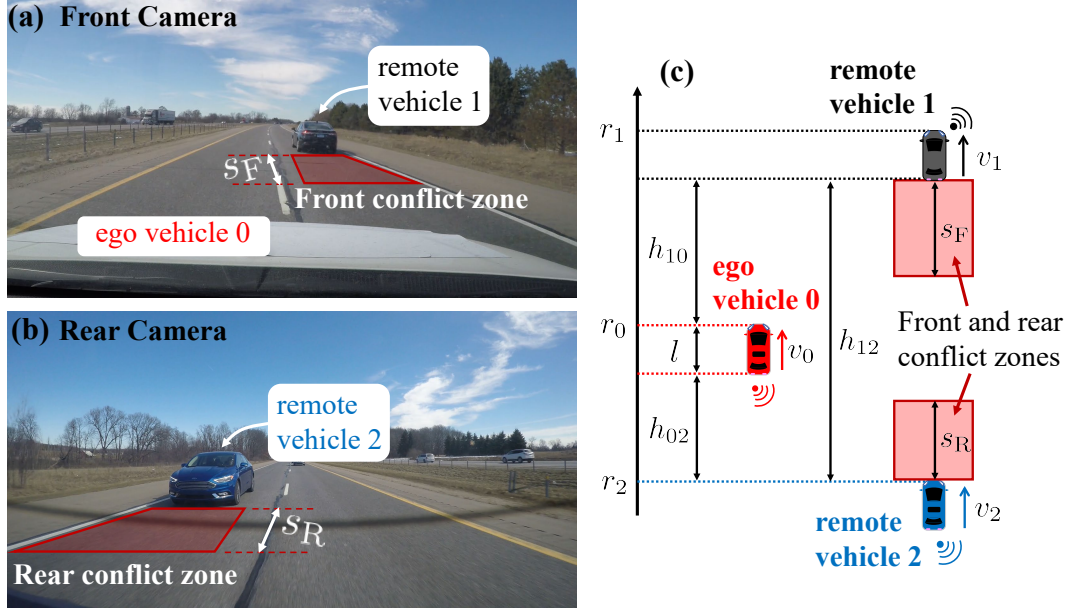


Figure 4.1: Potential conflict scenario in a cooperative maneuver between three vehicles. (a)-(b) Ego vehicle 0’s view from its front and rear cameras when performing a lane change between the remote vehicles 1 and 2. (c) Model showing the general scenario. Here, the front and rear conflict zones are highlighted by rectangles with red shadings.

conflict zones before initiating the lateral move. Note that the size and shape of conflict zones can vary depending on the traffic and road conditions.

As shown in Fig. 4.2, we consider two types of time delays in the system. On one hand, communication delay (highlighted by green shading) is associated with generating and compiling the V2X messages on the remote vehicles, transmitting these messages, and pre-processing the received data on the ego vehicle. On the other hand, time delay in the dynamics of the ego vehicle (indicated by red shading) results from on-board computation time, and from the actuation time in the powertrain and braking systems.

After incorporating these time delays, this chapter resolves conflicts from the ego vehicle’s viewpoint. Using reachability analysis, we propose a scalable method to calculate numerically the so-called no-conflict, uncertain, and conflict sets, which partition the state space into different domains with regard to conflict prevention. This enables fast and reliable decision making and control of the ego vehicle to guarantee conflict-free maneuvers. We study the effects of time delays on conflict prevention, and show that the information of intent substantially improves the decision and performance of the ego vehicle. Moreover, we propose a so-called goal-oriented controller to guarantee conflict-free maneuvers under time delays. This type of controller provides the designers with the freedom in choosing appropriate “goal state” to realize desired performance according to different design metrics (e.g., time and energy efficiencies, robustness). The extended framework

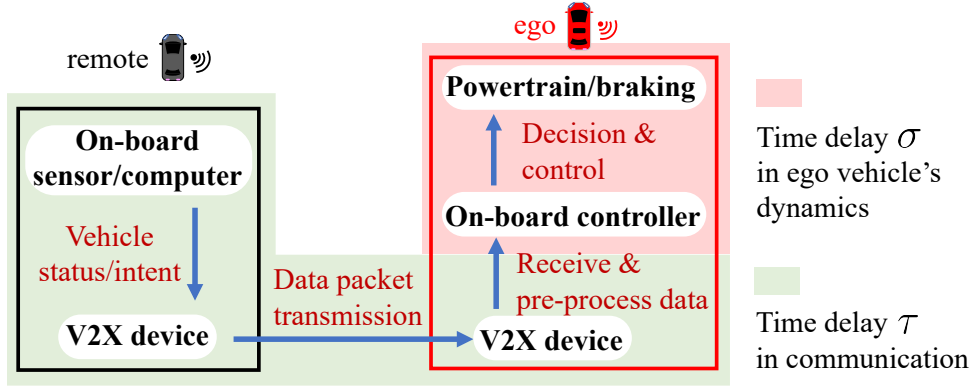


Figure 4.2: Time delays in the ego vehicle's dynamics and in the V2X communication between ego and remote vehicles.

of conflict analysis and the designed controller are demonstrated by utilizing real highway traffic data.

The contributions of this chapter are summarized below. (i) We generalize the conflict analysis framework to multi-vehicle case while accommodating time delays existing in both vehicle dynamics and V2X communication; (ii) we systematically quantify the effects of time delays on conflict in mixed autonomy environments, while revealing the benefits of intent sharing cooperation; (iii) we develop goal-oriented controller under time delays and demonstrate its applicability with real data.

The remainder of this chapter is structured in the following way. In Section 4.1, we mathematically construct the dynamic models of vehicles and provide details on the communication between vehicles. In Section 4.2, we build conflict analysis with status sharing while investigating the effects of time delays. Conflict analysis is then extended in Section 4.3 under intent sharing. In Section 4.4, we design goal-oriented controller and present simulations using real traffic data. Finally, Section 4.5 concludes this chapter.

4.1 Modeling Vehicle Dynamics and Communication

Fig. 4.1(a)-(b) show the scenario considered in this chapter, where the ego vehicle 0 intends to perform a lane change between the remote vehicles 1 and 2. For such maneuver, as previously stated, our analysis focuses on step (i), i.e., on vehicle 0 creating appropriate longitudinal distances before starting its lateral motion. In order to prevent conflicts, the minimum front and rear gaps represented by the lengths of conflict zones, s_F and s_R , must be secured by the ego vehicle. Here, to highlight the main idea of conflict analysis, we adopt a reasonable simplification by using constant s_F and s_R values, as given in Table 4.1. Such simplification is appropriate considering the limited

speed domains in scenarios of normal highway driving, while the results in this chapter can be extended to cases where s_F and s_R are not constant. The general model is shown in Fig. 4.1(c) where r_0 , r_1 and r_2 denote the vehicles' front bumper positions, and v_0 , v_1 and v_2 denote the vehicles' longitudinal velocities.

We describe the vehicles' longitudinal dynamics below, with the aerodynamic drag and rolling resistance neglected, as

$$\begin{aligned} \dot{r}_0(t) &= v_0(t), & \dot{v}_0(t) &= \text{sat}(u_0(t - \sigma)), \\ \dot{r}_i(t) &= v_i(t), & \dot{v}_i(t) &= \text{sat}(u_i(t)), \quad i = 1, 2, \end{aligned} \quad (4.1)$$

where the dot denotes the derivative with respect to time t , and u_0 , u_1 and u_2 are the control inputs. The limits of acceleration are modeled by the saturation function $\text{sat}(\cdot)$. For $v \in (v_{\min}, v_{\max})$, one has

$$\text{sat}(u) = \max \{ \min \{ u, a_{\max} \}, a_{\min} \}. \quad (4.2)$$

For $v = v_{\min}$, one shall substitute a_{\min} with 0, because the vehicle does not decelerate; for $v = v_{\max}$, one shall substitute a_{\max} with 0, since the vehicle does not accelerate. We remark that the values of acceleration and velocity limits depend on the road conditions and driving scenarios. Here we use limits corresponding to the typical driving behaviors on highways, with the assumption that the ego vehicle has the knowledge about their values; see Table 4.1. Note that the analysis in this chapter can be carried out with different parameter values, as demonstrated through simulations in Section 4.4.

We use σ to denote the time delay in the ego vehicle's dynamics, which comes from its on-board computation for decision making and control, and its powertrain and braking system; see the red-shaded part in Fig. 4.2. Note that delays in the dynamics of remote vehicles are not explicitly included in their models, representing the ego vehicle's limited knowledge about remote vehicles' dynamics. Still, as will be shown further below, our analysis implicitly handles the potential delays in the remote vehicles' dynamics.

We consider that the vehicles can use messages pertaining to two classes of cooperation via V2X communication: status sharing and intent sharing. In case of status sharing, the remote vehicles transmit their current positions r_1 , r_2 and velocities v_1 , v_2 . When the ego vehicle receives these messages, it can use the information for decision making and determining the control input u_0 . In case of intent sharing, the remote vehicles share information about their future trajectory, such as the range of speed and acceleration in addition to their current state. This allows the ego vehicle to obtain a better prediction of the future state of the remote vehicles. Note that we do not have control over the remote vehicles' motions, i.e., cannot prescribe inputs u_1 and u_2 .

As highlighted by the green shading in Fig. 4.2, time delay exists in the communication between

the remote and ego vehicles due to on-board sensing, and due to the transmission, propagation, and processing of V2X data packets. This type of delay is often referred to as communication latency. That is, the status and intent messages received by the ego vehicle contain delayed information of the remote vehicles. We use τ_1 and τ_2 to denote the communication delays of remote vehicles 1 and 2. For instance, the status messages received by the ego vehicle from the remote vehicles at a given time t contain $r_1(t - \tau_1)$, $v_1(t - \tau_1)$, $r_2(t - \tau_2)$, and $v_2(t - \tau_2)$. We assume that the values of τ_1 and τ_2 are known to the ego vehicle based on the GPS time stamps of the messages. Without loss of generality, we assume that the ego vehicle receives the V2X messages synchronously from both remote vehicles. The moment when the ego vehicle first receives a pair of status packets is defined as the system's initial time.

The vehicles' relative distances are defined as

$$h_{10} := r_1 - r_0 - l, \quad h_{02} := r_0 - r_2 - l, \quad h_{12} := r_1 - r_2 - l, \quad (4.3)$$

where h_{10} and h_{02} denote the front and rear gaps between the ego vehicle 0 and remote vehicles 1 and 2, respectively, and h_{12} denotes the total gap between the two remote vehicles; see Fig. 4.1(c). These gaps are signed bumper-to-bumper distances, where all three vehicles are assumed to have length l . Notice that $h_{12} = h_{10} + h_{02} + l \geq 0$ since we assume the remote vehicle 2 to be always traveling behind vehicle 1, which yields $h_{10} + h_{02} \geq -l$. Because of the critical role of relative distances (4.3) in lane change maneuvers, the state of the system (4.1) is defined as

$$x := [h_{10}, h_{02}, v_0, v_1, v_2]^T \in \Omega, \quad (4.4)$$

where Ω is given by

$$\Omega := \{[h_{10}, h_{02}]^T \in \mathbb{R}^2 \mid h_{10} + h_{02} \geq -l\} \times [v_{\min,0}, v_{\max,0}] \times [v_{\min,1}, v_{\max,1}] \times [v_{\min,2}, v_{\max,2}]. \quad (4.5)$$

In summary, so far we have established models for vehicle dynamics and communication. In the following sections we will carry out conflict analysis on these models.

Table 4.1: Parameters values used in the Chapter 4.

s_F, s_R	10 [m]	l	5 [m]
$a_{\min,0}$	-8 [m/s ²]	$a_{\min,1}, a_{\min,2}$	-4 [m/s ²]
$a_{\max,0}$	4 [m/s ²]	$a_{\max,1}, a_{\max,2}$	2 [m/s ²]
$v_{\min,0}$	22 [m/s]	$v_{\min,1}, v_{\min,2}$	25 [m/s]
$v_{\max,0}$	38 [m/s]	$v_{\max,1}, v_{\max,2}$	35 [m/s]

4.2 Multi-Vehicle Conflict Analysis with Status-sharing

This section establishes conflict analysis with status-sharing. We first provide a rigorous description of conflict using formal logic. Then we develop a method based on reachability analysis to construct disjoint sets in state space with distinct qualitative behaviors in terms of conflict prevention. In addition, we study the effects of delays, appearing in the dynamics and in communication, on conflict resolution.

Recall that to prevent conflict, the ego vehicle must secure the required relative distances before changing lanes in between the two remote vehicles. Such a conflict-free condition can be formalized by the proposition

$$P := \{\exists t \geq 0, h_{10}(t) \geq s_F \wedge h_{02}(t) \geq s_R\}, \quad (4.6)$$

where we use the symbol \wedge (and). Proposition P can be further decomposed into three cases:

- (i) No-conflict case: ego vehicle 0 is able to prevent conflict independent of the motion of remote vehicles 1 and 2.
- (ii) Uncertain case: ego vehicle 0 may be able to prevent conflict depending on the motion of remote vehicles 1 and 2.
- (iii) Conflict case: ego vehicle 0 is not able to prevent conflict independent of the motion of remote vehicles 1 and 2.

These cases correspond to three pairwise disjoint sets within Ω . Namely, we define

$$\mathcal{P}_g := \{x(0) \in \Omega \mid \forall u_1(t), \forall u_2(t), \exists u_0(t), P\}, \quad (4.7)$$

$$\mathcal{P}_y := \{x(0) \in \Omega \mid (\exists u_1(t), \exists u_2(t), \forall u_0(t), \neg P) \wedge (\exists u_1(t), \exists u_2(t), \exists u_0(t), P)\}, \quad (4.8)$$

$$\mathcal{P}_r := \{x(0) \in \Omega \mid \forall u_1(t), \forall u_2(t), \forall u_0(t), \neg P\}, \quad (4.9)$$

where the symbol \neg means negation, and $u_0(t)$, $u_1(t)$, and $u_2(t)$ are functions of time $t \geq 0$. These sets are referred to as no-conflict set, uncertain set, and conflict set, respectively. The corresponding domains are visualized in the state space with green, yellow, and red colors in the remaining of the chapter, and therefore, we use “g”, “y”, and “r” as subscripts. Note that the definition (4.8) contains two predicates which negate those of (4.7) and (4.9), i.e.,

$$(\exists u_1, \exists u_2, \forall u_0, \neg P) \iff \neg(\forall u_1, \forall u_2, \exists u_0, P), \quad (4.10)$$

$$(\exists u_1, \exists u_2, \exists u_0, P) \iff \neg(\forall u_1, \forall u_2, \forall u_0, \neg P). \quad (4.11)$$

Therefore, the sets \mathcal{P}_g , \mathcal{P}_y , and \mathcal{P}_r are indeed pairwise disjoint, and $\mathcal{P}_g \cup \mathcal{P}_y \cup \mathcal{P}_r = \Omega$.

4.2.1 Conflict analysis with time delay in dynamics

In this subsection, we develop theorems for conflict analysis considering time delay in the ego vehicle's dynamics while assuming zero communication delays for both remote vehicles.

Figure 4.3(a) and (b) show the sets \mathcal{P}_g , \mathcal{P}_y , and \mathcal{P}_r in (h_{10}, h_{02}) -plane for delays $\sigma = 0$ [s] and $\sigma = 0.5$ [s] in the ego vehicle's dynamics, respectively, while considering the velocities $(v_0, v_1, v_2) = (27, 29, 28)$ [m/s]. The domain outside the set Ω is left blank; cf. (4.5). These are, again, referred to as conflict charts, and their derivations are discussed further below. Given the current vehicle status the conflict charts can be used to determine the possibility of conflict-free lane change in the future. Notice that for any finite delay σ in the ego vehicle's dynamics, we have $\mathcal{P}_r = \emptyset$ if the parameters of behavior limits satisfy the condition

$$(v_{\max,1} > v_{\min,2}) \wedge (v_{\max,0} > v_{\min,2}) \wedge (v_{\min,0} < v_{\max,1}), \quad (4.12)$$

cf. parameters in Table 4.1. This condition enables the remote vehicles to create sufficiently large distance between them (if vehicle 1 speeds up and vehicle 2 decelerates), such that the ego vehicle can eventually perform a conflict-free lane change. Therefore, our focus will be the sets \mathcal{P}_g and \mathcal{P}_y throughout the rest of this subsection. We remark that if a maneuver needs to be completed within certain time deadline, then $\mathcal{P}_r = \emptyset$ may no longer hold and additional investigation on \mathcal{P}_r is needed. This will be studied in detail in the next chapter.

Next we introduce a method to check whether a given initial state $x(0)$ is located in the set \mathcal{P}_g or in the set \mathcal{P}_y . One may construct these sets by examining each state within Ω , but it is not necessary to compute them on-board. Instead, once receiving the latest V2X information, the ego vehicle only needs to determine which set the current system state belongs to. At the initial time, if $h_{10}(0) \geq s_F \wedge h_{02}(0) \geq s_R$ holds, then $x(0) \in \mathcal{P}_g$ holds immediately since the required front and rear gaps are already formed. Otherwise, it becomes necessary to examine whether the proposition P in (2.6) holds for some $t > 0$, while taking into account the ego and remote vehicles' all possible future trajectories. The following Lemma states that the remote vehicles' behavior limits shall be used to check $x(0) \in \mathcal{P}_g$.

Lemma 1. *For any given initial state $x(0) \in \Omega$, the following relationship holds:*

$$\begin{aligned} \{\forall u_1(t), \forall u_2(t), \exists u_0(t), P\} &\iff \\ \{(u_1(t), u_2(t)) \equiv (a_{\min,1}, a_{\max,2}), \exists u_0(t), \exists t \in T, h_{10}(t) \geq s_F \wedge h_{02}(t) \geq s_R\}, \end{aligned} \quad (4.13)$$

where $T = \{t \geq 0 | h_{12}(t) \geq s_F + s_R + l\}$.

Proof. See Appendix F. □

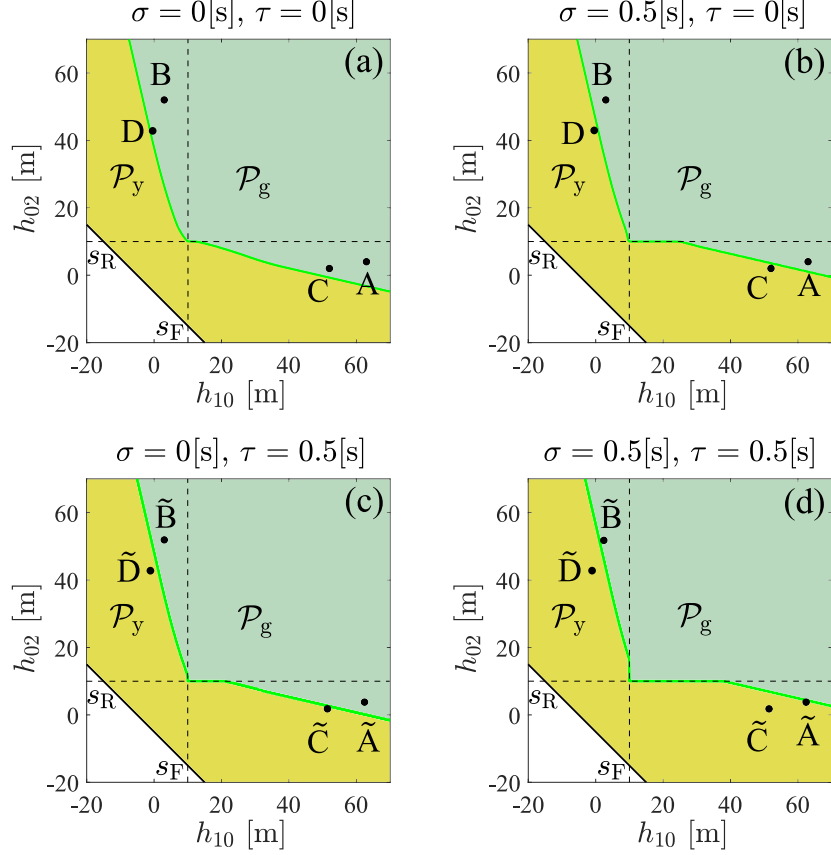


Figure 4.3: Conflict charts in (h_{10}, h_{02}) -plane under delay σ in the ego vehicle’s dynamics and communication delay $\tau_1 = \tau_2 = \tau$. (a) For initial velocities $(v_0(0), v_1(0), v_2(0)) = (27, 29, 28)$ [m/s] without delays. (b) For the same velocities as (a) with delay σ and control input history $u_0(t) = 0$ [m/s²], $t \in [-\sigma, 0]$. (c) For velocities $(v_0(0), v_1^{\text{est}}(0), v_2^{\text{est}}(0)) = (27, 26.7, 28.85)$ [m/s] with communication delay τ , where $v_1^{\text{est}}(0), v_2^{\text{est}}(0)$ are estimated based on Theorem 4. (d) For the same velocities as (c) with both delays σ and τ .

Here, T represents the time interval during which the total gap between the two remote vehicles is large enough for the ego vehicle to form the required front and rear gaps, assuming the remote vehicles’ worst-case behaviors given by their input limits. Combining (4.7) and (4.13), Lemma 1 suggests that to prevent conflict independent of remote vehicles’ behaviors, the ego vehicle must form the front and rear gaps within the time interval T . Thus, checking $x(0) \in \mathcal{P}_g$ is equivalent to checking the existences of an input $u_0(t)$ for $t \geq 0$ and a time $t \in T$ such that $h_{10}(t) \geq s_F \wedge h_{02}(t) \geq s_R$ holds under the remote vehicles’ worst-case behaviors. Note that with delay σ in the dynamics, control input assigned to the ego vehicle only “kicks in” after σ time. Therefore, the motion of the ego vehicle during the time interval $[0, \sigma]$ is determined by its control input history, i.e., $u_0(t)$, $t \in [-\sigma, 0]$. Also notice that the consideration of remote vehicles’ worst-case behaviors in Lemma 1 represents the most adversarial scenario even under the potential

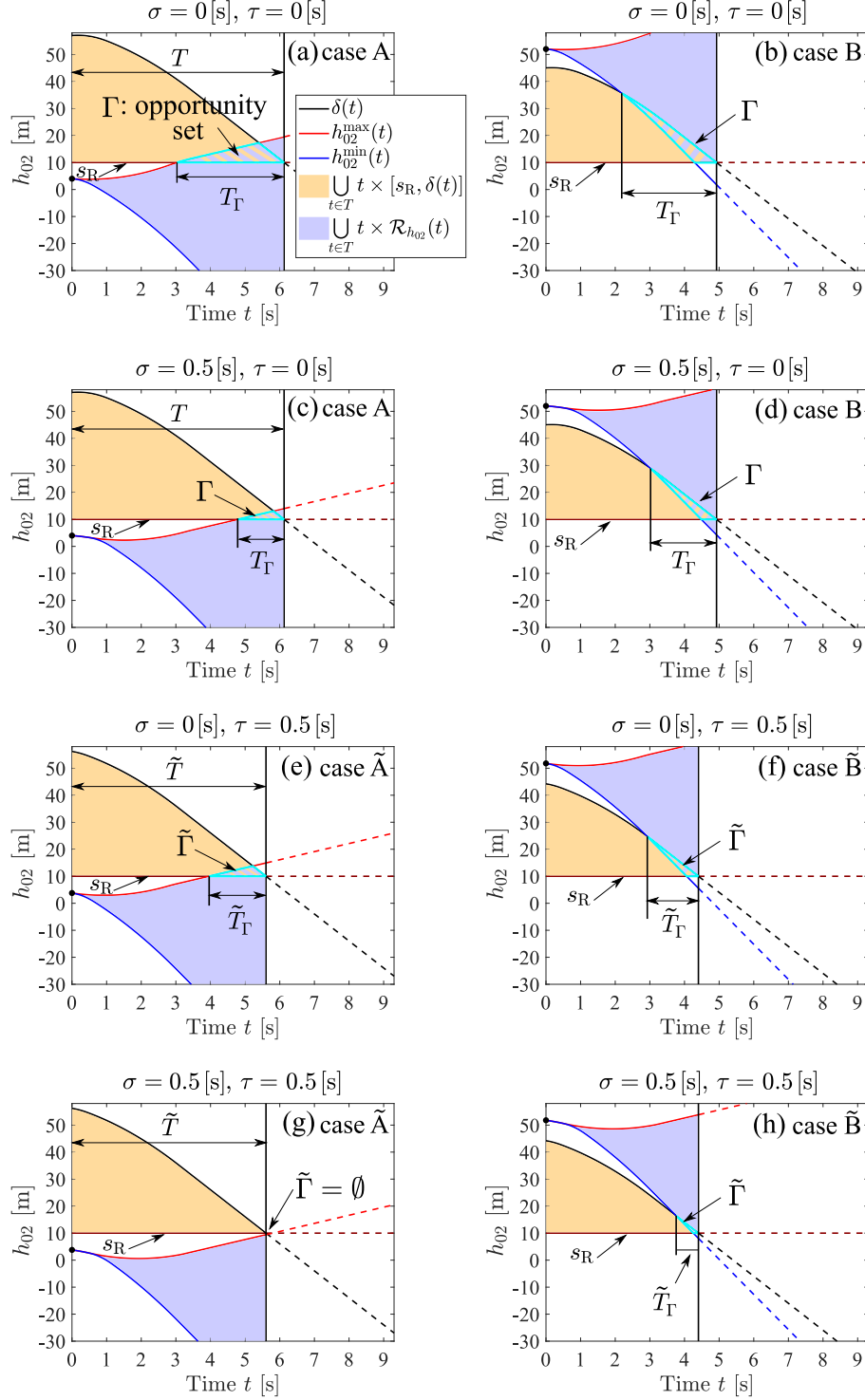


Figure 4.4: Opportunity set Γ for the indicated values of time delays with: (a)-(d) initial states corresponding to point A $(h_{10}(0), h_{02}(0)) = (63, 4)$ [m] and point B $(h_{10}(0), h_{02}(0)) = (3, 52)$ [m] in Fig. 4.3(a)-(b); (e)-(h) estimated initial states under communication delays corresponding to point \tilde{A} $(h_{10}^{\text{est}}(0), h_{02}^{\text{est}}(0)) = (62.43, 3.79)$ [m] and point \tilde{B} $(h_{10}^{\text{est}}(0), h_{02}^{\text{est}}(0)) = (2.43, 51.79)$ [m] in Fig. 4.3(c)-(d). Here, the input history $u_0(t) = 0$ [m/s²], $t \in [-\sigma, 0]$ is used for delay $\sigma > 0$.

delays in their dynamics. This conservatism implicitly includes the effects of the remote vehicles' unknown delays in their dynamics and the unknown control input histories. We remark that our analysis can be adapted to the case where the ego vehicle has the knowledge about the remote vehicles' delays in the dynamics and their corresponding control input histories, which will lead to less conservative results.

Now we are ready to state a theorem that allows us to determine whether conflict-free maneuvers are possible based on the behavioral limits of the ego vehicle and of the remote vehicles. More precisely, the Theorem below gives a reachability-based criterion to check $x(0) \in \mathcal{P}_g$.

Theorem 3. *Given the dynamics (4.1)-(4.2) and the initial state $x(0) \in \Omega$, $x(0) \in \mathcal{P}_g$ holds if and only if the condition*

$$\Gamma := \bigcup_{t \in T} t \times [s_R, \delta(t)] \cap \bigcup_{t \in T} t \times \mathcal{R}_{h_{02}}(t) \neq \emptyset, \quad (4.14)$$

is satisfied under $(u_1(t), u_2(t)) \equiv (a_{\min,1}, a_{\max,2})$, where

$$\delta(t) = h_{12}(t) - s_F - l, \quad (4.15)$$

$$\mathcal{R}_{h_{02}}(t) = [h_{02}^{\min}(t), h_{02}^{\max}(t)], \quad (4.16)$$

and the analytical forms of $\delta(t)$, $h_{02}^{\min}(t)$, and $h_{02}^{\max}(t)$ are given in Appendix G.

Proof. See Appendix H. □

Noting that $h_{02} = h_{12} - h_{10} - l$, the $\delta(t)$ given in (4.15) represents the maximum allowed rear gap at the time t to ensure a sufficiently large front gap, i.e., $h_{10}(t) \geq s_F$, given the total gap $h_{12}(t)$. Thus, the set $\bigcup_{t \in T} t \times [s_R, \delta(t)] \subseteq T \times \mathbb{R}$ contains the time t and the rear gap values h_{02} such that the conflict-free condition $h_{10}(t) \geq s_F \wedge h_{02}(t) \geq s_R$ holds under the remote vehicles' worst-case behaviors, while ignoring the ego vehicle's motion capability; see the orange shaded region in Fig. 4.4(a). Note that $\delta(t) \geq s_R$ defines the time interval T (cf. Lemma 1), when an adequate gap exists between the remote vehicles 1 and 2. On the other hand, the set $\bigcup_{t \in T} t \times \mathcal{R}_{h_{02}}(t) \subseteq T \times \mathbb{R}$ gives all rear gap values that the ego vehicle is able to reach along the time interval T , which corresponds to the projection of the (space-time) reachable tube of system (4.1) onto (t, h_{02}) ; see the light purple shaded region in Fig. 4.4(a). Note that for any given time $t > 0$, $\mathcal{R}_{h_{02}}(t)$ can be described by a lower bound $h_{02}^{\min}(t)$ and an upper bound $h_{02}^{\max}(t)$; see the blue and red curves in Fig. 4.4(a). They are calculated using the input limits $(u_0(t), u_2(t)) \equiv (a_{\min,0}, a_{\max,2})$ and $(u_0(t), u_2(t)) \equiv (a_{\max,0}, a_{\max,2})$ on $t > 0$, while considering a given input history $u_0(t)$ on $t \in [-\sigma, 0]$. Thus, the intersection Γ of the sets $\bigcup_{t \in T} t \times [s_R, \delta(t)]$ and $\bigcup_{t \in T} t \times \mathcal{R}_{h_{02}}(t)$ defined in (4.14) gives all feasible rear gaps and the corresponding times when the ego vehicle can secure

$h_{10}(t) \geq s_F \wedge h_{02}(t) \geq s_R$ independent of the remote vehicles' behaviors; see the striped region in Fig. 4.4(a). Such set Γ is referred to as opportunity set, and the time window covered, called opportunity window, is denoted by T_Γ .

Note that since the ego vehicle has the knowledge of its own control input history, it is sufficient to construct the opportunity set Γ for the given history of $u_0(t)$ under delay σ . On the other hand, to ensure that a conflict-free maneuver exists independent of the ego vehicle's control input history, the set Γ needs to be constructed considering all possible histories, i.e., all functions $u_0(t)$, $t \in [-\sigma, 0]$. We remark that this is consistent with the infinite-dimensional nature of time delay systems [114, 115], but is outside the scope of this study. We leave the corresponding analysis for future work.

It is emphasized that using Theorem 3, checking $x(0) \in \mathcal{P}_g$ is converted to examining the intersection of two analytically given sets. This is implementable in real time by applying simple yet efficient numerical algorithms. On the other hand, with more detailed vehicle dynamics, analytical form of the set $\mathcal{R}_{h_{02}}(t)$ may no longer be available. In this case reachable sets can still be constructed using a plethora of approximation techniques [116]. The ego vehicle's decision on its maneuver can be made based on the opportunity set Γ . If $\Gamma \neq \emptyset$, i.e., $x(0) \in \mathcal{P}_g$, then conflict is preventable, and the ego vehicle shall decide to pursue the opportunity of changing the lane. If $\Gamma = \emptyset$, i.e., $x(0) \in \mathcal{P}_y$, then a conflict-free lane change is not guaranteed. In such a scenario the ego vehicle shall decide to stay in its current lane.

Having established the theoretical base for conflict analysis under time delay σ , let us now investigate the effects of σ on conflict resolution. Fig. 4.4(a)-(b) illustrate the opportunity sets corresponding to the initial states given by points A and B in the conflict chart in Fig. 4.3(a) without delay ($\sigma = 0$ [s]). Note that in case A the ego vehicle is initially behind both remote vehicles, while in case B the ego vehicle is initially in front of them. For delay $\sigma = 0.5$ [s], the opportunity sets for initial states A and B are constructed in Fig. 4.4(c)-(d) for the control input history $u_0(t) \equiv 0$ on $t \in [-\sigma, 0]$; see also Fig. 4.3(b) for the corresponding conflict chart. In fact, as delay σ in the dynamics increases, the opportunity set Γ shrinks, independent of the given initial state and control command history. This is summarized in the following corollary.

Corollary 3. *Given initial state $x(0) \in \Omega$, let Γ and $\hat{\Gamma}$, and T_Γ and \hat{T}_Γ be the opportunity sets and their time windows under delays σ and $\hat{\sigma}$ in the ego vehicle's dynamics, such that $\sigma \leq \hat{\sigma}$. Then, we have*

$$\Gamma \supseteq \hat{\Gamma}, \quad T_\Gamma \supseteq \hat{T}_\Gamma. \quad (4.17)$$

Moreover, let \mathcal{P}_g and $\hat{\mathcal{P}}_g$, and \mathcal{P}_y and $\hat{\mathcal{P}}_y$ be the no-conflict sets and uncertain sets corresponding

to σ and $\hat{\sigma}$. Then

$$\mathcal{P}_g \supseteq \hat{\mathcal{P}}_g, \quad \mathcal{P}_y \subseteq \hat{\mathcal{P}}_y. \quad (4.18)$$

That is, the green no-conflict set shrinks whereas the yellow uncertain set expands as delay σ increases. The relationship (4.17) can be shown from the fact that larger delay in the dynamics leads to smaller set $\mathcal{R}_{h_{02}}(t)$ in (4.14). The relationship (4.18) can then be derived from (4.17) and Theorem 3.

The heat map shown in Fig. 4.5(a) quantifies the decrease of the opportunity window $\Delta T_\Gamma := |\hat{T}_\Gamma| - |T_\Gamma|$ when delay in the dynamics increases from 0 [s] to 0.5 [s]. Solid and dashed green curves correspond to the boundaries between the no-conflict and uncertain domains for $\sigma = 0$ [s] and $\sigma = 0.5$ [s] respectively. Here, the norm $|\cdot|$ measures the length of one-dimensional set. The stripped region corresponds to scenarios where the no-conflict domain changed to the uncertain domain as the delay in dynamics increased; see initial states represented by points C and D. In this region the ego vehicle cannot be certain of a conflict-free lane change any more, and thus decides not to undertake a lane change between the remote vehicles. In the region where the decision of the ego vehicle remains to change lane, the opportunity window still decreases; see the region above the dashed green boundary.

Figure 4.5(b) quantifies the opportunity window length $|T_\Gamma|$ while varying delay σ in the dynamics for initial states A-D. The slopes of the indicated segments on these curves being smaller than -1 reveals that the increase of delay in the dynamics can result in significantly larger decrease of opportunity window for conflict-free maneuvers. This contradicts an intuition that every 0.1 [s] of delay results in 0.1 [s] degradation of the opportunity window. The slope differences between cases A and B (and also between cases C and D) result from the fact that the ego vehicle was initially traveling slower than both remote vehicles. Thus, the increase of delay σ impacts more opportunity of changing lane from back (cases A and C) than changing lane from front (cases B and D).

To summarize, so far we have developed an efficient method for conflict analysis with time delay in vehicle dynamics via Theorem 3. This allowed us to quantify the effects of this delay in terms of the degradation of opportunity window for a conflict-free lane change. The established theory provides a basis for further analysis under the communication time delays as discussed in the subsection below.

4.2.2 Conflict analysis with time delays in communication

In this subsection, we extend conflict analysis to the case when communication delays τ_1 and τ_2 exist in the status information of the remote vehicles 1 and 2.

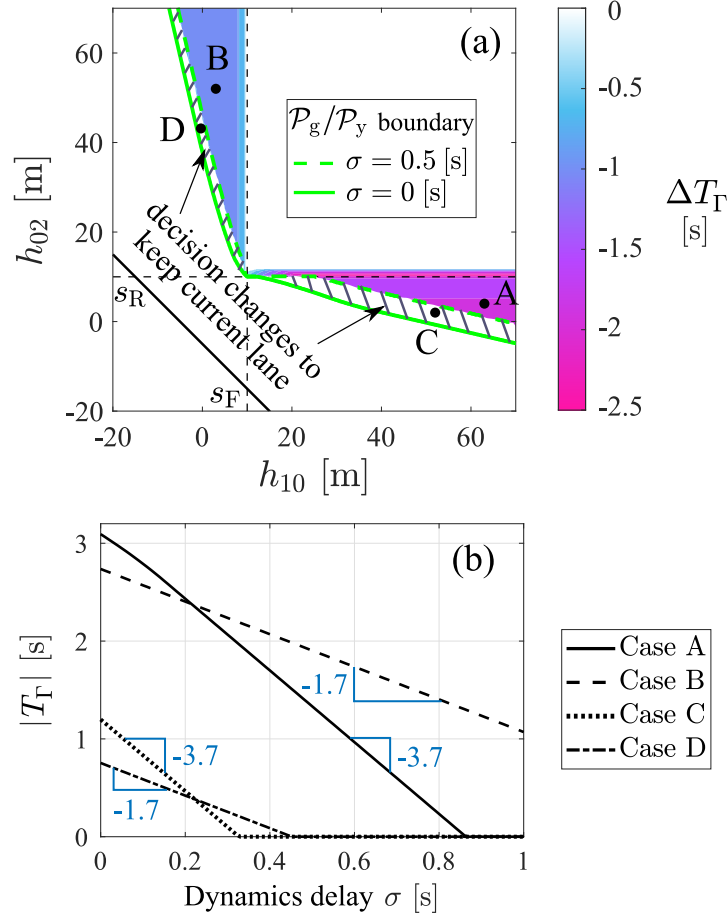


Figure 4.5: (a) Heat map showing the decrease of opportunity window $\Delta T_\Gamma = |\hat{T}_\Gamma| - |T_\Gamma|$ when delay in the ego vehicle's dynamics increases from $\sigma = 0$ [s] to $\sigma = 0.5$ [s]. (b) Opportunity window length evaluated as a function of delay σ for initial state cases represented by points A-D in Fig. 4.3(a)-(b), where $(v_0(0), v_1(0), v_2(0)) = (27, 29, 28)$ [m/s], and A $(h_{10}(0), h_{02}(0)) = (63, 4)$ [m], B $(h_{10}(0), h_{02}(0)) = (3, 52)$ [m], C $(h_{10}(0), h_{02}(0)) = (52, 2)$ [m], and D $(h_{10}(0), h_{02}(0)) = (-0.5, 43)$ [m].

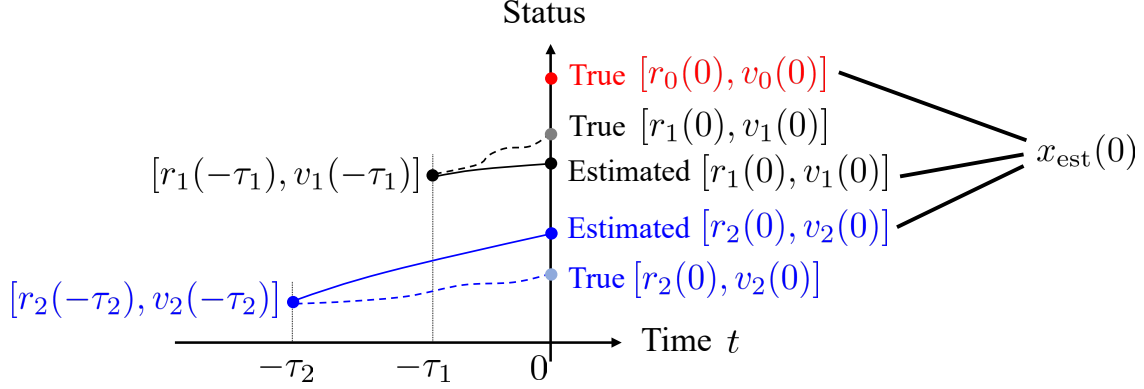


Figure 4.6: Conceptual illustration of estimating current system state at the initial time $t = 0$ under communication delays τ_1 and τ_2 . The dashed curves represent the remote vehicles' true behaviors during the time intervals $[-\tau_1, 0]$ and $[-\tau_2, 0]$, while the solid curves represent the worst case estimation according to Theorem 4.

As illustrated in Fig. 4.6, at the initial time, the ego vehicle has access to its own current status $r_0(0), v_0(0)$, and the remote vehicles' delayed status $r_1(-\tau_1), v_1(-\tau_1), r_2(-\tau_2)$, and $v_2(-\tau_2)$. That is, the exact initial state $x(0)$ is no longer available to the ego vehicle, and thus, checking $x(0) \in \mathcal{P}_g$ is not implementable. We remark, however, that while the communication delays compromise the ego vehicle's awareness of the exact current state, the sets $\mathcal{P}_g, \mathcal{P}_y$, and \mathcal{P}_r remain the same, still representing the ground truth of conflict prevention based on state values; see definitions in (4.7)-(4.9).

Since the ego vehicle has no knowledge about the actual behaviors of the remote vehicles 1 and 2 during the past time intervals $[-\tau_1, 0]$ and $[-\tau_2, 0]$, we modify the propositions corresponding to no-conflict, uncertain, and conflict cases as

$$\tilde{\mathcal{P}}_g := \{\forall u_1(t) \text{ on } t \geq -\tau_1, \forall u_2(t) \text{ on } t \geq -\tau_2, \exists u_0(t) \text{ on } t \geq 0, P\}, \quad (4.19)$$

$$\tilde{\mathcal{P}}_y := \{\exists u_1(t) \text{ on } t \geq -\tau_1, \exists u_2(t) \text{ on } t \geq -\tau_2, \forall u_0(t) \text{ on } t \geq 0, \neg P\} \quad (4.20)$$

$$\wedge \{\exists u_1(t) \text{ on } t \geq -\tau_1, \exists u_2(t) \text{ on } t \geq -\tau_2, \exists u_0(t) \text{ on } t \geq 0, P\}, \quad (4.21)$$

$$\tilde{\mathcal{P}}_r := \{\forall u_1(t) \text{ on } t \geq -\tau_1, \forall u_2(t) \text{ on } t \geq -\tau_2, \forall u_0(t) \text{ on } t \geq 0, \neg P\}, \quad (4.22)$$

cf. in (4.7)-(4.9). Note that independent of the given (delayed) vehicle status, the parameter condition (4.12) still allows the remote vehicles to form adequately large distance to eventually enable a conflict-free lane change, which yields $\tilde{\mathcal{P}}_r = \text{false}$ (and thus, $\mathcal{P}_r = \emptyset$ still holds). Therefore, we focus on propositions $\tilde{\mathcal{P}}_g$ and $\tilde{\mathcal{P}}_y$ in the rest of this subsection.

The following Theorem reveals that by appropriately estimating the current state, the methodology introduced in the previous subsection can be applied to determine if a conflict is preventable

under communication delays.

Theorem 4. *Given the dynamics (4.1)-(4.2) and vehicle status $r_0(0)$, $v_0(0)$, $r_1(-\tau_1)$, $v_1(-\tau_1)$, $r_2(-\tau_2)$, and $v_2(-\tau_2)$, the following relationships hold:*

$$\tilde{\mathcal{P}}_g \iff x_{\text{est}}(0) \in \mathcal{P}_g, \quad (4.23)$$

$$\tilde{\mathcal{P}}_y \iff x_{\text{est}}(0) \in \mathcal{P}_y, \quad (4.24)$$

where $x_{\text{est}}(0)$ is the estimated initial state using $u_1(t) \equiv a_{\min,1}$ for $t \in [-\tau_1, 0)$ and $u_2(t) \equiv a_{\max,2}$ for $t \in [-\tau_2, 0)$.

Proof. See Appendix I. □

Theorem 4 suggests that under communication delays, conflict shall be reasoned about using the estimated initial state $x_{\text{est}}(0)$, considering the remote vehicles' worst-case behaviors during the communication delay intervals; see Fig. 4.6 for a conceptual illustration. Theorem 3 can then be applied to check $x_{\text{est}}(0) \in \mathcal{P}_g$ by constructing the opportunity set using $x_{\text{est}}(0)$. This way, although the actual initial state $x(0)$ is unknown to the ego vehicle, $x(0) \in \mathcal{P}_g$ can be inferred by checking $x_{\text{est}}(0) \in \mathcal{P}_g$ since

$$x_{\text{est}}(0) \in \mathcal{P}_g \implies x(0) \in \mathcal{P}_g. \quad (4.25)$$

Note that the reverse direction in (4.25) does not hold, implying the conservatism in estimating $x_{\text{est}}(0)$. On the other hand, as discussed in the next section, this conservatism can be mitigated when the intent information of remote vehicles is available.

In the rest of this chapter, we use $\tau_1 = \tau_2 = \tau$ for simplicity of presentation, but all results can be easily generalized for $\tau_1 \neq \tau_2$. Fig. 4.3(c)-(d) show conflict charts for the same delay σ in the dynamics as Fig. 4.3(a)-(b), but with communication delays $\tau_1 = \tau_2 = \tau = 0.5$ [s]. Here, we use the velocities $(v_0(0), v_1^{\text{est}}(0), v_2^{\text{est}}(0)) = (27, 28.2, 28.35)$ [m/s], where $v_1^{\text{est}}(0)$ and $v_2^{\text{est}}(0)$ are the estimated initial velocities of remote vehicles based on Theorem 4, for the given delayed velocities $(v_1(-\tau), v_2(-\tau)) = (28.7, 27.85)$ [m/s]. Note that in this example, the actual behaviors of remote vehicles on $t \in [-\tau, 0)$ are given as $u_1(t) \equiv 0.6$ [m/s²] and $u_2(t) \equiv 0.3$ [m/s²] such that the actual initial velocities $v_1(0)$ and $v_2(0)$ are the same as in Fig. 4.3(a)-(b). In general, the actual behaviors of remote vehicles during the delay time intervals may be given by any (infinitely-many) feasible functions $u_1(t)$ and $u_2(t)$ on $t \in [-\tau, 0)$, and the delayed status of remote vehicles, i.e., $r_1(t)$, $v_1(t)$, $r_2(t)$, $v_2(t)$, $t \in [-\tau, 0)$, correspond to these histories. This again reflects the infinite-dimensional nature of time delay systems, which makes the analysis challenging. However, this difficulty is bypassed by the conservatism in our approach, where the worst-case behaviors of remote vehicles are considered over the delay intervals for any given delayed status; see Theorem 4.

We also remark that compared to Fig. 4.3(a)-(b), the conflict charts under communication delays in Fig. 4.3(c)-(d) in fact show a different 2D slice of the set Ω corresponding to the estimated initial velocities. Due to conservatism in estimating the remote vehicles' velocities, the 2D slice of no-conflict set \mathcal{P}_g in (h_{10}, h_{02}) -plane shrinks, while the 2D slice of uncertain set \mathcal{P}_y expands (although \mathcal{P}_g and \mathcal{P}_y remain the same in the 5D set Ω).

Now we are ready to investigate the effects of communication delay in conflict resolution. The points \tilde{A} - \tilde{D} in Fig. 4.3(c)-(d) represent the estimated initial states $x_{\text{est}}(0)$ corresponding to the actual initial states A-D in Fig. 4.3(a)-(b) given the communication delay $\tau = 0.5$ [s]. The conflict analysis of cases \tilde{A} and \tilde{B} are shown in Fig. 4.4(e)-(h) for the indicated time delays. For the same delay in the dynamics, the additional communication delay makes the opportunity set shrink; cf. Fig. 4.4(a)-(d). With both delays considered, the opportunity set vanishes for case \tilde{A} , which corresponds to \tilde{A} being in the uncertain set \mathcal{P}_y in Fig. 4.3(d). In fact, as the communication delay increases, the ego vehicle expects a shorter opportunity window for conflict-free lane change, and smaller freedom in choosing proper front and rear gap values to achieve the maneuver. This is summarized in the following corollary.

Corollary 4. *Given delay σ in the dynamics, the ego vehicle's initial status at $t = 0$, and the remote vehicles' delayed status at times $t = -\tau$ and $t = -\tilde{\tau}$, where $0 \leq \tau \leq \tilde{\tau}$. Let Γ and $\tilde{\Gamma}$, and T_Γ and \tilde{T}_Γ be the opportunity sets and the corresponding opportunity windows for the communication delays τ and $\tilde{\tau}$. Then we have*

$$T_\Gamma \supseteq \tilde{T}_\Gamma, \quad |\Gamma(t)| \geq |\tilde{\Gamma}(t)|, \quad \forall t \in T_\Gamma, \quad (4.26)$$

where $\Gamma(t)$ and $\tilde{\Gamma}(t)$ are slices of Γ and $\tilde{\Gamma}$ at time t .

This relationship can be shown from the fact that larger communication delay results in more conservative estimated initial state $x_{\text{est}}(0)$. Note that $\Gamma \supseteq \tilde{\Gamma}$ does not hold in general. Fig. 4.7(a)-(b) quantify the opportunity window length $|T_\Gamma|$ while varying communication delay τ for delays $\sigma = 0$ and 0.5 [s] in the dynamics. Again, increasing communication delay results in the shrinking of the opportunity window at a rate higher than 1, suggesting an amplified effect of communication delay. This again contradicts the intuition that every 0.1 [s] of delay results in 0.1 [s] degradation of the opportunity window.

The lower 3D surface in Fig. 4.8(a) illustrates the opportunity window length $|T_\Gamma|$ as a function of delays in both dynamics and communication for initial state case A, while Fig. 4.8(b) shows the contours of $|T_\Gamma|$ on the (σ, τ) -plane. The contour $|T_\Gamma| = 0$ gives the critical value combinations of delays σ and τ such that the opportunity set disappears, i.e., a conflict-free lane change is no longer guaranteed for larger delay values. We remark that the gradient of the 3D surface and the critical delay combination indeed depend on the initial states, but the qualitative behaviors remain similar.

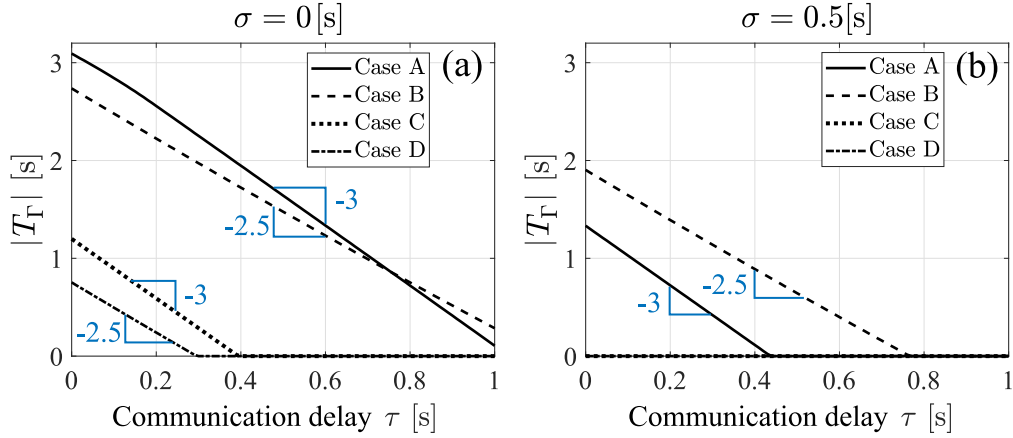


Figure 4.7: The length of the opportunity window evaluated as a function of communication delay τ for initial state cases A-D and different delays σ in the dynamics of ego vehicle.

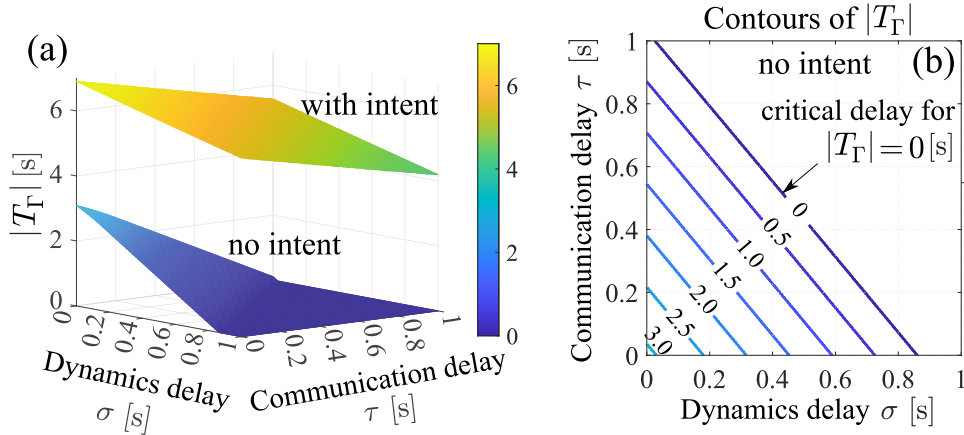


Figure 4.8: (a) Length of the opportunity window while varying the delay σ in the dynamics and communication delay τ with and without the intent information from remote vehicles for initial state case A. (b) Contours of opportunity window of the lower 3D surface (no-intent case).

In summary, we extended the conflict analysis framework to include time delays in communication by using the estimated initial state as illustrated by Theorem 4. The effects of both delays in vehicle dynamics and communication have been quantified. The next section introduces a V2X connectivity-enabled approach to compensate the negative effects of time delays by utilizing the remote vehicles' intent information.

4.3 Multi-Vehicle Conflict Analysis with Intent Information

This section extends conflict analysis to the case where the ego vehicle receives the remote vehicles' intent information. We show that intent sharing helps the ego vehicle to predict more accurately the

behaviors of the remote vehicles, and thus, facilitates less conservative decision making. Similar to Definition 2 in Section 2.3, intent information is formally defined as follows.

Definition 3. *Given the dynamics (4.1)-(4.2), the intent of remote vehicle i is represented by a restricted velocity domain $v_i(t) \in [\underline{v}_i, \bar{v}_i]$ and acceleration (input) domain $u_i(t) \in [\underline{a}_i, \bar{a}_i]$ over the time period $t \in [t_i, t_i + \Delta t_i]$, where $v_{\min,i} \leq \underline{v}_i \leq \bar{v}_i \leq v_{\max,i}$, $a_{\min,i} \leq \underline{a}_i \leq \bar{a}_i \leq a_{\max,i}$, and t_i is the time when this intent is generated. ■*

In the scenario of highway driving, for instance, an intent message may encode the information that the remote vehicle i will be traveling with velocity between $\underline{v}_i = 30$ and $\bar{v}_i = 32$ [m/s], and acceleration between $\underline{a}_i = -0.5$ and $\bar{a}_i = 0.8$ [m/s²], for the next $\Delta t_i = 6$ seconds. Note that Definition 3 uses constant bounds for velocity and acceleration in intent information, but our analysis below can be adapted to the case where these bounds are time-varying.

As with status information, we assume that the ego vehicle receives intent information from remote vehicles in a synchronized manner. Intent information can also have communication delay; see Fig. 4.2. For example, if intent information from vehicle i is received at time $t = 0$ with communication delay τ_i , then the time domain where this intent remains valid is $t \in [-\tau_i, \Delta t_i - \tau_i]$. When intent information is received together with status information, Theorem 4 still holds when estimating the initial state $x_{\text{est}}(0)$ using

$$u_1(t) = \begin{cases} \underline{a}_1, & \text{if } t \in [-\tau_1, \min\{0, \Delta t_1 - \tau_1\}), \\ a_{\min,1}, & \text{if } t \in [\min\{0, \Delta t_1 - \tau_1\}, 0), \end{cases} \quad (4.27)$$

$$u_2(t) = \begin{cases} \bar{a}_2, & \text{if } t \in [-\tau_2, \min\{0, \Delta t_2 - \tau_2\}), \\ a_{\max,2}, & \text{if } t \in [\min\{0, \Delta t_2 - \tau_2\}, 0), \end{cases} \quad (4.28)$$

which represents the remote vehicles' worst-case behaviors on the communication delay intervals under the given intent information. Notice that intent information leads to less conservative estimation $x_{\text{est}}(0)$. Similarly, Lemma 1 and Theorem 3 still hold when replacing $u_1(t) \equiv a_{\min,1}$ and $u_2(t) \equiv a_{\max,2}$ with

$$u_1(t) = \begin{cases} \underline{a}_1, & \text{if } t \in [0, \max\{0, \Delta t_1 - \tau_1\}), \\ a_{\min,1}, & \text{otherwise,} \end{cases} \quad (4.29)$$

$$u_2(t) = \begin{cases} \bar{a}_2, & \text{if } t \in [0, \max\{0, \Delta t_2 - \tau_2\}), \\ a_{\max,2}, & \text{otherwise,} \end{cases} \quad (4.30)$$

which correspond to the worst-case future motion of remote vehicles based on the intent. Note that intent information improves the ego vehicle's prediction on the remote vehicles' motions, while the

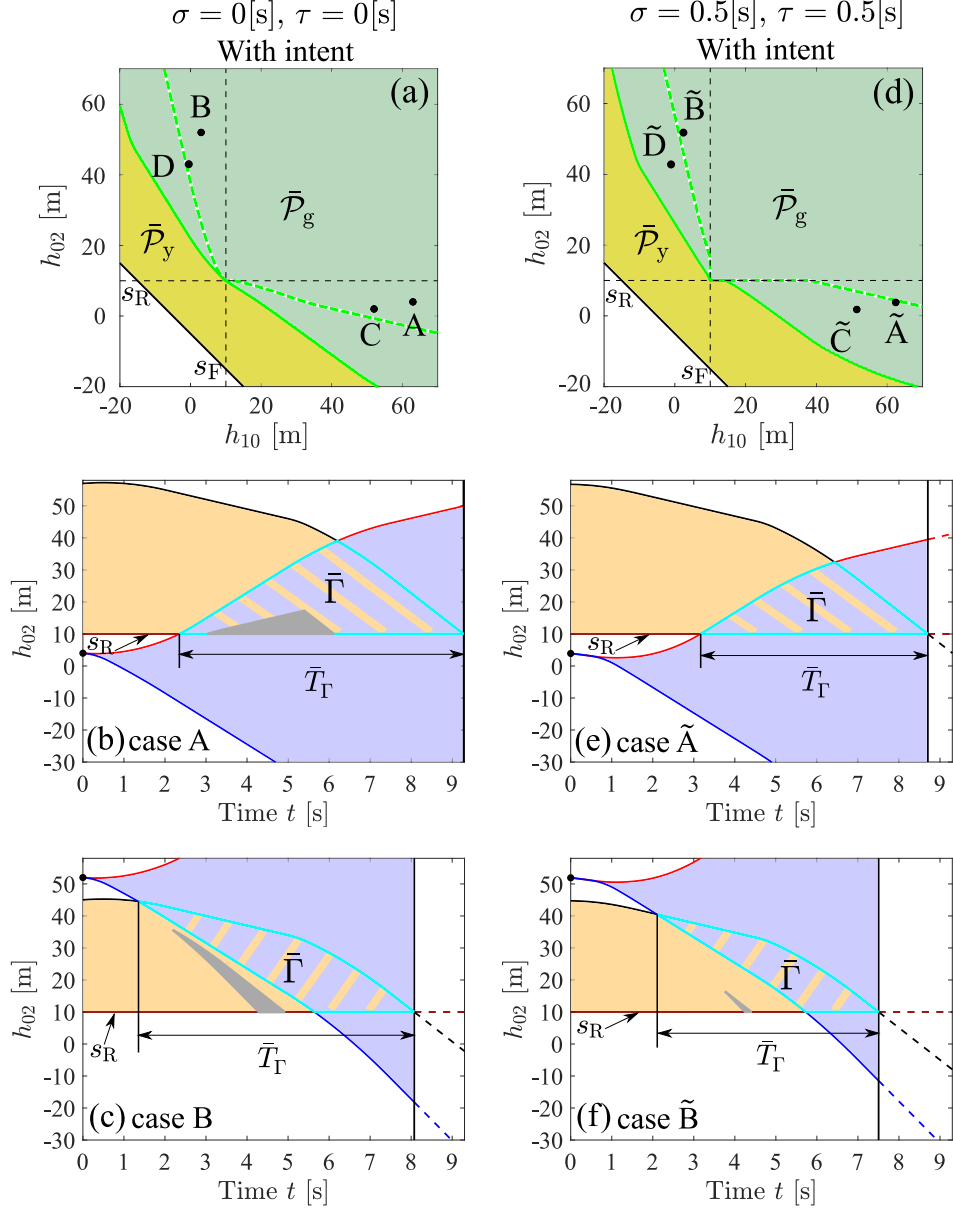


Figure 4.9: Conflict analysis with intent $v_1(t), v_2(t) \in [27, 30]$ [m/s], $u_1(t), u_2(t) \in [-1, 1]$ [m/s²], and $\Delta t_1 = \Delta t_2 = 5$ [s]. (a)-(c) Conflict chart and opportunity set without time delays for the same initial velocities as in Fig. 4.3(a). (d)-(f) Conflict chart and opportunity set with delay in dynamics $\sigma = 0.5$ [s] and communication delay $\tau = 0.5$ [s]. The gray regions indicate the corresponding opportunity sets in Fig. 4.4(a)-(b) and (g)-(h) without intent.

delay in the ego vehicle's dynamics can be similarly handled as in Theorem 3. Thus, the conflict analysis framework built in the previous section can be still applied.

Denoting the no-conflict, uncertain, and conflict sets under intent information as $\bar{\mathcal{P}}_g$, $\bar{\mathcal{P}}_y$, and

$\bar{\mathcal{P}}_r$, the following relationships can be derived:

$$\mathcal{P}_g \subseteq \bar{\mathcal{P}}_g, \quad \mathcal{P}_y \supseteq \bar{\mathcal{P}}_y, \quad \mathcal{P}_r = \bar{\mathcal{P}}_r = \emptyset. \quad (4.31)$$

This reveals that the green no-conflict set expands and the yellow uncertain set shrinks due to the intent; see the conflict charts in Fig. 4.9(a) and (d) where the dashed green boundaries correspond to the no-intent case in Fig. 4.3(a) and (d). A large portion of the originally yellow domain converts to green, indicating the ego vehicle's increased confidence in deciding to change lane.

Furthermore, given the time delays, the initial status of the ego vehicle, and the delayed status of the remote vehicles, the opportunity set $\bar{\Gamma}$ and the opportunity window \bar{T}_Γ under intent information satisfy

$$T_\Gamma \subseteq \bar{T}_\Gamma, \quad |\Gamma(t)| \leq |\bar{\Gamma}(t)|, \quad \forall t \in T_\Gamma, \quad (4.32)$$

where Γ and T_Γ correspond to the no-intent case. This suggests that an enlarged opportunity window is now accessible for the ego vehicle because of the intent information. This is illustrated in Fig. 4.9(b)-(c) for initial states A and B and in Fig. 4.9(e)-(f) for initial states \tilde{A} and \tilde{B} . The gray regions mark the opportunity sets without intent information; cf. Fig. 4.4(a)-(b) and Fig. 4.4(g)-(h). Notice that with intent the opportunity set of case \tilde{A} is no longer empty, since the enlarged green (no-conflict) set now contains the point \tilde{A} in Fig. 4.9(d). The methodology developed in Section 4.2 still enables the computation of the opportunity set $\bar{\Gamma}$ as detailed in Appendix G.

We quantify the benefits of intent with respect to decision making in Fig. 4.10. Panel (a) is obtained by superimposing the conflict chart in Fig. 4.9(d) and Fig. 4.3(d). Regions where ego vehicle's decision regarding lane change changes are shaded green. The heat map in panel (b) quantifies the growth of the opportunity window $\Delta T_\Gamma = |\bar{T}_\Gamma| - |T_\Gamma|$ due to intent. We can observe an ubiquitous increase of the opportunity window inside the set $\bar{\mathcal{P}}_g$, while substantial benefits are gained around the boundary dividing the sets \mathcal{P}_g and \mathcal{P}_y . Note that even though we used the intent horizon $\Delta t_1 = \Delta t_2 = 5$ [s] the opportunity window expands more than 5 [s] for some initial states. Even in the region where the decision remains pursuing lane change, the opportunity window increases.

The upper 3D surface in Fig. 4.8(a) quantifies the opportunity window length as a function of the time delays under the intent information for initial state case A. Apart from increasing the value of opportunity window, intent information also reduces the opportunity window's degradation rate as time delays increase; notice the milder slope of the upper surface compared to the lower one.

In Fig. 4.11(a) we highlight the effect of the intent horizon $\Delta t_1 = \Delta t_2 = \Delta t$ on the length of the opportunity window $|\bar{T}_\Gamma|$. Initially, the opportunity window increases with the intent horizon with a rate higher than 1, and then eventually saturates for higher Δt values. The first slope

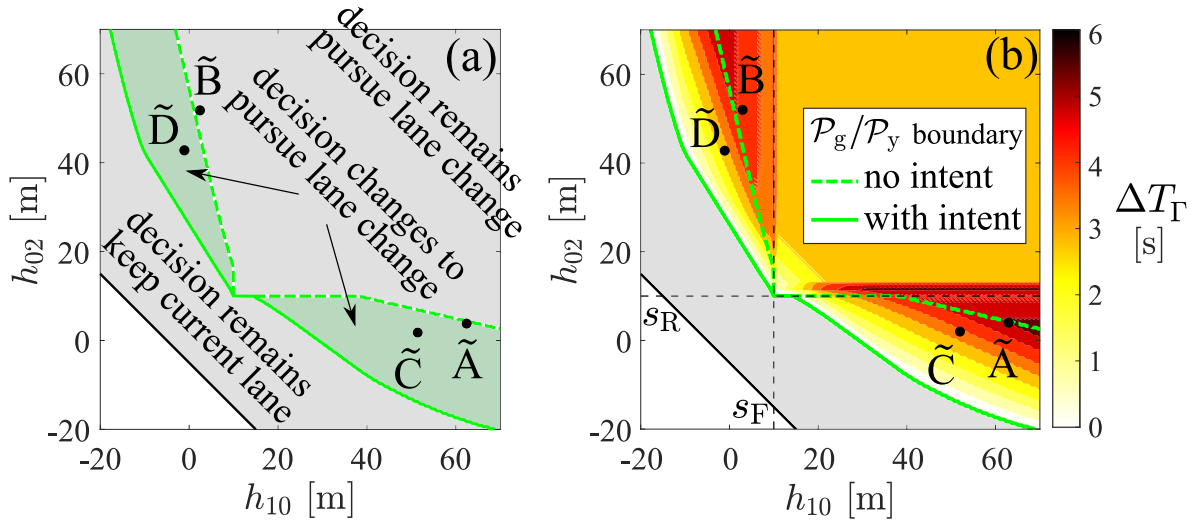


Figure 4.10: (a) Chart showing the decision change under the same intent information, time delays, and estimated initial velocities as in Fig. 4.9(d)-(f). (b) Heat map of opportunity window expansion $\Delta T_\Gamma = |\bar{T}_\Gamma| - |T_\Gamma|$.

change at $\Delta t \approx 2.5$ [s] corresponds to speed limit being reached inside the intent horizon. The saturation of $|\bar{T}_\Gamma|$ suggests that the benefit of increasing intent horizon is bounded. This is illustrated in Fig. 4.11(b) where the intent horizon Δt exceeds the length of the opportunity window \bar{T}_Γ . We remark that for intent information with less restricted velocity and acceleration bounds, the opportunity window length $|\bar{T}_\Gamma|$ saturates at a smaller value for shorter horizon Δt . We also remark that in our intent definition the velocity and acceleration bounds remain unchanged during the intent horizon Δt . However, our theories and numerical tools can be adapted to the case where the remote vehicles update their intent within the Δt horizon. This is outside the scope of this chapter and left as our future work.

In this section, we extended conflict analysis for the case when the remote vehicles' intent is available. We showed that intent information can significantly increase the ego vehicle's capability for a conflict-free maneuver and compensate for the shrink of the opportunity set caused by time delays. Using the theories developed so far, the next section discusses controller design and presents simulation results to demonstrate the power of the developed framework.

4.4 Controller Design and Simulation

In this section, a controller is designed for the ego vehicle to secure the required longitudinal distances for a non-conflicting lane change with time delays in both dynamics and communication. Feeding real highway data into numerical simulations, we validate the effectiveness of the extended conflict analysis framework and demonstrate the benefits of intent sharing.

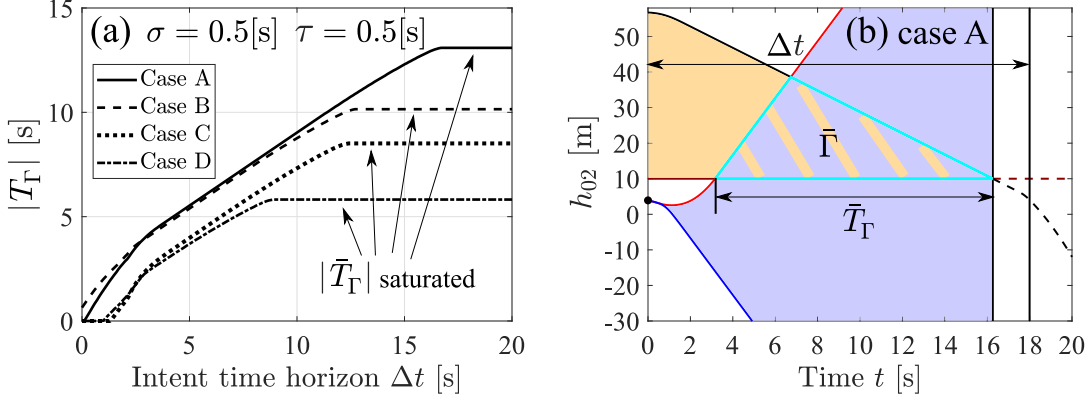


Figure 4.11: (a) Length of the opportunity window as a function of intent horizon for initial state cases A-D and time delays indicated. (b) Mechanism behind the saturation of the opportunity window.

4.4.1 Goal-oriented control

For $x(0) \in \mathcal{P}_g$ (or $x_{\text{est}}(0) \in \mathcal{P}_g$ under communication delay), we have a non-empty opportunity set $\Gamma \neq \emptyset$ and each point in this set $(t, h_{02}) \in \Gamma$ provides a feasible rear gap and a corresponding time. Securing such rear gap simultaneously guarantees the formation of the required front gap. Therefore, one can design the control input $u_0(t)$ by selecting an appropriate goal point $(t^G, h_{02}^G) \in \Gamma$ for the ego vehicle to pursue. We refer to this as goal-oriented control. We emphasize that the existence of such control input $u_0(t)$ is guaranteed by the non-empty opportunity set Γ . One may design $u_0(t)$ to realize a variety of desired performances of the ego vehicle, e.g., optimal time efficiency and/or energy efficiency.

From the robustness perspective, we choose the goal point to be the “center” of the opportunity set, that is, we select t^G in the middle of T_Γ and h_{02}^G in the middle of the slice $\Gamma(t^G)$; see the black dots in Fig. 4.12(a) and (e). Under time delays in both dynamics and communication, we propose a goal-oriented control input of constant value, i.e., $u_0(t) = u_0^G$, with which the goal point $(t^G, h_{02}^G) \in \Gamma$ can be pursued by the ego vehicle. Appendix J gives the analytical expression of u_0^G . Under this constant-value input, the expected trajectory $h_{02}(t)$ is illustrated in Fig. 4.12(a) and (e) by gray arrows. Notice that the goal-oriented controller automatically guarantees the invariance of domain \mathcal{P}_g (or $\bar{\mathcal{P}}_g$ when intent is shared) independent of the future motions of remote vehicles. If the ego vehicle receives the remote vehicles’ updated status and intent information, it may recompute the opportunity set Γ , update the goal point $(t^G, h_{02}^G) \in \Gamma$, and recalculate the corresponding goal-oriented control input u_0^G ; see Fig. 4.12(b)-(d) and (f)-(h). Simulation results in the next subsection demonstrate that the ego vehicle’s passenger comfort and time efficiency can benefit from the frequent status and intent updates.

Table 4.2: Maneuver results under different V2X conditions.

V2X condition	Maneuver result case (i)	Maneuver result case (ii)
Status sharing only	Lane change opportunity missed	Lane change opportunity missed
Status and intent sharing 1 [s] update rate	Lane change opportunity secured Maneuver time 9.0 [s]	Lane change opportunity secured Maneuver time 7.0 [s]
Status and intent sharing 0.1 [s] update rate	Lane change opportunity secured Maneuver time 8.4 [s]	Lane change opportunity secured Maneuver time 6.4 [s]

4.4.2 Simulations with real highway data

We represent the remote vehicles' motion by utilizing real data recorded on human-driven vehicles involved in a lane change scenario on highway I-94 in south-east Michigan. In this maneuver, the front remote vehicle 1 was decelerating while the rear remote vehicle 2 was accelerating and it traveled faster than vehicle 1; see the speed and acceleration data in Fig. 4.13(a)-(b) and (d)-(e). This represents an adversarial scenario where the two remote vehicles were shortening the distance between them; see the gap h_{12} in Fig. 4.13(c) and (f). The ego vehicle is assumed to be a connected automated vehicle which attempts to enter the target lane between the remote human-driven vehicles. We consider the delay in the ego vehicle's dynamics to be $\sigma = 0.5$ [s], while the communication delays associated with both remote vehicles to be $\tau = 0.1$ [s].

At time $t = 0$, the remote vehicles have initial positions $(r_1(0), r_2(0)) = (61.52, 0)$ [m] and initial velocities $(v_1(0), v_2(0)) = (36.46, 36.62)$ [m/s]. Here, without loss of generality, we set the initial position of remote vehicle 2 as the origin. For the ego vehicle, we consider two different initial states. In case (i) we set $r_0(0) = -5.43$ [m] and $v_0(0) = 38.57$ [m/s], that is, the ego vehicle initially travels behind the remote vehicles; while in case (ii) we set $r_0(0) = 66.57$ [m] and $v_0(0) = 32.77$ [m/s], that is, the ego vehicle initially travels in front of the remote vehicles. Note that at $t = 0$ the ego vehicle only has access to the remote vehicles' delayed status $(r_1(-0.1), r_2(-0.1)) = (57.95, -3.64)$ [m] and $(v_1(-0.1), v_2(-0.1)) = (36.46, 36.62)$ [m/s], and it is necessary to estimate their current status based on Theorem 4. We use $(v_{\max,0}, v_{\max,1}, v_{\max,2}) = (42, 40, 40)$ [m/s] as speed limits corresponding to highway driving, while other parameters remain unchanged as in Table 4.1. This adapts the conflict analysis to the driving scenario considered.

With status-sharing information only, the estimated initial state is such that $x_{\text{est}}(0) \in \mathcal{P}_y$ holds for both cases (i) and (ii), and thus, status information does not provide the ego vehicle with enough confidence for pursuing the lane change. Therefore, the chance to change lanes may be missed if the remote vehicles share only their status. However, the ego vehicle's decision can be improved when intent information is shared. The remote vehicles' in-

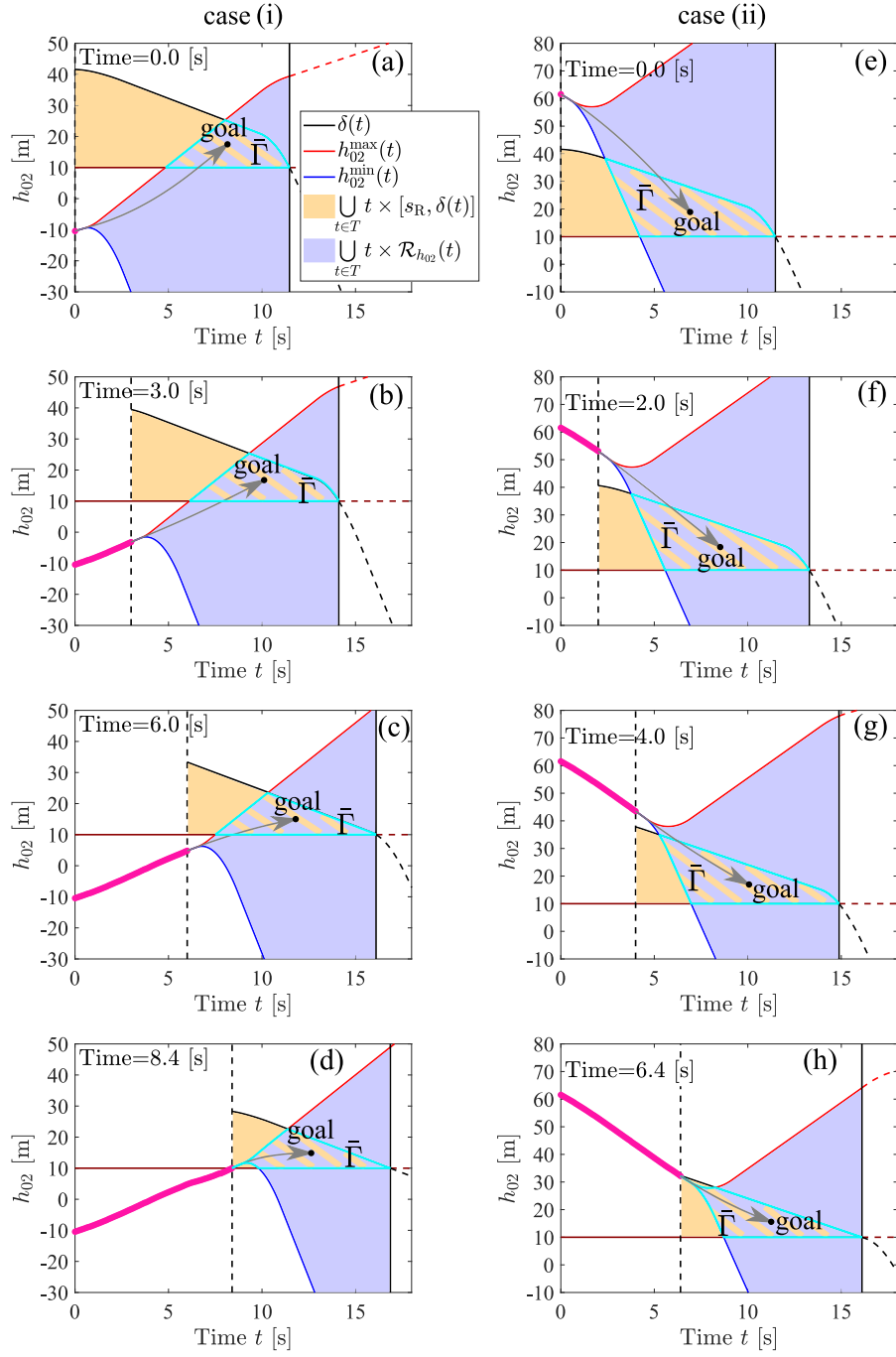


Figure 4.12: Evolution of opportunity set $\bar{\Gamma}$, goal point, and trajectory $h_{02}^{\text{est}}(t)$ under delay $\sigma = 0.5$ [s] in the ego vehicle's dynamics, and communication delay $\tau = 0.1$ [s], with intent information $v_1 \in [34.9, 36.7]$ [m/s], $v_2 \in [36.5, 37.2]$ [m/s], $u_1 \in [-0.6, 0.4]$ [m/s²], $u_2 \in [-1.5, 0.5]$ [m/s²], $\Delta t_1 = \Delta t_2 = 10$ [s]. The goal-oriented controller $u_0(t) = u_0^G$ is used with status and intent updates every 0.1 [s]. (a)-(d) Case (i) where the ego vehicle is initially traveling behind the remote vehicles. (e)-(h) Case (ii) where the ego vehicle is initially traveling in front of the remote vehicles.

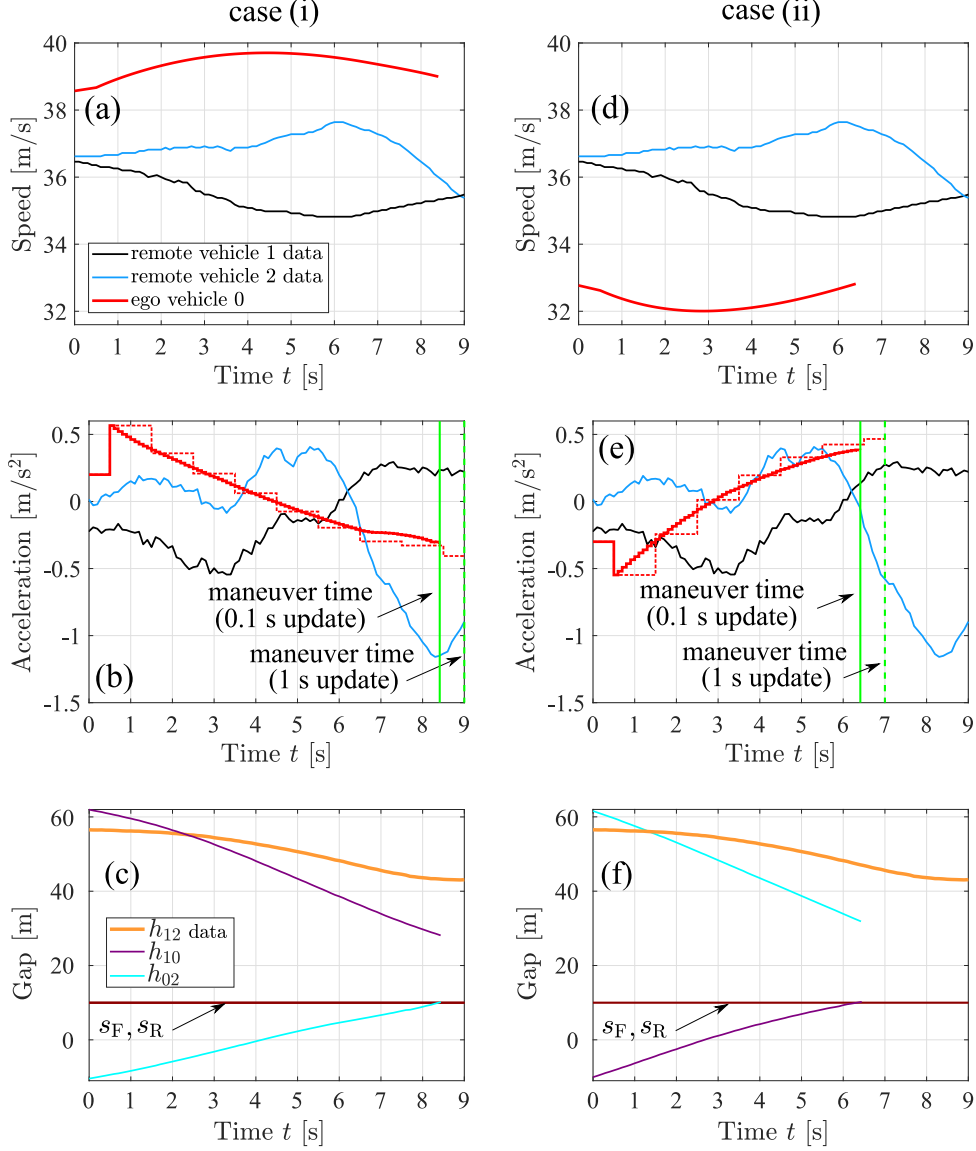


Figure 4.13: Simulation results under the same time delays, initial states, and intent as in Fig. 4.12. (a)-(c) Results for case (i). (d)-(f) Results for case (ii). The dashed magenta curves in (b) and (e) correspond to status and intent updates every 1 [s].

tent can be extracted from the data as $v_1(t) \in [34.9, 36.7]$ [m/s], $u_1(t) \in [-0.6, 0.4]$ [m/s²], $v_2(t) \in [36.5, 37.2]$ [m/s], and $u_2(t) \in [-1.5, 0.5]$ [m/s²]. This yields the estimated initial speeds $(v_1^{\text{est}}(0), v_2^{\text{est}}(0)) = (36.4, 36.67)$ [m/s] and the estimated initial front and rear gaps $(h_{10}^{\text{est}}(0), h_{02}^{\text{est}}(0)) = (62.03, -10.45)$ [m] for case (i), and $(h_{10}^{\text{est}}(0), h_{02}^{\text{est}}(0)) = (-9.97, 61.55)$ [m] for case (ii), assuming the intent of both vehicles covers $\Delta t_1 = \Delta t_2 = 10$ [s]. This leads to $\bar{x}_{\text{est}}(0) \in \bar{\mathcal{P}}_{\text{g}}$ for both cases. Accordingly, the decision of changing lane is made by the ego vehicle, and executed by the goal-oriented controller $u_0(t) = u_0^{\text{G}}$. Note that the value of input u_0^{G} is updated each time the ego vehicle

receives a status and/or intent information update.

Figure 4.12(a)-(d) illustrate the evolution of opportunity set $\bar{\Gamma}$, the goal point $(t^G, h_{02}^G) \in \bar{\Gamma}$, and the trajectory $h_{02}^{\text{est}}(t)$ (magenta curve) with status and intent updates in every 0.1 [s] for case (i). Panels (e)-(h) show the corresponding evolution for case (ii). Notice that when intent is updated, its horizon is extended, but the bounds of velocity and acceleration do not change. At $t = 8.4$ [s] and $t = 6.4$ [s] for cases (i) and (ii), respectively, the required rear gap (and front gap) are already formed by the ego vehicle. This can be confirmed by noticing that $(t, h_{02}^{\text{est}}(t)) \in \bar{\Gamma}$ holds, and thus, $x(t) \in \mathcal{P}_g$ holds according to (4.25). Then, the ego vehicle can initiate the lateral lane change motion immediately without further pursuing the goal point. Thus, goal point is functioning as a guidance for the motion of ego vehicle until sufficient relative distances are formed, while it is not necessary to actually reach it.

Figure 4.13(a)-(b) and (d)-(e) depict the ego vehicle's time profiles by solid red curves for update rates 0.1 [s] and 1 [s], respectively. Notice that when the ego vehicle receives status and intent updates less frequently, conflict-free lane change can still be performed but the required front and rear distances are secured at a later time, at $t = 9.0$ [s] and $t = 7.0$ [s] for cases (i) and (ii), respectively. Also, less smooth control command is prescribed as shown in the dashed red curves. Therefore, by receiving updated status and intent information frequently, the ego vehicle can significantly improve its time efficiency and passenger comfort. Table 4.2 summarizes these results.

4.5 Summary

This chapter scaled up the conflict analysis framework for multiple vehicles possessing different levels of automation in cooperative maneuvering, under time delays in vehicle dynamics and V2X communication. The merits of communication in conflict prevention were examined in the presence of delays by conducting conflict analysis. In particular, we considered status sharing and intent sharing communication. The effects of time delays on conflicts in a mixed-autonomy environment were systematically studied and quantified. It was revealed that conflict-free maneuvers can be facilitated by receiving status information, but time delays can compromise such opportunities. It was also shown that receiving intent information compensates the effects of delays, reduces unnecessary conservatism in decision making, and improves the efficiency of controllers of connected vehicles. A goal-oriented controller was designed for a connected automated vehicle to guarantee conflict-free maneuvers, and the benefits of different types of V2X information exchange were demonstrated via real highway data-based simulations. It is shown that receiving the remote vehicles' status and intent information more frequently further benefits the passenger comfort and time efficiency of the connected automated vehicle.

In the next chapter, we will examine in further detail the scalability and implementability of the conflict analysis framework. In particular, we will consider additional maneuver constraints in conflict resolution and demonstrate with a larger number of vehicles in a mixed traffic environment.

CHAPTER 5

Scalability of Conflict Analysis

In Chapter 4, we have developed a multi-vehicle conflict analysis framework, and applied it to a lane change scenario involving three vehicles on a road that may be infinitely long. To further demonstrate the generalizability and scalability of this framework, this chapter extends multi-vehicle conflict analysis to scenarios with more remote vehicles while considering additional maneuver constraints. Examples include highway merges and maneuvers at roundabouts, where conflicts must be resolved within a designated time and/or spatial domain. For instance, as shown in Fig. 5.1(a), a merge may be considered as a lane change which has to happen within a given road section, called merge zone, before the merging vehicle runs out of its on-ramp. Realizing a conflict-free lane change while satisfying such extra constraints, especially when more neighboring vehicles exist (see Fig. 5.4(a)), is indeed more difficult than the pure lane change considered in the previous chapter. Throughout the analysis below, we show that our conflict analysis framework can be extended to manage such challenging scenarios. In the meantime, the extended framework still allows for efficient consideration of different V2X information, delay effects, and flexible control design. These results will be demonstrated using simulations with real traffic data.

5.1 Extending Multi-Vehicle Conflict Analysis

In this section, we first extend multi-vehicle conflict analysis to accommodate additional maneuver constraints, while still considering only three vehicles – one ego vehicle and two remote vehicles. We then generalize our analysis to be able to handle conflicts with more remote vehicles.

5.1.1 Conflict analysis under additional maneuver constraints

Consider the merge scenario depicted in Fig. 5.1(a)-(b), where an ego vehicle 0 seeks to merge onto the main road between remote vehicles 1 and 2. To perform a conflict-free merge, the following two steps are needed for the ego vehicle: (i) Keep on the ramp and create adequate longitudinal

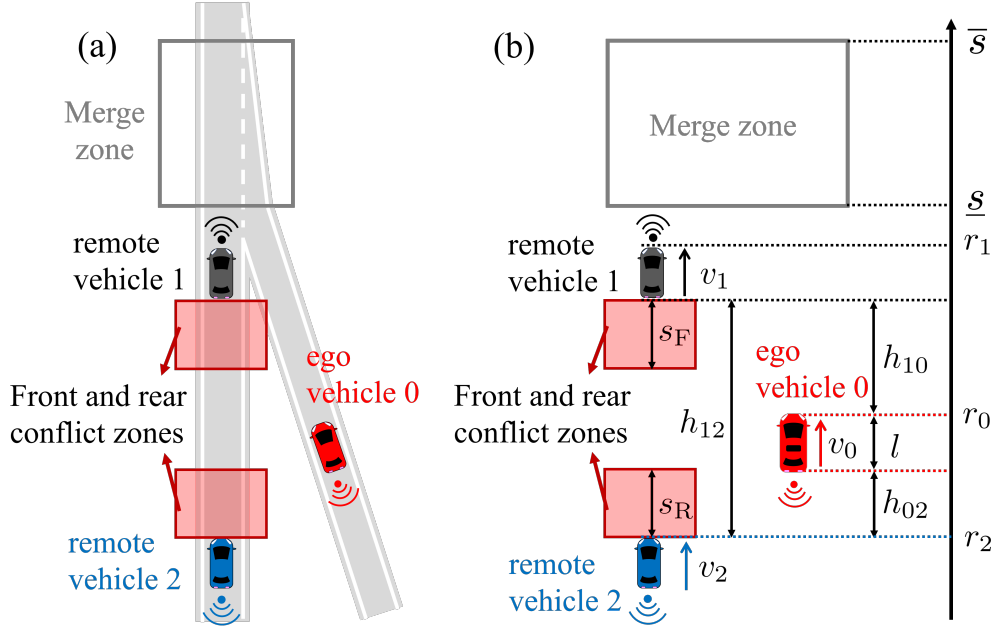


Figure 5.1: (a) A merge scenario involving an ego vehicle 0, and two remote vehicles 1 and 2. The ego vehicle must form necessary front and rear gaps inside the merge zone to enable a conflict-free merge. (b) Generalized model of the merge scenario.

distances from the two remote vehicles while remaining inside a designated merge zone; (ii) move into the main road by changing its lateral position. We focus on step (i) and assume that step (ii) is carried out by lateral motion planners and controllers once the longitudinal distances are ensured within the merge zone. Here, the merge zone is defined towards the end of the ramp, fixed to the ground and of finite length, occupying the position domain $[\underline{s}, \bar{s}]$; see Fig. 5.1(b). We emphasize that compared to the lane change scenario considered in Chapter 4, the requirement of creating necessary gaps within a finite merge zone constitutes a stricter, time-critical maneuver constraint. Similar to Chapter 4, the necessary front and rear gaps to ensure a conflict-free merge are represented by the constant lengths s_F and s_R of the two moving conflict zones. Our analysis below, however, can be generalized to non-constant values of s_F and s_R .

We use the same vehicle dynamics model given in (4.1) and still aim to resolve conflicts from the ego vehicle's perspective. Again, it is assumed that the remote vehicles are out of our control,

Table 5.1: Parameters values used in the Chapter 5.

s_F, s_R	10 [m]	l	5 [m]
$a_{\min,0}$	-8 [m/s ²]	$a_{\min,1}, a_{\min,2}$	-4 [m/s ²]
$a_{\max,0}$	4 [m/s ²]	$a_{\max,1}, a_{\max,2}$	2 [m/s ²]
$v_{\min,0}$	17 [m/s]	$v_{\min,1}, v_{\min,2}$	20 [m/s]
$v_{\max,0}$	33 [m/s]	$v_{\max,1}, v_{\max,2}$	30 [m/s]

but the ego vehicle has the knowledge about their velocity and acceleration limits corresponding to typical highway driving; see Table 5.1. Moreover, all vehicles are assumed to be capable of V2X communication. The communication setup remains the same as in Chapter 4, i.e., the ego vehicle receives two types of V2X information from the remote vehicles: status and intent. The status information from a remote vehicle i contains its instantaneous position r_i and velocity v_i , whereas the intent information follows the Definition 3, encoding a restricted velocity domain $v_i(t) \in [\underline{v}_i, \bar{v}_i]$ and acceleration domain $u_i(t) \in [\underline{a}_i, \bar{a}_i]$ over a future time horizon of length Δt_i . For simplicity, we assume that the status and intent are shared in a synchronized manner from both remote vehicles. The problem of unsynchronized transmission of status and intent information, however, is covered in the next chapter. Here, we still consider two types of time delays: the delay σ in the ego vehicle's dynamics and the communication delays τ_1 and τ_2 associated with the remote vehicles. Similar to the previous chapter, we first construct theorems for conflict analysis considering the time delay in the ego vehicle's dynamics only, and then we show how communication delays may be incorporated into the same framework.

Due to the existence of merge zone, the absolute position r_0 of the ego vehicle becomes important in this merge scenario. Accordingly, we define the state of the system (4.1) as

$$x := [h_{10}, h_{02}, r_0, v_0, v_1, v_2]^\top \in \Omega, \quad (5.1)$$

where Ω is given by

$$\begin{aligned} \Omega := & \{ [h_{10}, h_{02}]^\top \in \mathbb{R}^2 \mid h_{10} + h_{02} \geq -l \} \times (-\infty, \bar{s}] \\ & \times [v_{\min,0}, v_{\max,0}] \times [v_{\min,1}, v_{\max,1}] \times [v_{\min,2}, v_{\max,2}]. \end{aligned} \quad (5.2)$$

Note that compared to the lane change scenario in Chapter 4, the state variable r_0 adds one dimension to the state space; cf. (4.5). Also notice that we focus on $r_0 \in (-\infty, \bar{s}]$, since $r_0 > \bar{s}$ means that the ego vehicle has already exited the merge zone, and a merge may no longer happen.

As mentioned above, to be able to merge from the on-ramp to the main road between remote vehicles 1 and 2 without a conflict, the ego vehicle must secure necessary front and rear gaps while it is inside the merge zone. Such a conflict-free condition can be formally described by the proposition

$$M := \{ \exists t \geq 0, h_{10}(t) \geq s_F \wedge h_{02}(t) \geq s_R \wedge r_0(t) \in [\underline{s}, \bar{s}] \}, \quad (5.3)$$

where the predicate $h_{10}(t) \geq s_F \wedge h_{02}(t) \geq s_R$ remains the same as in the proposition P for describing a conflict-free lane change in Chapter 4; cf. (4.6). However, the additional predicate $r_0(t) \in [\underline{s}, \bar{s}]$ represents a time-critical constraint for a conflict-free merge maneuver. The proposition M can be similarly decomposed into three cases as follows.

- (i) No-conflict case: ego vehicle 0 is able to prevent conflict independent of the motion of remote vehicles 1 and 2.
- (ii) Uncertain case: ego vehicle 0 may be able to prevent conflict depending on the motion of remote vehicles 1 and 2.
- (iii) Conflict case: ego vehicle 0 is not able to prevent conflict independent of the motion of remote vehicles 1 and 2.

The three cases above correspond to three pairwise disjoint sets within Ω :

$$\mathcal{M}_g := \{x(0) \in \Omega | \forall u_1(t), \forall u_2(t), \exists u_0(t), M\}, \quad (5.4)$$

$$\mathcal{M}_y := \{x(0) \in \Omega | (\exists u_1(t), \exists u_2(t), \forall u_0(t), \neg M) \wedge (\exists u_1(t), \exists u_2(t), \exists u_0(t), M)\}, \quad (5.5)$$

$$\mathcal{M}_r := \{x(0) \in \Omega | \forall u_1(t), \forall u_2(t), \forall u_0(t), \neg M\}. \quad (5.6)$$

These sets are referred to as no-conflict set, uncertain set, and conflict set, respectively. The subscripts “g”, “y”, and “r” still correspond to the colors green, yellow, and red in visualizing these domains in the state space. Noting that the first and second predicates in (5.5) negates those in (5.4) and (5.6), i.e.,

$$(\exists u_1, \exists u_2, \forall u_0, \neg M) \iff \neg(\forall u_1, \forall u_2, \exists u_0, M), \quad (5.7)$$

$$(\exists u_1, \exists u_2, \exists u_0, M) \iff \neg(\forall u_1, \forall u_2, \forall u_0, \neg M), \quad (5.8)$$

the sets \mathcal{M}_g , \mathcal{M}_y , and \mathcal{M}_r are indeed pairwise disjoint, and $\mathcal{M}_g \cup \mathcal{M}_y \cup \mathcal{M}_r = \Omega$. An example of these sets in (h_{10}, h_{02}) -plane is shown in Fig. 5.3(a) for the indicated ego vehicle position r_0 , merge zone location $[\underline{s}, \bar{s}]$, and velocities (v_0, v_1, v_2) . This is still referred to as conflict chart, whose derivation is discussed further below. We emphasize that compared to the pure lane change case (see, e.g., Fig. 4.3) where the conflict set was empty, here the red region indeed shows up due to having stricter maneuver constraint, i.e., $\mathcal{M}_r \neq \emptyset$.

Now we develop methods to check whether a given initial state $x(0)$ is located in the set \mathcal{M}_g , \mathcal{M}_y , or \mathcal{M}_r . At the initial time, if $h_{10}(0) \geq s_F \wedge h_{02}(0) \geq s_R \wedge r_0(0) \in [\underline{s}, \bar{s}]$ holds, then $x(0) \in \mathcal{M}_g$ holds immediately since the ego vehicle already formed necessary gaps inside the merge zone; otherwise, one needs to check if proposition M is true for some $t > 0$, considering all possible future behaviors of the ego and remote vehicles. The Lemma below shows that the behavioral limits of remote vehicles shall be used to check $x(0) \in \mathcal{M}_g$.

Lemma 2. *The following relationship holds for any given initial state $x(0) \in \Omega$:*

$$\{\forall u_1(t), \forall u_2(t), \exists u_0(t), M\} \iff \{(u_1(t), u_2(t)) \equiv (\underline{u}_1(t), \bar{u}_2(t)), \exists u_0(t), \exists t \in [0, t_{\max,0}], h_{10}(t) \geq s_F \wedge h_{02}(t) \geq s_R \wedge r_0(t) \in [\underline{s}, \bar{s}]\}, \quad (5.9)$$

where

$$\underline{u}_1(t) = \begin{cases} \underline{a}_1, & \text{if } t \in [0, \Delta t_1], \\ a_{\min,1}, & \text{otherwise,} \end{cases} \quad (5.10)$$

$$\bar{u}_2(t) = \begin{cases} \bar{a}_2, & \text{if } t \in [0, \Delta t_2], \\ a_{\max,2}, & \text{otherwise,} \end{cases} \quad (5.11)$$

with $t_{\max,0}$ being the time t such that $r_{-0}^*(t) = \bar{s}$, and $r_{-0}^*(t)$ is given in (G.6) in Appendix G.

Proof. See Appendix K. □

Here, $r_{-0}^*(t)$ gives the smallest position that the ego vehicle may reach, under its input limits and delay σ in its dynamics. Accordingly, $t_{\max,0}$ gives the latest possible time of the ego vehicle remaining inside the merge zone. Also, $\underline{u}_1(t)$ and $\bar{u}_2(t)$ are the input lower and upper bounds of the remote vehicles 1 and 2, respectively, given the available intent information. These inputs represent the remote vehicles' worst-case behaviors that shrink the total gap h_{12} the most. Thus, Lemma 2 suggests that to prevent conflict independent of the remote vehicles' motion, the ego vehicle must form the necessary gaps inside the merge zone within the time window $[0, t_{\max,0}]$, assuming the worst-case motion of remote vehicles. This way, checking $x(0) \in \mathcal{M}_g$ is reduced to checking the existence of an input $u_0(t)$ for $t \geq 0$ and a time $t \in [0, t_{\max,0}]$ such that $h_{10}(t) \geq s_F \wedge h_{02}(t) \geq s_R \wedge r_0(t) \in [\underline{s}, \bar{s}]$ holds under the remote vehicles' deterministic (worst-case) behaviors.

A similar relationship can be derived for checking $x(0) \in \mathcal{M}_r$ as stated by the following Lemma.

Lemma 3. *The following relationship holds for any given initial state $x(0) \in \Omega$:*

$$\{\forall u_1(t), \forall u_2(t), \forall u_0(t), \neg M\} \iff \{(u_1(t), u_2(t)) \equiv (\bar{u}_1(t), \underline{u}_2(t)), \forall u_0(t), \forall t \in [0, t_{\max,0}], \neg(h_{10}(t) \geq s_F \wedge h_{02}(t) \geq s_R \wedge r_0(t) \in [\underline{s}, \bar{s}])\}, \quad (5.12)$$

where

$$\bar{u}_1(t) = \begin{cases} \bar{a}_1, & \text{if } t \in [0, \Delta t_1], \\ a_{\max,1}, & \text{otherwise,} \end{cases} \quad (5.13)$$

$$\underline{u}_2(t) = \begin{cases} \underline{a}_2, & \text{if } t \in [0, \Delta t_2], \\ a_{\min,2}, & \text{otherwise,} \end{cases} \quad (5.14)$$

and $t_{\max,0}$ is given in Lemma 2.

Proof. See Appendix L. □

Here, $\bar{u}_1(t)$ and $\underline{u}_2(t)$ are the upper and lower input bounds of the remote vehicles 1 and 2, respectively. Such inputs give the remote vehicles' best-case behaviors that enlarge the total gap h_{12} the most. Lemma 3 suggests that a conflict-free merge maneuver being impossible is equivalent to the fact that the ego vehicle is not able to form the necessary gaps inside the merge zone within the time window $[0, t_{\max,0}]$, assuming the best-case motion of remote vehicles. That is, checking $x(0) \in \mathcal{M}_r$ is reduced to showing the inexistence of an input $u_0(t)$ for $t \geq 0$ and a time $t \in [0, t_{\max,0}]$ to satisfy the condition $h_{10}(t) \geq s_F \wedge h_{02}(t) \geq s_R \wedge r_0(t) \in [\underline{s}, \bar{s}]$ under the remote vehicles' deterministic (best-case) behaviors.

With Lemmas 2 and 3, we are now ready to develop criteria for checking $x(0) \in \mathcal{M}_g$ and $x(0) \in \mathcal{M}_r$. To this aim, we reuse the lane change opportunity set Γ defined in (4.14) in the previous chapter. Recall that the set Γ contains all feasible values of the rear gap h_{02} and the corresponding time t such that the condition $h_{10}(t) \geq s_F \wedge h_{02}(t) \geq s_R$ holds. Fig. 5.2 (a) illustrates an example of the set Γ under the indicated initial conditions. The set Γ can be alternatively described in closed form as

$$\Gamma = \bigcup_{t \geq 0} t \times [\underline{\Gamma}(t), \bar{\Gamma}(t)], \quad (5.15)$$

where $\underline{\Gamma}(t) = \max\{s_R, h_{02}^{\min}(t)\}$ and $\bar{\Gamma}(t) = \min\{\delta(t), h_{02}^{\max}(t)\}$ describe the lower and upper bounds of the set Γ at time t . Note that the set Γ is defined only at the times t when $\underline{\Gamma}(t) \leq \bar{\Gamma}(t)$ holds. Also notice that $\delta(t)$, $h_{02}^{\min}(t)$, and $h_{02}^{\max}(t)$ are analytically given in Appendix G. By transforming the set Γ from (t, h_{02}) -domain to (t, r_0) -domain, a criterion to check $x(0) \in \mathcal{M}_g$ is provided by the following Theorem.

Theorem 5. *Given the dynamics (4.1)-(4.2) and the initial state $x(0) \in \Omega$, $x(0) \in \mathcal{M}_g$ holds if and*

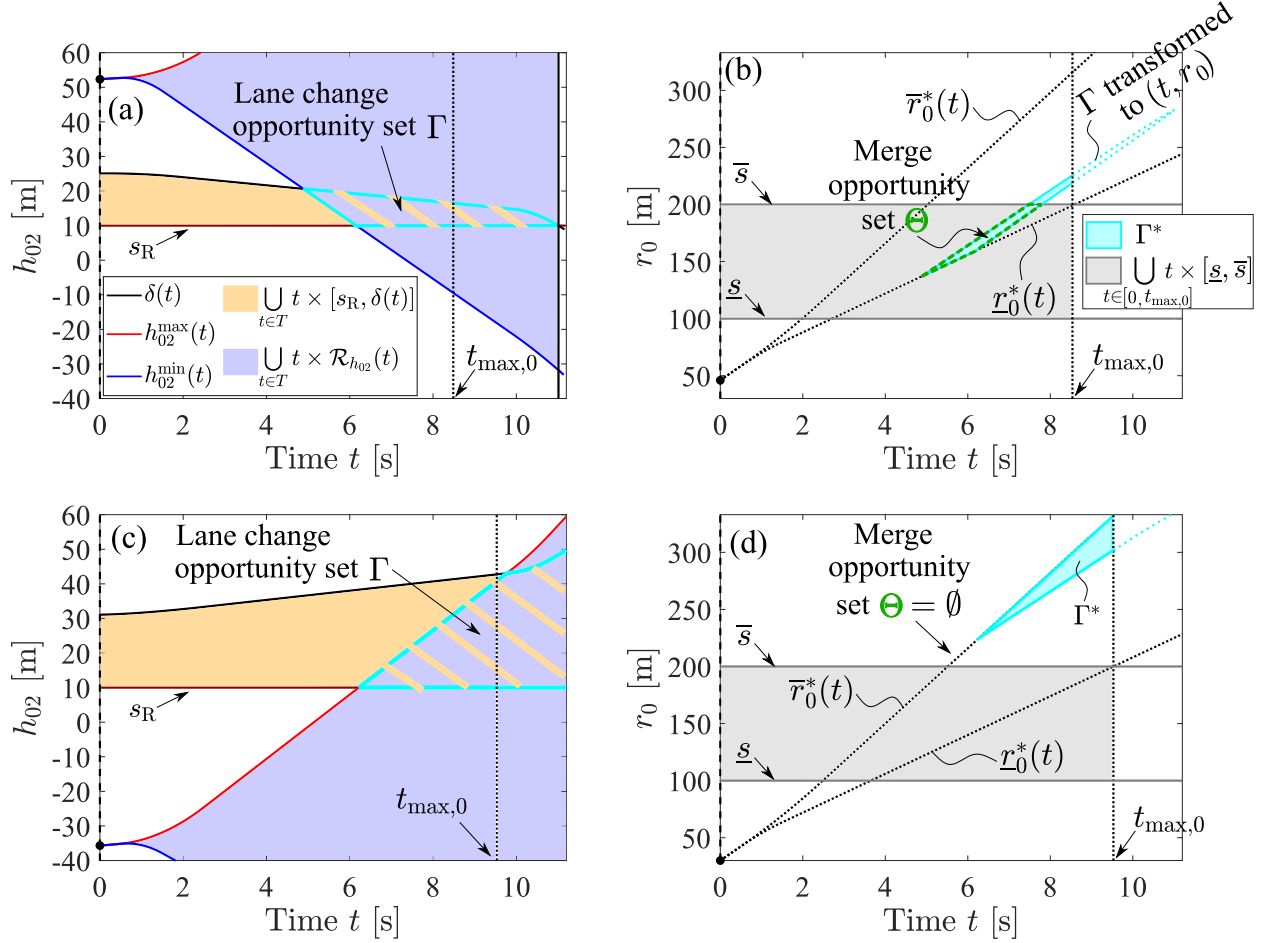


Figure 5.2: Extending multi-vehicle conflict analysis to the merge scenario. (a)-(b) Checking $x(0) \in \mathcal{M}_g$ according to Theorem 5 with initial condition $(h_{10}(0), h_{02}(0), r_0(0)) = (-17.3, 52.3, 46)$ [m] and $(v_0(0), v_1(0), v_2(0)) = (25, 24.22, 24.09)$ [m/s], where (a) constructs the lane change opportunity set Γ , and (b) constructs the corresponding merge opportunity set Θ ; (c)-(d) Checking $x(0) \in \mathcal{M}_r$ according to Theorem 6 with initial condition $(h_{10}(0), h_{02}(0), r_0(0)) = (76.7, -35.7, 30)$ [m] and $(v_0(0), v_1(0), v_2(0)) = (25, 24.25, 23.99)$ [m/s], where (c) and (d) visualize the constructions of the sets Γ and Θ , respectively. Here, the merge zone is located at $[100, 200]$ [m] and time delay $\sigma = 0.5$ [s] is used in the ego vehicle's dynamics. Intent of remote vehicles are assumed to be $v_1(t) \in [24.22, 25.04]$ [m/s], $u_1(t) \in [-0.2, 0.3]$ [m/s²], $v_2(t) \in [23.70, 25.36]$ [m/s], and $u_2(t) \in [-0.3, 0.7]$ [m/s²], with intent horizons $\Delta t_1 = \Delta t_2 = 10$ [s].

only if the condition

$$\Theta := \Gamma^* \cap \bigcup_{t \in [0, t_{\max, 0}]} t \times [\underline{s}, \bar{s}] \neq \emptyset, \quad (5.16)$$

is satisfied under $(u_1(t), u_2(t)) \equiv (\underline{u}_1(t), \bar{u}_2(t))$, where

$$\Gamma^* := \bigcup_{t \in [0, t_{\max, 0}]} t \times [\underline{\Gamma}(t) + r_2(t) + l, \bar{\Gamma}(t) + r_2(t) + l]. \quad (5.17)$$

Proof. See Appendix M. □

To understand the physical meaning of the set Θ defined in (5.16), we first recall from the definition (4.3) of rear gap h_{02} , that is, $r_0 = h_{02} + r_2 + l$. Noting that the set Γ is expressed in terms of h_{02} , one confirms from (5.15) and (5.17) that the set Γ^* is in fact the set Γ transformed from (t, h_{02}) -plane to (t, r_0) -plane, on the time domain $t \in [0, t_{\max, 0}]$; see the cyan shaded region in Fig. 5.2(b). The set Γ^* thus gives all feasible values of the position r_0 that the ego vehicle is able to reach, and the corresponding time $t \in [0, t_{\max, 0}]$ such that $h_{10}(t) \geq s_F \wedge h_{02}(t) \geq s_R$ holds under the worst-case behaviors of remote vehicles. Thus, the intersection Θ of the sets Γ^* and $\bigcup_{t \in [0, t_{\max, 0}]} t \times [\underline{s}, \bar{s}]$ gives all feasible r_0 values and the corresponding times such that $h_{10}(t) \geq s_F \wedge h_{02}(t) \geq s_R \wedge r_0(t) \in [\underline{s}, \bar{s}]$ holds. Therefore, based on Lemma 2, $\Theta \neq \emptyset$ is equivalent to the ego vehicle being able to secure the necessary front and rear gaps inside the merge zone independent of the remote vehicles' behaviors, that is, $x(0) \in \mathcal{M}_g$. We refer to the set Θ as the merge opportunity set, as opposed to the lane change opportunity set Γ . We remark that here, the time delay σ in the ego vehicle's dynamics is taken into account when the set Γ is constructed.

Similarly, by constructing the set Γ (and accordingly the set Γ^*) using the remote vehicles' best-case behaviors; see Lemma 3, one is able to derive a similar criterion to check $x(0) \in \mathcal{M}_r$, given by the following Theorem.

Theorem 6. *Given the dynamics (4.1)-(4.2) and the initial state $x(0) \in \Omega$, $x(0) \in \mathcal{M}_r$ holds if and only if the condition*

$$\Theta = \emptyset, \quad (5.18)$$

is satisfied under $(u_1(t), u_2(t)) \equiv (\bar{u}_1(t), \underline{u}_2(t))$, for the set Θ defined in (5.16).

Proof. See Appendix N. □

That is, the merge opportunity set Θ being empty under the remote vehicles' best-case behaviors is equivalent to the ego vehicle not being able to secure the necessary front and rear gaps inside

the merge zone, i.e., $x(0) \in \mathcal{M}_r$. Fig. 5.2(c)-(d) visualize an example of the sets Γ and Γ^* under the indicated initial conditions such that $\Theta = \emptyset$. Notice from Fig. 5.2(c) that the set Γ may be unbounded depending on the input limits of remote vehicles, but the consideration of a finite time window $[0, t_{\max,0}]$ ensures that the set Γ^* is always bounded; see Fig. 5.2(d), thereby avoiding infinite (and unnecessary) set calculation. We also emphasize that the construction of the set Θ is highly efficient as the set Γ^* is analytically given, and checking its intersection with the set $\bigcup_{t \in [0, t_{\max,0}]} t \times [\underline{s}, \bar{s}]$ is numerically fast.

In summary, Theorems 5 and 6 reveal that a simple adaptation of the reachability-based approach developed in the previous chapter allows for efficient study of conflicts under stricter maneuver constraints. This demonstrates the scalability and efficient implementability of the conflict analysis framework. By applying these Theorems to check the states within the set Ω , one obtains the conflict chart mentioned earlier in this section; see Fig. 5.3(a) for an example.

In practice, however, the ego vehicle does not necessarily have to construct the whole conflict chart, but may simply check which subset the current system state is in. Based on this, the ego vehicle's maneuver decision can be made. If $x(0) \in \mathcal{M}_g$, then the ego vehicle shall pursue the opportunity to merge. If $x(0) \in \mathcal{M}_r$, then a conflict-free merge is not possible and the ego vehicle shall not merge between these two remote vehicles. If, however, $x(0) \notin \mathcal{M}_g \cup \mathcal{M}_r$, then $x(0) \in \mathcal{M}_y$ holds. In this case, a conflict-free merge is not guaranteed. Thus, the ego vehicle shall still decide not to merge between the two remote vehicles.

Our analysis so far ignored the communication delays τ_1 and τ_2 associated with the V2X information from the remote vehicles. When communication delays exist, the actual state $x(0)$ becomes unavailable and the intent information is also delayed. However, one may estimate the current state $x_{\text{est}}(0)$ similar to the Theorem 4 in Chapter 4, and use it in conflict analysis. Following the discussion in Section 4.3, by constructing $x_{\text{est}}(0)$ using (4.27)-(4.28) one obtains

$$x_{\text{est}}(0) \in \mathcal{M}_g \implies x(0) \in \mathcal{M}_g, \quad (5.19)$$

while the Lemma 2 and Theorem 5 hold when replacing $(u_1(t), u_2(t)) \equiv (\underline{u}_1(t), \bar{u}_2(t))$ with (4.29)-(4.30). Recall that (4.27)-(4.28) represent the remote vehicles' worst-case behaviors on the communication delay intervals $[-\tau_1, 0]$ and $[-\tau_2, 0]$, respectively, and (4.29)-(4.30) give the worst future motion of remote vehicles based on the delayed intent. This way, although the actual state $x(0)$ is unknown, $x(0) \in \mathcal{M}_g$ can be inferred by checking $x_{\text{est}}(0) \in \mathcal{M}_g$.

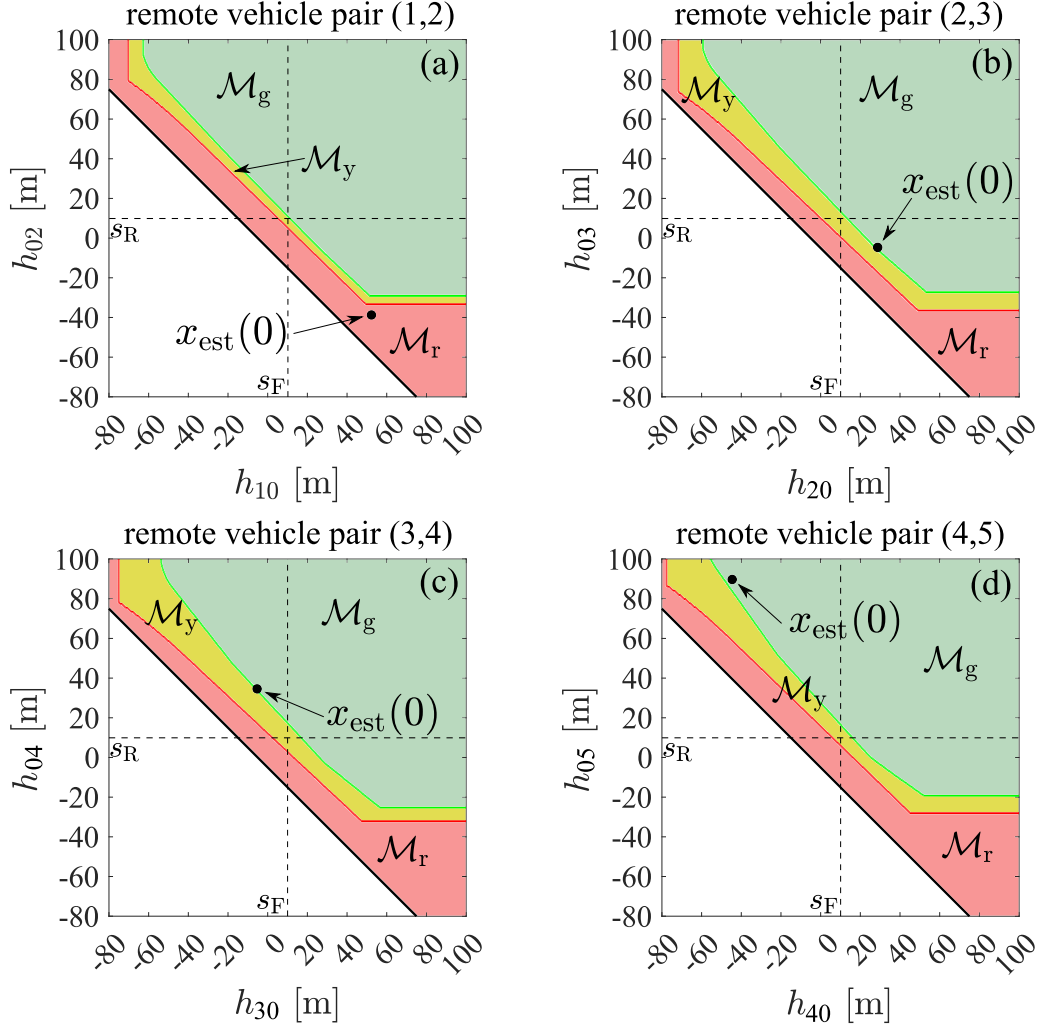


Figure 5.3: Conflict charts in the plane of front and rear gaps corresponding to different remote vehicle pairs in Fig. 5.4, under delay $\sigma = 0.5$ [s] in the ego vehicle's dynamics and delay $\tau = 0.1$ [s] in the remote vehicles' V2X information, for velocities (a) $(v_0(0), v_1(-0.1), v_2(-0.1)) = (25, 24.58, 24.22)$ [m/s]; (b) $(v_0(0), v_2(-0.1), v_3(-0.1)) = (25, 24.22, 24.02)$ [m/s]; (c) $(v_0(0), v_3(-0.1), v_4(-0.1)) = (25, 24.02, 25.50)$ [m/s]; and (d) $(v_0(0), v_4(-0.1), v_5(-0.1)) = (25, 25.50, 26.28)$ [m/s]. Here, the ego vehicle's initial position is given as $r_0(0) = 0$ [m] and the merge zone is located at [100, 200] [m]. The estimated initial state encoded in $x_{\text{est}}(0)$ for each panel is summarized in Table 5.2.

Table 5.2: Estimated initial state encoded in $x_{\text{est}}(0)$ for each panel of Fig. 5.3.

(a)	$(h_{10}^{\text{est}}(0), h_{02}^{\text{est}}(0)) = (52.30, -38.75)$ [m], $(v_1^{\text{est}}(0), v_2^{\text{est}}(0)) = (24.60, 24.22)$ [m/s]
(b)	$(h_{20}^{\text{est}}(0), h_{03}^{\text{est}}(0)) = (28.75, -4.67)$ [m], $(v_2^{\text{est}}(0), v_3^{\text{est}}(0)) = (24.22, 24.09)$ [m/s]
(c)	$(h_{30}^{\text{est}}(0), h_{04}^{\text{est}}(0)) = (-5.33, 34.58)$ [m], $(v_3^{\text{est}}(0), v_4^{\text{est}}(0)) = (23.99, 25.50)$ [m/s]
(d)	$(h_{40}^{\text{est}}(0), h_{05}^{\text{est}}(0)) = (-44.58, 89.72)$ [m], $(v_4^{\text{est}}(0), v_5^{\text{est}}(0)) = (25.47, 26.32)$ [m/s]

Similarly, by constructing $x_{\text{est}}(0)$ using

$$u_1(t) = \begin{cases} \bar{a}_1, & \text{if } t \in [-\tau_1, \min\{0, \Delta t_1 - \tau_1\}), \\ a_{\max,1}, & \text{if } t \in [\min\{0, \Delta t_1 - \tau_1\}, 0), \end{cases} \quad (5.20)$$

$$u_2(t) = \begin{cases} \underline{a}_2, & \text{if } t \in [-\tau_2, \min\{0, \Delta t_2 - \tau_2\}), \\ a_{\min,2}, & \text{if } t \in [\min\{0, \Delta t_2 - \tau_2\}, 0), \end{cases} \quad (5.21)$$

one obtains

$$x_{\text{est}}(0) \in \mathcal{M}_r \implies x(0) \in \mathcal{M}_r. \quad (5.22)$$

Here, (5.20)-(5.21) represent the remote vehicles' best-case behaviors on their communication delay intervals. Also, the Lemma 3 and Theorem 6 hold by replacing $(u_1(t), u_2(t)) \equiv (\bar{u}_1(t), \underline{u}_2(t))$ with

$$u_1(t) = \begin{cases} \bar{a}_1, & \text{if } t \in [0, \max\{0, \Delta t_1 - \tau_1\}), \\ a_{\max,1}, & \text{otherwise,} \end{cases} \quad (5.23)$$

$$u_2(t) = \begin{cases} \underline{a}_2, & \text{if } t \in [0, \max\{0, \Delta t_2 - \tau_2\}), \\ a_{\min,2}, & \text{otherwise,} \end{cases} \quad (5.24)$$

which correspond to the best future motion of remote vehicles based on their delayed intent.

Thus, the efficiency in incorporating communication delays is preserved in the extended conflict analysis under stricter maneuver constraints.

5.1.2 Conflict analysis with more remote vehicles

So far, we developed tools to study conflicts between one ego vehicle and two remote vehicles in merge scenarios. In this subsection we generalize conflict analysis to the case where more remote vehicles exist.

Consider the scenario shown in Fig. 5.4(a) where the red ego vehicle 0 seeks to merge onto a main road along which a chain of remote vehicles are approaching. The task for the ego vehicle is

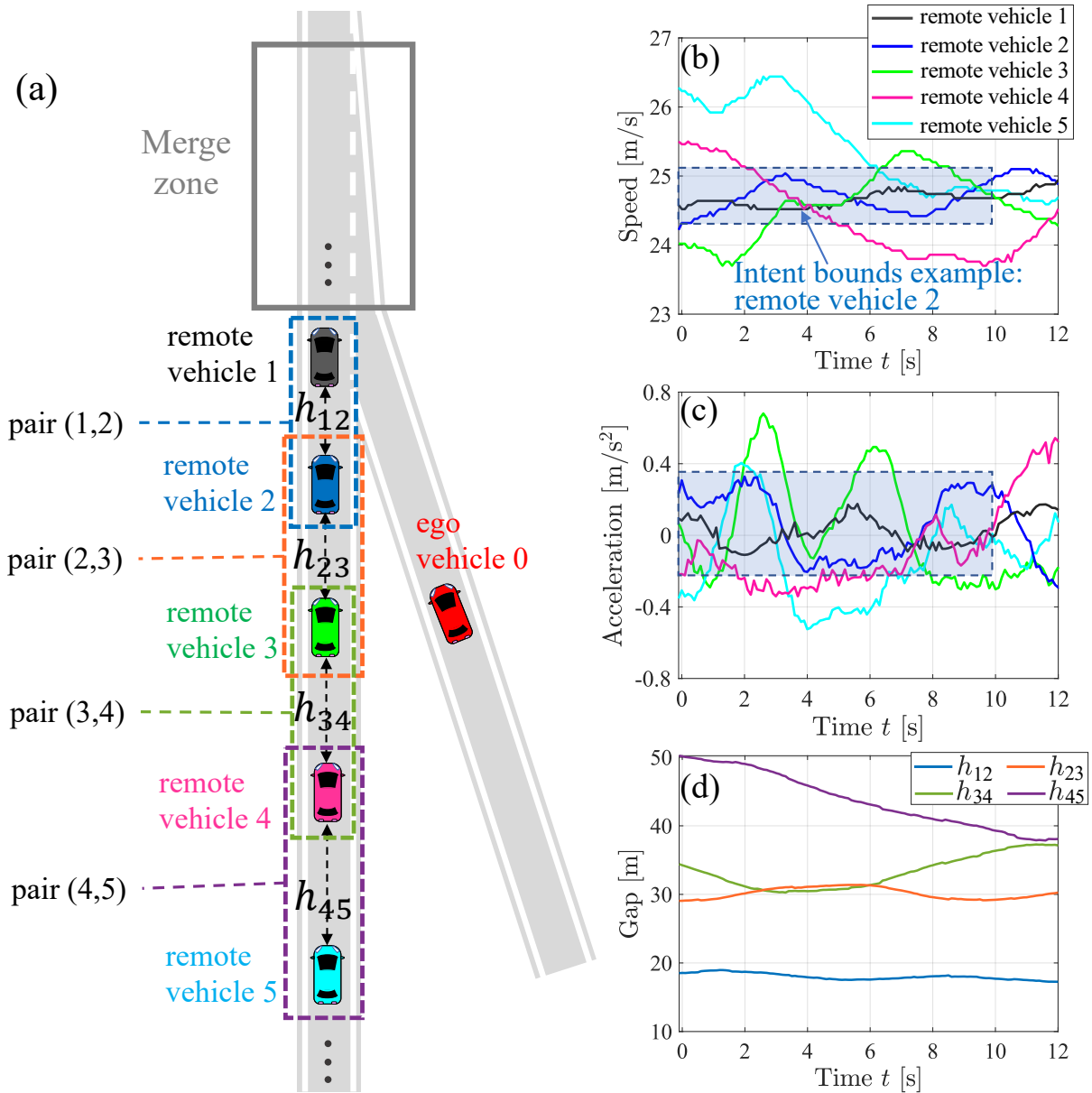


Figure 5.4: An extended merge scenario where the ego vehicle 0 attempts to merge onto the main road as a chain of remote vehicles are approaching. (a) Pairwise conflict analysis when five remote vehicles are inside the ego vehicle’s communication range. (b) Remote vehicles’ behaviors represented by real highway driving data.

to select a pair of remote vehicles to perform a conflict-free merge maneuver between them. The methodology developed above can be naturally applied to this scenario by considering “pairwise” conflicts. This idea is illustrated in Fig. 5.4(a) where the ego vehicle checks merge opportunities with each pair of remote vehicles inside its communication range. More specifically, consider that N remote vehicles indexed $1, \dots, N$ are within the ego vehicle’s communication range at the initial time. The ego vehicle shall perform conflict analysis sequentially with each pair of remote vehicles from the pair $(1, 2)$ to the pair $(N - 1, N)$; see Fig. 5.4(a) for $N = 5$. The farthest pair ahead whose status and intent yield $x(0) \in \mathcal{M}_g$ (or $x_{\text{est}}(0) \in \mathcal{M}_g$ if communication delays exist), shall be selected as target vehicles to pursue a conflict-free merge. Such selection maximizes the ego vehicle’s time efficiency since a further ahead longitudinal position can be achieved.

To demonstrate the proposed pairwise conflict analysis, we represent the motion of five remote vehicles by real data collected on highway US-23 in south-east Michigan. Fig. 5.4(b)-(d) show the profiles of the remote vehicles’ speeds, accelerations, and inter-vehicle distances h_{12} , h_{23} , h_{34} , and h_{45} . We assume the ego vehicle 0 to be a connected automated vehicle with initial position $r_0(0) = 0$ [m] and initial speed $v_0(0) = 25$ [m/s]. The ego vehicle attempts to select a pair of remote vehicles to merge between, within the merge zone located at $[100, 200]$ [m]. The remote vehicles’ initial positions and speeds are given as $(r_1(0), r_2(0), r_3(0), r_4(0), r_5(0)) = (57.3, 33.7, -0.3, -39.6, -94.7)$ [m] and $(v_1(0), v_2(0), v_3(0), v_4(0), v_5(0)) = (24.52, 24.32, 24.02, 25.46, 26.23)$ [m/s]. That is, the ego vehicle initially travels near remote vehicle 3 (in terms of longitudinal position); see Fig. 5.4(a) for a conceptual illustration. We consider the delay $\sigma = 0.5$ [s] in the ego vehicle’s dynamics and the communication delay $\tau = 0.1$ [s] associated with all remote vehicles. At the initial time $t = 0$, the ego vehicle is aware of the remote vehicles’ delayed status: $(r_1(-0.1), r_2(-0.1), r_3(-0.1), r_4(-0.1), r_5(-0.1)) = (54.9, 31.3, -2.7, -42.1, -97.3)$ [m] and $(v_1(-0.1), v_2(-0.1), v_3(-0.1), v_4(-0.1), v_5(-0.1)) = (24.58, 24.22, 24.02, 25.50, 26.28)$ [m/s], as well as the remote vehicles’ delayed intent shared at time $t = -0.1$ [s]. The remote vehicles’ intent can be extracted from the data. An example of the remote vehicle 2’s intent at $t = -0.1$ [s] with a 10 [s] horizon is visualized by the blue shadings in Fig. 5.4(b)-(c) over the time span of $[-0.1, 9.9]$ [s]. On the other hand, all remote vehicles’ behavior limits follow the values in Table 5.1.

At the initial time, the ego vehicle first estimates the remote vehicles’ current status based on our discussion in the previous subsection. Then it performs conflict analysis according to Theorems 5 and 6 with each pair of remote vehicles sequentially. The conflict charts associated with four possible pairs of remote vehicles – $(1, 2)$, $(2, 3)$, $(3, 4)$, and $(4, 5)$ – are shown in Fig. 5.3(a)-(d) in the plane of front and rear gaps. In the conflict chart in Fig. 5.3(a), the estimated initial state $x_{\text{est}}(0)$ is in the conflict set \mathcal{M}_r , if the remote vehicles 1 and 2 are considered. Therefore, the ego

vehicle shall not decide to merge between remote vehicles 1 and 2. On the other hand, Fig. 5.3(c)-(d) reveal that the remote vehicle pairs (2, 3), (3, 4), and (4, 5) all yield $x_{\text{est}}(0) \in \mathcal{M}_g$. That is, conflict-free merge opportunities exist in all these remote vehicle pairs. For the best time efficiency, the ego vehicle shall select the farthest pair (2, 3) ahead to pursue a conflict-free merge. This way, conflict analysis is naturally scaled up to scenarios where more remote vehicles exist, while avoiding significant increase in computational load caused by increased dimensionality.

In the next section, we discuss controller design and demonstrate its effectiveness via simulations using real highway data.

5.2 Controller Design and Simulation

For $x(0) \in \mathcal{M}_g$ (or $x_{\text{est}}(0) \in \mathcal{M}_g$ under communication delays), we have a non-empty merge opportunity set Θ ; see Theorem 5. Each point in this set, $(t, r_0) \in \Theta$, provides a feasible position and a corresponding time for the ego vehicle's conflict-free merge. Therefore, similar to the previous chapter, one can design the control input $u_0(t)$ by selecting an appropriate goal point $(t^G, r_0^G) \in \Theta$ for the ego vehicle to pursue, that is, to construct a goal-oriented controller as proposed in Section 4.4.1. In what follows, we demonstrate that such goal-oriented controller can be applied to enable the ego vehicle's conflict-free merge maneuver.

While one may choose different goal points in the set Θ to realize a variety of desired performances of the ego vehicle, here we choose the goal point to be the “center” of the opportunity set, that is, we select t^G in the middle of the time span of the set Θ and r_0^G in the middle of the slice $\Theta(t^G)$; see the black dot in Fig. 5.5(a). Similar to the Section 4.4.1, we design a goal-oriented control input of constant value, i.e., $u_0(t) = u_0^G$, with which the goal point $(t^G, r_0^G) \in \Theta$ can be pursued by the ego vehicle. The analytical expression of u_0^G remains the same as in Appendix J, except that one needs to replace the s^G used therein as $s^G = r_0^G - r_0(\sigma)$. Under this constant-value input, the expected trajectory $r_0(t)$ is illustrated in Fig. 5.5(a) by the red arrow. Such controller provides guarantees on the formation of necessary front and rear gaps inside the merge zone. If the ego vehicle receives the remote vehicles' updated status and intent information, it may recompute the opportunity set Θ , update the goal point $(t^G, r_0^G) \in \Theta$, and recalculate the corresponding goal-oriented control input u_0^G ; see Fig. 5.5(b)–(d). We will now use simulations to demonstrate the performance of this controller.

Let us revisit the highway merge scenario in Fig. 5.4 involving five remote vehicles. Recall from the conflict charts in Fig. 5.3 and the discussions in Section 5.1.2 that, the ego vehicle shall select the remote vehicles 2 and 3 to perform a conflict-free merge. This decision is executed by the goal-oriented controller $u_0(t) = u_0^G$. Fig. 5.5(a)-(d) show the evolution of the merge opportunity set Θ , goal point $(t^G, r_0^G) \in \Theta$, and the positions r_0 , r_2 , and r_3 , as the ego vehicle 0 pursues its merge

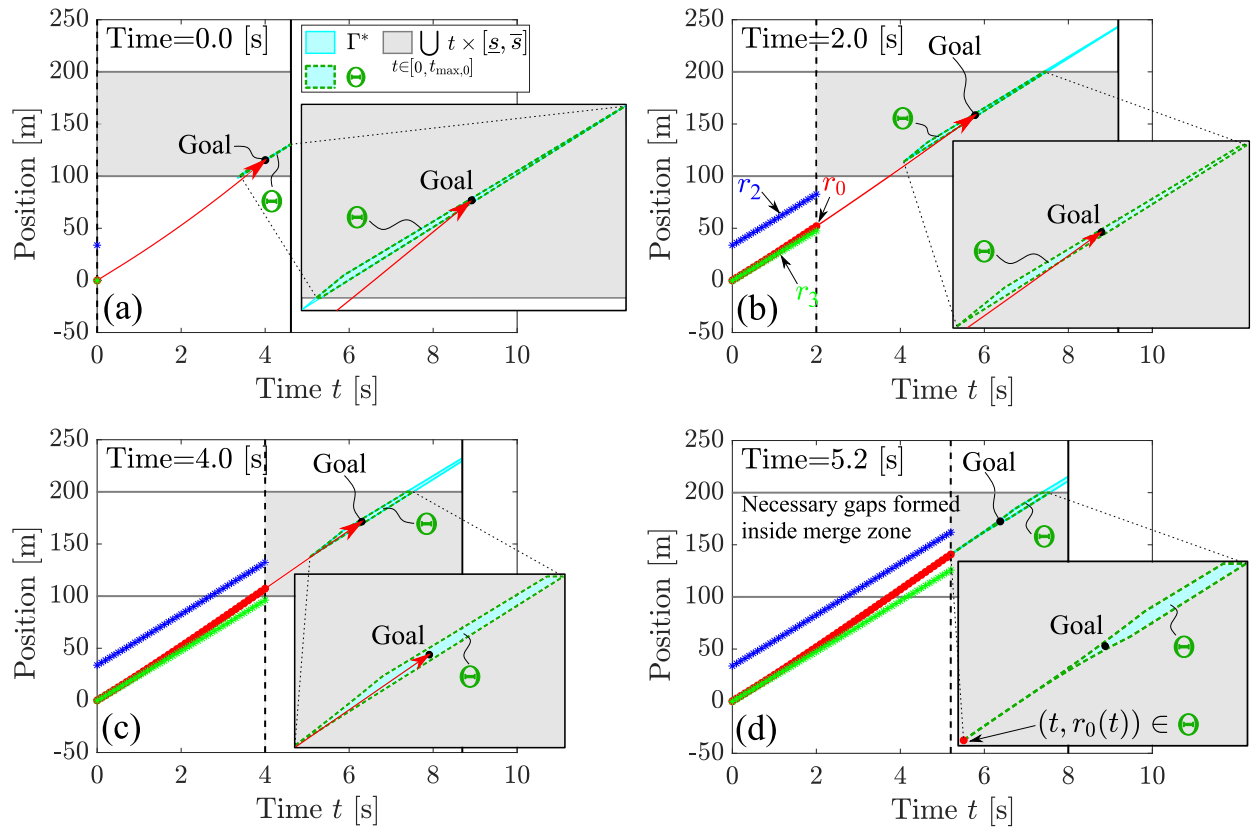


Figure 5.5: Evolution of merge opportunity set Θ , goal point $(t^G, r_0^G) \in \Theta$, and positions r_0 , r_2 , and r_3 , corresponding to the merge scenario in Fig. 5.4. Here, the ego vehicle 0 pursues merge opportunity between remote vehicles 2 and 3 using goal-oriented controller $u_0(t) = u_0^G$ with status and intent updates every 0.1 [s].

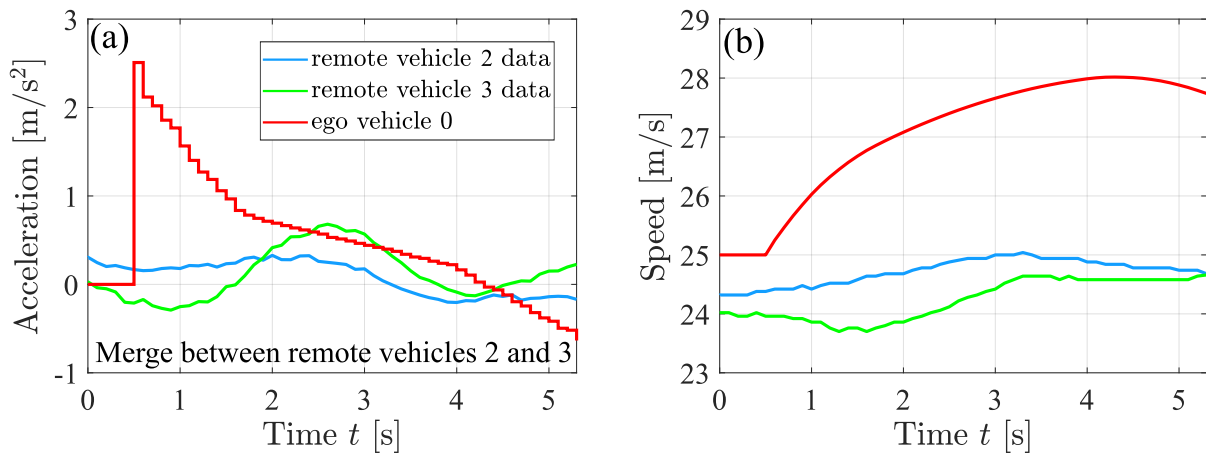


Figure 5.6: Simulation results of the ego vehicle 0 pursuing merge opportunity between remote vehicles 2 and 3, corresponding to Fig. 5.5.

opportunity between the remote vehicles 2 and 3. Under the designed goal-oriented controller, at time $t = 5.2$ [s], the ego vehicle forms the necessary front and rear gaps while remaining inside the merge zone; see Fig. 5.5(d). This can be confirmed by noticing that $(t, r_0(t)) \in \Theta$ holds, and thus, $x(t) \in \mathcal{M}_g$ holds according to (5.19). Then the ego vehicle may start its lateral motion to complete the merge maneuver. Notice that here, the goal point is still functioning as a guidance for the ego vehicle’s conflict-free and feasible maneuver, while it is not necessary to actually reach it. The ego vehicle’s speed and acceleration profiles when merging between remote vehicles 2 and 3 are shown in Fig. 5.6(a)-(b). We remark that the goal-oriented controller may also be applied for the ego vehicle to merge between the remote vehicle pairs (3, 4) and (4, 5) without a conflict, but choosing one of these pairs lead to worse time efficiency. These results demonstrate the effectiveness of goal-oriented control under the extended conflict analysis framework.

5.3 Summary

In this chapter, we investigated the scalability of multi-vehicle conflict analysis by considering more challenging mixed traffic scenarios where stricter maneuver constraints apply and more road users are involved. After a straightforward adaptation of the reachability-based approach built in Chapter 4, we derived conflict analysis algorithms that are implementable in real-time. The extended conflict analysis preserves advantages such as simplicity in investigating delay effects, capability of accommodating different V2X information, and flexibility in control design. These results were validated using simulations based on real traffic data in a multi-vehicle merge scenario. This way, the scalability of conflict analysis framework was demonstrated.

So far conflict analysis has allowed us to study conflict resolution under different cooperation classes – status sharing and intent sharing – from a theoretical perspective. In the next chapter, we will bridge the gap between theory and practice by implementing intent sharing communication on real vehicles, which validates on-board conflict analysis in the real world.

CHAPTER 6

Intent-based Conflict Analysis and Experimental Evaluation

Throughout Chapters 2-5, we have built a scalable framework of conflict analysis for mixed traffic. We studied the benefits of status and intent sharing and investigated the effects of time delays. In this chapter, we bring our theoretical analysis to practice.

We first revisit and generalize the representation of vehicle intent from the perspective of input/output relationship in dynamical systems. Such representation allows us to describe the intent of vehicles possessing different automation levels. We then implement, test, and systematically evaluate intent sharing using commercially available V2X communication devices on real production vehicles. We extend the conflict analysis framework such that the information encoded in status and intent messages can be tailored for both automated and human-driven vehicles. This enables personalized decision-making assistance that considers user-based preferences for conflict prevention during cooperative maneuvers.

Using merge scenarios as an application example, we test intent sharing for conflict resolution at a closed test track where a main road vehicle approaches a merge zone while sending both status and intent messages. These V2X messages are received by a human-driven vehicle seeking to join the main road. We use the extended conflict analysis to assist the decision-making of the merging vehicle. Through experiments, we validate an on-board warning system for human drivers that enhances maneuver safety. Results show that, compared to status sharing, receiving additional intent messages can substantially mitigate a human driver's decision inefficiency, leading to more time-efficient, yet still safe, maneuvers. Such merits are quantified by a proposed metric.

To further investigate intent sharing in the real world, we test intent messages on public highways. The communication performance is evaluated via the packet delivery ratio, i.e., the percentage of intent packets received out of those have been sent. We feed the collected data into numerical simulations to study the effects of communication conditions (e.g., intent message sending rate, intent horizon, and packet drops) on the benefits of intent sharing in conflict resolution.

The major contributions of this chapter are threefold. (i) We generalize the representation of

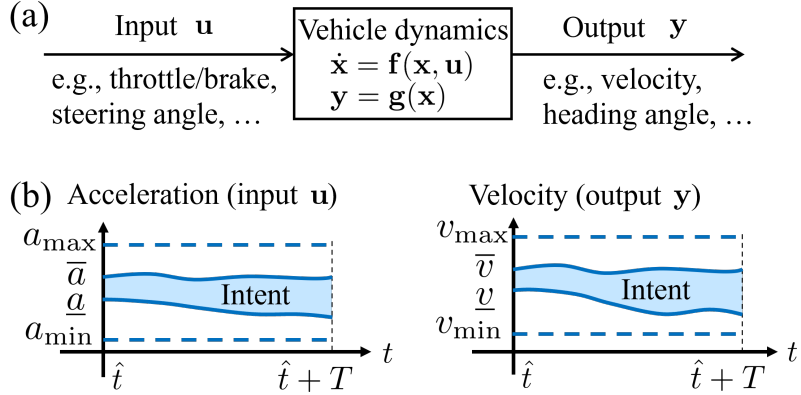


Figure 6.1: Modeling vehicle intent from dynamical systems viewpoint. (a) Diagram showing the input/output representation of a vehicle’s motion. (b) Conceptual illustration of a vehicle’s longitudinal motion intent.

vehicle intent from a dynamical systems viewpoint and establish the corresponding framework of conflict analysis. (ii) Test-track experiments of intent-based conflict analysis are presented to demonstrate personalized on-board decision assistance. (iii) Real highway data is collected and utilized to evaluate the benefits of intent sharing under different transmission conditions and imperfect communication. Insights from this analysis may benefit the on-going standardization and future real-world deployment.

The remainder of this chapter is organized as follows. In Section 6.1 we define vehicle motion intent. In Section 6.2 we establish the extended conflict analysis framework. In Section 6.3 we implement intent messages and test intent-based conflict analysis experimentally. In Section 6.4, highway data is used to investigate the benefits of sharing intent. Finally, Section 6.5 concludes the chapter.

6.1 Generalizing Motion Intent of Vehicles

To provide a rigorous definition of vehicle intent, we consider a vehicle’s motion from a dynamical systems viewpoint. As shown in Fig. 6.1(a), the vehicle’s behavior may be described by some observable quantities that we refer to as *outputs*, for example, the vehicle’s velocity and the heading angle. Such outputs are influenced by some other quantities called *inputs* that are applied to the vehicle. Examples of inputs are the throttle/brake and steering angle applied by the human driver or set by the autonomous driving system. Note that depending on the fidelity of the model describing the vehicle’s motion, different quantities may be considered as inputs and outputs. Based on this, we represent the vehicle’s motion intent by the bounded domains of inputs and outputs over a time horizon; see Fig. 6.1(b) for a conceptual illustration using the acceleration as input and the velocity

as output. Note that the domains specified in intent are more restricted than the vehicle's physical behavior limits since uncertainties are reduced when anticipating the vehicle's future maneuver. A formal definition of such vehicle intent is given below.

Definition 4. *A vehicle's motion intent is represented by the restricted domains $\mathbf{u}(t) \in [\underline{\mathbf{u}}(t), \overline{\mathbf{u}}(t)]$ and $\mathbf{y}(t) \in [\underline{\mathbf{y}}(t), \overline{\mathbf{y}}(t)]$ of the input and output over the time period $t \in [\hat{t}, \hat{t} + T]$, where \hat{t} is the time when the intent is generated, and T is the intent horizon. The vectors $\underline{\mathbf{u}}$, $\overline{\mathbf{u}}$, $\underline{\mathbf{y}}$, and $\overline{\mathbf{y}}$ collect the lower and upper bounds of the input vector \mathbf{u} and the output vector \mathbf{y} , and these bounds can be time-dependent. ■*

It is emphasized that according to Definition 4, a vehicle's intent can be compactly encoded into the input/output bounds, enabling an efficient implementation of intent sharing communication. Note that such intent information does not specify the intent sender's vehicle dynamics; see Fig. 6.1(a). However, the encoded input bounds and output constraints can be interpreted by an intent receiver using an appropriately chosen dynamical model, which allows the calculation of possible future trajectories of the intent sender in continuous time. We remark that Definition 4 is kept general such that one can describe a vehicle's intent for different scenarios under a unified framework, by selecting appropriate input/output quantities. Below we provide a more specific definition for a vehicle's longitudinal motion intent, which considers acceleration as input and velocity as output along a planned path; see Fig. 6.1(b) for an illustration.

Definition 5. *A vehicle's longitudinal motion intent is represented by a lane index I , a restricted acceleration (input) domain $u(t) \in [a(t), \bar{a}(t)]$ and velocity (output) domain $v(t) \in [v(t), \bar{v}(t)]$ over the time period $t \in [\hat{t}, \hat{t} + T]$, where \hat{t} is the time when this intent is generated, T is the intent horizon. Also, $a_{\min} \leq a(t) \leq \bar{a}(t) \leq a_{\max}$ and $v_{\min} \leq v(t) \leq \bar{v}(t) \leq v_{\max}$ where a_{\min} , a_{\max} , v_{\min} , and v_{\max} denote the physical acceleration and velocity limits. ■*

For instance, in a highway driving scenario, an intent message may convey the information that for the next $T = 8$ [s], the vehicle will be traveling on the leftmost lane (i.e., $I = 1$) while having its velocity between $v(t) \equiv 29$ [m/s] and $\bar{v}(t) \equiv 32$ [m/s], and acceleration between $a(t) \equiv -0.7$ [m/s²] and $\bar{a}(t) \equiv 0.9$ [m/s²]. It will be demonstrated below experimentally that the intent given by Definition 5 can be decoded to predict the intent sender's future behaviors using a simple first-principle model of longitudinal dynamics.

We remark that the intent of an automated vehicle may be given by specifying its future trajectory [30, 83, 86]. However, a major advantage of our representation is the capability of encoding uncertainties into motion intent (through input/output bounds) in an easy-to-interpret fashion. Thus, Definitions 4 and 5 can be implemented for vehicles possessing various automation degrees. For a connected automated vehicle, such intended input bounds and output constraints may

be extracted from its on-board motion planner that prescribes the vehicle's future behaviors. On the other hand, for a connected human-driven vehicle, the intent bounds may be determined in a data-driven manner for a specific human driver involved in similar traffic scenarios. Section 6.3 discusses in detail the implementation of intent sharing communication. We also remark that Definition 5 can be easily extended to include lane changes by specifying lane indices that correspond to different time periods. Alternatively, lateral motion can be incorporated into the definition of intent, by specifying the steering angle as an input, in accordance with Definition 4.

With the definition of vehicle intent, the next section provides theoretical preparation for the application of intent sharing for conflict resolution in cooperative maneuvering.

6.2 Generalizing Conflict Analysis

In this section, we generalize the framework of conflict analysis by considering multiple vehicles with general dynamical models and general cooperative driving scenarios. Under this extension, the received V2X messages can be interpreted in a personalized manner for both automated and human-driven vehicles considering their user-determined behavior preferences. Fig. 6.2 shows an illustration of the intent-based conflict analysis that we develop in this section. This generalized framework is then applied to investigate conflicts in a merge scenario.

6.2.1 Intent-based conflict analysis

Consider a cooperative maneuver involving an ego vehicle indexed 0, and N remote vehicles indexed $1, \dots, N$, whose dynamics are modeled by:

$$\begin{aligned}\dot{\mathbf{x}}_i(t) &= \mathbf{f}_i(\mathbf{x}_i(t), \mathbf{u}_i(t)), \\ \mathbf{y}_i(t) &= \mathbf{g}_i(\mathbf{x}_i(t)), \quad i = 0, 1, \dots, N.\end{aligned}\tag{6.1}$$

Here the dot denotes time derivative, $\mathbf{x}_i \in \Omega_i \subseteq \mathbb{R}^n$ is the state of vehicle i , $\mathbf{u}_i \in \mathbb{R}^m$ is the input, $\mathbf{y}_i \in \mathbb{R}^q$ is the output, and $\mathbf{f}_i : \Omega_i \times \mathbb{R}^m \rightarrow \Omega_i$, $\mathbf{g}_i : \Omega_i \rightarrow \mathbb{R}^q$ are continuous functions. Each vehicle $i \in \{0, 1, \dots, N\}$ is subject to

$$\mathbf{u}_i(t) \in [\mathbf{u}_{\min,i}, \mathbf{u}_{\max,i}], \quad \mathbf{y}_i(t) \in [\mathbf{y}_{\min,i}, \mathbf{y}_{\max,i}], \quad \forall t,\tag{6.2}$$

where $\mathbf{u}_{\min,i}, \mathbf{u}_{\max,i} \in \mathbb{R}^m$ and $\mathbf{y}_{\min,i}, \mathbf{y}_{\max,i} \in \mathbb{R}^q$ contain the (constant) lower and upper bounds for the input and output, imposed by the vehicle's physical behavior limits.

From the perspective of the ego vehicle 0, the remote vehicles $1, \dots, N$ are not controllable. That is, we cannot prescribe the inputs $\mathbf{u}_1, \dots, \mathbf{u}_N$, nor do we have the knowledge about their exact

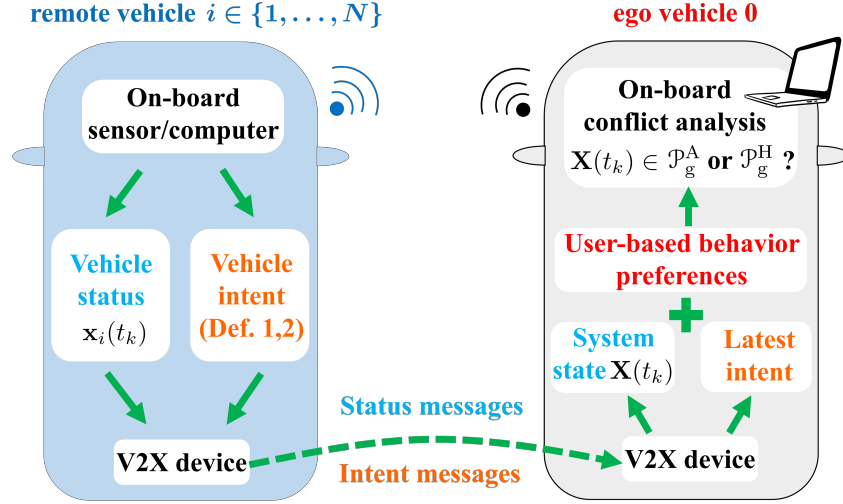


Figure 6.2: Schematic diagram of on-board conflict analysis that provides real-time decision assistance to the ego vehicle based on the remote vehicles' status and intent messages.

values. However, the remote vehicles' physical behavior limits in (6.2) are assumed to be known to the ego vehicle based on general knowledge of vehicle capabilities and traffic rules. Moreover, the remote vehicles may share their status \mathbf{x}_i and intent (cf. Definition 4) with the ego vehicle at given time instants. For example, knowing the intent of a remote vehicle $i \in \{1, \dots, N\}$ generated at time \hat{t} , in addition to (6.2), imposes the following input and output bounds:

$$\mathbf{u}_i(t) \in [\underline{\mathbf{u}}_i(t), \bar{\mathbf{u}}_i(t)], \quad \mathbf{y}_i(t) \in [\underline{\mathbf{y}}_i(t), \bar{\mathbf{y}}_i(t)], \quad t \in [\hat{t}, \hat{t} + T], \quad (6.3)$$

where the conditions $\mathbf{u}_{\min,i} \leq \underline{\mathbf{u}}_i(t) \leq \bar{\mathbf{u}}_i(t) \leq \mathbf{u}_{\max,i}$ and $\mathbf{y}_{\min,i} \leq \underline{\mathbf{y}}_i(t) \leq \bar{\mathbf{y}}_i(t) \leq \mathbf{y}_{\max,i}$ hold (element-wise). Given the remote vehicle's current status \mathbf{x}_i , its future evolution can be predicted from (6.1) under the constraints (6.2)-(6.3). We leave the details of communication setups for the next subsection, while here we present the main idea of conflict analysis.

We define the overall state of the system (6.1) as

$$\mathbf{X} := \begin{bmatrix} \mathbf{x}_0 \\ \mathbf{x}_1 \\ \vdots \\ \mathbf{x}_N \end{bmatrix} \in \Omega := \Omega_0 \times \Omega_1 \times \dots \times \Omega_N, \quad (6.4)$$

where Ω contains the states of interest when reasoning about conflicts between vehicles. We formally describe a conflict-free maneuver using the proposition

$$P := \{\forall t, \mathbf{X}(t) \notin \Omega^* \subseteq \Omega\}, \quad (6.5)$$

where Ω^* is the set that the states $\mathbf{X}(t)$ must avoid for all time t to ensure that a conflict never occurs during the maneuver. Note that encoding conflict conditions in the set Ω^* is a general representation which can be used to describe conflicts in a multitude of traffic scenarios.

Our goal is to ensure that the proposition P holds, by assisting the maneuver of the ego vehicle 0 while considering the environmental uncertainty coming from the remote vehicles. Such assistance may be provided at the decision level (e.g., whether the ego vehicle is able to merge ahead of an approaching remote vehicle without a conflict) and/or at the control level (e.g., what control input $\mathbf{u}_0(t)$ should be used to execute the corresponding decision). In this study, we focus on providing decision-level assistance to the ego vehicle (which may be either automated or human-driven), while leaving the control-level assistance for future work. To provide a personalized decision assistance, we consider the ego vehicle's user-based behavior preferences, modeled as input bounds and output constraints:

$$\mathbf{u}_0(t) \in [\underline{\mathbf{u}}_0(t), \bar{\mathbf{u}}_0(t)], \quad \mathbf{y}_0(t) \in [\underline{\mathbf{y}}_0(t), \bar{\mathbf{y}}_0(t)], \quad (6.6)$$

similar to the intent Definition 4. We assume that these bounds cover the whole time span of the ego vehicle's maneuver.

For an automated ego vehicle, such preference may be preset according to different metrics (e.g., passenger comfort and energy efficiency). When the ego vehicle is human-driven, these preference bounds may be extracted from specific human drivers' historical data when they were involved in similar maneuvers. Notice that for an automated ego vehicle, the behavior preference (6.6) represents the constraints in designing control strategies for completing a given maneuver. For the human-driven case, however, such preference represents the uncertainty in a human driver's behavior when performing the maneuver. In this case we assist the human driver's decision, but the vehicle is maneuvered by the driver.

With the ego vehicle's behavior preference and the remote vehicles' behavior uncertainty in mind, proposition P in (6.5) can be decomposed into three cases:

- (i) No-conflict case: Independent of the motion of remote vehicles $1, \dots, N$, the ego vehicle 0 is able to perform a conflict-free maneuver under its behavior preference.
- (ii) Uncertain case: Depending on the motion of remote vehicles $1, \dots, N$, the ego vehicle 0 may be able to perform a conflict-free maneuver under its behavior preference.
- (iii) Conflict case: Independent of the motion of remote vehicles $1, \dots, N$, the ego vehicle 0 is not able to perform a conflict-free maneuver under its behavior preference.

These three cases correspond to three pairwise disjoint sets within the set Ω . Depending on whether the ego vehicle 0 is automated or human-driven, different expressions are required for

these sets. For an automated ego vehicle, we have

$$\mathcal{P}_g^A := \{\mathbf{X} \in \Omega | \forall \mathbf{u}_1(t), \dots, \mathbf{u}_N(t), \exists \mathbf{u}_0(t), P\}, \quad (6.7)$$

$$\mathcal{P}_y^A := \{\mathbf{X} \in \Omega | (\exists \mathbf{u}_1(t), \dots, \mathbf{u}_N(t), \forall \mathbf{u}_0(t), \neg P) \wedge (\exists \mathbf{u}_1(t), \dots, \mathbf{u}_N(t), \exists \mathbf{u}_0(t), P)\}, \quad (6.8)$$

$$\mathcal{P}_r^A := \{\mathbf{X} \in \Omega | \forall \mathbf{u}_1(t), \dots, \mathbf{u}_N(t), \forall \mathbf{u}_0(t), \neg P\}, \quad (6.9)$$

where the symbol \neg means “negation” and \wedge means “and”. The inputs $\mathbf{u}_0, \mathbf{u}_1, \dots, \mathbf{u}_N$ are subject to their corresponding bounds imposed by the physical behavior limits (6.2), the intent (6.3) of remote vehicles, and the behavior preference (6.6) of ego vehicle. The superscript “A” corresponds to the ego vehicle being automated, while the subscripts “g”, “y”, and “r” correspond to the convention of using green, yellow, and red colors to visualize the no-conflict, uncertain, and conflict sets[95]. If the ego vehicle is human-driven, we have

$$\mathcal{P}_g^H := \{\mathbf{X} \in \Omega | \forall \mathbf{u}_1(t), \dots, \mathbf{u}_N(t), \forall \mathbf{u}_0(t), P\}, \quad (6.10)$$

$$\mathcal{P}_y^H := \{\mathbf{X} \in \Omega | (\exists \mathbf{u}_1(t), \dots, \mathbf{u}_N(t), \exists \mathbf{u}_0(t), \neg P) \wedge (\exists \mathbf{u}_1(t), \dots, \mathbf{u}_N(t), \forall \mathbf{u}_0(t), P)\}, \quad (6.11)$$

$$\mathcal{P}_r^H := \{\mathbf{X} \in \Omega | \forall \mathbf{u}_1(t), \dots, \mathbf{u}_N(t), \exists \mathbf{u}_0(t), \neg P\}, \quad (6.12)$$

where the superscript “H” is used for the human-driven case.

We emphasize that the no-conflict set \mathcal{P}_g^A in (6.7) requires the existence of an input for the automated ego vehicle (i.e., $\exists \mathbf{u}_0$), which steers the system state \mathbf{X} such that the proposition P remains true. In contrast, the no-conflict set \mathcal{P}_g^H in (6.10) requires the proposition P to hold for any input of the human-driven ego vehicle (i.e., $\forall \mathbf{u}_0$) under the behavior preference (6.6). Such difference accounts for the behavior uncertainty associated with the ego vehicle’s human driver, while considering that an automated counterpart can execute a prescribed input without significant uncertainty. One may observe similar difference between the conflict sets \mathcal{P}_r^A and \mathcal{P}_r^H . These yield the relations

$$\mathcal{P}_g^A \supseteq \mathcal{P}_g^H, \quad \mathcal{P}_r^A \subseteq \mathcal{P}_r^H. \quad (6.13)$$

That is, under the behavior uncertainty of ego vehicle’s human driver, the no-conflict set shrinks while the conflict set enlarges compared to the automated case. We remark that for both the automated and human-driven cases, the two predicates of the uncertain set \mathcal{P}_y^* negate those of the no-conflict set \mathcal{P}_g^* and conflict set \mathcal{P}_r^* (where “*” denotes either “A” or “H”). For human-driven

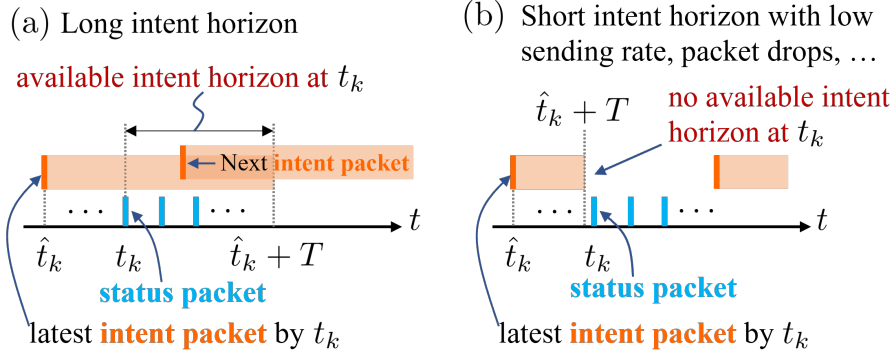


Figure 6.3: Visualizing packet receiving timing of V2X messages. (a) When intent packet has sufficient horizon. (b) When intent packet has short horizon while being sent with a low rate or when packet drops occur.

case (6.10)-(6.12), we have

$$(\exists \mathbf{u}_1(t), \dots, \mathbf{u}_N(t), \exists \mathbf{u}_0(t), \neg P) \iff \neg(\forall \mathbf{u}_1(t), \dots, \mathbf{u}_N(t), \forall \mathbf{u}_0(t), P), \quad (6.14)$$

$$(\exists \mathbf{u}_1(t), \dots, \mathbf{u}_N(t), \forall \mathbf{u}_0(t), P) \iff \neg(\forall \mathbf{u}_1(t), \dots, \mathbf{u}_N(t), \exists \mathbf{u}_0(t), \neg P), \quad (6.15)$$

which explains why the sets \mathcal{P}_g^H , \mathcal{P}_y^H , and \mathcal{P}_r^H are mutually disjoint and $\mathcal{P}_g^H \cup \mathcal{P}_y^H \cup \mathcal{P}_r^H = \Omega$. Similar relationships hold for the sets \mathcal{P}_g^A , \mathcal{P}_y^A , and \mathcal{P}_r^A .

By checking which subset of Ω the system state \mathbf{X} is currently located at, one can assist the ego vehicle to identify the opportunity in completing a conflict-free maneuver, resulting in safe and efficient decision. Note that such checking is made possible by the status and intent of the remote vehicles shared via V2X communication. The corresponding communication setup is provided in the next subsection.

6.2.2 Communication setup

We consider that all vehicles are equipped with V2X devices. The ego vehicle may acquire information regarding the remote vehicles' motion via status sharing and intent sharing. In status sharing, the ego vehicle 0 receives status information from the remote vehicles $1, \dots, N$ at discrete time moments t_k , $k = 0, 1, \dots$, i.e., it obtains $[\mathbf{x}_1(t_k)^\top, \dots, \mathbf{x}_N(t_k)^\top]^\top$. Here, for simplicity, we assume that the reception of status messages from all N remote vehicles is synchronized at each t_k . Due to the discrete nature of status information, the ego vehicle has the accurate knowledge of system state \mathbf{X} at times t_k only. In intent sharing, the remote vehicles transmit their intent messages at discrete time moments according to Definition 4. Similar to status sharing, we assume that the reception of intent messages are synchronized for all N remote vehicles.

For both status and intent packets, the transmission time delay is assumed to be negligible such

that a message is delivered immediately to the ego vehicle once generated from the remote vehicle. For analysis with time delays, we refer the readers to Chapter 4. However, the two types of messages (status and intent) may be transmitted with different sending rates, and therefore, they may not arrive at the ego vehicle’s V2X port in a synchronized fashion. A conceptual visualization of the message reception timing is shown in Fig. 6.3(a). For simplicity of notation, we avoid introducing a new index of intent messages, but simply use $\hat{t}_k \leq t_k$ to denote the latest time when the intent packets were received by the ego vehicle, at the status receiving time t_k . This corresponds to the notation used in (6.3) if one substitutes \hat{t} with \hat{t}_k for all remote vehicles.

At each time t_k , the available intent information, that the ego vehicle may use to predict the remote vehicle’s future trajectory, covers the time horizon $[t_k, \hat{t}_k + T]$; see Fig. 6.3(a). If intent packets are designed with a short horizon T , while subject to low sending rate and/or to packet drops, then $t_k \geq \hat{t}_k + T$ may occur; see Fig. 6.3(b). In this case, the information in the latest intent packet already expires at t_k and may not be used to facilitate the ego vehicle’s prediction. This suggests that a sufficient intent horizon together with appropriate communication conditions are needed to secure a satisfactory performance of intent sharing. Detailed evaluation of these communication factors are given in Section 6.4 via real highway data.

With this communication setup, one is able to check the system state \mathbf{X} at each time t_k while using the latest (available) intent information. If $\mathbf{X}(t_k) \in \mathcal{P}_g^A$ or $\mathbf{X}(t_k) \in \mathcal{P}_g^H$ (depending on whether the ego vehicle is automated or human-driven), then a conflict is guaranteed not to happen, and the ego vehicle may confidently initiate such a maneuver according to its behavior preference. Otherwise, the ego vehicle should not execute the maneuver to prevent potential conflicts caused by the behavior uncertainties of the remote and the ego vehicles. In the next subsection, we apply this conflict analysis framework to a merge scenario and develop an efficient algorithm to check whether $\mathbf{X}(t_k) \in \mathcal{P}_g^A$ or $\mathbf{X}(t_k) \in \mathcal{P}_g^H$.

6.2.3 Conflict analysis for a merge scenario

As an application of intent-based conflict analysis, we focus on the example of a merge scenario illustrated in Fig. 6.4(a). This maneuver is selected because it is one of the most challenging driving scenarios that frequently involves conflicts. Nevertheless, the results of the following analysis can be applied to a much broader set of conflict scenarios, such as intersections, unprotected left/right turns, and roundabouts.

In Fig. 6.4(a), the blue remote vehicle 1 is approaching a merge zone (yellow rectangle) while traveling along the main road. In the meantime, the white ego vehicle 0 is attempting to merge onto the main road. The conflict zone (red rectangle) is located towards the end of the merge zone. A conflict occurs when the two vehicles appear simultaneously inside the conflict zone, even

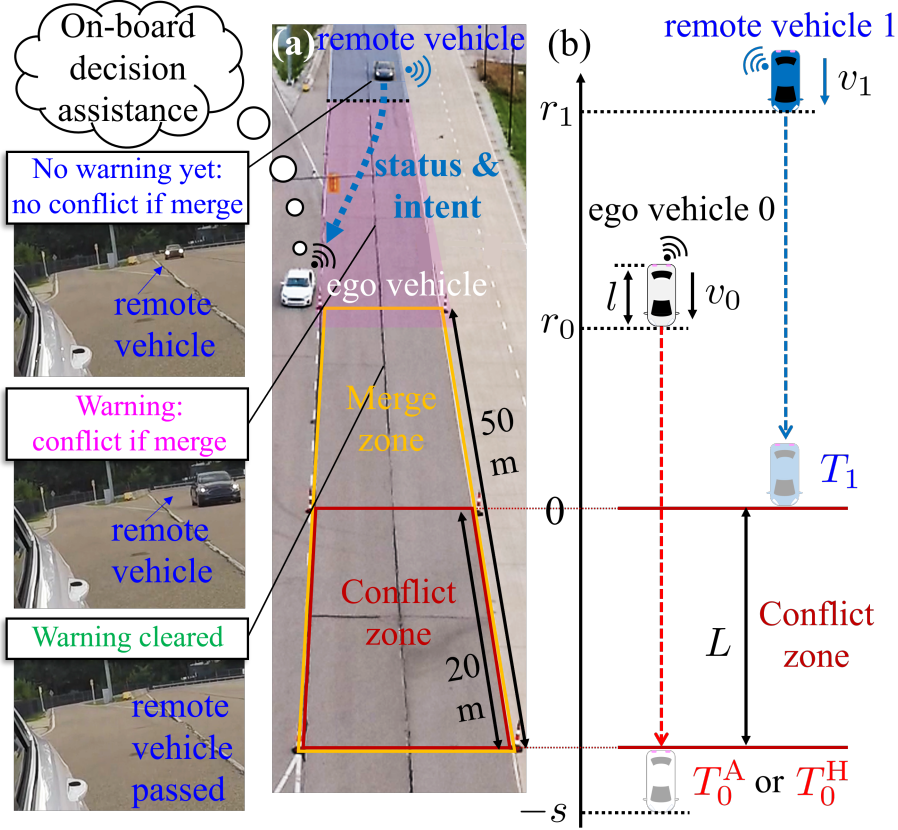


Figure 6.4: Validating intent sharing cooperation in a merge scenario using real vehicles at Mcity test track. (a) Experiments where intent-based conflict analysis provides on-board decision assistance to an ego vehicle attempting to merge. The rear mirror views of the ego vehicle are shown in the left column. (b) A generalized model of the merge scenario.

partially. Fig. 6.4(b) shows a generalized model for this scenario, while considering the vehicles' longitudinal dynamics only. We place the origin at the entry point of the conflict zone and use L to denote the conflict zone length. The front bumper positions of the vehicles are denoted by r_0 and r_1 , and the corresponding velocities are v_0 and v_1 . The same vehicle length ℓ is assumed for both vehicles and we define the variable $s := L + \ell$.

For simplicity, we model the vehicles' longitudinal dynamics while neglecting rolling resistance and air drag:

$$\begin{aligned} \dot{r}_i(t) &= -v_i(t), \\ \dot{v}_i(t) &= u_i(t), \quad i = 0, 1. \end{aligned} \tag{6.16}$$

Here, u_i is the control input (acceleration) of vehicle i , and the negative sign in front of the velocity corresponds to the fact that vehicles travel towards the negative direction (towards the conflict zone); see Fig. 6.4(b). The state and output of vehicle i are defined as $\mathbf{x}_i = [r_i \ v_i]^\top$ and $\mathbf{y}_i = v_i$. The

physical behavior limits of both vehicles, in terms of the input (acceleration) bounds and output (velocity) constraints, are given as

$$u_i(t) \in [a_{\min,i}, a_{\max,i}], \quad v_i(t) \in [v_{\min,i}, v_{\max,i}], \quad \forall t, \quad (6.17)$$

cf. (6.2). Table 2.1 gives the corresponding values drawn from the experiments performed at a closed test track; see more details in Section 6.3. For vehicle i , the set $\Omega_i = [-s, \infty) \times [v_{\min,i}, v_{\max,i}]$ in state space is used to reason about conflict. Hence the overall state of the system (6.16) is $\mathbf{X} := [\mathbf{x}_0^\top \ \mathbf{x}_1^\top]^\top \in \Omega := \Omega_0 \times \Omega_1$.

We are interested in whether the ego vehicle is able to merge ahead of the remote vehicle without a conflict. Such a conflict-free merge ahead is given by the proposition

$$P := \{\exists t, r_0(t) < -s \wedge r_1(t) = 0\}, \quad (6.18)$$

which states that by the time the remote vehicle enters the conflict zone, the ego vehicle has passed it; see Fig. 6.4(b). Here, we exploited the fact that vehicles only move forward during the merge (i.e., r_0 and r_1 are non-increasing functions of time t). Proposition (6.18) can be converted to the general form (6.5):

$$P = \{\forall t, \neg (r_0(t) \geq -s \wedge -s \leq r_1(t) \leq 0)\}, \quad (6.19)$$

see the proof in Appendix O. That is, to ensure a conflict-free merge ahead, the set

$$\Omega^* = [-s, \infty) \times [v_{\min,0}, v_{\max,0}] \times [-s, 0] \times [v_{\min,1}, v_{\max,1}], \quad (6.20)$$

must be avoided by the system state \mathbf{X} . Here, $\mathbf{X} \in \Omega^* \subset \Omega$ describes the scenario when the remote vehicle 1 is inside the conflict zone while the ego vehicle 0 has not yet exited it: it is either in the conflict zone, or has not yet reached the conflict zone. In this case a conflict-free merge ahead is not possible.

Following the communication setup given in the previous subsection, the ego vehicle has access to the system state $\mathbf{X}(t_k)$ at status message receiving times t_k . The available intent information at

Table 6.1: Parameters values used in the experiments at Mcity.

d	20 [m]	l	5 [m]
$a_{\min,0}$	-4 [m/s ²]	$a_{\min,1}$	-4 [m/s ²]
$a_{\max,0}$	4 [m/s ²]	$a_{\max,1}$	4 [m/s ²]
$v_{\min,0}$	0 [m/s]	$v_{\min,1}$	8 [m/s]
$v_{\max,0}$	15 [m/s]	$v_{\max,1}$	15 [m/s]

t_k is encoded in the latest intent message received from the remote vehicle 1 at \hat{t}_k :

$$u_1(t) \in [\underline{a}_1(t), \bar{a}_1(t)], \quad v_1(t) \in [\underline{v}_1(t), \bar{v}_1(t)], \quad t \in [t_k, \hat{t}_k + T]; \quad (6.21)$$

cf. Definition 5 and Fig. 6.3. For the ego vehicle 0, the behavior preference

$$u_0(t) \in [\underline{a}_0(t), \bar{a}_0(t)], \quad v_0(t) \in [\underline{v}_0(t), \bar{v}_0(t)], \quad (6.22)$$

holds until it exits the conflict zone, cf. (6.6). Fig. 6.6(a)-(b) show an example of such preference bounds associated with a human driver performing a merge maneuver.

Using the available intent (6.21) and behavior preference (6.22), if $\mathbf{X}(t_k)$ is in the set \mathcal{P}_g^A or in the set \mathcal{P}_g^H then the ego vehicle shall pursue the merge ahead opportunity; otherwise it shall yield to the approaching remote vehicle to avoid potential conflicts. This is summarized in the following decision-making rules:

$$\text{decision for an \textbf{automated} ego vehicle} = \begin{cases} \text{merge ahead,} & \text{if } \mathbf{X}(t_k) \in \mathcal{P}_g^A, \\ \text{yield,} & \text{otherwise.} \end{cases} \quad (6.23)$$

$$\text{decision for a \textbf{human-driven} ego vehicle} = \begin{cases} \text{merge ahead,} & \text{if } \mathbf{X}(t_k) \in \mathcal{P}_g^H, \\ \text{yield,} & \text{otherwise.} \end{cases} \quad (6.24)$$

The following two Theorems provide criteria to check $\mathbf{X}(t_k) \in \mathcal{P}_g^A$ (for an automated ego vehicle) and $\mathbf{X}(t_k) \in \mathcal{P}_g^H$ (for a human-driven ego vehicle), respectively.

Theorem 7. *Given the dynamics (6.16)-(6.17), the current system state $\mathbf{X}(t_k)$, the remote vehicle's latest available intent (6.21), and the behavior preference (6.22) of an **automated** ego vehicle, we have*

$$\mathbf{X}(t_k) \in \mathcal{P}_g^A \iff T_0^A < T_1, \quad (6.25)$$

where T_0^A is the time such that $r_0(T_0^A) = -s$ under

$$u_0(t) \equiv \bar{a}_0(t), \quad t \geq t_k, \quad (6.26)$$

and T_1 is the time such that $r_1(T_1) = 0$ under

$$u_1(t) = \begin{cases} \bar{a}_1(t), & \text{if } t \in [t_k, \hat{t}_k + T], \\ a_{\max,1}, & \text{otherwise.} \end{cases} \quad (6.27)$$

Proof. See Appendix P. □

Theorem 8. *Given the dynamics (6.16)-(6.17), the current system state $\mathbf{X}(t_k)$, the remote vehicle's latest available intent (6.21), and the behavior preference (6.22) of a **human-driven** ego vehicle, we have*

$$\mathbf{X}(t_k) \in \mathcal{P}_g^H \iff T_0^H < T_1, \quad (6.28)$$

where T_0^H is the time such that $r_0(T_0^H) = -s$ under

$$u_0(t) \equiv \underline{a}_0(t), \quad t \geq t_k, \quad (6.29)$$

while T_1 is the same as in Theorem 7.

Proof. See Appendix Q. □

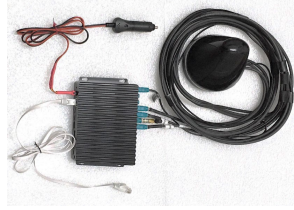
As depicted in Fig. 6.4(b), T_0^A in Theorem 7 calculates the time of an automated ego vehicle 0 exiting the conflict zone under its best-case behavior (input upper bound). In comparison, T_0^H in Theorem 8 corresponds to the time when a human-driven ego vehicle exits the conflict zone under its worst-case behavior (input lower bound) due to the uncertainty in human behavior. On the other hand, T_1 gives the time of the remote vehicle 1 entering the conflict zone under its worst-case future behavior, that is, when using the input upper bound in its intent (6.21) and in its physical behavior limits (6.17). As indicated by (6.27), with intent information, the ego vehicle can estimate the evolution of its environment with reduced uncertainty. It will be shown later experimentally that sharing intent significantly improves the efficiency in decision making. Notice that if $t_k \geq \hat{t}_k + T$ happens due to short intent horizon and/or improper communication conditions, then the intent is no longer available at t_k and (6.27) degrades to $u_1(t) \equiv a_{\max,1}$ for $t \geq t_k$.

Based on Theorems 7 and 8, examining $\mathbf{X}(t_k) \in \mathcal{P}_g^A$ or $\mathbf{X}(t_k) \in \mathcal{P}_g^H$ (i.e., whether a conflict-free merge ahead is guaranteed for an automated or a human-driven ego vehicle) reduces to calculating the time parameters T_0^A , T_0^H , and T_1 . Such calculation can be done efficiently by performing numerical integration for the corresponding dynamics model using the indicated (deterministic) control inputs while satisfying output constraints. In the next section, we implement this intent-based conflict analysis algorithm on production vehicles to provide real-time decision assistance to human drivers.

6.3 Experiments at Mcity Test Track

In this section, we first discuss the implementation of vehicle intent (defined in Section 6.1) in V2X messages. Then we present the experimental results obtained on a closed test track. These

(a) V2X OBU



(b) Intent message example 1: cruise control

Current	Device ID	GPS time [ms]	Latitude	Longitude	Speed [cm/s]	
GPS	3460933077	1668181920900	423017075	-836983479	1338	
Intent	0	-0.550000	0.437000	-0.300000	0.300000	10.000000
	Lane	Lower and upper bounds of speed deviation from current speed [m/s]		Lower and upper bounds of acceleration [m/s ²]		Intent horizon [s]

(c) Intent message example 2: human driving

Current						
GPS	3460933077	1668194727100	423016591	-836974119	1283	
Intent	0	-2.500000	0.000000	-1.000000	0.300000	10.000000

Figure 6.5: Implementing intent messages using the V2X protocol WSMP. (a) Commercially available V2X Onboard Unit (OBU). (b)-(c) Examples of intent messages transmitted in the experiments.

experiments validate the intent-based conflict analysis using connected vehicles. Experimental data is used to quantify the benefits of receiving intent messages.

6.3.1 Creating intent messages

We encode the longitudinal motion intent of Definition 5 into wireless messages using commercially available V2X communication devices; see Fig. 6.5(a). For simplicity, we focus on constant intent bounds for both acceleration (input) and velocity (output). The vehicle’s longitudinal intent is packaged into a few parameters, which requires small data space to store and transmit, and uses communication resources efficiently. For time-dependent intent bounds, one may still parameterize them as functions of time to enable compact representation. Details on such implementation can be found in our recent work [99].

To implement intent messages, we adopt the WAVE Short Message Protocol (WSMP) [88], an efficient network layer messaging protocol that is able to transmit custom messages with standardized security [87]. Using the V2X Onboard Units (OBUs) shown in Fig. 6.5(a), we create secured intent messages in C language via the OBU supplier’s application programming interface (API). We design appropriate data structures to store the intent parameters and specify the sending rate of intent packets. By running the developed C program on a computer connected to the OBU via

Ethernet, intent messages can be sent/received by the OBU at a user-determined rate.

Two of intent message examples, corresponding to two different driving scenarios in our experiments are shown in Fig. 6.5(b)-(c). They were transmitted from a vehicle during a driving test whose details are given in the next subsection. The vehicle's current GPS information and its intent over a future horizon of 10 [s] are included in each message. Note that the intended velocity bounds are expressed relative to the current velocity of the vehicle. For instance, the intent message in Fig. 6.5(b) encodes a velocity range of $[13.38 - 0.55, 13.38 + 0.437]$ [m/s]. Examples of such intent bounds can be seen in Fig. 6.6(c)-(d). Thanks to the data-compact description of vehicle intent, the messages are contained in small packets of the size 51 bytes. One may further downsize intent packets by using data types that occupy less storage. Such lightweight design is important since smaller packet size contributes to less packet drops in real traffic [97].

6.3.2 Experiments in Mcity

Having implemented intent messages, we test intent sharing for conflict resolution using two human-driven vehicles equipped with V2X OBUs; see Fig. 6.5(a). Each OBU is equipped with a GPS unit, gyroscope, accelerometer, and magnetometer. Our OBUs communicate in a peer-to-peer manner through V2X antennas, using Cellular-V2X (C-V2X) direct communications [117]. Such C-V2X adopts an efficient wireless access technology – single carrier frequency division multiple access (SC-FDMA) at the medium access control (MAC) layer [118], contributing to good communication range and reliability. During the tests, our OBUs operated at the 5.9 GHz frequency band with 20 dBm transmit power.

The experiments were performed at the Mcity test track of the University of Michigan. Fig. 6.4(a) shows the experimental setup, in which the ego vehicle (white) intends to merge onto the main road inside a 50 [m] long merge zone as the remote vehicle (blue) approaches on the main road. Notice that the merge zone does not exactly correspond to that of the actual on-ramp. Such design allows a longer section of the main road to be used by the remote vehicle to perform the required maneuvers (as specified below) before the ego vehicle merges. We define a conflict zone of length 20 [m]. To avoid danger to the experiment participants while studying conflicts, the second to the rightmost lane was used by the remote vehicle when approaching on the main road.

We define the initial time of each merge experiment as the moment when the distance between the remote vehicle and the conflict zone's entry point is 150 [m]. The ego vehicle's initial position is set at the entry point of the merge zone (30 [m] in front of the entry of the conflict zone), while its initial speed is set as zero; see Fig. 6.4(a). Such experimental setup replicates one of the most challenging merge scenarios where a merge has to be initiated from standstill; see Fig. 6.10(a)-(b) for a public road example that is often seen on US expressways. Note, however, that our

methodology and qualitative results can be extended to many other traffic scenarios.

Two different behaviors were exhibited by the remote vehicle when driving along the main road: (i) cruise control with speed set to 30 [mi/hr] \approx 13.4 [m/s]; (ii) human driving with speed decreasing from 30 [mi/hr]. Accordingly, we created intent messages for these two scenarios with the intent parameters given in the examples in Fig. 6.5(b)-(c). Examples of the remote vehicle's speed and acceleration profiles when performing such maneuvers are shown in Fig. 6.6(c)-(d). Blue shadings indicate the intent bounds which were determined based on data collected while the vehicle repeatedly performed such maneuvers. Indeed in practice, the parameters of human driving intent may be determined based on such historical data. The consideration of different remote vehicle behaviors allow us to demonstrate personalized decision assistance while responding to different intent information. The sending rate of intent messages was set to 1 [message/s]. Meanwhile, we used standard BSMs to transmit the remote vehicle's status information (position r_1 and velocity v_1) in every 0.1 [s].

In our experiments, the ego vehicle was human driven. We extracted the human driver's behavior preference beforehand by collecting data of the driver performing merge maneuvers multiple times at the test track. The cumulative min/max values of the speed and acceleration profiles yield the lower/upper bounds of the driver's preferred behavior shown in Fig. 6.6(a)-(b). The uncertainty in human driving is highlighted by the gray region between the bounds. Inside the ego vehicle, we used a computer to manage the reception of status and intent messages. The conflict analysis algorithm in Theorem 8 was implemented through MATLAB real-time. Decision assistance to the ego vehicle's human driver was provided on-board based on the decision rule (6.24) and Theorem 8, that is,

$$\text{decision assistance} = \begin{cases} \text{no warning,} & \text{if } T_0^H(t_k) < T_1(t_k), \\ \text{warning issued,} & \text{if } T_0^H(t_k) \geq T_1(t_k), \end{cases} \quad (6.30)$$

where t_k is status receiving time. Warning was issued from the computer running conflict analysis as audible beep sounds with a corresponding warning message displayed on the screen.

We performed experiments in two different ways. In the first case, highlighted in Figs. 6.4(a) and 6.6(e)-(f), on-board conflict analysis was performed while the ego vehicle stayed stationary at its initial position. These experiments were used to demonstrate the utility of intent sharing in resolving conflicts, and to quantify the benefits of intent. In the second case, shown in Fig. 6.7, on-board conflict analysis was performed while the ego vehicle's driver was asked to initiate the merge maneuver with different timings before/after the issuance of warning. These experiments enabled the validation of the intent-based conflict analysis for real human drivers' merge maneuvers. The results of these two categories of experiments are presented in detail in the next two subsections.

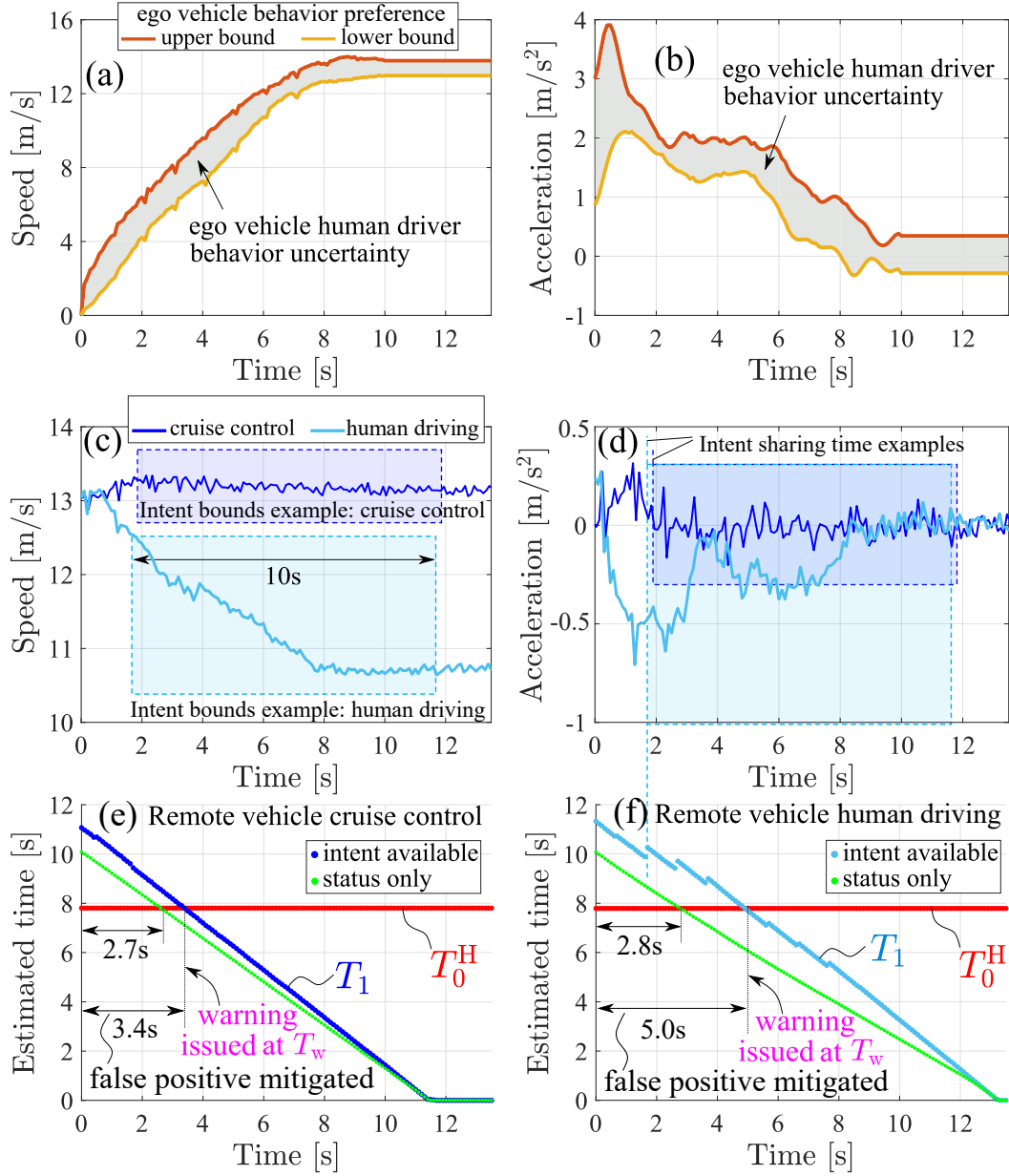


Figure 6.6: Benefits evaluation of intent sharing in Mcity experiments where the ego vehicle performed on-board conflict analysis while maintaining standstill. (a)-(b) Ego vehicle's behavior preference. (c)-(d) Remote vehicle's maneuvers while using cruise control and when the human driver decreases the speed. Examples of intent bounds are highlighted as blue shadings. (e)-(f) Evolution of estimated times T_0^H and T_1 under the aforementioned two different behaviors of the remote vehicle. The warning issuance times T_w highlight the benefits of intent sharing in mitigating false positive decisions.

6.3.3 Evaluating benefits of intent sharing

An experiment performed with stationary ego vehicles is illustrated in Fig. 6.4(a) through the ego vehicle's rear view camera images. With the remote vehicle being far away, the on-board conflict analysis does not predict a conflict upon the ego vehicle merging ahead, and accordingly, no warning is issued. As the remote vehicle approaches the ego vehicle from behind, a potential conflict between the two vehicles is predicted for the merge. Thus, a warning is generated, which continues until the remote vehicle passes the ego vehicle. Fig. 6.6(e)-(f) visualize the conflict analysis of two such experiments under the aforementioned two different behaviors of the remote vehicle (cruise control and human driving). Each time when a status update is received, the time parameters T_0^H and T_1 are calculated utilizing the ego vehicle's behavior preference and the remote vehicle's latest intent and status information. The small jumps (appearing every 1 [s]) in T_1 in Fig. 6.6(f) correspond to receiving new intent messages.

In what follows, we discuss the benefits quantification of intent sharing based on experimental results. To start, note that an ideal decision assistance shall (i) avoid *false negative* decisions, i.e., a conflict happens while a warning is not provided in time; (ii) minimize *false positive* decisions, i.e., a warning is provided while the ego vehicle can still confidently merge ahead without a conflict. Since our framework considers the worst-case behaviors of the remote and ego vehicles (see Theorem 8), the absence of *false negative* decisions is guaranteed theoretically, and this is also demonstrated empirically in the next subsection. Thus, mitigating *false positive* decisions is of our main interest. This is related to the *warning issuance time*, which is the time when the warning first appears after the experiment is initiated. A too early warning can lead to the human driver missing the opportunity to pursue a non-conflicting merge ahead, making the driver wait longer than necessary. Such unnecessary delays compromise the efficiency of the on-ramp.

According to (6.30) warnings are issued when $T_0^H \geq T_1$. Thus, to quantify the benefits, we use the warning issuance time

$$T_w = \min t_k \in \{t_0, t_1, \dots\}, \quad \text{s.t.} \quad T_0^H(t_k) \geq T_1(t_k), \quad (6.31)$$

where t_k are the times when status are received. In Fig. 6.6(e) and (f) we have $T_w = 3.4$ [s] for the cruise control scenario and $T_w = 5.0$ [s] for the human-driving scenario, respectively.

To highlight the benefits of intent sharing, we compare the warning issuance time T_w with a baseline case: when only status sharing messages are used. Suppose that intent messages had not been transmitted, the time parameter T_1 would be calculated with smaller values due to more conservative prediction on the remote vehicle's future behavior; see green curves in Fig. 6.6(e)-(f). In both cases, the warning issuance times shrink (to $T_w = 2.7$ [s] and 2.8 [s], respectively). Therefore, intent sharing indeed mitigates *false positive* decisions in conflict resolution compared

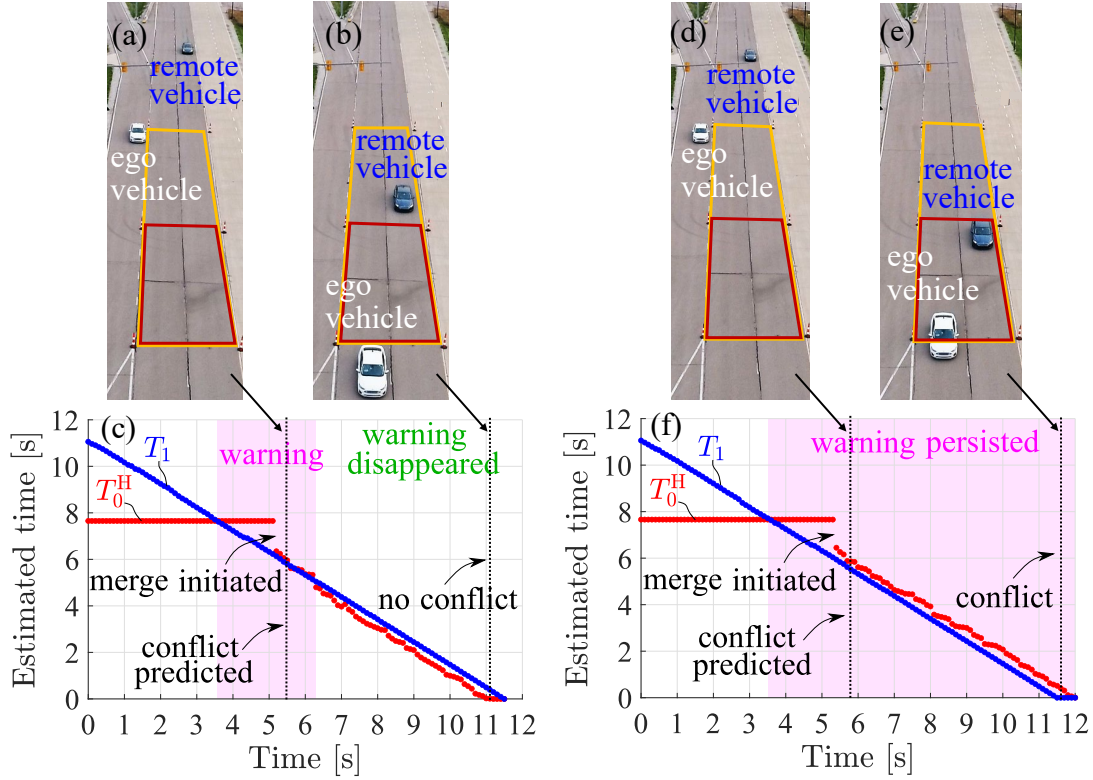


Figure 6.7: Two examples of Mcity experiments where the remote vehicle approaches with cruise control and the ego vehicle driver merges after the issuance of warning. (a)-(c) A scenario where the warning disappears automatically during the maneuver based on the ego vehicle’s actual behavior and the updated V2X messages. No conflict happens after all as illustrated in panel (b). (d)-(f) A scenario where the warning persists after being issued. Here an actual conflict happens as shown in panel (e).

to status sharing.

Notice that for status sharing only, the difference between the warning issuing times associated with the cruise control and human driving cases is small. This is because of the similar status of remote vehicle at the beginning of both maneuvers. In contrast, with the anticipation of future motion encoded in the intent messages, different remote vehicle behaviors (intentions) were distinguished by our framework through the different warning issuing times.

6.3.4 Validating intent-based conflict analysis

Here we describe the experiments when the ego vehicle’s human driver starts to merge with designated timings before/after the issuance of the warning, while conflict analysis is performed. These experiments demonstrate that our framework enhances the safety of the ego vehicle by providing on-board warnings with no *false negative* decision and that the algorithm can self-correct the *false positive* decision in real-time during a merge.

In the experiment shown in Fig. 6.7(a)-(c), the remote vehicle is using cruise control while the ego vehicle's driver initiates the merge after the warning starts. As panel (c) depicts, the value of T_0^H drops at around 5.4 [s] when the ego vehicle begins to move (whose actual behavior is better than the worst-case input used for conflict analysis). Then the on-board warning automatically disappears during the maneuver at around 6.3 [s] based on the updated status and intent information. As shown in panel (b) conflict does not happen after all. Such self-adjustment of the warning showcased our framework's capability of real-time decision assistance. Another experiment is shown in Fig. 6.7(d)-(f), where the remote vehicle attempts to merge ahead amid the warning (which persists throughout the maneuver), and this leads to an actual conflict under the behavior uncertainty of the ego driver. We emphasize again that the warning was tailored to the specific driver's behavior preference.

By varying the ego vehicle's merge initiation timing, the experiments were repeated multiple times. For the case of cruise control, the experimental results are summarized in Fig. 6.8(a), depicting the ego vehicle's merge starting time and the remote vehicle's corresponding position, and representing the merge results by colors. As shown by the blue points, the ego vehicle was always able to merge ahead without a conflict when initiating a merge before the warning was issued, i.e., no *false negative* decision was observed. On the other hand, the yellow points correspond to *false positive* decisions, which stem from using the ego drivers' worst-case behaviors when dealing with the uncertainties in human driving. Intent sharing indeed reduces such *false positive* decisions as highlighted by the larger average warning issuance times, compared to the status sharing only case. Such *false positive* warnings were self-corrected in real-time during the maneuver based on the updated information; see Fig. 6.7(a)-(c). The necessity of having conservatism in conflict analysis is, however, justified by a segment of data points with mixed yellow and red colors in Fig. 6.8(a), that is, conflicts could occur depending on the ego driver's actual behavior. With the remote vehicle being closer, merge ahead was no longer achievable without a conflict, as shown by the red points. Finally, the green points indicate that, by following the warning, a conflict-free merge behind was always realizable.

As shown in Fig. 6.8(b), when the remote vehicle was operated by a human driver, the experimental results remained qualitatively similar. In fact, the on-board warning system was also tested under a different human driver of the ego vehicle, who drove more aggressively (with higher values of the preferred velocity and acceleration bounds). While the detailed results of such experiments are omitted in this chapter due to qualitative similarity, we observed larger warning issuance times due to a more aggressive behavior preference. These experiments validated the capability of the conflict analysis in providing personalized decision assistance tailored to different ego drivers under different remote vehicle intentions. We demonstrated that the real-time on-board warning provided a sufficient safety margin in alerting the human driver of the ego vehicle of a potential conflict. At the same time our intent-based warning led to a significant reduction in *false positives* compared to

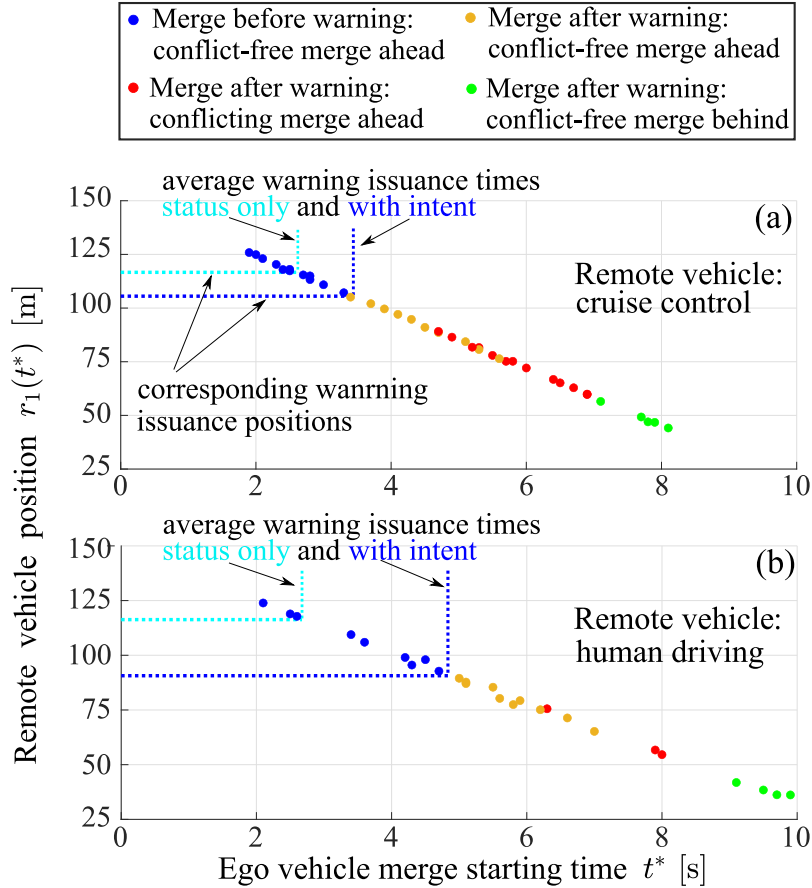


Figure 6.8: Experimental results validating the on-board decision assistance enabled by intent-based conflict analysis. Each data point marks an experiment, showing the merge starting time of the ego vehicle and the corresponding position of the remote vehicle. Colors indicate different merge results. (a) Remote vehicle uses cruise control. (b) Remote vehicle is human-driven.

a status-based warning.

6.4 Evaluating Intent Sharing using Real Highway Data

So far we validated intent sharing at the Mcity test track. In this section we bring intent sharing to public roads. We first test intent messages on real highways. Then we perform numerical simulations to investigate the effects of communication conditions on the benefits of intent sharing.

6.4.1 Packet delivery ratios on public highways

The transmission of intent messages was tested using connected human-driven vehicles on two different highways in south-east Michigan: on a rural section of highway US-23; and on an urban section of highway I-275.

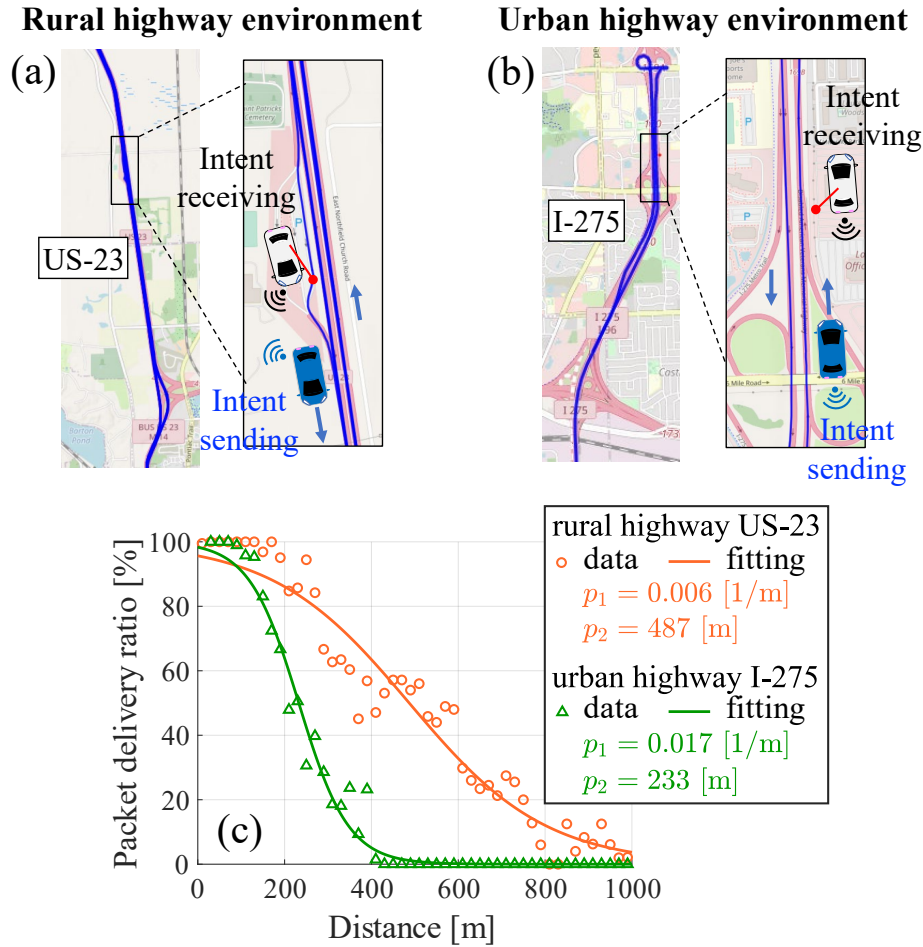


Figure 6.9: Testing packet delivery ratio of intent messages (a) on a rural section of highway US-23, and (b) on an urban section of highway I-275. (c) The corresponding packet delivery ratios as a function of distance between intent sender and receiver.

The experimental setup used on highway US-23 is depicted in Fig. 6.9(a). While traveling along the highway, the blue vehicle sends status messages via BSMs and intent messages as described in Section 6.3.1, both at a rate of every 0.1 [s]; see the blue trajectory for the route taken. The white vehicle receives the messages while staying next to the highway at a rest area. The collected data allows for the calculation of intent packet delivery ratio, i.e., the percentage of packets received versus those have been sent, under different inter-vehicle distances. Note that here we are interested in testing the intent packet reception on public roads, while the exact intent parameter values in each message are not important. Similar experimental setup is shown in Fig. 6.9(b) for the experiments conducted on an urban section of highway I-275.

The reception of intent packets is indeed affected by the distance and the environment in which the vehicles were operating; see data points in Fig. 6.9(c). To capture the trend of decreasing packet

delivery ratio as a function of the inter-vehicle distance d , we fit the sigmoid function

$$S(d) = 1 - \frac{1}{1 + e^{-p_1(d-p_2)}}, \quad (6.32)$$

to the data where parameter p_1 describes the decreasing rate (steepness) while parameter p_2 corresponds to the d value at the function's midpoint. Such function has been widely used in the literature for evaluating wireless messages' packet delivery ratios [119]. To fit the function (6.32) to the data, we minimize the root mean square error

$$\text{RMSE} = \sqrt{\frac{1}{M} \sum_{k=1}^M (S(d_k) - \hat{S}_k)^2}, \quad (6.33)$$

where d_1, \dots, d_M represent distances where packet delivery ratio data $\hat{S}_1, \dots, \hat{S}_M$ are available. The fitted functions are depicted as solid curves in Fig. 6.9(c) with the corresponding parameter values shown on the right.

For the rural highway section on US-23, relatively high packet delivery ratio is maintained until 200 [m], while gradual drops appeared for larger distances. Notice that intent packets could be received up to 1000 [m]. For the urban highway environment on I-275, the packet delivery ratio drops earlier and more sharply as inter-vehicle distance increases; see larger p_1 and smaller p_2 values. This deterioration is due to obstructions such as dense traffic, buildings and overpasses. We remark that these observations are representative – our further tests revealed more intent packet drops on urban roads compared to urban highways, due to more obstacle-related communication interruptions. The qualitative trend, however, remains similar. On the other hand, the packet delivery ratio in the Mcity experiments (Fig. 6.7) was almost 100% due to the small size of the test track.

These data-based results of packet delivery ratio will be used in the next subsection to evaluate the effects of communication conditions on the benefits of intent sharing in resolving conflicts for cooperative maneuvers.

6.4.2 Effects of communication conditions

In this subsection, we study the benefits of intent sharing under imperfect communication where intent packet drops exist, while considering different intent sending conditions (e.g., rate and horizon). To this aim, we perform numerical simulations for a highway merge scenario in a real-world road configuration using real human driving data. We select the on-ramp of highway M-14 near Barton Drive in Ann Arbor, Michigan, as our simulation example, which requires a highway merge to be initiated from a stop sign with zero initial speed; see Fig. 6.10(a)-(b). For this highway

merge section, we define a conflict zone shown as the red rectangle in Fig. 6.10(a). The entry point of the conflict zone is where the lane width of the on-ramp shrinks to 1.2 [m], which is narrower than a typical vehicle and a conflict with adjacent lane vehicles becomes apparent. The conflict zone ends at the end of the ramp. This yields a conflict zone size of 24.5 [m]. We remark that when choosing a slightly different start/end points for the conflict zone the simulation results remain similar.

We consider the scenario that a human-driven ego vehicle attempts to merge from standstill at the highway entrance, while a remote vehicle is approaching along the rightmost lane. To obtain behavior preference of a human driver’s merge maneuver, we collected data from a driver who merged multiple times from the M-14 entrance. Similar to the Mcity experiments, we extracted the lower/upper bounds of preferred speed and acceleration shown in Fig. 6.10(c)-(d). The initial position of the ego vehicle (at the stop sign) is 111.4 [m] away from the entry point of the conflict zone. To represent the remote vehicle’s behavior for the simulation, we use data collected by a human-driven vehicle; see the blue curves in Fig. 6.10(c)-(d). The initial position of remote vehicle is selected as 450 [m] from the conflict zone. That is, the two vehicles are (roughly) 338.6 [m] apart at the initial time, enabling the exchange of intent messages (with packet drops); cf. Fig. 6.9(c).

In the simulation, the remote vehicle shares its status (position and speed) every 0.1 [s], while the intent information (of Definition 5) is shared with different sending rates and intent horizons. At any intent sharing time, the bounds of the intended speed and acceleration are extracted from the remote vehicle’s data. The blue shadings in Fig. 6.10(c)-(d) illustrate an example of intent shared at 1 [s] with a horizon of 10 [s], where the min/max values of the corresponding data segment yield the bounds. Note that in reality intent may not be generated this way as one does not know exactly the future profile, but simulations with such “accurate” intent allow us to focus on investigating the effects of communication conditions.

As the remote vehicle approaches, the ego vehicle performs on-board conflict analysis while staying at the stop sign. Corresponding to highway driving, the speed limits of the remote vehicle are set as $v_{\min,1} = 20$ [m/s] and $v_{\max,1} = 32$ [m/s], while its acceleration limits are the same as in Table 6.1. The simulation results in Fig. 6.10(e) show the estimated times T_0^H and T_1 calculated via conflict analysis. Here, we incorporated the intent packet delivery ratio of the rural highway US-23 (orange curve in Fig. 6.9(c)) into the simulation. Namely, the reception of intent packets is modeled by a Bernoulli process such that the probability of receiving a packet is given by the packet delivery ratio corresponding to the current distance between vehicles.

Three different intent sharing conditions are simulated for the remote vehicle. Without intent sharing (green curve), the warning starts at $T_w = 3.1$ [s]. When intent is sent every 0.1 [s] with horizon 5 [s] (purple curve), the warning starts later at $T_w = 4.3$ [s], giving more opportunity for the ego vehicle to pursue merge ahead. As the intent horizon is increased to 10 [s] while maintaining

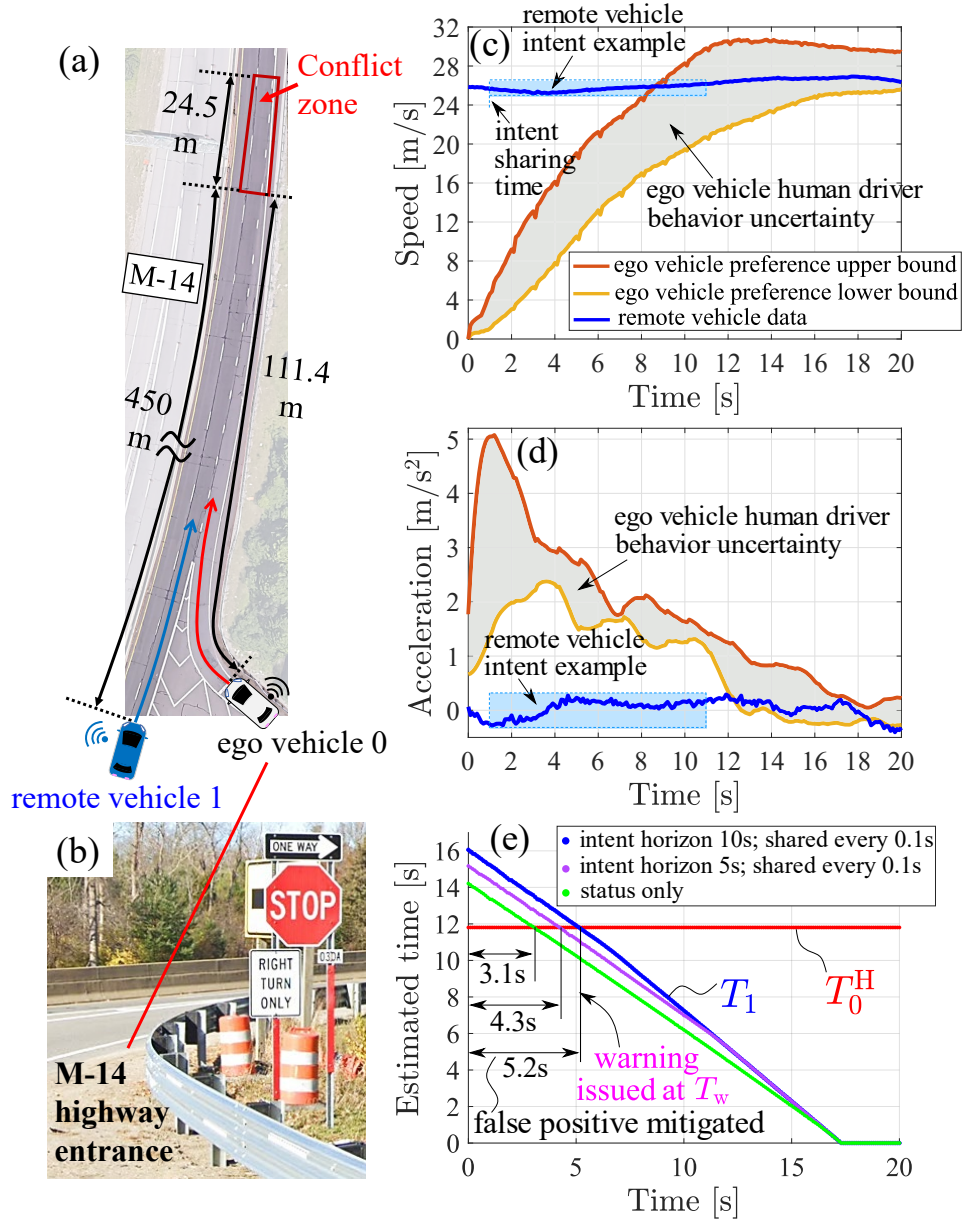


Figure 6.10: Data-based simulation of a merge scenario at the on-ramp of highway M-14 near Barton Drive, Ann Arbor, Michigan. (a)-(b) Simulation setup where the ego vehicle merges from a stop sign. (c)-(d) The ego vehicle’s behavior preference and remote vehicle’s speed profile (extracted from a real human driver data). (e) Conflict analysis showing the estimated times T_0^H and T_1 . The warning issuance times are highlighted for different intent sending conditions.

the same sending rate, the warning issuance time is pushed to $T_w = 5.2$ [s]. Such improvement is because longer intent horizon enables a more accurate (less conservative) prediction of the remote vehicle’s future maneuver; cf. (6.27). Thus, longer intent horizon boosts the time efficiency of the ego vehicle (and those queuing behind it). Simulations with a worse packet delivery ratio associated with the urban highway I-275 (green curve in Fig. 6.9(c)) yield slightly smaller warning issuance

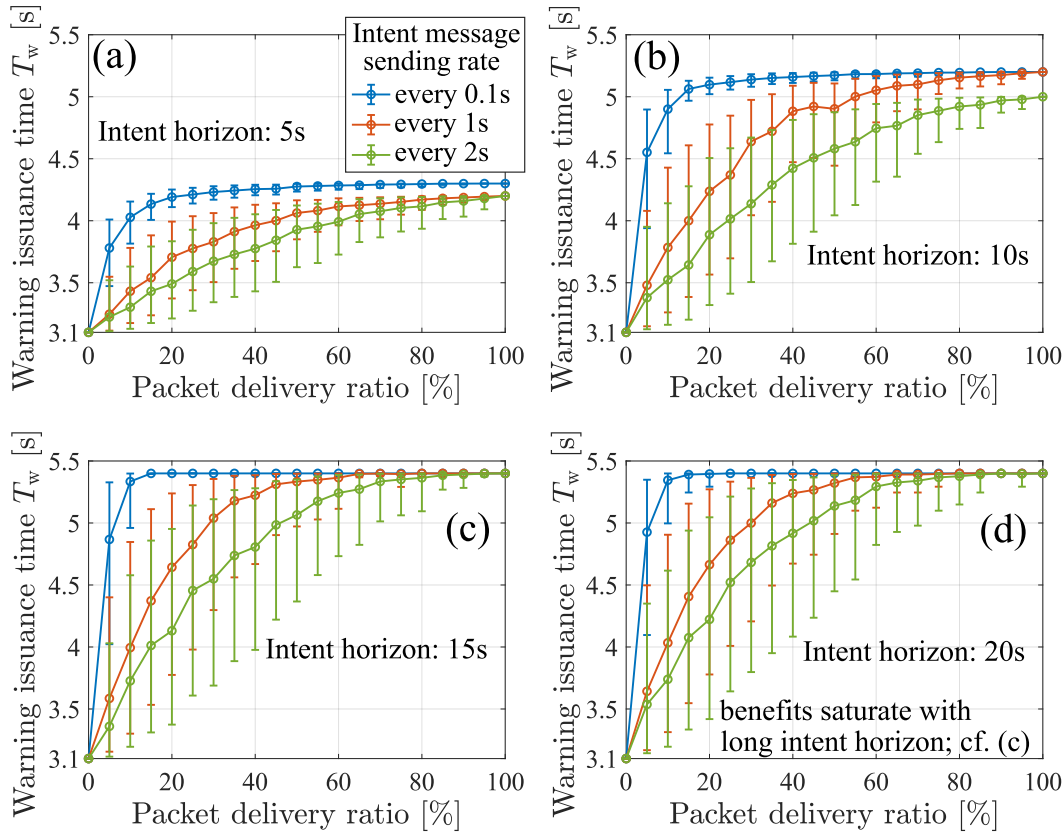


Figure 6.11: Evaluating the effects of communication conditions (intent horizon, sending rate, and packet delivery ratio) on the benefits of intent sharing via simulations. The warning issuance time is plotted as a function of packet delivery ratio with the indicated intent horizons and sending rates. The dots mark mean values while the error bars show the standard deviations.

times, but the qualitative trend remains similar.

To further quantify the effects of communication conditions, we repeat the simulations for different values of packet delivery ratio under different sending rates and intent horizons. Here we adopt the simplification that packet delivery ratio is independent from the inter-vehicle distance. Fig. 6.11(a) plots the warning issuance time T_w as a function of packet delivery ratio for intent horizon 5 [s] with the three sending rates as indicated. Each dot marks the mean value of 500 simulations while error bars represent standard deviations. The latter are calculated separately above and below the mean to reflect more accurate distribution. For sending rate 0.1 [s] (blue curve), the warning issuance time remain almost constant between 20 – 100% packet delivery ratios, indicating that intent sharing has good tolerance against packet drops. For lower sending rates (orange and green curves), the system becomes less resilient to packet loss as shown by the lower mean values and higher variance. Having higher sending rate boosts the chance of the ego vehicle obtaining an intent packet, which can provide information regarding its future environment.

The intent horizon also affects the merge performance significantly. When the horizon is

increased to 10 [s] as in Fig. 6.11(b), the warning issuance times witness a significant increase, while the qualitative trends remain similar. As the horizon is increased further to 15 [s] as in Fig. 6.11(c), we observe further (but moderate) increase in warning issuance times and improved tolerance to packet drops. These benefits eventually saturate as shown in Fig. 6.11(d) for horizon 20 [s] which is long enough to cover the rest of the merge maneuver.

The above data-based simulations enable a systematic evaluation of communication factors in intent sharing. These results provide insights into designing efficient generation rules of intent messages. For instance, an adaptive transmission rate may be imposed such that under reliable communication, long-horizon intent is sent with lower rate to save communication channels while maintaining comparable performance; cf. Fig. 6.11(c)-(d). Our studies are expected to benefit standardization and future deployments.

6.5 Summary

In this chapter, we proposed a generalized representation of vehicle motion intent from a system dynamics viewpoint. We extended conflict analysis to incorporate intent information for conflict resolution for an ego vehicle (which may be either automated or human-driven), while considering user-determined behavior preference. We implemented and tested intent messages using real vehicles equipped with commercially available V2X devices. An on-board decision assistance system was developed and validated through experiments at a test track to facilitate the decision-making of human drivers in merge scenarios. It was shown that such system can provide individualized assistance to human drivers while utilizing intent information. Experimental results demonstrated that receiving intent messages, in addition to status information, can significantly improve a vehicle's safety and time efficiency in cooperative maneuvers, by mitigating the uncertainty of its future environments. Furthermore, highway data was used together with numerical simulations to investigate the effects of communication conditions (e.g., intent sending rate, horizon, and packet drops) on the obtained benefits.

CHAPTER 7

Conclusions and Future Work

7.1 Conclusions

In this dissertation, we developed and experimentally validated a framework of conflict analysis for conflict detection, management, and resolution in mixed traffic, where vehicles with different automation levels coexist. This framework allowed us to systematically study the impacts of two different classes of cooperation enabled by V2X communication: status sharing and intent sharing.

We started with conflict analysis between two vehicles in Chapter 2, where conflict charts were analytically derived to interpret the dynamical information encoded in wireless V2X messages. This enabled quick decision-making and reliable control design. We derived communication range requirements to guarantee the existence of conflict-free maneuvering strategies. Moreover, we showed that sharing intent information that bounds the future speed and acceleration of remote vehicles leads to improved efficiency in the decision making of the ego vehicle. It was found that the performance improvements brought by intent messages cannot be replicated by merely increasing the transmission rates of current status information. We demonstrated these results by experimental data collected from field tests and by numerical simulations utilizing real highway data.

In Chapter 3 we proposed an optimization-based opportunistic strategy for conflict prevention. This strategy significantly improved the time efficiency of the ego vehicle by online adjusting its decision based on status updates received via V2X, while guaranteeing a conflict-free maneuver. It was revealed that V2X connectivity plays an essential role in applying such a strategy since regular status updates are necessary for successful decision adjustment.

We then scaled up our conflict analysis framework to multi-vehicle cases in Chapter 4, by developing numerical approaches in the presence of time delays associated with vehicle dynamics and V2X communication. Using a lane change scenario as an application example, we carefully investigated the effects of time delays on conflict resolution in mixed-autonomy environments. It was shown that the conflict-free maneuvering opportunities, facilitated by status sharing, can deteriorate under time delays. On the other hand, receiving additional intent information can

compensate the effects of delays, reduce unnecessary conservatism in decision-making, and improve the efficiency in control design for connected vehicles. Finally, we proposed a goal-oriented controller for CAVs to secure conflict-free maneuvers, which provides the designers with the freedom in choosing a proper (i.e., reachable) “goal state” to realize desired performances.

To further investigate the scalability of our framework, in Chapter 5 we extended conflict analysis to more challenging mixed traffic scenarios, which included additional maneuver constraints and involved more road users. Multi-vehicle merge scenarios were used to demonstrate the applicability of this extension. A straightforward adaptation of the framework built in Chapter 4 yielded real-time implementable algorithms for the extended conflict analysis. This enabled us to preserve advantages such as simplicity in investigating delay effects, capability of accommodating different V2X information, and flexibility in control design. Simulations based on real traffic data were used to demonstrate the scalability of our conflict analysis framework.

In Chapter 6, we generalized the representation of vehicles’ motion intent from a system dynamics viewpoint. Considering user-determined behavior preferences, we extended conflict analysis to incorporate intent information for a personalized conflict resolution for an ego vehicle, which may be either automated or human-driven. Intent messages were implemented using real vehicles equipped with commercially available V2X devices. We developed an on-board decision assistance system to facilitate the decision-making of human drivers in merge scenarios, and validated it using experiments at Mcity test track. We showed that such system can provide individualized assistance to human drivers of an ego vehicle based on intent information received from a remote vehicle. The experimental results demonstrated that, in addition to receiving status information, intent messages can significantly improve a vehicle’s safety and time efficiency in cooperative maneuvers. We quantified such benefits with a proposed metric. Moreover, intent sharing was tested on public highways. The collected data were used in simulations to study the effects of communication conditions (e.g., intent sending rate, horizon, and packet drops) on the obtained benefits.

7.2 Future Work

The results developed in this dissertation opened up multiple avenues for future research on conflict resolution in mixed-autonomy environments. To begin with, one may consider more detailed models of vehicle dynamics in conflict analysis to account for effects such as rolling resistance and air drag. Designing more sophisticated controllers is also an interesting research direction. For example, one may optimize the goal-oriented controllers (developed in Chapters 4 and 5) based on different metrics such as time efficiency, energy consumption, and passenger comfort.

Another potential research task is to design intent messages containing more sophisticated motion information. Preliminary results are reported in our recent work [99], where planned

paths and time-varying bounds of velocity and acceleration were encoded in intent messages in a compact, parameterized form. One may further implement intent messages in an adaptive manner, where a vehicle's intent can be updated online according to real-time traffic and communication conditions. This may be merged using data-driven and learning-based techniques. Moreover, our intent-based conflict analysis may be extended to accommodate the existence of non-connected vehicles. In the absence of connectivity, vehicles' status and intent information may be estimated through perception, which is expected to be less accurate and computationally more expensive than V2X-based status and intent information. The corresponding impact on traffic safety and efficiency shall be investigated.

In addition, our experimental work on validating conflict analysis may be extended from human-driven cases (as presented in Chapter 6) to automated vehicles. The decision-making rules and control algorithms designed in this dissertation shall be implemented on a CAV and demonstrated through real-world tests. To this end, a software interface that incorporates different types of V2X information to the automated vehicle's motion planner and controller needs to be built. This may be realized using Robot Operating System (ROS), through which custom applications can be developed to perform on-board conflict analysis for different testing scenarios.

Moreover, conflict analysis may be extended to higher levels of cooperation, for example, to the negotiation between multiple road users. Note that in this dissertation, conflict analysis was always performed from the perspective of a single ego vehicle, based on the available V2X information via status and intent sharing. The resultant decision-making is indeed passive. That is, the ego vehicle cannot cancel an unfavorable intended maneuver of a neighboring vehicle. Also, uncertainties in status and intent can still lead to inefficient decisions. Instead, negotiation, by allowing vehicles to actively reach agreements about their future maneuvers, may contribute to a more efficient conflict resolution. Our recent work [99] used conflict analysis to develop such a negotiation protocol between two CAVs, where conflict charts were generated from both vehicles' perspectives. It was shown that, based on the shared status and intent, conflict analysis can enable guaranteed feasibility in request initiation and response generation, which satisfy both vehicles' user-based behavior preferences. The theoretical results were experimentally demonstrated using real vehicles.

On the other hand, constructing an efficient negotiation framework that guarantees maneuver feasibility in mixed traffic settings remains challenging. Research efforts are needed to investigate how conflict analysis may contribute to negotiation in the presence of vehicles with lower levels of automation and cooperation. It is also an important research task to systematically study the effects of time delays associated with negotiation in a dynamic environment where vehicles move with high speeds, especially when multiple rounds of requests and responses are needed. Furthermore, this research shall be extended to more general traffic environments where multiple negotiation participants and/or non-connected road users exist.

APPENDIX A

Decoupling a conflict-free merge maneuver

In this appendix, we prove the relationship (2.7) in Chapter 2, i.e., $P \vee Q \iff \neg C$.

To prove $P \vee Q \implies \neg C$, we only need to prove that $(P \implies \neg C) \wedge (Q \implies \neg C)$. Let us first focus on the proposition P . Let t_P be the time such that $r_1(t_P) = 0$ and $r_2(t_P) < -s$ hold. Since $r_1(t)$ is monotonously decreasing, and $r_2(t)$ is non-increasing with respect to t , the following statements hold:

$$\forall t < t_P, \quad r_1(t) > 0, \tag{A.1}$$

$$\forall t \geq t_P, \quad r_2(t) < -s. \tag{A.2}$$

Thus, $P \implies \neg C$. Similarly, for proposition Q , let t_Q be the time such that $r_1(t_Q) = -s$ and $r_2(t_Q) > 0$ hold. Then we have

$$\forall t > t_Q, \quad r_1(t) < -s, \tag{A.3}$$

$$\forall t \leq t_Q, \quad r_2(t) > 0. \tag{A.4}$$

Thus, $Q \implies \neg C$. Therefore, $P \vee Q \implies \neg C$.

To prove $P \vee Q \iff \neg C$, we prove its contrapositive $(\neg P \wedge \neg Q) \implies C$. From (2.6), we have

$$\begin{aligned} \neg P &= \{\forall t, r_1(t) \neq 0 \vee r_2(t) \geq -s\}, \\ \neg Q &= \{\forall t, r_1(t) \neq -s \vee r_2(t) \leq 0\}. \end{aligned} \tag{A.5}$$

If $(\neg P \wedge \neg Q) = \text{true}$, then both $\neg P = \text{true}$ and $\neg Q = \text{true}$. Let t_P and t_Q be the times such that $r_1(t_P) = 0$ and $r_1(t_Q) = -s$, respectively. Based on (A.5), $r_2(t_P) \geq -s$ and $r_2(t_Q) \leq 0$ must hold. Then we have $\neg P \implies P_1 \vee P_2$, where P_1 and P_2 are the propositions

$$\begin{aligned} P_1 &:= \{\exists t_P, r_1(t_P) = 0 \wedge r_2(t_P) \in [-s, 0]\}, \\ P_2 &:= \{\exists t_P, r_1(t_P) = 0 \wedge r_2(t_P) \in (0, \infty)\}. \end{aligned} \tag{A.6}$$

Note that here we divided $r_2(t_P) \geq -s$ into two cases: $r_2(t_P) \in [-s, 0]$ and $r_2(t_P) \in (0, \infty)$. Similarly, we obtain $\neg Q \implies Q_1 \vee Q_2$, where Q_1 and Q_2 are

$$\begin{aligned} Q_1 &:= \{\exists t_Q, r_1(t_Q) = -s \wedge r_2(t_Q) \in [-s, 0]\}, \\ Q_2 &:= \{\exists t_Q, r_1(t_Q) = -s \wedge r_2(t_Q) \in (-\infty, -s)\}. \end{aligned} \tag{A.7}$$

Therefore, $(\neg P \wedge \neg Q) \implies (P_1 \vee P_2) \wedge (Q_1 \vee Q_2)$. On the other hand,

$$\begin{aligned} &(P_1 \vee P_2) \wedge (Q_1 \vee Q_2) \\ &= (P_1 \wedge Q_1) \vee (P_1 \wedge Q_2) \vee (P_2 \wedge Q_1) \vee (P_2 \wedge Q_2). \end{aligned} \tag{A.8}$$

One can confirm that $(P_2 \wedge Q_2) \implies C$. Also, $P_1 \implies C$ and $Q_1 \implies C$. Thus, it follows from (A.8) that $(\neg P \wedge \neg Q) \implies C$. These complete the proof.

APPENDIX B

Conflict Chart Boundaries

Boundaries p_1 and p_2 in (2.15), (2.16), and (2.17) are given by

$$r_2 = p_1(r_1, v_1, v_2) = p(t_{p1}, v_2), \quad (\text{B.1})$$

$$r_2 = p_2(r_1, v_1, v_2) = p(t_{p2}, v_2), \quad (\text{B.2})$$

where

$$p(t_{p1}, v_2) = \begin{cases} t_{p1}v_2 + \frac{1}{2}t_{p1}^2 a_{\max,2} - s & \text{if } v_2 \leq v_{\max,2} - t_{p1} a_{\max,2}, \\ -\frac{(v_{\max,2} - v_2)^2}{2a_{\max,2}} + t_{p1}v_{\max,2} - s & \text{if } v_2 > v_{\max,2} - t_{p1} a_{\max,2}, \end{cases} \quad (\text{B.3})$$

with $t_{p1} = t_p(a_{\max,1})$ and $t_{p2} = t_p(a_{\min,1})$, where the function $t_p(a)$ is given by the following three cases depending on the sign of its argument.

(i) For $a > 0$,

$$t_p(a) = \begin{cases} \frac{\sqrt{v_1^2 + 2ar_1} - v_1}{a} & \text{if } r_1 \leq \frac{v_{\max,1}^2 - v_1^2}{2a}, \\ \frac{v_{\max,1} - v_1}{a} + \frac{r_1 - \frac{v_{\max,1}^2 - v_1^2}{2a}}{v_{\max,1}} & \text{if } r_1 > \frac{v_{\max,1}^2 - v_1^2}{2a}. \end{cases} \quad (\text{B.4})$$

(ii) For $a = 0$,

$$t_p(a) = \frac{r_1}{v_1}. \quad (\text{B.5})$$

(iii) For $a < 0$,

$$t_p(a) = \begin{cases} -\frac{v_1 - \sqrt{v_1^2 + 2ar_1}}{a} & \text{if } r_1 \leq -\frac{v_1^2 - v_{\min,1}^2}{2a}, \\ -\frac{v_1 - v_{\min,1}}{a} + \frac{r_1 + \frac{v_1^2 - v_{\min,1}^2}{2a}}{v_{\min,1}} & \text{if } r_1 > -\frac{v_1^2 - v_{\min,1}^2}{2a}. \end{cases} \quad (\text{B.6})$$

Note that t_{p1} and t_{p2} are the time needed for the remote vehicle to reach conflict zone, with $u_1(t) \equiv a_{\max,1}$ and $u_1(t) \equiv a_{\min,1}$, respectively. Thus, the relation $t_{p2} \geq t_{p1}$ always holds, and therefore, we have $p_2(r_1, v_1, v_2) \geq p_1(r_1, v_1, v_2)$.

Boundaries q_1 and q_2 in (2.18), (2.19), and (2.20) are given by

$$r_2 = q_1(r_1, v_1, v_2) = q(t_{q1}, v_2), \quad (\text{B.7})$$

$$r_2 = q_2(r_1, v_1, v_2) = q(t_{q2}, v_2), \quad (\text{B.8})$$

where

$$q(t_{q1}, v_2) = \begin{cases} t_{q1} v_2 + \frac{1}{2} t_{q1}^2 a_{\min,2} & \text{if } v_2 \geq -t_{q1} a_{\min,2}, \\ -\frac{v_2^2}{2a_{\min,2}} & \text{if } v_2 < -t_{q1} a_{\min,2}, \end{cases} \quad (\text{B.9})$$

with $t_{q1} = t_q(a_{\min,1})$ and $t_{q2} = t_q(a_{\max,1})$, where the function $t_q(a)$ is defined below.

(i) For $a > 0$,

$$t_q(a) = \begin{cases} \frac{\sqrt{v_1^2 + 2a(r_1 + s)} - v_1}{a} & \text{if } r_1 \leq \frac{v_{\max,1}^2 - v_1^2}{2a} - s, \\ \frac{v_{\max,1} - v_1}{a} + \frac{r_1 + s - \frac{v_{\max,1}^2 - v_1^2}{2a}}{v_{\max,1}} & \text{if } r_1 > \frac{v_{\max,1}^2 - v_1^2}{2a} - s. \end{cases} \quad (\text{B.10})$$

(ii) For $a = 0$,

$$t_q(a) = \frac{r_1 + s}{v_1}. \quad (\text{B.11})$$

(iii) For $a < 0$,

$$t_q(a) = \begin{cases} -\frac{v_1 - \sqrt{v_1^2 + 2a(r_1 + s)}}{a} & \text{if } r_1 \leq -\frac{v_1^2 - v_{\min,1}^2}{2a} - s, \\ -\frac{v_1 - v_{\min,1}}{a} + \frac{r_1 + s + \frac{v_1^2 - v_{\min,1}^2}{2a}}{v_{\min,1}} & \text{if } r_1 > -\frac{v_1^2 - v_{\min,1}^2}{2a} - s. \end{cases} \quad (\text{B.12})$$

We remark that in the above equations $a_{\max,2} > 0$, $a_{\min,2} < 0$, and $0 < v_{\min,1} < v_{\max,1}$ hold by definition, and thus, the fractions are well-defined.

APPENDIX C

Proof of Theorem 1

In this appendix, we prove the communication requirement stated in Theorem 1.

Notice that boundary q_1 is upper bounded by $r_2 = f(v_2) = -v_2^2/(2a_{\min,2})$. Thus, to prove that $x(0) \in \mathcal{P}_g \cup \mathcal{Q}_g$ holds for $r_1 \geq r_1^*$, it is sufficient to show that $r_1 \geq r_1^* \Rightarrow p_1(r_1, v_1, v_2) > f(v_2)$, $\forall v_1 \in [v_{\min,1}, v_{\max,1}]$, $\forall v_2 \in [0, v_{\max,2}]$.

Let us define

$$\delta(r_1, v_1, v_2) := p_1(r_1, v_1, v_2) - f(v_2). \quad (\text{C.1})$$

By calculating $\frac{\partial \delta}{\partial v_2}(r_1, v_1, v_2)$, one may show that δ first increases and then decreases with respect to v_2 on $[0, v_{\max,2}]$. That is, δ takes minimum value at $v_2 = 0$ or $v_2 = v_{\max,2}$.

Now consider the inequalities

$$\delta(r_1, v_1, 0) > 0 \iff r_1 > g_1(v_1), \quad (\text{C.2})$$

$$\delta(r_1, v_1, v_{\max,2}) > 0 \iff r_1 > g_2(v_1), \quad (\text{C.3})$$

where g_1 and g_2 are functions of v_1 . One can confirm that the \underline{r}_1 and \bar{r}_1 given in (2.22) correspond to the maximum values of g_1 and g_2 on $v_1 \in [v_{\min,1}, v_{\max,1}]$. Thus, if $r_1 \geq r_1^* = \max\{\underline{r}_1, \bar{r}_1\}$, then both (C.2) and (C.3) hold independent of v_1 . This yields that $\delta(r_1, v_1, v_2) > 0$, i.e., $p_1(r_1, v_1, v_2) > f(v_2)$, $\forall v_1 \in [v_{\min,1}, v_{\max,1}]$, $\forall v_2 \in [0, v_{\max,2}]$.

APPENDIX D

Proof of Theorem 2

In this appendix, we prove Theorem 2, i.e., the relationships between the sets with and without intent information.

To prove (2.31) and (2.32), let us first prove the following two statements under vehicle 1's intent $v_1 \in [\underline{v}_1, \bar{v}_1]$ and $u_1 \in [\underline{a}_1, \bar{a}_1]$:

$$\begin{aligned} \bar{p}_1(r_1, v_1, v_2) &\geq p_1(r_1, v_1, v_2), \\ \bar{p}_2(r_1, v_1, v_2) &\leq p_2(r_1, v_1, v_2), \\ \forall r_1 \in (0, \infty), v_1 \in [\underline{v}_1, \bar{v}_1], v_2 \in [0, v_{\max,2}], \end{aligned} \tag{D.1}$$

and

$$\begin{aligned} \bar{q}_1(r_1, v_1, v_2) &\leq p_1(r_1, v_1, v_2), \\ \bar{q}_2(r_1, v_1, v_2) &\geq q_2(r_1, v_1, v_2), \\ \forall r_1 \in [-s, \infty), v_1 \in [\underline{v}_1, \bar{v}_1], v_2 \in [0, v_{\max,2}]. \end{aligned} \tag{D.2}$$

Using (B.4)-(B.6) and (B.10)-(B.12), we calculate \bar{t}_{p1} , \bar{t}_{p2} , \bar{t}_{q1} , and \bar{t}_{q2} with the remote vehicle's velocity and acceleration limits given by its intent. Since these limits never exceed the range $[v_{\min,1}, v_{\max,1}]$ and $[a_{\min,1}, a_{\max,1}]$ (cf. Definition 2), one can confirm that $\bar{t}_{p1} \geq t_{p1}$, $\bar{t}_{p2} \leq t_{p2}$, $\bar{t}_{q1} \leq t_{q1}$ and $\bar{t}_{q2} \geq t_{q2}$. Moreover, from (B.3) and (B.9), the function p monotonically increases with respect to t_{p1} and t_{p2} , and q monotonically increases with respect to t_{q1} and t_{q2} . Then, (D.1) and (D.2) follow from (B.1)-(B.2) and (B.7)-(B.8).

Finally, (2.31) is proved by combining (D.1) with (2.15)-(2.17) and (2.25)-(2.27), and (2.32) is proved by combining (D.2) with (2.18)-(2.20) and (2.28)-(2.30).

APPENDIX E

Prove the optimality of opportunistic control law

In this appendix, we prove the optimality of the solution (3.3).

From the dynamics (2.1), one can calculate

$$T_{\text{exit},2}(t) = \begin{cases} \frac{\sqrt{v_2^2(t) + 2a_{\max,2}(r_2(t) + s)} - v_2(t)}{a_{\max,2}}, & \text{if } r_2(t) \leq \frac{v_{\max,2}^2 - v_2^2(t)}{2a_{\max,2}} - s, \\ \frac{v_{\max,2} - v_2(t)}{a_{\max,2}} + \frac{r_2(t) + s}{v_{\max,2}} - \frac{v_{\max,2}^2 - v_2^2(t)}{2a_{\max,2}v_{\max,2}}, & \text{otherwise.} \end{cases} \quad (\text{E.1})$$

which yields that

$$J(t) = \frac{d}{dt} T_{\text{exit},2}(t) = \begin{cases} -f_1(t) \text{sat}(u_2(t)) - f_2(t), & \text{if } r_2(t) \leq \frac{v_{\max,2}^2 - v_2^2(t)}{2a_{\max,2}} - s, \\ -g_1(t) \text{sat}(u_2(t)) - g_2(t), & \text{otherwise,} \end{cases} \quad (\text{E.2})$$

where

$$\begin{aligned} f_1(t) &= \frac{1}{a_{\max,2}} \left(1 - \frac{v_2(t)}{\sqrt{v_2^2(t) + 2a_{\max,2}(r_2(t) + s)}} \right), \\ f_2(t) &= \frac{v_2(t)}{\sqrt{v_2^2(t) + 2a_{\max,2}(r_2(t) + s)}}, \\ g_1(t) &= \frac{1}{a_{\max,2}} \left(1 - \frac{v_2(t)}{v_{\max,2}} \right), \quad g_2(t) = \frac{v_2(t)}{v_{\max,2}}. \end{aligned} \quad (\text{E.3})$$

Thus, from (E.2), for all $t \in [t_k, t_{k+1})$, independent of the value of $r_2(t)$ and $v_2(t)$, maximizing $\text{sat}(u_2(t))$ minimizes the cost function $J(t)$. This implies $u_2(t) \equiv a_{\max,2}$. Moreover, the constraint $x(t) \in \mathcal{A}_Q$ must hold. Since vehicle 1's status is unknown until t_{k+1} , we must assume the worst-case scenario $u_1(t) \equiv a_{\min,1}$ for $t > t_k$, and predict time t_k^* such that $x(t_k^*)$ reaches the boundary of \mathcal{A}_Q . Based on the definition of \mathcal{A}_Q , $a_{\min,2}$ is the only input that can keep a state staying on the boundary of \mathcal{A}_Q under the worst-case scenario. Therefore, (3.3) is the optimal solution to (3.2).

APPENDIX F

Proof of Lemma 1

(\Rightarrow). The left hand side of (4.13) implies that for $(u_1, u_2) \equiv (a_{\min,1}, a_{\max,2})$, one has $\exists u_0, \exists t \geq 0, h_{10}(t) \geq s_F \wedge h_{02}(t) \geq s_R$. Therefore, $h_{12}(t) = h_{10}(t) + h_{02}(t) + l \geq s_F + s_R + l$, implying that $t \in T$ is satisfied by such t .

(\Leftarrow). The right hand side of (4.13) implies that for $(u_1, u_2) \equiv (a_{\min,1}, a_{\max,2})$, one has $\exists u_0, P$. Let u_0^* and t^* be an input u_0 and a time t such that $h_{10}(t^*) \geq s_F \wedge h_{02}(t^*) \geq s_R$ under $(u_1, u_2) \equiv (a_{\min,1}, a_{\max,2})$. For $(u_1, u_2) \neq (a_{\min,1}, a_{\max,2})$, even larger h_{10} and h_{02} values are generated by the same input u_0^* at t^* , that is, $h_{10}(t^*) \geq s_F \wedge h_{02}(t^*) \geq s_R$ still holds. Therefore, $\forall u_1, \forall u_2, \exists u_0, P$.

APPENDIX G

Analytical forms of the boundaries that construct the opportunity set

In this appendix, we derive the analytical forms of the boundaries $\delta(t)$, $h_{02}^{\min}(t)$, and $h_{02}^{\max}(t)$

With status information only, one has $\delta(t) = r_1^*(t) - r_2^*(t) - s_F - 2l$, where

$$r_1^*(t) = g(r_1(0), v_1(0), a_{\min,1}, v_{\min,1}, v_{\max,1}, t), \quad (\text{G.1})$$

$$r_2^*(t) = g(r_2(0), v_2(0), a_{\max,2}, v_{\min,2}, v_{\max,2}, t), \quad (\text{G.2})$$

and the function $g(r(0), v(0), a, v_{\min}, v_{\max}, t)$ is defined as

(i) For $a > 0$,

$$g(r(0), v(0), a, v_{\min}, v_{\max}, t) = \begin{cases} r(0) + v(0)t + \frac{1}{2}at^2 & \text{if } t \leq \frac{(v_{\max} - v(0))}{a}, \\ r(0) - \frac{(v_{\max} - v(0))^2}{2a} + v_{\max}t & \text{otherwise,} \end{cases} \quad (\text{G.3})$$

(ii) For $a = 0$,

$$g(r(0), v(0), a, v_{\min}, v_{\max}, t) = r(0) + v(0)t, \quad (\text{G.4})$$

(iii) For $a < 0$,

$$g(r(0), v(0), a, v_{\min}, v_{\max}, t) = \begin{cases} r(0) + v(0)t + \frac{1}{2}at^2 & \text{if } t \leq \frac{(v_{\min} - v(0))}{a}, \\ r(0) - \frac{(v_{\min} - v(0))^2}{2a} + v_{\min}t & \text{otherwise,} \end{cases} \quad (\text{G.5})$$

and $h_{02}^{\min}(t) = \underline{r}_0^*(t) - r_2^*(t) - l$, $h_{02}^{\max}(t) = \bar{r}_0^*(t) - r_2^*(t) - l$, where

$$\underline{r}_0^*(t) = \begin{cases} \tilde{g}(r_0(0), v_0(0), t) & \text{if } t \leq \sigma, \\ g(r_0(\sigma), v_0(\sigma), a_{\min,0}, v_{\min,0}, v_{\max,0}, t - \sigma) & \text{otherwise,} \end{cases} \quad (\text{G.6})$$

$$\bar{r}_0^*(t) = \begin{cases} \tilde{g}(r_0(0), v_0(0), t) & \text{if } t \leq \sigma, \\ g(r_0(\sigma), v_0(\sigma), a_{\max,0}, v_{\min,0}, v_{\max,0}, t - \sigma) & \text{otherwise,} \end{cases} \quad (\text{G.7})$$

$$\tilde{g}(r_0(0), v_0(0), t) = r_0(0) + v_0(0)t + \int_0^t \int_0^{\bar{t}} \text{sat}(u(\bar{t} - \sigma)) d\bar{t} d\bar{t}, \quad (\text{G.8})$$

$$r_0(\sigma) = \tilde{g}(r_0(0), v_0(0), \sigma), \quad (\text{G.9})$$

$$v_0(\sigma) = v_0(0) + \int_0^\sigma \text{sat}(u(\bar{t} - \sigma)) d\bar{t}. \quad (\text{G.10})$$

Note that for $t \in [0, \sigma]$, $u(t - \sigma)$ represents the control command history of the ego vehicle, and thus, is a given deterministic function.

Under remote vehicles' intent, one shall calculate $\delta(t)$, $h_{02}^{\min}(t)$, and $h_{02}^{\max}(t)$ in a similar way utilizing the previously given formulae, where $r_1^*(t)$ and $r_2^*(t)$ need to be updated as

$$r_1^*(t) = \begin{cases} g(r_1(0), v_1(0), \underline{a}_1, \underline{v}_1, \bar{v}_1, t) & \text{if } t \leq \Delta t_1, \\ g(r_1^*(\Delta t_1), v_1^*(\Delta t_1), a_{\min,1}, v_{\min,1}, v_{\max,1}, t - \Delta t_1) & \text{otherwise,} \end{cases} \quad (\text{G.11})$$

$$r_2^*(t) = \begin{cases} g(r_2(0), v_2(0), \bar{a}_2, \underline{v}_2, \bar{v}_2, t) & \text{if } t \leq \Delta t_2, \\ g(r_2^*(\Delta t_2), v_2^*(\Delta t_2), a_{\max,2}, v_{\min,2}, v_{\max,2}, t - \Delta t_2) & \text{otherwise,} \end{cases} \quad (\text{G.12})$$

where $v_1^*(\Delta t_1) = \hat{g}(v_1(0), \Delta t_1, \underline{a}_1, \underline{v}_1, \bar{v}_1)$ and $v_2^*(\Delta t_2) = \hat{g}(v_2(0), \Delta t_2, \bar{a}_2, \underline{v}_2, \bar{v}_2)$, with the function $\hat{g}(v(0), \Delta t, a, \underline{v}, \bar{v})$ given as

$$\hat{g}(v(0), \Delta t, a, \underline{v}, \bar{v}) = \begin{cases} \max\{v(0) + a\Delta t, \underline{v}\} & \text{if } a \leq 0, \\ \min\{v(0) + a\Delta t, \bar{v}\} & \text{otherwise,} \end{cases} \quad (\text{G.13})$$

Notice that under communication delay, one needs to replace $r_1(0)$, $v_1(0)$, $r_2(0)$, and $v_2(0)$ in (G.1), (G.2), (G.11), and (G.12) with their estimated values based on Theorem 4. Also, Δt_1 and Δt_2 shall be substituted by $\max\{0, \Delta t_1 - \tau_1\}$ and $\max\{0, \Delta t_2 - \tau_2\}$, respectively.

APPENDIX H

Proof of Theorem 3

If $\Gamma \neq \emptyset$, then according to the definition of Γ in (4.14), under $(u_1, u_2) \equiv (a_{\min,1}, a_{\max,2})$, one has $\exists u_0, \exists t \in T, s_R \leq h_{02}(t) \leq \delta(t)$. Substituting $\delta(t) = h_{12}(t) - s_F - l$ gives $h_{02}(t) \leq h_{12}(t) - s_F - l$, i.e., $s_F \leq h_{10}(t)$. These and Lemma 1 yield $\mathbf{x}(0) \in \mathcal{P}_g$.

If $\Gamma = \emptyset$, then under $(u_1, u_2) \equiv (a_{\min,1}, a_{\max,2})$, one has $\forall u_0(t), \forall t \in T, \neg\{s_R \leq h_{02}(t) \leq \delta(t)\}$, i.e., $\neg\{h_{10}(t) \geq s_F \wedge h_{02}(t) \geq s_R\}$. Also, $\forall t \notin T$ one still obtains $\neg\{h_{10}(t) \geq s_F \wedge h_{02}(t) \geq s_R\}$. Therefore, for $(u_1, u_2) \equiv (a_{\min,1}, a_{\max,2})$, $\forall u_0, \neg P$. This yields $\mathbf{x}(0) \notin \mathcal{P}_g$.

APPENDIX I

Proof of Theorem 4

By noting that $\mathbf{x}_{\text{est}}(0) \in \mathcal{P}_g$ is equivalent to $\{u_1(t) \equiv a_{\min,1}, t \in [-\tau_1, 0], u_2(t) \equiv a_{\max,2}, t \in [-\tau_2, 0], \forall u_1(t), t > 0, \forall u_2(t), t > 0, \exists u_0(t), t > 0, P\}$, $\tilde{P}_g \implies \mathbf{x}_{\text{est}}(0) \in \mathcal{P}_g$ is obvious based on the definition of \tilde{P}_g in (4.19).

If $\mathbf{x}_{\text{est}}(0) \in \mathcal{P}_g$ holds, let u_0^* and t^* be an input u_0 and a time t such that the proposition P holds, i.e., $h_{10}(t^*) \geq s_F \wedge h_{02}(t^*) \geq s_R$. Then, $\forall u_1(t) \neq a_{\min,1}, t \in [-\tau_1, 0], \forall u_2(t) \neq a_{\max,2}, t \in [-\tau_2, 0]$, at time t^* even larger h_{10} and h_{02} values are obtained by the same input u_0^* , that is, $h_{10}(t^*) \geq s_F \wedge h_{02}(t^*) \geq s_R$ still holds. Thus, $\tilde{P}_g \iff \mathbf{x}_{\text{est}}(0) \in \mathcal{P}_g$. These give (4.23).

On the other hand, (4.24) is obtained from (4.23) by noting that $\tilde{P}_y = \neg \tilde{P}_g \wedge \neg \tilde{P}_r = \neg \tilde{P}_g \wedge \text{True} = \neg \tilde{P}_g$ and $\mathbf{x}_{\text{est}}(0) \in \mathcal{P}_y \iff \mathbf{x}_{\text{est}}(0) \notin \mathcal{P}_g$.

These complete the proof of Theorem 4.

APPENDIX J

Analytical form of goal-oriented controller

Given a goal point $(t^G, h_{02}^G) \in \Gamma$ (or $\bar{\Gamma}$), we have

$$u_0^G = \begin{cases} \frac{2(s^G - (t^G - \sigma)v_0)}{(t^G - \sigma)^2}, & \text{if } s^G \in \left[\frac{(t^G - \sigma)(v_0 + v_{\min,0})}{2}, \frac{(t^G - \sigma)(v_0 + v_{\max,0})}{2} \right], \\ f_1(v_0, t^G, s^G), & \text{if } s^G \in \left[0, \frac{(t^G - \sigma)(v_0 + v_{\min,0})}{2} \right], \\ f_2(v_0, t^G, s^G), & \text{otherwise.} \end{cases} \quad (\text{J.1})$$

Here, v_0 represents $v_0(\sigma)$ given in (G.10), and s^G represents the distance that the ego vehicle shall travel for $t > \sigma$ to form the rear gap h_{02}^G at t^G considering the remote vehicle 2's worst-case behavior. Thus, $s^G = r_2^*(t^G) - r_0(\sigma) + h_{02}^G + l$ for the $r_2^*(\cdot)$ in (G.2) or (G.12) depending on whether intent of remote vehicle 2 is available, and $r_0(\sigma)$ in (G.9).

$$f_1(v_0, t^G, s^G) = \begin{cases} \frac{2(s^G - (t^G - \sigma)v_0)}{(t^G - \sigma)^2}, & \text{if } a_{\min,0} \geq \frac{v_{\min,0} - v_0}{t^G - \sigma}, \\ \frac{(v_0 - v_{\min,0})^2}{2((t^G - \sigma)v_{\min,0} - s^G)}, & \text{otherwise,} \end{cases} \quad (\text{J.2})$$

$$f_2(v_0, t^G, s^G) = \begin{cases} \frac{2(s^G - (t^G - \sigma)v_0)}{(t^G - \sigma)^2}, & \text{if } a_{\max,0} \leq \frac{v_{\max,0} - v_0}{t^G - \sigma}, \\ \frac{(v_0 - v_{\max,0})^2}{2((t^G - \sigma)v_{\max,0} - s^G)}, & \text{otherwise.} \end{cases} \quad (\text{J.3})$$

Notice that in (J.1), we divide u_0^G into three cases to deal with the speed saturation of the ego vehicle as it travels distance s^G during the time interval $(\sigma, t^G]$.

APPENDIX K

Proof of Lemma 2

Here we prove (5.9).

(\Rightarrow) From the left hand side, we know that for $(u_1(t), u_2(t)) \equiv (\underline{u}_1(t), \bar{u}_2(t))$, $\exists u_0(t), \exists t \geq 0, h_{10}(t) \geq s_F \wedge h_{02}(t) \geq s_R \wedge r_0(t) \in [\underline{s}, \bar{s}]$. Such t must satisfy $t \in [0, t_{\max,0}]$, since $r_0(t) \in [\underline{s}, \bar{s}]$ implies $t \in [0, t_{\max,0}]$. Thus, the right hand side holds.

(\Leftarrow) The right hand side implies that for $(u_1(t), u_2(t)) \equiv (\underline{u}_1(t), \bar{u}_2(t))$, $\exists u_0(t), M$. Let u_0^* and t^* denote an input u_0 and a time t such that $h_{10}(t^*) \geq s_F \wedge h_{02}(t^*) \geq s_R \wedge r_0(t^*) \in [\underline{s}, \bar{s}]$ holds under $(u_1(t), u_2(t)) \equiv (\underline{u}_1(t), \bar{u}_2(t))$. Now consider any $(u_1(t), u_2(t)) \neq (\underline{u}_1(t), \bar{u}_2(t))$ and the same u_0^* . $r_0(t^*)$ remains unchanged, while both $h_{10}(t^*) = r_1(t^*) - r_0(t^*)$ and $h_{02}(t^*) = r_0(t^*) - r_2(t^*)$ become larger. Thus, $h_{10}(t^*) \geq s_F \wedge h_{02}(t^*) \geq s_R \wedge r_0(t^*) \in [\underline{s}, \bar{s}]$ still holds, i.e., the left hand side.

APPENDIX L

Proof of Lemma 3

Below we prove (5.12).

(\Rightarrow) The left hand side implies that for $(u_1(t), u_2(t)) \equiv (\bar{u}_1(t), \underline{u}_2(t))$, we have $\forall u_0(t), \forall t \geq 0$, $\neg(h_{10}(t) \geq s_F \wedge h_{02}(t) \geq s_R \wedge r_0(t) \in [\underline{s}, \bar{s}])$. This follows directly the right hand side for $t \in [0, t_{\max,0}]$.

(\Leftarrow) We first note that $t \notin [0, t_{\max,0}]$ implies $r_0(t) \notin [\underline{s}, \bar{s}]$. Thus, given the right hand side, we have that $\forall u_0(t), \forall t \geq 0$, $\neg(h_{10}(t) \geq s_F \wedge h_{02}(t) \geq s_R \wedge r_0(t) \in [\underline{s}, \bar{s}])$ under $(u_1(t), u_2(t)) \equiv (\bar{u}_1(t), \underline{u}_2(t))$. Moreover, for any $(u_1(t), u_2(t)) \neq (\bar{u}_1(t), \underline{u}_2(t))$, both $h_{10}(t)$ and $h_{02}(t)$ become smaller under any given $u_0(t)$. Thus, $\neg(h_{10}(t) \geq s_F \wedge h_{02}(t) \geq s_R \wedge r_0(t) \in [\underline{s}, \bar{s}])$ still holds. This proves the left hand side.

APPENDIX M

Proof of Theorem 5

Here we prove (5.16).

(\Rightarrow) $\Theta \neq \emptyset$ implies that for $(u_1(t), u_2(t)) \equiv (\underline{u}_1(t), \bar{u}_2(t))$, we have $\exists u_0(t), \exists t \in [0, t_{\max,0}], r_0(t) \in [\underline{s}, \bar{s}] \wedge r_0(t) \in \Gamma^*(t)$, where $\Gamma^*(t)$ denotes the slice of the set Γ^* at time t . From the definition of Γ^* , $r_0(t) \in \Gamma^*(t) \iff \Gamma(t) \neq \emptyset$, where $\Gamma(t)$ is the slice of the set Γ at a given time t . From this, one can derive that $h_{10}(t) \geq s_F \wedge h_{02}(t) \geq s_R$ holds. These and Lemma 2 imply that $\mathbf{x}(0) \in \mathcal{M}_g$.

(\Leftarrow) We prove this by contrapositive. If $\Theta = \emptyset$, then under $(u_1(t), u_2(t)) \equiv (\underline{u}_1(t), \bar{u}_2(t))$, $\forall u_0(t), \forall t \in [0, t_{\max,0}], \neg(r_0(t) \in [\underline{s}, \bar{s}] \wedge r_0(t) \in \Gamma^*)$. That is, similar to the argument above, $\neg(r_0(t) \in [\underline{s}, \bar{s}] \wedge h_{10}(t) \geq s_F \wedge h_{02}(t) \geq s_R)$. Also, $\forall t \notin [0, t_{\max,0}]$, we always have $r_0(t) \notin [\underline{s}, \bar{s}]$. Therefore, for $(u_1(t), u_2(t)) \equiv (\underline{u}_1(t), \bar{u}_2(t))$, $\forall u_0(t), \neg M$. This implies $\mathbf{x}(0) \notin \mathcal{M}_g$.

APPENDIX N

Proof of Theorem 6

Below we prove (5.18).

(\Rightarrow) If $\Theta = \emptyset$ under $(u_1(t), u_2(t)) \equiv (\bar{u}_1(t), \underline{u}_2(t))$, then $\forall u_0(t), \forall t \in [0, t_{\max,0}]$, $\neg(r_0(t) \in [\underline{s}, \bar{s}] \wedge r_0(t) \in \Gamma^*(t))$ holds. Since $r_0(t) \in \Gamma^*(t) \iff h_{10}(t) \geq s_F \wedge h_{02}(t) \geq s_R$, we have $\neg(r_0(t) \in [\underline{s}, \bar{s}] \wedge h_{10}(t) \geq s_F \wedge h_{02}(t) \geq s_R)$. These and Lemma 3 imply that $\mathbf{x}(0) \in \mathcal{M}_r$.

(\Leftarrow) We prove this by contrapositive. If $\Theta \neq \emptyset$ under $(u_1(t), u_2(t)) \equiv (\bar{u}_1(t), \underline{u}_2(t))$, then we have $\exists u_0(t), \exists t \in [0, t_{\max,0}], r_0(t) \in [\underline{s}, \bar{s}] \wedge r_0(t) \in \Gamma^*(t)$. That is, $r_0(t) \in [\underline{s}, \bar{s}] \wedge h_{10}(t) \geq s_F \wedge h_{02}(t) \geq s_R$. Thus, for $(u_1(t), u_2(t)) \equiv (\bar{u}_1(t), \underline{u}_2(t))$, $\exists u_0(t), M$. This implies $\mathbf{x}(0) \notin \mathcal{M}_r$.

APPENDIX O

Proof of the relationship in equation 5.19

For simplicity of notation, we define a proposition

$$Q := \{r_0(t) \geq -s \wedge -s \leq r_1(t) \leq 0\}, \quad (\text{O.1})$$

then (6.19) becomes $P \iff \{\forall t, \neg Q\}$.

We first prove $P \implies \{\forall t, \neg Q\}$. If $P = \text{true}$, then according to definition (6.18), one can find such a time $t = \bar{t}$ that $r_0(\bar{t}) < -s \wedge r_1(\bar{t}) = 0$ holds. This yields immediately $\neg Q = \text{true}$ at such \bar{t} . Since the vehicles do not move backward, for any given $t > \bar{t}$, $r_0(t) < -s$ still holds, while for any given $t < \bar{t}$, one has $r_1(t) > 0$. Therefore, $\neg Q = \text{true}$ also holds for any $t \neq \bar{t}$. These lead to $\{\forall t, \neg Q\}$.

To show $P \impliedby \{\forall t, \neg Q\}$, we prove its contrapositive, i.e., $\neg P \implies \{\exists t, Q\}$. From (6.18) we have $\neg P = \{\forall t, r_0(t) \geq -s \vee r_1(t) \neq 0\}$. Since $r_1(t)$ monotonically decreases along t with $\dot{r}_1 \leq -v_{\min,1} < 0$, there must exist a time \tilde{t} , such that $r_1(\tilde{t}) = 0$. If $\neg P = \text{true}$, then at such \tilde{t} we have $r_0(\tilde{t}) \geq -s$. Hence, $\neg P \implies \{\exists t = \tilde{t}, r_0(\tilde{t}) \geq -s \wedge r_1(\tilde{t}) = 0\} \implies \{\exists t, Q\}$. These complete the proof of (6.19).

APPENDIX P

Proof of Theorem 7

The relationship (6.25) is shown below.

(\implies). We prove its contrapositive, i.e., $\mathbf{X}(t_k) \notin \mathcal{P}_g^A \iff T_0^A \geq T_1$. If $T_0^A \geq T_1$, then for any admissible input u_0 , we have $\bar{T}_0^A \geq T_0^A \geq T_1$, where \bar{T}_0^A represents the time such that $r_0(t) = -s$ under the given u_0 . Thus, $\exists u_1$ in (6.27), $\forall u_0, r_0(T_1) \geq r_0(\bar{T}_0^A) \geq -s \wedge r_1(T_1) = 0$, implying $\{\exists t = T_1, Q\}$, where proposition Q is defined by (O.1) in Appendix K. Based on (6.19), we have $\exists u_1, \forall u_0, \neg P$, that is, $\mathbf{X}(t_k) \notin \mathcal{P}_g^A$.

(\impliedby). If $T_0^A < T_1$, then for any admissible input u_1 , we have $T_0^A < T_1 \leq \bar{T}_1$, where \bar{T}_1 represents the time such that $r_1(t) = 0$ under the given u_1 . Thus, $\forall u_1, \exists u_0$ in (6.26), $r_0(\bar{T}_1) < r_0(T_0^A) = -s \wedge r_1(\bar{T}_1) = 0$. That is, $\forall u_1, \exists u_0, P$, i.e., $\mathbf{X}(t_k) \in \mathcal{P}_g^A$.

APPENDIX Q

Proof of Theorem 8

Below we prove the relationship (6.28).

(\implies). If $\mathbf{x}(t_k) \in \mathcal{P}_g^H$, then for the inputs u_0 and u_1 in (6.29) and (6.27), we have $\exists t, r_0(t) < -s \wedge r_1(t) = 0$. Such t must be unique since $r_1(t)$ is monotonic along t , yielding $t = T_1$. Thus, $T_0^H < T_1$ holds obviously.

(\impliedby). If $T_0^H < T_1$, then for the inputs u_0 and u_1 in (6.29) and (6.27), we have $r_0(T_1) < -s \wedge r_1(T_1) = 0$. For any admissible u_0 and u_1 other than (6.29) and (6.27), let \bar{T}_0^H and \bar{T}_1 be the times such that $r_0 = -s$ and $r_1 = 0$. We have $\bar{T}_0^H < T_0^H < T_1 < \bar{T}_1$. Thus, $r_0(\bar{T}_1) < -s \wedge r_1(\bar{T}_1) = 0$. These imply $\mathbf{x}(t_k) \in \mathcal{P}_g^H$.

BIBLIOGRAPHY

- [1] F. H. Amundsen and C. Hyden. Proceedings of first workshop on traffic conflicts. *Oslo, TTI, Oslo, Norway and LTH Lund, Sweden*, 78, 1977.
- [2] W. D. Glauz and D. J. Migletz. Application of traffic conflict analysis at intersections. Technical report, Transportation Research Board, 1980.
- [3] H.-C. Chin and S.-T. Quek. Measurement of traffic conflicts. *Safety Science*, 26(3):169–185, 1997.
- [4] D. Shinar. *Traffic safety and human behavior*. Emerald Group Publishing, 2017.
- [5] K. Bucsuházy, E. Matuchová, R. Zůvala, P. Moravcová, M. Kostíková, and R. Mikulec. Human factors contributing to the road traffic accident occurrence. *Transportation research procedia*, 45:555–561, 2020.
- [6] D. González, J. Pérez, V. Milanés, and F. Nashashibi. A review of motion planning techniques for automated vehicles. *IEEE Transactions on intelligent transportation systems*, 17(4):1135–1145, 2015.
- [7] S. E. Shladover. Connected and automated vehicle systems: Introduction and overview. *Journal of Intelligent Transportation Systems*, 22(3):190–200, 2018.
- [8] G. Meyer and S. Beiker. *Road vehicle automation*, volume 201955. Springer, 2019.
- [9] H. Zhu, K.-V. Yuen, L. Mihaylova, and H. Leung. Overview of environment perception for intelligent vehicles. *IEEE Transactions on Intelligent Transportation Systems*, 18(10):2584–2601, 2017.
- [10] J. V. Brummelen, M. O’Brien, D. Gruyer, and H. Najjaran. Autonomous vehicle perception: The technology of today and tomorrow. *Transportation research part C: Emerging technologies*, 89:384–406, 2018.
- [11] S. Zeadally, M. A. Javed, and E. B. Hamida. Vehicular communications for ITS: Standardization and challenges. *IEEE Communications Standards Magazine*, 4(1):11–17, 2020.
- [12] S. A. A. Shah, E. Ahmed, M. Imran, and S. Zeadally. 5G for vehicular communications. *IEEE Communications Magazine*, 56(1):111–117, 2018.

- [13] S. A. A. Hakeem, A. A. Hady, and H. Kim. Current and future developments to improve 5G-newradio performance in vehicle-to-everything communications. *Telecommunication systems*, 75:331–353, 2020.
- [14] V. Milanés, J. Alonso, L. Bouraoui, and J. Ploeg. Cooperative maneuvering in close environments among cybercars and dual-mode cars. *IEEE Transactions on Intelligent Transportation Systems*, 12(1):15–24, 2011.
- [15] L. Hobert, A. Festag, I. Llatser, L. Altomare, F. Visintainer, and A. Kovacs. Enhancements of V2X communication in support of cooperative autonomous driving. *IEEE Communications Magazine*, 53(12):64–70, 2015.
- [16] J. Ploeg, E. S.-Kazerooni, A. I. M. Medina, J. F. C. M. de Jongh, J. van de Sluis, A. Voronov, C. Englund, R. J. Bril, H. Salunkhe, Á. Arrúe, et al. Cooperative automated maneuvering at the 2016 grand cooperative driving challenge. *IEEE Transactions on Intelligent Transportation Systems*, 19(4):1213–1226, 2017.
- [17] B. Häfner, V. Bajpai, J. Ott, and G. A. Schmitt. A survey on cooperative architectures and maneuvers for connected and automated vehicles. *IEEE Communications Surveys & Tutorials*, 24(1):380–403, 2021.
- [18] SAE J3216. Taxonomy and Definitions for Terms Related to Cooperative Driving Automation for On-Road Motor Vehicles. Technical report, SAE International, 2021.
- [19] S. Chen, J. Hu, Y. Shi, Y. Peng, J. Fang, R. Zhao, and L. Zhao. Vehicle-to-everything (V2X) services supported by LTE-based systems and 5G. *IEEE Communications Standards Magazine*, 1(2):70–76, 2017.
- [20] T. Ersal, I. Kolmanovsky, N. Masoud, N. Ozay, J. Scruggs, R. Vasudevan, and G. Orosz. Connected and automated road vehicles: State of the art and future challenges. *Vehicle System Dynamics*, 58(5):672–704, 2020.
- [21] SAE J2735. Dedicated Short Range Communications (DSRC) Message Set Dictionary Set. Technical report, SAE International, 2016.
- [22] J. B. Kenney. Dedicated short-range communications (DSRC) standards in the United States. *Proceedings of the IEEE*, 99(7):1162–1182, 2011.
- [23] X. Wu, S. Subramanian, R. Guha, R. G. White, J. Li, K. W. Lu, A. Buccheri, and T. Zhang. Vehicular communications using DSRC: Challenges, enhancements, and evolution. *IEEE Journal on Selected Areas in Communications*, 31(9):399–408, 2013.
- [24] J.-K. Bae, M.-C. Park, E.-J. Yang, and D.-W. Seo. Implementation and performance evaluation for DSRC-based vehicular communication system. *IEEE Access*, 9:6878–6887, 2020.
- [25] 3GPP, TS 33.885. Universal mobile telecommunications system (UMTS); LTE; Architecture enhancements for V2X services, Rel-14 V14.2.0. Technical report, 3GPP, 2017.

- [26] 5GAA. An assessment of LTE-V2X (PC5) and 802.11p direct communications technologies for improved road safety in the EU. Technical report, 5GAA, 2017.
- [27] H. Abou-zeid, F. Pervez, A. Adinoyi, M. Aljlayl, and H. Yanikomeroglu. Cellular V2X transmission for connected and autonomous vehicles standardization, applications, and enabling technologies. *IEEE Consumer Electronics Magazine*, 8(6):91–98, 2019.
- [28] E. Moradi-Pari, D. Tian, M. Bahramgiri, S. Rajab, and S. Bai. DSRC versus LTE-V2X: Empirical performance analysis of direct vehicular communication technologies. *IEEE Transactions on Intelligent Transportation Systems*, 24(5):4889–4903, 2023.
- [29] K. Abboud, H. A. Omar, and W. Zhuang. Interworking of DSRC and cellular network technologies for V2X communications: A survey. *IEEE Transactions on Vehicular Technology*, 65(12):9457–9470, 2016.
- [30] B. Lehmann, H.-J. Günther, and L. Wolf. A generic approach towards maneuver coordination for automated vehicles. In *2018 21st International Conference on Intelligent Transportation Systems (ITSC)*, pages 3333–3339. IEEE, 2018.
- [31] I. Llatser, T. Michalke, M. Dolgov, F. Wildschütte, and H. Fuchs. Cooperative automated driving use cases for 5G V2X communication. In *2nd IEEE 5G World Forum (5GWF)*, pages 120–125, 2019.
- [32] A. Correa, S. Maerivoet, E. Mintsis, A. Wijbenga, M. Sepulcre, M. Rondinone, J. Schindler, and J. Gozalvez. Management of transitions of control in mixed traffic with automated vehicles. In *16th International Conference on Intelligent Transportation Systems Telecommunications (ITST)*, pages 1–7, 2018.
- [33] Y.-T. Lin, H. Hsu, S.-C. Lin, C.-W. Lin, I. H.-R. Jiang, and C. Liu. Graph-based modeling, scheduling, and verification for intersection management of intelligent vehicles. *ACM Transactions on Embedded Computing Systems (TECS)*, 18(5s):1–21, 2019.
- [34] N. Arechiga. Specifying safety of autonomous vehicles in signal temporal logic. In *2019 IEEE Intelligent Vehicles Symposium (IV)*, pages 58–63. IEEE, 2019.
- [35] K. X. Cai, T. Phan-Minh, S.-J. Chung, and R. M. Murray. Rules of the road: Formal guarantees for autonomous vehicles with behavioral contract design. *IEEE Transactions on Robotics*, 2023.
- [36] A. I. M. Medina, N. van de Wouw, and H. Nijmeijer. Automation of a T-intersection using virtual platoons of cooperative autonomous vehicles. In *the 18th International Conference on Intelligent Transportation Systems*, pages 1696–1701, Las Palmas, Spain, 2015.
- [37] C. Liu, C.-W. Lin, S. Shiraishi, and M. Tomizuka. Distributed conflict resolution for connected autonomous vehicles. *IEEE Transactions on Intelligent Vehicles*, 3(1):18–29, 2020.

- [38] R. Hult, M. Zanon, S. Gros, H. Wymeersch, and Paolo Falcone. Optimisation-based coordination of connected, automated vehicles at intersections. *Vehicle System Dynamics*, 58(5):726–747, 2020.
- [39] J. Rios-Torres and A. A. Malikopoulos. A survey on the coordination of connected and automated vehicles at intersections and merging at highway on-ramps. *IEEE Transactions on Intelligent Transportation Systems*, 18(5):1066–1077, 2016.
- [40] A. A. Malikopoulos, L. Beaver, and I. V. Chremos. Optimal time trajectory and coordination for connected and automated vehicles. *Automatica*, 125:109469, 2021.
- [41] B. Chalaki and A. A. Malikopoulos. Time-optimal coordination for connected and automated vehicles at adjacent intersections. *IEEE Transactions on Intelligent Transportation Systems*, 23(8):13330–13345, 2021.
- [42] I. B. Viana, H. Kanchwala, and N. Aouf. Cooperative trajectory planning for autonomous driving using nonlinear model predictive control. In *IEEE International Conference on Connected Vehicles and Expo (ICCVE)*, pages 1–6, 2019.
- [43] A. Katriniok, B. Rosarius, and P. Mähönen. Fully distributed model predictive control of connected automated vehicles in intersections: Theory and vehicle experiments. *IEEE Transactions on Intelligent Transportation Systems*, 23(10):18288–18300, 2022.
- [44] M. R. Hafner and D. D. Vecchio. Computational tools for the safety control of a class of piecewise continuous systems with imperfect information on a partial order. *SIAM Journal on Control and Optimization*, 49(6):2463–2493, 2011.
- [45] R. Kianfar, P. Falcone, and J. Fredriksson. Safety verification of automated driving systems. *IEEE Intelligent Transportation Systems Magazine*, 5(4):73–86, 2013.
- [46] M. R. Hafner, D. Cunningham, L. Caminiti, and D. D. Vecchio. Cooperative collision avoidance at intersections: Algorithms and experiments. *IEEE Transactions on Intelligent Transportation Systems*, 14(3):1162–1175, 2013.
- [47] S. Bansal, M. Chen, S. Herbert, and C. J. Tomlin. Hamilton-Jacobi reachability: A brief overview and recent advances. In *the 56th IEEE Conference on Decision and Control*, pages 2242–2253, Melbourne, Australia, 2017.
- [48] Z. Lin, L. Castano, E. Mortimer, and H. Xu. Fast 3D collision avoidance algorithm for fixed wing UAS. *Journal of Intelligent and Robotic Systems*, 97(3):577–604, 2020.
- [49] J. N. Yasin, S. A. S. Mohamed, M. Haghbayan, J. Heikkonen, H. Tenhunen, and J. Plosila. Unmanned aerial vehicles (UAVs): Collision avoidance systems and approaches. *IEEE Access*, 8:105139–105155, 2020.
- [50] M. A. Hinostroza, H. Xu, and C. G. Soares. Cooperative operation of autonomous surface vehicles for maintaining formation in complex marine environment. *Ocean Engineering*, 183:132–154, 2019.

- [51] SAE J3016. Taxonomy and Definitions for Terms Related to Driving Automation Systems for On-Road Motor Vehicles. Technical report, SAE International, 2021.
- [52] J. I. Ge, S. S. Avedisov, C. R. He, W. B. Qin, M. Sadeghpour, and G. Orosz. Experimental validation of connected automated vehicle design among human-driven vehicles. *Transportation Research Part C*, 91:335–352, 2018.
- [53] S. S. Avedisov, G. Bansal, and G. Orosz. Impacts of connected automated vehicles on freeway traffic patterns at different penetration levels. *IEEE Transactions on Intelligent Transportation Systems*, 23(5):4305–4318, 2022.
- [54] A. Bajcsy, S. L. Herbert, D. Fridovich-Keil, J. F. Fisac, S. Deglurkar, A. Dragan, and C. Tomlin. A scalable framework for real-time multi-robot, multi-human collision avoidance. *2019 International Conference on Robotics and Automation (ICRA)*, pages 936–943, 2019.
- [55] B. M. Albaba and Y. Yildiz. Modeling cyber-physical human systems via an interplay between reinforcement learning and game theory. *Annual Reviews in Control*, 48:1–21, 2019.
- [56] Y. E. Sahin, Z. Liu, K. Rutledge, D. Panagou, S. Z. Yong, and N. Ozay. Intention-aware supervisory control with driving safety applications. In *2019 IEEE Conference on Control Technology and Applications (CCTA)*, pages 1–8, 2019.
- [57] T. G. Molnar, A. K. Kiss, A. D. Ames, and G. Orosz. Safety-critical control with input delay in dynamic environment. *IEEE Transactions on Control Systems Technology*, pages 1–14, 2022.
- [58] N. Mehdipour, M. Althoff, R. D. Tebbens, and C. Belta. Formal methods to comply with rules of the road in autonomous driving: State of the art and grand challenges. *Automatica*, 152:110692, 2023.
- [59] K. Esterle, V. Aravantinos, and A. Knoll. From specifications to behavior: Maneuver verification in a semantic state space. In *2019 IEEE Intelligent Vehicles Symposium (IV)*, pages 2140–2147. IEEE, 2019.
- [60] T. Wongpiromsarn, K. Slutsky, E. Frazzoli, and U. Topcu. Minimum-violation planning for autonomous systems: Theoretical and practical considerations. In *2021 American Control Conference (ACC)*, pages 4866–4872. IEEE, 2021.
- [61] C. Belta, B. Yordanov, and E. A. Gol. *Formal methods for discrete-time dynamical systems*, volume 89. Springer, 2017.
- [62] Y. E. Sahin, R. Quirynen, and S. D. Cairano. Autonomous vehicle decision-making and monitoring based on signal temporal logic and mixed-integer programming. In *2020 American Control Conference (ACC)*, pages 454–459. IEEE, 2020.
- [63] M. Koschi and M. Althoff. Set-based prediction of traffic participants considering occlusions and traffic rules. *IEEE Transactions on Intelligent Vehicles*, 6(2):249–265, 2021.

- [64] J. Guo, S. Cheng, and Y. Liu. Optimal control of connected and automated vehicles at roundabouts: An investigation in a mixed-traffic environment. *IFAC-PapersOnLine*, 51(9):73–78, 2018. 15th IFAC Symposium on Control in Transportation Systems CTS 2018.
- [65] V.-A. Le, H. M. Wang, G. Orosz, and A. A. Malikopoulos. Coordination for connected automated vehicles at merging roadways in mixed traffic environment. In *2023 62nd IEEE Conference on Decision and Control (CDC)*, pages 4150–4155, 2023.
- [66] Z. Sun, T. Huang, and P. Zhang. Cooperative decision-making for mixed traffic: A ramp merging example. *Transportation Research Part C: Emerging Technologies*, 120:102764, 2020.
- [67] M. Karimi, C. Roncoli, C. Alecsandru, and M. Papageorgiou. Cooperative merging control via trajectory optimization in mixed vehicular traffic. *Transportation Research Part C: Emerging Technologies*, 116:102663, 2020.
- [68] J. Bethge, B. Morabito, H. Rewald, A. Ahsan, S. Sorgatz, and R. Findeisen. Modelling human driving behavior for constrained model predictive control in mixed traffic at intersections. *IFAC-PapersOnLine*, 53(2):14356–14362, 2020.
- [69] J. Guo, S. Cheng, and Y. Liu. Merging and diverging impact on mixed traffic of regular and autonomous vehicles. *IEEE Transactions on Intelligent Transportation Systems*, 22(3):1639–1649, 2021.
- [70] J. Hu, X. Li, Y. Cen, Q. Xu, X. Zhu, and W. Hu. A roadside decision-making methodology based on deep reinforcement learning to simultaneously improve the safety and efficiency of merging zone. *IEEE Transactions on Intelligent Transportation Systems*, 23(10):18620–18631, 2022.
- [71] Y. T. Chow, J. Darbon, S. Osher, and W. Yin. Algorithm for overcoming the curse of dimensionality for time-dependent non-convex Hamilton–Jacobi equations arising from optimal control and differential games problems. *Journal of Scientific Computing*, 73:617–643, 2017.
- [72] T. Wongpiromsarn, S. Karaman, and E. Frazzoli. Synthesis of provably correct controllers for autonomous vehicles in urban environments. In *2011 14th International IEEE Conference on Intelligent Transportation Systems (ITSC)*, pages 1168–1173. IEEE, 2011.
- [73] M. Bui, M. Lu, R. Hojabr, M. Chen, and A. Shriraman. Real-time Hamilton-Jacobi reachability analysis of autonomous system with an FPGA. In *2021 IEEE/RSJ International Conference on Intelligent Robots and Systems (IROS)*, pages 1666–1673. IEEE, 2021.
- [74] ETSI TR 103 578. *Intelligent Transport Systems (ITS); Vehicular Communications; Informative report for the Maneuver Coordination Service*. European Telecommunications Standards Institute, ETSI Standard, draft 0.0.7, Feb. 2022.
- [75] ETSI TS 103 561. *Intelligent Transport Systems (ITS); Vehicular Communications; Basic Set of Applications; Maneuver Coordination Service*. European Telecommunications Standards Institute, draft 0.0.6, Jan. 2024.

- [76] D. Heß, R. Lattarulo, J. Pérez, T. Hesse, and F. Köster. Negotiation of cooperative maneuvers for automated vehicles: Experimental results. In *2019 IEEE Intelligent Transportation Systems Conference (ITSC)*, pages 1545–1551, 2019.
- [77] D. Maksimovski, A. Festag, and C. Facchi. A survey on decentralized cooperative maneuver coordination for connected and automated vehicles. In *VEHITS*, pages 100–111, 2021.
- [78] D. Maksimovski and C. Facchi. Negotiation patterns for V2X cooperative driving: How complex maneuver coordination can be? In *IEEE 98th Vehicular Technology Conference (VTC2023-Fall)*, pages 1–7, 2023.
- [79] ETSI EN 302 637-2 V1.4.1. *Intelligent Transport Systems (ITS); Vehicular Communications; Basic Set of Applications; Part 2: Specification of Cooperative Awareness Basic Service*. European Telecommunications Standards Institute, ETSI Standard, 2019.
- [80] M. Wu, T. Louw, M. Lahijanian, W. Ruan, X. Huang, N. Merat, and M. Kwiatkowska. Gaze-based intention anticipation over driving manoeuvres in semi-autonomous vehicles. In *2019 IEEE/RSJ International Conference on Intelligent Robots and Systems (IROS)*, pages 6210–6216, 2019.
- [81] Y. Chen, N. Sohani, and H. Peng. Modelling of uncertain reactive human driving behavior: A classification approach. In *2018 IEEE Conference on Decision and Control (CDC)*, pages 3615–3621, 2018.
- [82] SAE J3186. Application Protocol and Requirements for Maneuver Sharing and Coordinating Service. Technical report, SAE International, 2023.
- [83] A. Correa, R. Alms, J. Gozalvez, M. Sepulcre, M. Rondinone, R. Blokpoel, L. Lüken, and G. Thandavarayan. Infrastructure support for cooperative maneuvers in connected and automated driving. In *2019 IEEE Intelligent Vehicles Symposium (IV)*, pages 20–25. IEEE, 2019.
- [84] R. Molina-Masegosa, S. S. Avedisov, M. Sepulcre, Y. Z. Farid, J. Gozalvez, and O. Altintas. V2X communications for maneuver coordination in connected automated driving: Message generation rules. *IEEE Vehicular Technology Magazine*, 18(3):91–100, 2023.
- [85] R. Molina-Masegosa, S. S. Avedisov, M. Sepulcre, Y. Z. Farid, J. Gozalvez, and O. Altintas. Insights into the design of V2X-based maneuver coordination for connected automated driving. In *96th IEEE Vehicular Technology Conference (VTC2022-Fall)*, pages 1–5, 2022.
- [86] R. van Hoek, J. Ploeg, and H. Nijmeijer. Cooperative driving of automated vehicles using B-splines for trajectory planning. *IEEE Transactions on Intelligent Vehicles*, 6(3):594–604, 2021.
- [87] IEEE 1609.2-2016. *IEEE Standard for Wireless Access in Vehicular Environments—Security Services for Applications and Management Messages*. IEEE, Jan. 2016.
- [88] IEEE 1609.3-2020. *IEEE Standard for Wireless Access in Vehicular Environments (WAVE)—Networking Services*. IEEE, Dec. 2020.

- [89] H. M. Wang, T. G. Molnár, S. S. Avedisov, A. H. Sakr, O. Altintas, and G. Orosz. Conflict analysis for cooperative merging using V2X communication. In *2020 IEEE Intelligent Vehicles Symposium (IV)*, pages 1538–1543, 2020.
- [90] H. M. Wang, S. S. Avedisov, A. H. Sakr, O. Altintas, and G. Orosz. Opportunistic strategy for cooperative maneuvering using conflict analysis. In *2021 IEEE Intelligent Vehicles Symposium (IV)*, pages 348–353, 2021.
- [91] H. M. Wang, S. S. Avedisov, O. Altintas, and G. Orosz. Multi-vehicle conflict management under time delays. *IFAC-PapersOnLine*, 55(36):306–311, 2022. 17th IFAC Workshop on Time Delay Systems TDS 2022.
- [92] H. M. Wang, S. S. Avedisov, O. Altintas, and G. Orosz. Multi-vehicle conflict management with status and intent sharing. In *2022 IEEE Intelligent Vehicles Symposium (IV)*, pages 1321–1326, 2022.
- [93] H. M. Wang, S. S. Avedisov, A. H. Sakr, O. Altintas, and G. Orosz. Conflict charts: Effective design tools for cooperative driving strategies. In *the 28th ITS world congress*, 2022.
- [94] H. M. Wang, S. S. Avedisov, O. Altintas, and G. Orosz. Multi-vehicle conflict management with status and intent sharing under time delays. *IEEE Transactions on Intelligent Vehicles*, 8(2):1624–1637, 2023.
- [95] H. M. Wang, S. S. Avedisov, T. G. Molnár, A. H. Sakr, O. Altintas, and G. Orosz. Conflict analysis for cooperative maneuvering with status and intent sharing via V2X communication. *IEEE Transactions on Intelligent Vehicles*, 8(2):1105–1118, 2023.
- [96] H. M. Wang, S. S. Avedisov, O. Altintas, and G. Orosz. Experimental validation of intent sharing in cooperative maneuvering. In *2023 IEEE Intelligent Vehicles Symposium (IV)*, pages 1–6. IEEE, 2023.
- [97] H. M. Wang, S. S. Avedisov, O. Altintas, and G. Orosz. Evaluating intent sharing communication using real connected vehicles. In *2023 IEEE Vehicular Networking Conference (VNC)*, pages 69–72. IEEE, 2023.
- [98] H. M. Wang, S. S. Avedisov, O. Altintas, and G. Orosz. Intent sharing in cooperative maneuvering: Theory and experimental evaluation. *IEEE Transactions on Intelligent Transportation Systems*, 2024, doi: 10.1109/TITS.2024.3379994.
- [99] H. M. Wang, S. S. Avedisov, O. Altintas, and G. Orosz. Negotiation in cooperative maneuvering using conflict analysis: Theory and experimental evaluation. In *2024 Intelligent Vehicles Symposium*, under review. 2024.
- [100] A. Kondyli and L. Elefteriadou. Modeling driver behavior at freeway–ramp merges. *Transportation Research Record*, 2249(1):29–37, 2011.
- [101] D. Zhou, Z. Ma, and J. Sun. Autonomous vehicles’ turning motion planning for conflict areas at mixed-flow intersections. *IEEE Transactions on Intelligent Vehicles*, 5(2):204–216, 2020.

- [102] Y. Zhang, Q. Lin, J. Wang, S. Verwer, and J. M. Dolan. Lane-change intention estimation for car-following control in autonomous driving. *IEEE Transactions on Intelligent Vehicles*, 3(3):276–286, 2018.
- [103] Y. Zhang, C. Fu, and L. Hu. Yellow light dilemma zone researches: A review. *Journal of Traffic and Transportation Engineering (English Edition)*, 1(5):338–352, 2014.
- [104] C. Liu, R. Herman, and D. C. Gazis. A review of the yellow interval dilemma. *Transportation Research Part A: Policy and Practice*, 30(5):333–348, 1996.
- [105] L. Zhang and G. Orosz. Motif-based design for connected vehicle systems in presence of heterogeneous connectivity structures and time delays. *IEEE Transactions on Intelligent Transportation Systems*, 17(6):1638–1651, 2016.
- [106] W. B. Qin, M. M. Gomez, and G. Orosz. Stability and frequency response under stochastic communication delays with applications to connected cruise control design. *IEEE Transactions on Intelligent Transportation Systems*, 18(2):388–403, 2017.
- [107] H. Xing, J. Ploeg, and H. Nijmeijer. Padé approximation of delays in cooperative ACC based on string stability requirements. *IEEE Transactions on Intelligent Vehicles*, 1(3):277–286, 2016.
- [108] J. I. Ge and G. Orosz. Connected cruise control among human-driven vehicles: Experiment-based parameter estimation and optimal control design. *Transportation research part C: emerging technologies*, 95:445–459, 2018.
- [109] S. Beregi, S. S. Avedisov, C. R. He, D. Takacs, and G. Orosz. Connectivity-based delay-tolerant control of automated vehicles: Theory and experiments. *IEEE Transactions on Intelligent Vehicles*, 2021.
- [110] Z. H. Khattak, J. Rios-Torres, and M. D. Fontaine. Impact of communications delay on safety and stability of connected and automated vehicle platoons: Empirical evidence from experimental data. *IEEE Access*, 2023.
- [111] T. G. Molnár, W. B. Qin, T. Insperger, and G. Orosz. Application of predictor feedback to compensate time delays in connected cruise control. *IEEE Transactions on Intelligent Transportation Systems*, 19(2):545–559, 2018.
- [112] H. Xing, J. Ploeg, and H. Nijmeijer. Compensation of communication delays in a cooperative acc system. *IEEE Transactions on Vehicular Technology*, 69(2):1177–1189, 2019.
- [113] C. R. He, J. I. Ge, and G. Orosz. Fuel efficient connected cruise control for heavy-duty trucks in real traffic. *IEEE Transactions on Control Systems Technology*, 28(6):2474–2481, 2020.
- [114] G. Stépán. *Retarded dynamical systems: Stability and characteristic functions*. Longman Scientific & Technical, 1989.
- [115] M. Krstic. *Delay compensation for nonlinear, adaptive, and PDE systems*. Springer, 2009.

- [116] N. Kochdumper and M. Althoff. Sparse polynomial zonotopes: A novel set representation for reachability analysis. *IEEE Transactions on Automatic Control*, 66(9):4043–4058, 2021.
- [117] G. Cecchini, A. Bazzi, B. M. Masini, and A. Zanella. Localization-based resource selection schemes for network-controlled LTE-V2V. In *2017 International Symposium on Wireless Communication Systems (ISWCS)*, pages 396–401, 2017.
- [118] B. M. Masini, A. Bazzi, and E. Natalizio. Radio access for future 5G vehicular networks. In *86th IEEE Vehicular Technology Conference (VTC-Fall)*, pages 1–7, 2017.
- [119] M. Sepulcre, J. Gozalvez, B. Coll-Perales, M. C. Lucas-Estañ, and J. R. Gisbert. Empirical performance models for V2V communications. In *2015 IEEE International Conference on Computer and Information Technology; Ubiquitous Computing and Communications; Dependable, Autonomic and Secure Computing; Pervasive Intelligence and Computing*, pages 737–742, 2015.